8-2007

Identification and Characterization of Phenotypically Distinct Aggregates within Huntingtin-inducible PC12 Cell Models

Erica LeAnn Rowe
University of Tennessee - Knoxville

To the Graduate Council:

I am submitting herewith a dissertation written by Erica LeAnn Rowe entitled "Identification and Characterization of Phenotypically Distinct Aggregates within Huntingtin-inducible PC12 Cell Models." I have examined the final electronic copy of this dissertation for form and content and recommend that it be accepted in partial fulfillment of the requirements for the degree of Doctor of Philosophy, with a major in Life Sciences.

Ronald Wetzel, Major Professor

We have read this dissertation and recommend its acceptance:

Jonathan S. Wall, Stephen J. Kennel, Brynn H. Voy

Accepted for the Council:

Carolyn R. Hodges

Vice Provost and Dean of the Graduate School

(Original signatures are on file with official student records.)

To the Graduate Council:

I am submitting herewith a dissertation written by Erica LeAnn Rowe entitled "Identification and Characterization of Phenotypically Distinct Aggregates within Huntingtin-inducible PC12 Cell Models." I have examined the final electronic copy of this dissertation form and content and recommend that it be accepted in partial fulfillment of the requirements for the degree of Doctor of Philosophy, with a major in Life Sciences.

_____

Ronald Wetzel, PhD, Major Professor

We have read this dissertation
and recommend its acceptance.

_____

Jonathan S. Wall, PhD

_____

Stephen J. Kennel, PhD

_____

Brynn H. Voy, PhD

Accepted for the Council:

_____

Carolyn R. Hodges,
Vice Provost and Dean of the Graduate School

(Original signatures are on file with official student records.)

IDENTIFICATION AND CHARACTERIZATION OF PHENOTYPICALLY DISTINCT AGGREGATES WITHIN HUNTINGTIN-INDUCIBLE PC12 CELL MODELS

A Dissertation

Presented for the

Doctor of Philosophy

Degree

University of Tennessee, Knoxville

Erica LeAnn Rowe

August 2007

DEDICATION

This dissertation is dedicated to:

My loving Mother and late Father:

Patricia Ann Johnson

&

Tommy Ray Johnson

And also to my husband, son, and unborn daughter:

Anthony Shaun Rowe

&

Matthew Conner and Chloe Elizabeth Rowe

ACKNOWLEDGEMENTS

Thank you, Dr. Ron Wetzel for inviting me into your lab and for sharing with me some of your vast scientific knowledge. I'm grateful to have had the opportunity to study with one of the leading scientists in the Huntington's disease research field. I appreciate the freedom that you entrusted in me with designing and implementing my research project.

I would like to express my sincerest gratitude to all who have trained me and inspired me to become a researcher. To everyone in the laboratories of Drs. Alan Solomon and Ron Wetzel, I truly appreciate all the help each of you have offered me during my Ph.D. studies. I would like to thank Dr. Alex Osmand for answering my many questions regarding the various aspects of science and for sharing with me the wonderful stories of his life. I would like to especially thank Dr. Valerie Berthelier for all her wonderful advice, training, guidance, and encouragement. With her mentorship and friendship, I have developed the confidence necessary for a successful career. I will always remember our discussions and am grateful for the opportunity to have worked with her.

I am thankful for my wonderful committee members, Drs. Jonathan Wall, Steve Kennel, and Brynn Voy for their great support and guidance. Your encouragement is what kept my head above the water when I felt like all was lost. I will never be able to repay you for all that you've done for me. I would also like to include Dr. Doug Gillman in this group. Although his stay on my committee was shortened, I appreciate the advice that he offered during the time he was present. Dr. Jonathan Wall deserves a special

acknowledgement for taking on the advising role during my last several months of study and for providing me with space to finish my dissertation.

I would like to thank the Hereditary Disease Foundation and the Genome Science and Technology Program for funding a significant portion of my research. I would like to thank Dr. Cynthia Peterson for being so particularly understanding and supportive. I would also like to thank the Physcians' Medical Education and Research Foundation for providing me the opportunity to continue and finish my research when my advisor took a new position.

Finally, I am most thankful for my especially understanding family. My husband, Shaun, has been my biggest supporter. You will never know how much your encouragement and understanding has meant to me. You have been my rock on which I have leaned. Thank you so much for always believing in me. My son, Matthew, has also been very patient with his Mom. I know it's been difficult for him not having me at his disposal. Thank you, my angel, Mommy loves you. I am also thankful that our pending arrival has been cooperative and allowed her Mom to spend many long hours writing. I am grateful for my sisters' support. Tomi Lynn and Amy have always provided encouragement when I needed it most. I owe so much gratitude to my Granny, Aunt Jac, and, Aunt Muff for everything you have done for me over the years.Thank you Georgia and Dennis for all your support. Finally, I am very thankful for my Mom, who has always offered her encouragement. I know it wasn't always easy raising three girls alone. For that reason, you are my inspiration. Thanks for teaching me that you must always do your best and work your hardest for the most important things.

ABSTRACT

The role of various polyglutamine (polyGln) aggregated states in the disease mechanism of expanded CAG repeat disorders continues to be a perplexing subject. We are interested in learning more about these species and the relationship between the aggregation pathways. We have developed an innovative staining technique that allows, for the first time, the visualization of small polyGln aggregates, which we refer to as aggregation foci (AF), that are functionally distinguished by their ability to serve as seeds for amyloid growth. The aggregation foci stain should prove useful in the Huntington's disease research as a tool for the identification of a functional class of aggregates that was previously undescribed. The ability to account for different aggregates may provide a better correlation with neurodegeneration. Using this method we were able to detect at least four phenotypic classes of aggregates in stable PC12 cells engineered for inducible expression of different polyGln repeat length forms of a green fluorescent protein-fused huntingtin (htt) exon-1 fragment: 1) small, recruitment-competent, cytoplasmic AF, 2) large, cytoplasmic, perinuclear, green-fluorescent, recruitment-inert htt aggregates, 3) cytoplasmic, perinuclear, green-fluorescent, recruitment-competent aggregates, and 4) small, nuclear, recruitment-inert, green-fluorescent aggregates. Each species can be found either in isolation or co-existing within the same microscope field depending on the time post-induction and Gln repeat-length. In our studies, AF tend to be the earliest species that appear in the cells. The PC12 cells generally did not exhibit indications of toxicity due to the polyGln species, and thus provided a good model to study the aggregation pathway without the bias of cell death. Biochemical data were gathered to understand the

properties of each distinct aggregate specie. We also examined the ability of two separate compounds (curcumin and demecolcine) to alter the aggregation pathway. Each experiment was designed to obtain knowledge about possible precursor/product relationships that exist among the species, with the ultimate goal of gaining insight into the aggregation pathways responsible for the formation of the amyloid-like AF and larger inert aggregates that arise in these the cell lines expressing various polyGln repeat-lengths. We interpret this data as indicating that the two species are on competing assembly pathways.

TABLE OF CONTENTS

LIST OF TABLES

LIST OF FIGURES

CHAPTER 1

LITERATURE REVIEW

1.1 Protein folding disorders:

OVERVIEW

A large number of human diseases arise from the inability of peptides or proteins to properly assume their native conformation. These conditions, often collectively referred to as protein conformational, or protein folding disorders, span diverse conditions that are widespread and are not confined to any particular organ or tissue (see Table 1.1 for a summary of amyloidoses) [Carrell and Lomas 1997; Uversky 1999; Ahmad et al. 2005; Westermark et al. 2005; Chiti and Dobson 2006]. Conformational disorders arise when there is a change in the size, shape, or amount of a protein resulting in the deposition of an aberrant form – which may be amyloid or some other type of protein aggregate – within tissues. Protein folding disorders can be categorized into two major groups: 1) those involving only the brain, and 2) those affecting the remainder of the body. This section will provide a brief introduction to the protein folding disorders that result in amyloid or amyloid-like deposits; after which, a more detailed description of a subset of these illnesses, the polyglutamine (polyGln or polyQ) repeat diseases, will be provided.

Table 1.1: Human protein folding disorders (Amyloidoses)

Amyloid condition	Aggregating peptide or protein	Native structure(s) of peptide or protein [#]	Affected tissue / Syndrome
Cerebral (Localized)			
Expanded polyglutamine diseases	Various polyglutamine containing proteins (CAG)	Intrinsically unfolded; β-sheet; α-helices; combination α+β; unknown (See Table 1.2)	Cerebral cortex, Purkinje cells, basal ganglia, etc.
Alzheimer's disease	β-amyloid precursor protein (Aβ)	Intrinsically unfolded	Cerebral cortex, hippocampus, basal forebrain, etc.
Spongiform encephalopathies	Prion protein (APrP)	Intrinsically unfolded; α-helices	Brain
Parkinson's disease	α-synuclein	Intrinsically unfolded	Substantia nigra
Amyotrophic lateral sclerosis	Superoxide dismutase 1	β-sheet	Motor neurons
Pituitary prolactinoma	Prolactin (APro)	α-helices, 4-helical cytokines	Pituitary
Icelandic cerebral amyloid angiopathy (Systemic)	Cystatin C (ACys)	α+β, cystatin-like	Brain
Peripheral – Systemic (S) or Localized (L)			
AL amyloidosis – Light chain (S,L)	Immunoglobulin light chains (AL)	β-sheet	Skin, nerves, heart, GI tract (includes tongue), kidney, liver, spleen, blood vessels Myeloma-associated primary tumors
AH amyloidosis – Heavy chain (S,L)	Immunoglobulin heavy chains (AH)	β-sheet	
AA amyloidosis – Inflammation-associated (S)	Serum amyloid A protein (AA)	α/β	Spleen, liver, kidneys, adrenals, lymph nodes. vascular Secondary to chronic infections, reactive tumors
Familial & senile systemic amyloidosis (S,L)	Transthyretin (ATTR)	β-sheet	Predominately liver, most organs & tissues
Hemodialysis amyloidosis (S,L)	β_2-microglobulin ($A\beta_2M$)	β-sheet	Musculoskeletal, GI tract

Table 1.1. Continued

Amyloid condition	Aggregating peptide or protein	Native structure(s) of peptide or protein [#]	Affected tissue / Syndrome
Lysozyme amyloidosis (S)	Lysozyme (ALys)	α+β, lysozyme fold	Visceral organs & tissues
Familial, sporadic & aortic (S,L)	Apolipoprotein (AApoAI, AApoAII, AApoAIV)	α-helices	Visceral organs & tissues
Familial amyloidosis (S)	Gelsolin (AGel)	α+β, gelsolin-like	Eyes
Hereditary fibrinogen α-chain amyloidosis (S)	Fibrinogen α-chain (AFib)	Coil?	Kidney
Familial British dementia (S)	ABriPP (ABri)	Majority coil, some α+β	Central nervous system
Familial Danish dementia (S)	ADanPP (ADan)	Predicted β-sheet	Central nervous system
Diabetes mellitus type II (L)	Islet amyloid polypeptide (AIAPP) or amylin	Natively unfolded	Islets of Langerhans (pancreas)
Medullary thyroid carcinoma (L)	(Pro)calcitonin (ACal)	50% coil : 50% α-helix	C-cell thyroid tumors
Isolated atrial amyloidosis (L)	Atrial natriuretic factor (AANF)	50% coil : 50% α-helix	Heart
Iatrogenic insulin-dependent amyloidosis (L)	Insulin (AIns)	Largely α-helical	Liver, kidney, spleen, pancreas
Senile aortic, medin amyloidosis (L)	Lactadherin (AMed)	Coil	Heart
Familial corneal amyloidosis (L)	Kerato-epithelin (AKer)	Largely α-helical	Eyes
Familial corneal amyloidosis (L)	Lactoferrin (ALac)	α+β combination	Eyes

[#]Based on the Structural Classification of Proteins (SCOP), Protein Data Bank (PDB), or Advanced Protein Secondary Structure Prediction Server (APSSP).

A natively folded protein can become pathogenic for a variety of reasons, including posttranslational processing or the improper trafficking of the protein [Chai et al. 1999; Amaral 2004; Lee et al. 2004; Gunawardena and Goldstein 2005; Luo et al. 2005]. The majority of conformational disorders, however, occur as a result of a change in the protein from a normally soluble state into an aggregated state, where the aggregates range from soluble, oligomeric structures to large, insoluble, "amyloid" or amyloid-like fibrils. This aggregation is normally associated with a conformational change. Aggregated proteins either accumulate within the cell (examples are inclusions of huntingtin and neurofibrillary tangles of tau) or outside the cell (amyloid plaques in Alzheimer's disease, amyloid fibrils in other amyloid diseases, diffuse, non-amyloid deposits in AD). The overall effect is that there is a reduction in the amount of the normal protein and an increase in the misfolded protein. While some aggregation diseases may exhibit a component of a loss of function phenotype (generally intracellular aggregation disorders), due to the reduction in normal protein levels, for many of these diseases the principle effects appear to be due to toxic gains of function.

AMYLOID STRUCTURE

Amyloid fibrils, by classical definition, are extracellular protein aggregates [Pepys 2006] that: (a) exhibit a cross-β structure (β-sheets run parallel to the fibril axis, and the β-strand components run perpendicular to the axis) as demonstrated by x-ray diffraction (see Figure 1.1) [Sunde et al. 1997]; (b) that specifically bind Congo red (CR) dye, which is thought to bind between β-strands, with a green birefringence that is

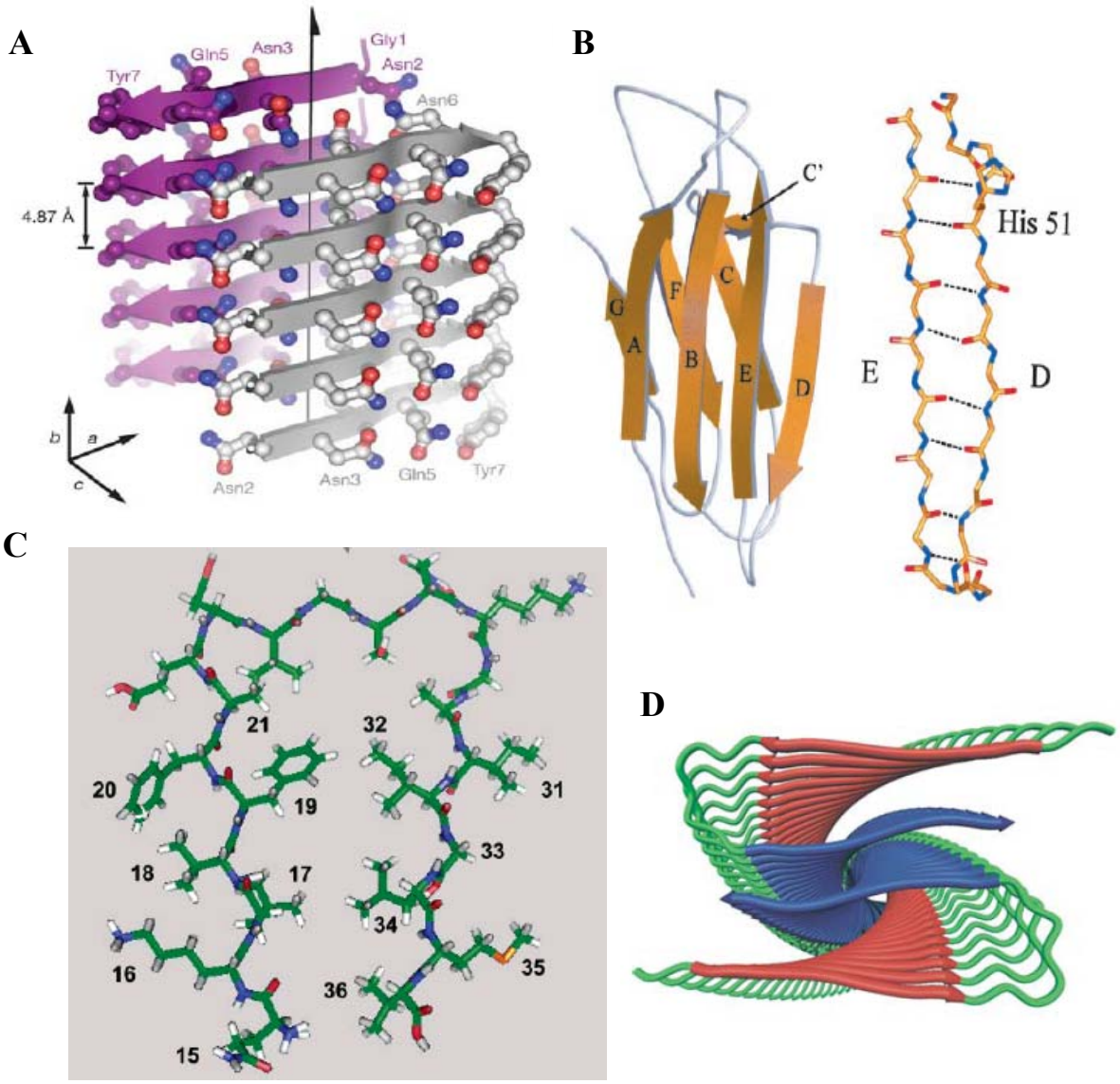

Figure 1.1: Proposed β-strand structures. *(A) Cross-β spine structure of amyloid fibrils* (Taken from [Nelson et al. 2005]). Carbon atoms are colored purple or gray/white, oxygen is red, and nitrogen is blue. The backbone of each β-strand is represented as an arrow with protruding side chains. The "dry" interface (composed of side chains Asn2, Gln4, and Asn6) is located between the two sheets, while the solvated surfaces are exposed. *(B) Ribbon diagram and detailed conformational views of the human monomeric β2-microglobulin* (Taken from [Trinh et al. 2002]). *(C) Model of a single strand of residues 15-36 of the amyloid fibril core β-sheet cross-section* (Adapted from [Shivaprasad and Wetzel 2004]). Model was created by J.T. Guo and Y. Xu based on cysteine accessibility and disulfide cross-linking [Shivaprasad and Wetzel 2006]. Carbon backbone is colored green, hydrogen is gray/white, oxygen is red, nitrogen is blue, and yellow is sulfur. *(D) Cartoon depiction of antiparallel β-sheets of Abeta fibril.* Residues 12-21 are red and residues 30-40 are blue. (Taken from [Tycko 2006]).

observed under polarized light microscopy [Puchtler 1962]; and (c) that bind the yellow fluorescent dye thioflavin T (ThT), another molecule thought to bind to β-sheets [Sunde, Serpell et al. 1997]. Actual amyloid deposits have also been shown to contain glycan molecules, such as heparan sulfate [Nelson et al. 1991] and to bind serum amyloid P (SAP) component [Pepys et al. 1994]. In contrast to the above restrictive definition of amyloid, the term has been adopted by the protein structural and biophysical community to refer to a type of aggregated protein folding motif that has the structural properties of amyloid (cross-β, dye-binding, etc.), even if the aggregate has been generated in vitro or intracellularly. Thus, for the purposes of this dissertation, the term amyloid or amyloid-like will be used interchangeably and will refer to non-native, aggregated, β-structures that have the ability to self-propagate.

Over the past decade, several structural models of this amyloid fibril folding motif have been proposed. These models include the cross-β spine (Figure 1.1A) proposed by Eisenberg and coworkers [Nelson, Sawaya et al. 2005], the polar zipper model [Perutz et al. 1994] (discussed in Section 1.2), as well as various other antiparallel β-strand models (Figure 1.1B-1D) [Trinh et al. 2002; Shivaprasad and Wetzel 2004; Shivaprasad and Wetzel 2006; Tycko 2006; Bu et al. 2007]. These structures are based on data obtained using a variety of methods including, solid-state NMR (SSNMR), hydrogen-deuterium exchange, mutational analysis, atomic force microscopy (AFM), X-ray diffraction, and transmission electron microscopy (TEM).

Each model has several similarities including the accepted cross-β structure, the intermolecular packing that occurs between the β-sheets [Shivaprasad and Wetzel 2004],

and the hydrogen bonding that occurs between the main chain and side chain amino acids [Perutz et al. 1994; Trinh et al. 2002]. Several of the proposed models suggest that the core region, despite differences among their primary sequences, is composed of two to four β-sheets that intimately interact with one another [Chiti and Dobson 2006].

Despite the observed similarities, there are also numerous differences among the various models. These differences include the nature of side chain involvement, β-strand length and arrangement (parallel or antiparallel), the conformation of regions outside of the core, and the number of β-sheets that comprise a protofilament (the filamentous fibril building block of amyloid fibrils). Other factors that differ significantly are the spacing between the β-sheets of the core and the number of peptide residues that are actually incorporated into the core [Fandrich and Dobson 2002]. In the case of insulin amyloid fibrils, the presence of disulfide bonds also affects the β-sheet packing [Jimenez et al. 2002]. In polyglutamine peptide amyloid, the side chains may become involved in hydrogen bonding to each other or to the β-sheet peptide backbone [Perutz et al. 2002].

The conformation found in isolated fibrils is ultimately determined by some combination of thermodynamics and kinetics. Protein aggregates tend to be quite stable, so that, whether the precursor is an intrinsically unfolded protein or a stably folded protein, fibrils occupy a lower free energy and hence are thermodynamically favored. At the same time, reaction kinetics can determine which of the essentially equally stable polymorphic amyloid states [Kodali and Wetzel 2007] are formed in a fibril formation reaction. More generally, even though the fibril state exists and is thermodynamically favored, fibrils will not form unless the reaction is kinetically feasible, for example by

virtue of a weakening of the native state of a folded precursor, the presence of a fibril seed, or a surmountable nucleation barrier [Kodali and Wetzel 2007].

FUNCTIONAL AMYLOID

Amyloid-like fibrils are not always associated with pathology. Some proteins have been shown to produce amyloid fibrils not associated with tissue toxicity [Stefani and Dobson 2003; Uversky and Fink 2004]. This type of amyloid is referred to as functional amyloid, where the amyloid structure is found to be beneficial to the living organism rather than associated with a disease-state. A few examples of functional amyloid are the bacterial protein curlin [Chapman et al. 2002] that is produced by *Escherichia coli* and used to mediate attachment to host proteins for colonization; the *Saccharomyces cerevisiae* (yeast) prion proteins Ure2p and Sup35p [Osherovich et al. 2004] that confer alternate non-pathogenic phenotypes; and mammalian melanosomes [Berson et al. 2003], which are lysosome-like organelles responsible for the production of the pigment melanin. There are also amyloid deposits not known to be either pathogenic or beneficial [Haggqvist et al. 1999].

NUCLEATION-DEPENDENT MECHANISM

Spontaneous amyloid fibril formation is normally considered to occur via nucleation-dependent polymerization (see Figure 1.2) [Ferrone 1999] followed by elongation or growth of the fibril. This is rather controversial, however, and in some cases fibrils grow without a required nucleation step by a process called “downhill aggregation” [Ferrone 1999; Modler et al. 2004].

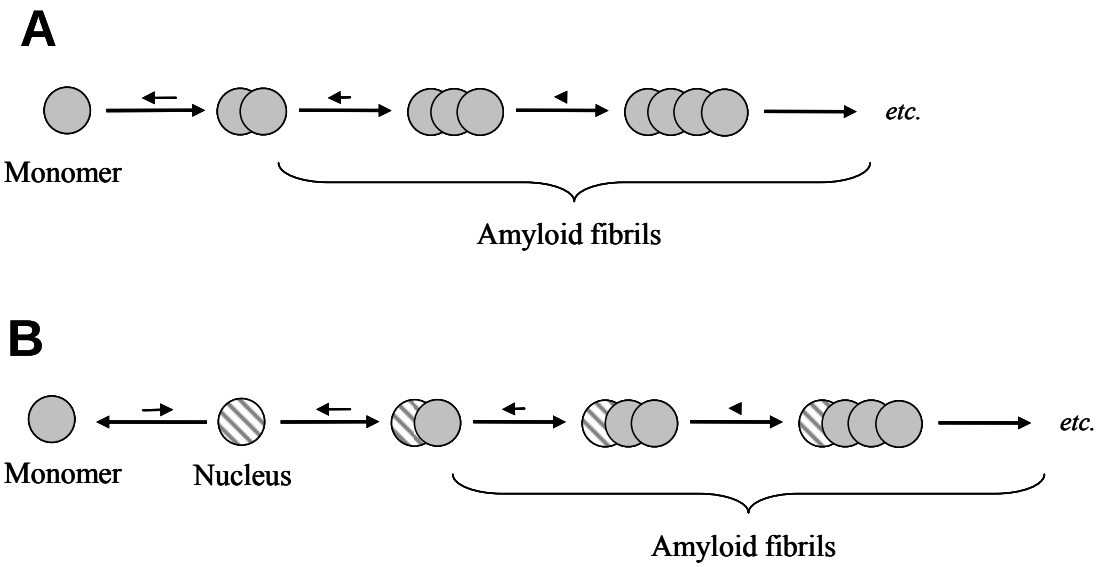

Figure 1.2: General schematic representations of aggregation initiation and growth by monomer addition. *(A) Downhill aggregation.* In this class of aggregate assembly, all monomers, and all aggregates, are equally capable of participating in an effective collision to form a larger particle. There is no energy barrier to initiation of the aggregation reaction (as indicated by the relative sizes of the arrows). *(B) Nucleated growth.* In this class of aggregate assembly, the overall reaction is limited by the energetically unfavorable formation of a critical species called the nucleus. Once the nucleus begins to elongate by monomer addition, the aggregation reaction becomes essentially irreversible. In this illustration, the nucleus is depicted as a special form of the monomer, but, classically, the nucleus is conceived as an oligomer; both appear to be possible. More complex schemes are also possible. For example, although spherical oligomers appear to form by downhill aggregation, their conversion to fibrils – if it happens – could be considered to be the nucleation event for amyloid formation, effectively drawing components of both A and B. These schemes ignore the further complexity that aggregation reactions often require an initial misfolding of the monomer. This is not a concern for amyloidogenic peptides like Aβ and polyglutamine, however, since they have no stable folded structure in solution.

The conversion of the protein into a fibril can be monitored by many means, including light scattering, ThT fluorescence, atomic force microscopy (AFM), electron microscopy (EM), and centrifugation coupled with high performance liquid chromatography (HPLC) (which is useful for following the disappearance of the monomeric species). Fibril formation is often preceded by a lag phase associated with the formation of a nucleus or other, oligomeric states. Once the nucleus has been established (rate-limiting step), the growth (elongation) of the fibril, by addition of either monomers [Lomakin et al. 1996; Lomakin et al. 1997; Collins et al. 2004; O'Nuallain et al. 2005] or oligomers [Kumar et al. 2007; Vestergaard et al. 2007] , occurs very rapidly. Whatever the mechanistic source of the lag phase (nucleus formation, oligomer formation), it may be eliminated by the addition of preformed fibrillar seeds [Naiki et al. 1997; Serio et al. 2000; O'Nuallain et al. 2005]. Experimental conditions as well as certain kinds of mutations have also been shown to decrease the lag phase [Uversky et al. 2002; Pedersen et al. 2004].

AGGREGATE MORPHOLOGIES

As mentioned above, there are a variety of aggregate types and morphologies that go well beyond the amyloid designation. Morphologies of protein aggregates in the literature include amyloid fibrils of various polymorphic states, spherical oligomers of various diameters, and linear and annular protofibrils. The word ‘amorphous’ is sometimes applied to protein aggregates that do not easily fit into previously described definitions or exist in highly variable structures or which maintain their native-like state in the aggregate. Proteins capable of making amyloid fibrils are often also capable of

making other aggregate morphologies, and it is frequently assumed – but rarely if ever proved – that there are precursor-product relationships between these forms.

In 1996, Wood and colleagues discussed the effects of pH on the ability of the amyloid beta peptide to form aggregates [Wood et al. 1996]. Their results demonstrated that aggregates grown at physiologically relevant pH (7.4) exhibit characteristics of standard amyloid fibrils, i.e. a high affinity for Congo red, possessed twists along the longitudinal axis, were approximately 100 Å in width, as evidenced by EM, and were excellent seeds for fibril elongation. In contrast, aggregates produced at a more acidic pH (5.8) did not bind CR, were thicker and shorter (Figure 1.3), and were also poor seeds for further fibril formation.

In another example, IAPP (a 37aa peptide associated with the amyloid found in patients with Type II diabetes), amorphous aggregates were observed to form *in vitro* via EM from a full-length synthetic human IAPP peptide [Higham et al. 2000]. Within 24 hours, these structures had completely converted into amyloid fibrils, which were confirmed not only by EM but also by ThT response, thus demonstrating the complicated nature of fibril formation.

Within the last decade, new aggregate species have been identified. One of these species was named protofibrils by the authors who first described them [Harper et al. 1997; Walsh et al. 1997]. Protofibrils are small, filamentous aggregates that appear early in fibril formation reactions. Their role in the mechanism of mature amyloid fibril assembly remains controversial, and may vary depending on the peptide involved [Kodali and Wetzel 2007]. Protofibrils are different from protofilaments, which are the actual

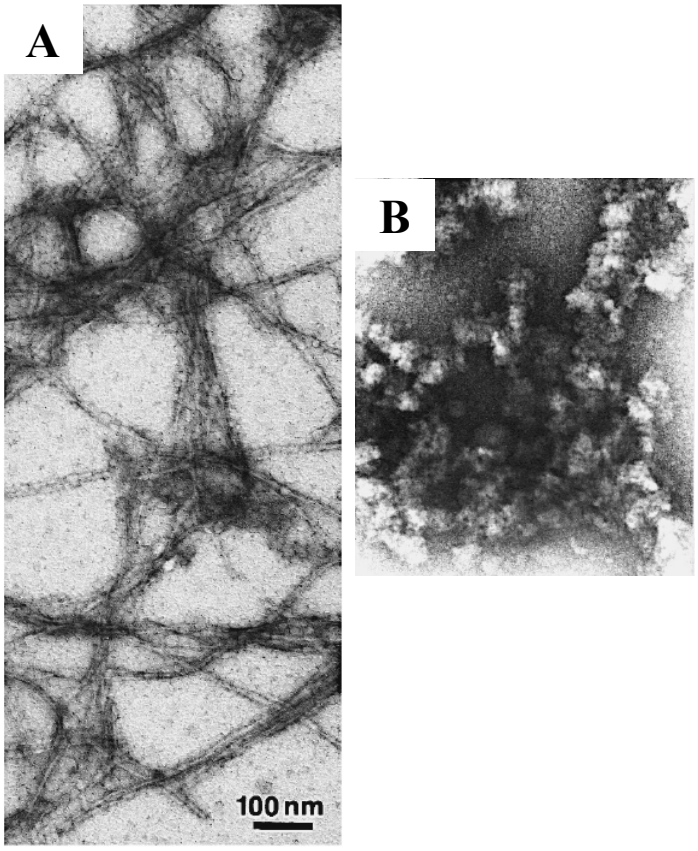

Figure 1.3: Electron micrographs of Aβ aggregates. (Images taken from [Wood, Maleeff et al. 1996]). *(A) pH 7.4 Aβ(1-40) fibrils.* 230μM peptide was incubated for 48 hours at 37°C in phosphate buffered saline. *(B) pH 5.8 Aβ(1-40) aggregates.* 230μM peptide was incubated for 48 hours at 37°C in 50mM 2-(N-morpholino)ethanesulfonic acid (Mes).

components of mature fibrils and not intermediates observed during fibril assembly. Some protofibrils are annular in shape, and this has suggested a particular hypothesis for their cytotoxicity [Harper et al. 1997; Walsh et al. 1999; Lashuel et al. 2002].

Another recently described aggregate is the class called spherical oligomers [Kayed et al. 2003]. These are sometimes referred to as ADDLs (Aβ diffusible ligands) [Lambert et al. 1998] or Aβ56* [Cheng et al. 2007]. The presence of various kinds of small, non-fibrillar Aβ aggregates *in vivo* has also been described [Roher et al. 1996; Cleary et al. 2005]. Oligomers and protofibrils have been identified *in vitro* in a host of protein systems, such as β-amyloid [Harper et al. 1997; Walsh et al. 1997; Kheterpal et al. 2003; Williams et al. 2005], α-synuclein [Conway et al. 2000], transthyretin [Quintas et al. 2001], polyGln proteins [Poirier et al. 2002], β2-microglobulin [Gosal et al. 2005], and immunoglobulin light chain [Ionescu-Zanetti et al. 1999]. Although they have a distinct, non-amyloid morphology, some oligomers/protofibrils give a ThT response and have significant β-structure (but not so much as mature fibrils) [Kodali and Wetzel 2007] (See Figure 1.4). The identification of such species has led to the idea that these smaller structures are responsible for the toxicity observed in neurodegenerative disorders [Conway et al. 2001; Klein et al. 2001; Bucciantini et al. 2002; Walsh et al. 2002; Schaffar et al. 2004; Malisauskas et al. 2005; Glabe and Kayed 2006]

Although it is well documented that protofibrils exist, a question remains whether they are "on-pathway" [Harper et al. 1999; Serio et al. 2000; Plakoutsi et al. 2005; Ellisdon et al. 2006] or "off-pathway" [Collins et al. 2004; Gosal et al. 2005]

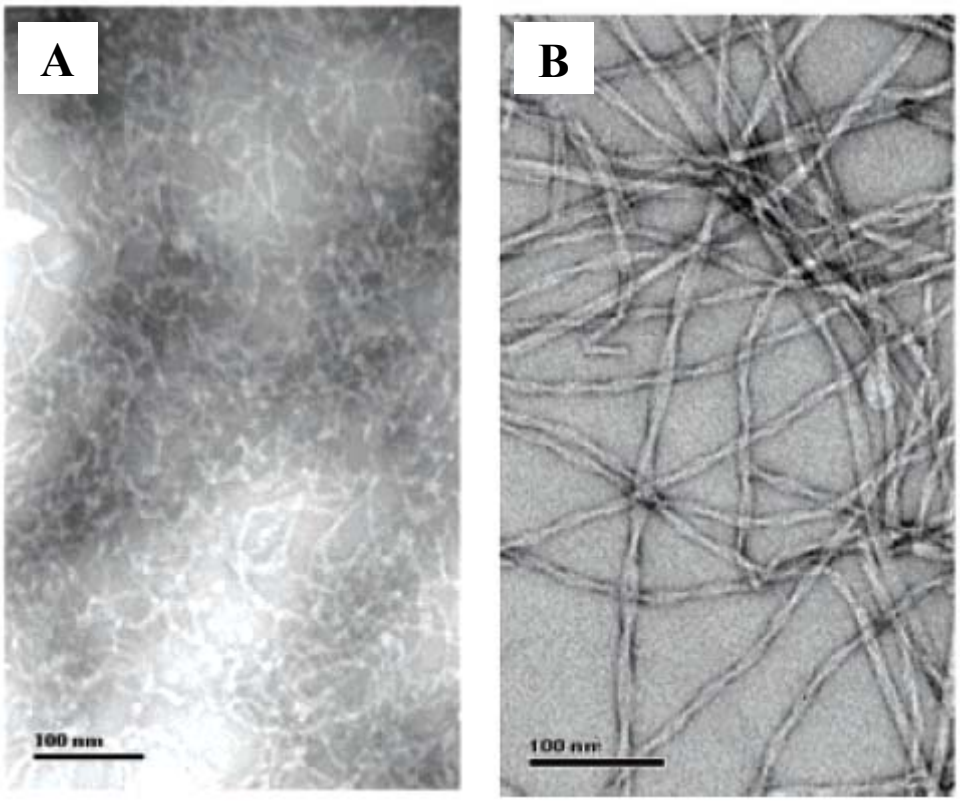

Figure 1.4: Electron micrograph images of Aβ arctic mutant protofibrils and fibrils. (Images adapted from [Kheterpal et al. 2003]). *(A) Aβ arctic mutant protofibrils obtained 16 hours post-incubation at room temp. (B) Negatively stained electron micrograph of mature Aβ arctic fibrils.* The arctic mutant is an Aβ peptide mutation at E22G that is responsible for an early onset familial Alzheimer's disease.

intermediates during the formation of fibrils. Several experiments conducted support both hypothesis (reviewed in [Kodali and Wetzel 2007]).

A particular example supporting an "on-pathway" role of oligomers in fibril formation was demonstrated in a yeast prion model [Serio et al. 2000; Serio et al. 2001] where the Lindquist group showed that fluid oligomeric intermediates underwent a "conformational conversion" upon association with the nucleus. Once the interaction had been established, rapid assembly of an amyloid fibril ensued. Other evidence for "on-pathway" fibril formation was demonstrated in the protein α/β acylphosphatase in *Sulfolobus solfataricus* [Plakoutsi et al. 2005] where early, enzymatically active aggregates were observed that had secondary structure but did not exhibit any β-structure by circular dichroism (CD) or fourier transform infrared spectroscopy (FTIR). As time progressed, these aggregates slowly converted to more amyloid-like structures: loss of enzymatic activity, contained extensive β-sheets, and were ThT and CR positive. Transmission EM also revealed that these latter aggregates contained structures reminiscent of spherical oligomers and protofibrils.

Two other pieces of evidence that suggest that oligomer/protofibrils are "on-pathway" intermediates come from polyglutamine diseases: Machado-Joseph Disease (MJD) [Ellisdon et al. 2006] and Huntington's disease (HD) [Poirier, Li et al. 2002]. In the first example, MJD, it was shown that the ataxin-3 protein formed fibrils through a two-step mechanism [Ellisdon, Thomas et al. 2006], and that fibril formation was nucleation-dependent [Ellisdon et al. 2007]. The first step involved the formation of a protofibril within the Josephin domain of the protein, and the second step involved the

conversion of the protofibril to a fibril. In the second example, HD, it was demonstrated that recombinant htt exon-1 fragments can be induced *in vitro* to form aggregates similar to the spherical oligomers and protofibrils described in other amyloid systems [Poirier et al. 2002; Wacker et al. 2004]. As in other amyloid systems, however, the mechanistic interrelationships between these various aggregated states and their possible roles in pathogenesis have not been established with certainty.

Contrastingly are the reports of oligomer/protofibrils being formed "off-pathway" [Collins et al. 2004; Gosal et al. 2005]. The Weissman group performed kinetic studies that showed, in a yeast prion model, that amyloid formation occurred from monomer addition to a nucleus and that this pathway was separate and competitive with the formation of potentially toxic oligomers [Collins et al. 2004]. Other evidence supporting an "off-pathway" mechanism was demonstrated *in vitro* by the use of a recombinant β_2M protein [Gosal, Morten et al. 2005] where two competing pathways were observed: a nucleation-dependent pathway leading to amyloid fibril formation and a rapid, nucleation-independent pathway yielding flexible "worm-like" fibrils.

As suggested in a current study, the aggregation pathway, not surprisingly, may involve the formation of both "on-" and "off-pathway" intermediates [Thakur unpublished data]. In recent years it has become increasingly clear that the sequences flanking the polyGln region are very important in modulating aggregation. For example, it has been shown that the polyproline region, C-terminal to the Gln stretch, alters the rate of aggregate formation and destabilizes the aggregate but does not change the aggregation mechanism, i.e. aggregation still occurs in a nucleation-dependent

mechanism [Bhattacharyya et al. 2006]. More recently, the effects of the first 17 aa on htt aggregation have also been explored [Rockabrand et al. 2007; Thakur unpublished data]. Our group has found that the presence of htt's first 17 aa rapidly accelerates polyGln aggregation, alters the aggregate morphology, and changes the aggregation mechanism (non-nucleated) [Thakur unpublished data]. For example, at least four morphologically different aggregates are formed. The earliest species appear to be recruitment-incompetent oligomers/protofibrils, while the later species that are formed are recruitment-competent fibrils (reminiscent of the fibrils produced from synthetic peptides containing only polyGln or polyGln and polyproline). The mechanistic relationship between the various types of aggregates is not clear; however, the data suggest that some of the observed aggregates may be "on-pathway", while other species may be "off-pathway".

The exact role(s) that oligomers, "off-pathway" aggregates, and protofibrils play in disease pathogenesis is contentious and unresolved. As alluded in the previous paragraph, perhaps, there are multiple pathways by which amyloid fibrils can form, some directly producing amyloid from monomers, and some involving on-pathway intermediates like protofibrils. Some may involve toxicity, while others do not. Indeed, accessibility to these pathways may even be protein specific. Further research is needed to address these critical questions.

1.2 Polyglutamine diseases:

OVERVIEW

The term neurodegenerative disease refers to any condition in which brain and/or spinal cord cells die or become dysfunctional. These diseases are comprised of a multitude of illnesses involving, but not limited to, dementia and/or the loss of motor skills (ataxia). In the early 1990s, it was found that the expansion of an unstable trinucleotide repeat was associated with several related neurological disorders [Fu et al. 1991; La Spada et al. 1991; Fu et al. 1992]. To date, at least 15 neurological disorders ranging from Huntington's disease to forms of mental retardation occur due to a triplet codon (trinucleotide) expansion (Table 1.2). Each of the trinucleotide repeat disorders can occur in either the coding exon sequences (such as in the polyglutamine repeat diseases), spliced out of the intron sequences (such as in Friedreich's ataxia), or in the 5' or 3' untranslated regions (as found in fragile X syndrome or myotonic dystrophy). A summary of these gene mutations are shown in Figure 1.5. Each mutation confers a different toxic effect, which will be discussed later in the chapter.

Of these trinucleotide repeat disorders, at least nine are caused by an expansion of a polyglutamine sequence (polyGln) within their respective proteins (Table 1.3), with Huntington's disease (HD) being the most common in the population. The remaining CAG repeat diseases are spinobulbar muscular atrophy (SBMA), dentatorubral-pallidoluysian atrophy (DRPLA), and the spinocerebellar ataxias (SCA) 1, 2, 3, 6, 7 and 17.

Table 1.2: Trinucleotide repeat disorders.

Disease	Triplet expansion		Clinical features upon expansion
	Normal	Pathological	
Fragile X syndrome (FRAXA)	$(CGG)_n$ 6-60	> 200	Mental retardation, enlarged testes, connective tissue defects, behavioral abnormalities
Fragile XE mental retardation (FRAXE)	$(CCG)_n$ 4-39	200-900	Mental retardation
Friedreich's ataxia (FRDA)	$(GAA)_n$ 6-32	200, 1700	Sensory ataxia, cardiomyopathy, diabetes
Myotonic dystrophy (DM1)	$(CTG)_n$ 5-37	50-10,000	Myotonia, weakness, cardiac conduction defects, insulin resistance, cataracts, testicular atrophy, and congenital mental retardation
Fragile X-associated tremor ataxia syndrome (FXTAS)	$(CGG)_n$ 6-60	60-200	Ataxia, tremor, Parkinsonism, dementia
Spinocerebellar ataxia 8 (SCA8)	$(CTG)_n$ 16-34	> 74	Ataxia, slurred speech, involuntary eye movements
Huntington disease-like 2 (HDL2)	$(CTG)_n$ 7-28	66-78	Chorea, dystonia, cognitive deficits, psychiatric problems (similar to HD)
SCA12	$(CAG)_n$ 7-45	55-78	Ataxia, seizures
Polyglutamine repeat diseases (CAG)	$(CAG)_n$ Varies per disease		Various

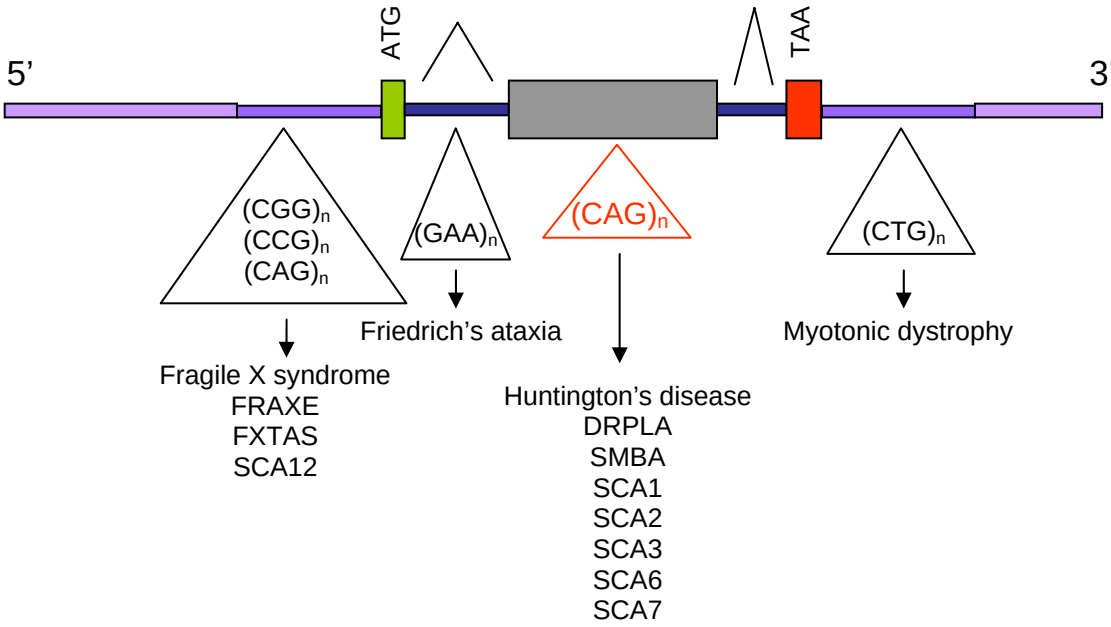

Figure 1.5: Gene location of trinucleotide expansions. Green represents the start codon (ATG) at the beginning of an exon (gray). Red is representative of a stop codon (TAA) signaling the end of the coding region. The purple areas represent untranslated regions, and the dark blue represents non-coding intron regions. Huntington's disease-like 2 (SCA 12) is not shown; however, the mutation occurs in a non-coding spliced exon of the junctophilin 3 gene.

Table 1.3: Polyglutamine neurodegenerative diseases.

Disease	Gene locus	CAG repeat length		Clinical features upon expansion
		Normal	Pathological	
Spinobulbar muscular atrophy (SBMA) – Kennedy's disease	Xq13-21	9-36	38-62	Motor weakness, swallowing, male breast enlargement, decreased fertility
Huntington's disease (HD)	4p16.3	6-34	36-121	Chorea, dystonia, cognitive deficits, psychiatric problems
Spinocerebellar ataxia 1 (SCA1)	6p23	6-44	39-82	Ataxia, slurred speech, spasms, cognitive impairments
SCA2	12q24.1	15-31	36-63	Ataxia, polyneuropathy, decreased reflexes, infancy variant with retinopathy
SCA3 – Machado-Joseph Disease (MJD)	14q32.1	12-41	62-84	Ataxia, Parkinsonism, spasms
SCA6	19p13	4-18	21-33	Ataxia, difficulty in articulating, involuntary eye movements, tremors
SCA7	3p12-21.1	4-35	37-306	Ataxia, blindness, infancy variant with cardiac failure
SCA17	6q27	25-42	47-63	Ataxia, cognitive decline, seizures, psychiatric problems
Dentatorubral-pallidoluysian atrophy (DRPLA)	12p13.31	6-36	49-84	Ataxia, seizures, choreoathetosis, dementia

For these expanded CAG repeat diseases, longer repeat expansions lead to earlier ages of onset and increased disease severity (Figure 1.6) [Gusella and MacDonald 2000]. In the remainder of this chapter, the polyGln diseases will be discussed with a particular emphasis on Huntington's disease, the proposed mechanisms of cell dystrophy, and the model systems that have been created in order to study these devastating diseases.

POLYGLUTAMINE DISEASE CHARACTERISTICS

There are many similarities and differences among the various polyglutamine diseases. This section will summarize some of the characteristics found among these diseases. For instance, all of the polyglutamine diseases, except spinobulbar muscular atrophy (SBMA), which is X-linked recessive [Belsham et al. 1992; Ferlini et al. 1995], are dominantly inherited [Wilmot 1998]. Also the diseases generally occur during mid-life and are progressive (see review by [Fischbeck 2001]), causing neuronal dysfunction and eventually neuronal death [Ross 1995; Taylor et al. 2002; Bates 2003]. The instabilities observed in these diseases occur in both germline and somatic cells (reviewed by [Bates 2002]). Especially in the case of HD, DRPLA, SCA1, and SCA3, somatic instabilities are generally higher in the central nervous system than in peripheral tissues [Telenius et al. 1994; Chong et al. 1995; Ueno et al. 1995; Lopes-Cendes et al. 1996; Tanaka et al. 1996; Hashida et al. 1997; Cancel et al. 1998]. As repeat length increases, the disease progresses more rapidly and onset appears earlier (see review by [Gusella and MacDonald 2000]).

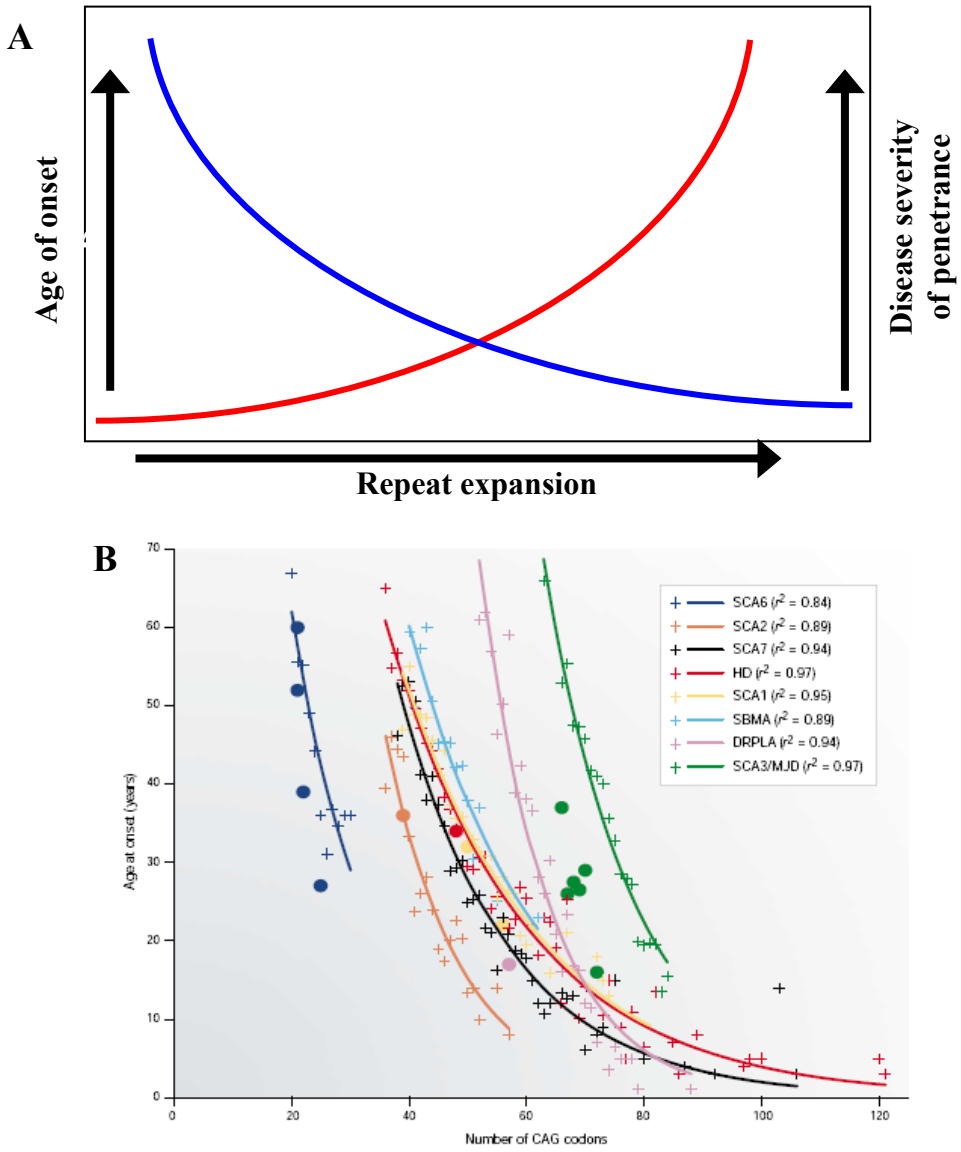

Figure 1.6: Observed inverse correlation between trinucleotide repeat expansion and age of onset. *(A)* The longer the glutamine repeat the more complete penetrance and earlier onset. *(B)* Data compiled from the literature (Figure and Legend from [Gusella and MacDonald 2000]) were used to calculate the mean age at onset (denoted by '+') associated with various CAG repeat lengths and the best-fit curve (denoted by a smooth line), using a simple exponential decay model for the relationship, in each of the polyglutamine disorders. The age of onset of homozygotes for the various disorders is also shown (filled circles), plotted according to the longer of their two expanded CAG repeats. (DRPLA, dentatorubropallidoluysian atrophy; HD, Huntington's disease; MJD, Machado-Joseph disease; SBMA, spinal and bulbar muscular atrophy; SCA, spinocerebellar ataxia.)

Interestingly, the proteins produced in each disease are expressed ubiquitously throughout the brain and other tissues; however, only a subset of neurons appear to be affected (Figure 1.7 for selective summary) [Young 1998; Bates 2002]. Some of the diseases share overlap of the affected regions; however, there are also differences in the areas attacked. Table 1.4 summarizes the proteins produced, the cells affected and the area(s) of the cell where detectable aggregates accumulate. Similar pathological thresholds are observed for the CAG repeat disorders (~35-40 Gln repeats), excluding SCA-6, which has a slightly lower threshold [Bates 2002]. Because of these very similar expansion-threshold lengths, a common pathogenic mechanism involving the polyGln-rich region has been suggested for these disorders [Cha and Dure 1994; Paulson and Fischbeck 1996].

Another major characteristic shared by the polyGln disorders is the formation of insoluble nuclear and/or cytoplasmic aggregates, which exhibit a fibrillar morphology [DiFiglia et al. 1997] and can be detected with antibodies to the disease protein [Davies et al. 1997; Scherzinger et al. 1997], ubiquitin, or polyGln (1C2). 1C2 is an antibody that was originally raised against TATA binding protein (TBP) and selectively recognizes polyGln stretches on Western blots [Trottier et al. 1995].

As mentioned in the preceding section, expansion of the polyglutamine sequence in the CAG trinucleotide diseases occurs in the coding region of the genes, resulting in the transcription and translation of the gene into the protein product, which then becomes misfolded and prone to aggregate. It is widely accepted that the mechanism by which the polyGln expansion causes diseases is by imparting a toxic “gain of function” (GOF)

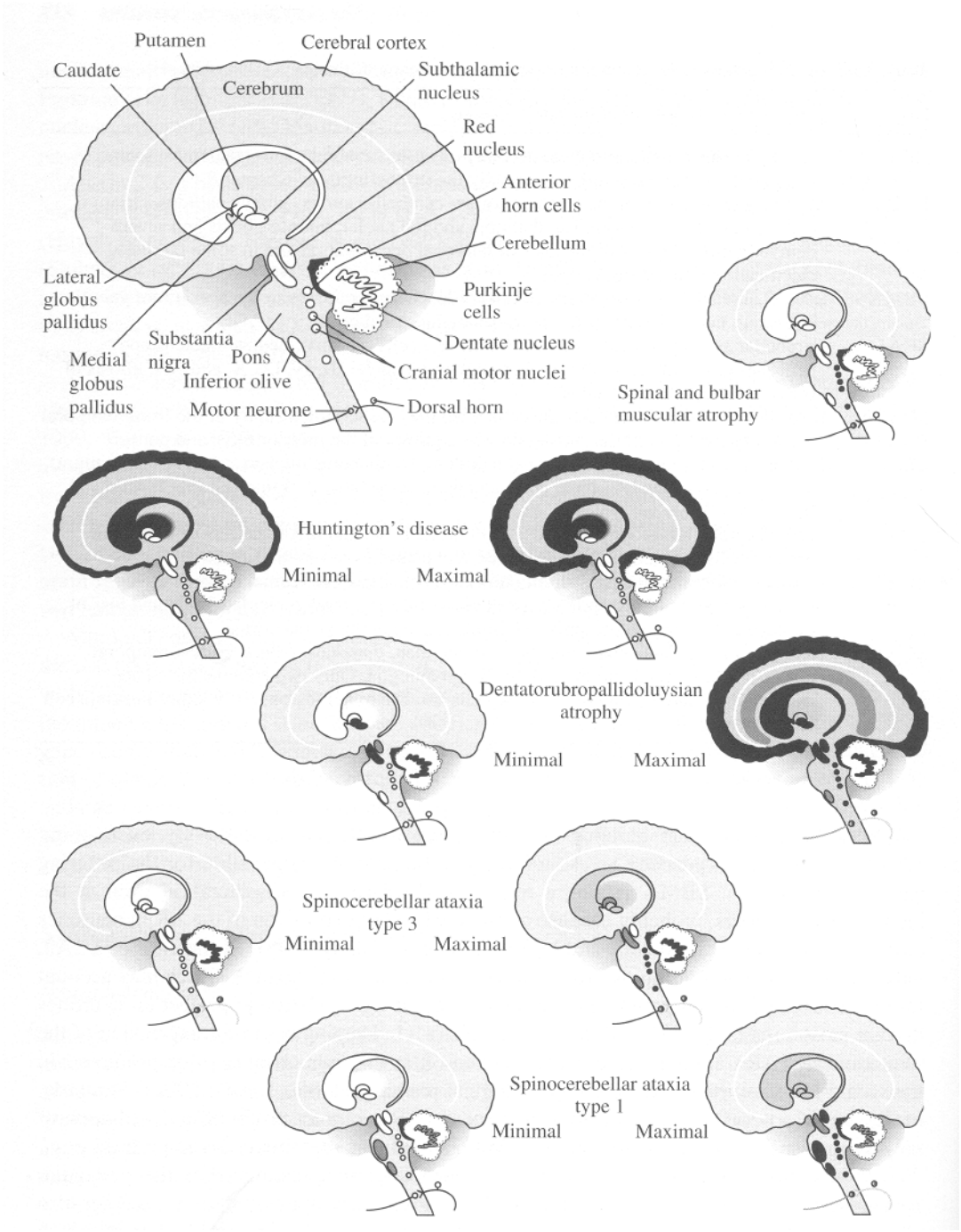

Figure 1.7: Depiction of the brain pathology in five of the polyGln diseases. Darker shaded areas represent severe pathology where the lighter shaded areas indicate varying degrees of intermediate pathology. (Image taken from [Bates 2002]).

Table 1.4: Polyglutamine localization.

Disease	Protein product	Expanded protein localization	Affected cells
SBMA	Androgen receptor (AR)	Nuclear / cytoplasmic	Anterior horn and bulbar neurons, dorsal root ganglia, brainstem
HD	Huntingtin (htt)	Nuclear / cytoplasmic	Striatum, cerebral cortex, caudate-putamen, globus pallidus, hippocampus, thalamus
SCA1	Ataxin-1 (At1)	Nuclear / cytoplasmic	Cerebellar Purkinje cells, dentate nucleus, inferior olive, brainstem
SCA2	Ataxin-2 (At2)	Cytoplasmic	Cerebellar Purkinje cells, brainstem, fronto-temporal lobes, substantia nigra, inferior olive and pons
SCA3 – MJD	Ataxin-3 (At3)	Nuclear / cytoplasmic	Cerebellar dentate neurons, basal ganglia, brainstem, spinal cord
SCA6	Calcium channel ($CACNAI_A$)	Cytoplasmic/ cell membrane	Cerebellar Purkinje cells, dentate nucleus, inferior olive, cerebellar granule cells
SCA7	Ataxin-7 (At7)	Nuclear / cytoplasmic	Cerebellum, brainstem, macula, visual cortex, inferior olive
SCA17	TATA box-binding protein (TBP)	Nuclear	Caudate nucleus, putamen, thalamus, frontal cortex, temporal cortex, Purkinje cells
DRPLA	Atrophin (drplap)	Nuclear / cytoplasmic	Cerebellum, cerebral cortex, basal ganglia, Luys body (subthalamic nucleus)

mutation to the affected protein [Wilmot 1998; Bates 2002] that increases with longer Gln repeats [Ross 1997; Klockgether and Evert 1998; Evert et al. 2000]. Evidence suggests that the gain of function is the ability of the protein to access a non-native state that is toxic to neurons. Supporting evidence for this discovery was presented by Ordway and colleagues who demonstrated that in an unrelated protein, *hprt* (hypoxanthine/guanine phosphoribosyltransferase), which exhibited an abnormal CAG expansion of 150 repeats, the polyGln tract was directly responsible for generating a similar late-onset, progressive, neurodegenerative disorder [Ordway et al. 1997]. This suggested that the polyGln tract was responsible for causing neuronal dysfunction and subsequent neurodegeneration and that the protein context played a role in defining other characteristics of the disease. Some groups interpret their data as indicating that toxicity is caused not by a gain of function but by the loss of normal protein function (LOF); this, however, is a much less widely-accepted theory [Zhuchenko et al. 1997; Cattaneo et al. 2001; Katsuno et al. 2004].

COMMON AMYLOID FEATURES

Polyglutamine proteins possess many of the same features as other amyloidogenic proteins (see Figure 1.8). Polyglutamine aggregates formed at 37°C have been shown to exhibit fibrillar morphology by EM that is comparable to an amyloid fibril [Scherzinger et al. 1997; Thakur and Wetzel 2002]. Earlier studies revealed huntingtin aggregates expressed in patient brains exhibited an apple green birefringence when stained with Congo red and examined using polarized light microscopy [Huang et al. 1998; McGowan et al. 2000], while other groups have found htt inclusions to be CR negative

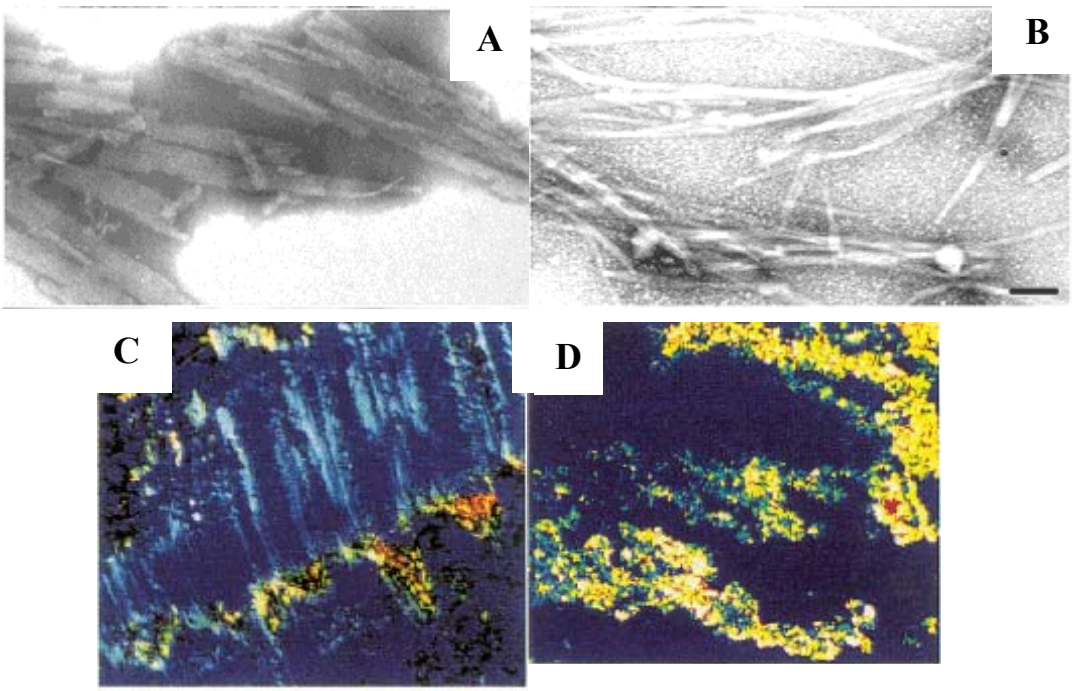

Figure 1.8: Common amyloid features exhibited by polyglutamine peptides/proteins. *(A) Electron micrographs of Q_{37} synthetic aggregates grown in PBS at 37 °C. (B) Aβ(1-40) fibrils grown in PBS at 37 °C.* A Hitachi 500 electron microscope was used to obtain images. Samples were adsorbed onto mica grids and stained with 0.05% potassium phosphor-tungstate (KPTA) solution. (Adapted from [Chen et al. 2002].) *(C) Congo red birefringence of isolated Huntington's disease frontal cortex. (D) Congo red birefringence of Alzheimer's disease frontal cortex.* C,D images were obtained via cross-polarizers and light microscopy. (Taken from [Huang et al. 1998]). Both types of images represent the fibrillar morphology and presence of cross β-sheets.

[Karpuj et al. 1999]. However, other data has shown that many aggregates generated from a synthetic polyglutamine peptide, while efficient in binding Congo red, are much less efficient in displaying the green birefringence seen in other amyloid fibrils [Chen, Berthelier et al. 2002]. Polyglutamine aggregates (synthetic, fusion, or natural) also exhibit a ThT response [Chen et al. 2002; Ellisdon et al. 2006]. Another commonality between aggregates of simple polyGln peptides and other amyloid fibril systems is the presence of a lag phase during fibril growth (see above) (Figure 1.9) that can be shortened or eliminated by the addition of pre-formed fibrillar seed [Chen et al. 2002; Thakur and Wetzel 2002; Bhattacharyya et al. 2005]. Amyloid-like character is also suggested by the microstructure EMs of neuronal inclusions [DiFiglia, Sapp et al. 1997] and the abilities of aggregates in brain tissue and transformed cells to recruit monomeric polyglutamine molecules [Osmand et al. 2006]. Finally, the most important similarity is that polyglutamine aggregates also exhibit a cross-β structure, which is the hallmark of all amyloid proteins (Figure 1.10) [Perutz et al. 1994; Thakur and Wetzel 2002; Sharma et al. 2005].

HUNTINGTON'S DISEASE

Huntington's disease (HD) is a progressive autosomal dominant neurodegenerative disorder that was first characterized in the late 1800s by Dr. George Huntington and is the most common of the nine CAG repeat diseases. Dr. Huntington published the seminal manuscript entitled *On chorea* [Huntington 1872] in 1872 that

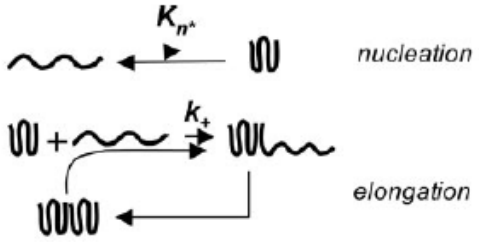

Figure 1.9: Polyglutamine nucleation-dependent polymerization by monomer addition. ([Bhattacharyya et al. 2005]) An unfavorable folding event (nucleation) occurs with monomeric polyGln. Elongation occurs after an initial binding step to an extended conformational monomer. Subsequent monomer additions to the altered conformation result in elongation.

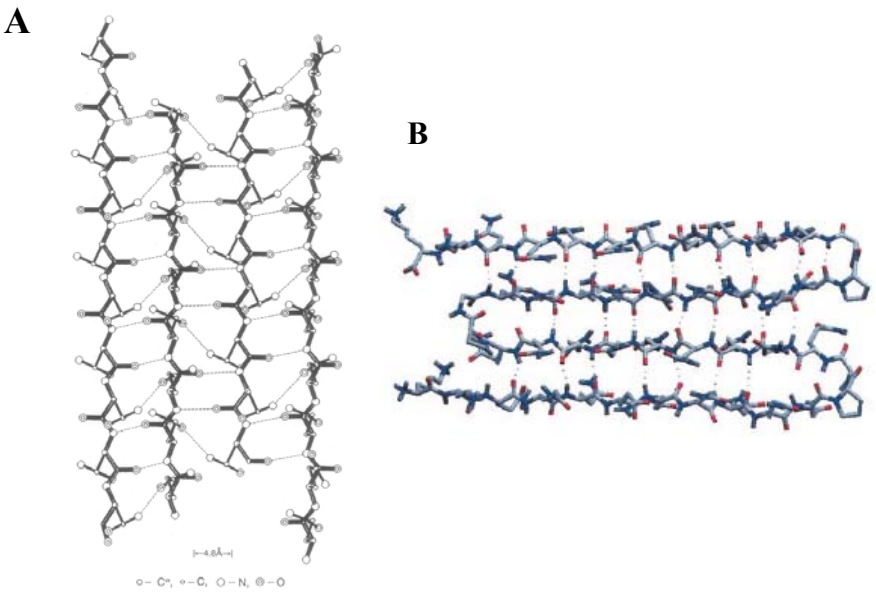

Figure 1.10: Proposed structural models for polyglutamine proteins are comparable to amyloid proteins. *(A) Computer-generated structure of two paired anti-parallel β-strands of polyGln linked together by main chain and side chain hydrogen bonds.* (Taken from [Perutz, Johnson et al. 1994]). *(B) β-sheet β-turn model of expanded polyGln.* Light blue – carbon, dark blue – nitrogen, red – oxygen. (Taken from [Ross et al. 2003]).

described the clinical manifestation of an illness ("hereditary chorea") he observed among three families residing in New York. Patients with the illness were described as having involuntary, jerky movements (chorea) and significantly retarded voluntary movements (bradykinesia), combined with cognitive impairment, and which had adult onset and an advancing development that was eventually fatal. He also noted the hereditary nature of the disease. Among people of European descent, the prevalence of the disease is 3-4 per 100,000 people, and it's estimated that another 15-30 out of 100,000 of the Caucasian population are at risk of developing the disease [Harper 2002].

In 1983, the HD gene (interesting transcript, *IT15*) was mapped near the vicinity of a DNA marker, *D4S10*, located on chromosome 4p16.3 [Gusella et al. 1983]. The gene contains 67 exons and spans ~180 kb (Figure 1.11). After 10 years of research, the genetic defect responsible for HD was found to be localized in the first exon of the *IT15* gene, which encodes a 350-kDa protein, huntingtin [Group 1993]. The disease-causing mutation is the expansion of an unstable, polymorphic CAG trinucleotide repeat within exon 1 of the HD gene. This CAG repeat (found in the N-terminus) translates into a polyGln tract that is expressed in the huntingtin (htt) protein. Located just downstream of the polyGln region there is also a proline-rich stretch containing approximately 21 prolines. The sequence of htt exon 1 is MATLEKLMKAFESLKSF$\mathbf{(Q)_n}$ $\mathbf{(P)_{11}}$Q**LPQPPPQ** A**QP**LL**PQPQ**$\mathbf{(P)_{10}}$G**P**A VAEE**P**LHR**P**KK. As discussed above for expanded CAG repeat diseases in general, polyGln repeat length is directly correlated to disease severity [Gusella and MacDonald 2000]. People who have a repeat length of $<Q_{35}$ do not develop the disease; whereas, people who have $>Q_{40}$ will invariably develop

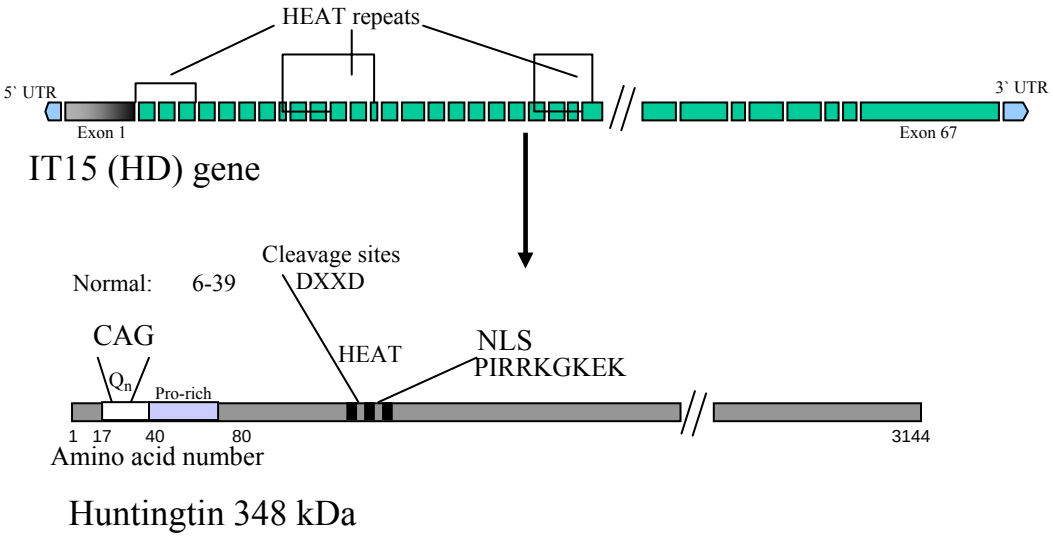

Figure 1.11: Structure of HD gene and translated protein.

HD (See Figure 1.6 and 1.12). There is an ambiguous CAG repeat length, 36-40, where some people develop the disease and others do not [Myers 1998]. As with the other polyGln diseases, there is an inverse correlation between repeat length and age of onset, where the longer the CAG repeat, the earlier the age of onset [Duyao et al. 1993] (see Figure 1.6).

CHARACTERISTICS OF NORMAL AND EXPANDED HUNTINGTIN

Huntingtin is a highly conserved protein that is expressed throughout the body and which has no functional homology to any known protein. However, it has been shown that wildtype htt plays important roles in embryonic development including gastrulation [Duyao et al. 1995; Nasir et al. 1995; Zeitlin et al. 1995; Dragatsis et al. 1998], neurogenesis [White et al. 1997; Reiner et al. 2003], and formation of extraneuronal tissue [Dragatsis et al. 1998]. In recent years, there has been growing evidence that normal htt is also involved in RNA biogenesis [Faber et al. 1998; Boutell et al. 1999; Passani et al. 2000; Takagaki and Manley 2000; Strehlow et al. 2007], membrane association and vesicle/protein trafficking [Li et al. 1995; Kalchman et al. 1997; Wanker et al. 1997; Truant et al. 2006; Truant et al. 2007], and iron homeostasis [Hilditch-Maguire et al. 2000].

Even though htt is ubiquitously expressed, the only known pathological changes that occur in HD are specific to the brain and are characterized by selective neuronal degeneration and loss [Ross 1995; Huq 1998; Bates 2002]. The most striking atrophy occurs in the caudate nucleus and putamen, which together form the neostriatum within the basal ganglia. A secondary effect due to caudate atrophy is an enlargement in the

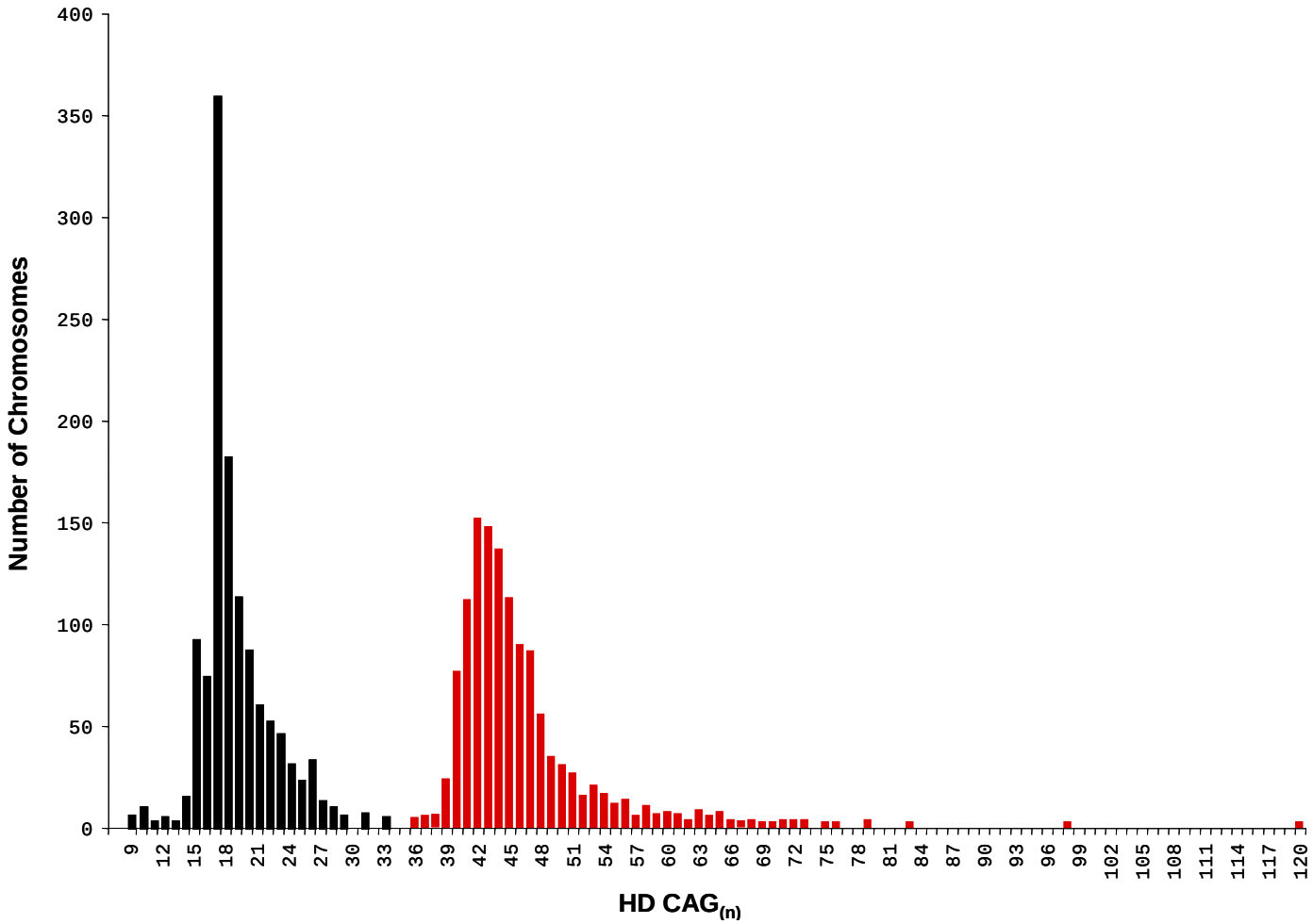

Figure 1.12: Distribution of HD CAG repeat lengths on normal and HD chromosomes. Histogram plot of HD CAG repeat sizes found on the1212 normal chromosomes (black bars) and 1212 HD chromosomes (red bars), from the same individuals, largely of western European ancestry [MacDonald personal communication].

lateral ventricles. Other than these major affected areas, there is 10-20% overall deterioration of the brain. The reduction occurs in the cerebral hemispheres, the cerebellum, the brainstem, the diencephalons, and the spinal cord [Forno 1979].

Loss of neurons in both the putamen and caudate show a gradient correlating to disease progression [Bruyn 1979; Roos et al. 1985; Vonsattel et al. 1985; Myers et al. 1988; Heinsen et al. 1994]. To determine the severity of neurodegeneration, a grading scale of 0 to 4 (mild to severe), based on microscopic and gross deterioration of the basal ganglion, was created so that a patient could be graded semiquantitatively on the severity of the disease (Figure 1.13) [Vonsattel et al. 1985; Myers et al. 1988]. Also, there is a severe loss in the medium-sized spiny neurons (MSNs) but a preservation of the large striatal neurons [Cicchetti et al. 2000]. MSNs are inhibitory projection neurons that encompass more than 95% of the neuronal cells in the striatum and use γ-aminobutyric acid (GABA) as their neurotransmitter. Other than the basal ganglion, the next most severely affected region is the cerebral cortex, with the greatest loss in layer VI and significant loss in layers III and V [de la Monte et al. 1988].

At the subcellular level, normal length huntingtin is most often localized in the cytoplasm as a soluble protein; however, aggregates arising from the expanded form are often found in the nucleus as well as the cytoplasm. As mentioned previously, the expanded protein accumulates into insoluble, fibrillar aggregates [Davies et al. 1997; Scherzinger et al. 1997] that primarily contain N-terminal htt fragments that leads to pathology [DiFiglia et al. 1997; Sapp et al. 1997; Gutekunst et al. 1999]. A hallmark of HD is the appearance of protein aggregates as neuronal intranuclear inclusions (NII)

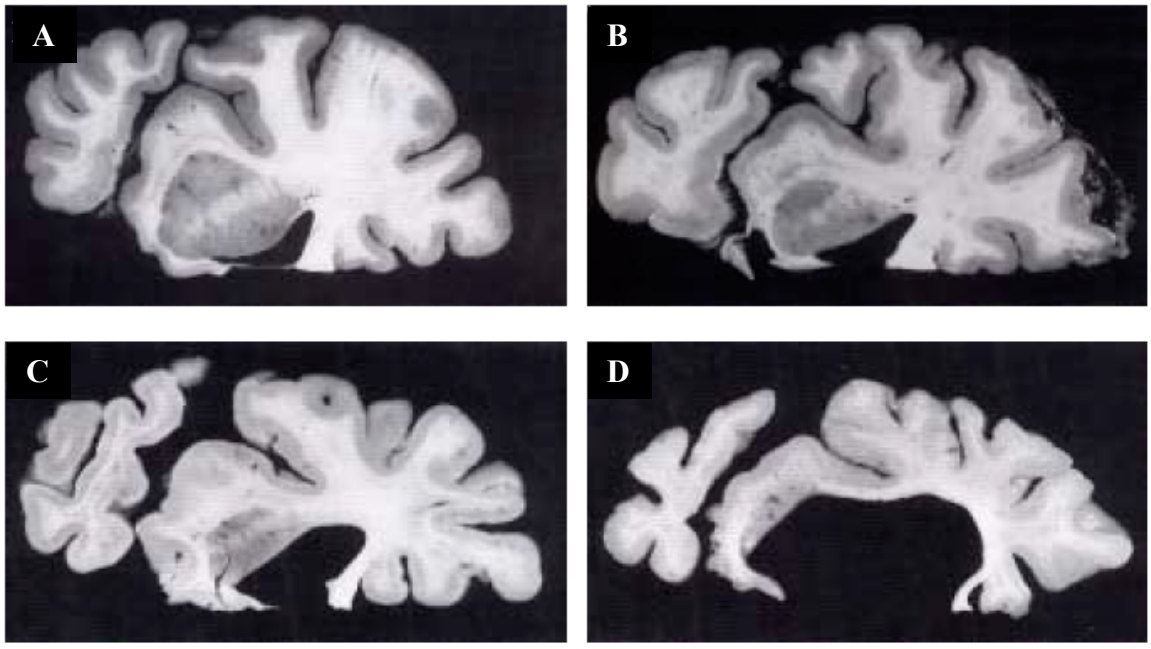

Figure 1.13: Huntingtin accumulation causes neurodegeneration of the brain. *(A) Normal brain section of the caudate nucleus, nucleus accumbens, and putamen.* (B-D) Progressive neuronal loss of HD patients' brain sections as graded via the Vonsattel method. *(B) early HD grade 2, (C) mid HD grade 3, (D) late HD grade 4.* (Images taken from [Myers 1998].)

[Davies et al. 1997; DiFiglia et al. 1997; Gutekunst et al. 1999; Sieradzan et al. 1999; Wheeler et al. 2000]. NII have been found in the MSNs of the striatum but are most prevalent in the large striatal neuron, which do not undergo neurodegeneration [Kuemmerle et al. 1999]. Moreover, NII are rarely observed in neurons of the globus pallidus and cerebellum [Gutekunst et al. 1999]. In general, NIIs range from 3 – 5μm in diameter and generally adopt one of two shapes: the majority are spherical (55%); while the remainder are elliptical (ovoid) [DiFiglia et al. 1997; Becher et al. 1998; Gutekunst et al. 1999].

Other aggregated states of huntingtin, besides NII, have been described. Neuropil aggregates (NA) localize in the white matter outside of discernable cell bodies and are assumed to be located in the axons, dendrites, and synapses. They tend to be round to oval in shape [DiFiglia et al. 1997; Gutekunst et al. 1999] and are typically larger than NII. Both NII and NA have been shown to stain positively for ubiquitin (an indication that the protein has been targeted for degradation [Alves-Rodrigues et al. 1998; Sieradzan et al. 1999]) and CREB binding protein (CBP) (which also contains a polyGln tract and therefore indicates that huntingtin inclusions can sequester other polyGln-containing proteins) [DiFiglia et al. 1997; Preisinger et al. 1999; Nucifora et al. 2001]. Another class of aggregates, often seen in conjunction with NII, is perikaryal aggregates. This type of aggregate is generally smaller (0.3 – 1.5μm) than the NII and exhibit a round to oval appearance [Gutekunst 2002]. However, these structures are found in a perinuclear location [Huang et al. 1998; Heiser et al. 2000]. Each of these types of aggregates have been shown to exihibit Congo red blue-green birefringence, again suggestive of an

amyloid-like structure [McGowan et al. 2000]. *In vitro* data have shown that it is possible to produce both detergent-soluble [Muchowski et al. 2000] and detergent-resistant htt aggregates [Cooper et al. 1998; Kazantsev et al. 1999; Chen et al. 2001], with the latter representing end-stage aggregates.

It has long been recognized that the aggregation and deposition of misfolded proteins are the pathological hallmarks for many neurodegenerative diseases [Ross and Poirier 2005]. However, the presence of these inclusion bodies correlate poorly with other neurodegenerative characteristics [Terry et al. 1991; Tompkins and Hill 1997], especially in HD [Gutekunst, Li et al. 1999], introducing questions about the role of aggregates in the disease process. It has been hypothesized that inclusion bodies may represent an end stage structure in a multi-step aggregation process [Ross and Poirier 2005] and that early events, including the formation of misfolded monomers [Weissmann 2005; Nagai et al. 2007] or soluble oligomeric/protofibrillar intermediates [Poirier et al. 2002; Bucciantini et al. 2004; Katsuno et al. 2004; Wacker et al. 2004; Mukai et al. 2005], which directly arise from the presence of an expanded polyGln sequence, may be responsible for cellular toxicity. However, there is no consensus on what the toxic species is, whether the intermediates are “on-pathway” or “off-pathway”, or the precise role of aggregation in the disease mechanism.

1.3 Disease Mechanisms in Huntington's Disease:

OVERVIEW

Despite the fact that the genetic abnormality is well characterized, the underlying mechanism of neurodegeneration in Huntington's disease has not yet been unequivocally elucidated [Ross et al. 1999; Ross 2002; Ross 2004; Bett 2006]. A schematic representation of the proposed pathogenic mechanisms is shown in Figure 1.14. The widely accepted view is that the HD mutation causes a toxic gain of function, where the aberrant protein inherits additional properties that render it cytotoxic [Ross 1997; Wilmot 1998; Bates 2002]. Alternatively, there may be a loss of normal htt functionality that results in neurodegeneration [Cattaneo et al. 2001]. In support of a loss of function mechanism, huntingtin gene expression must be required for normal development, since huntingtin knock-out mice die early in embryogenesis [Duyao et al. 1995; Jones 2002]. At the same time, several lines of evidence argue against loss-of-function being the major disease mechanism. Patients homozygous for the HD mutation are not more severely affected than patients who are heterozygous for the mutation [Wexler et al. 1987; Myers et al. 1989], and a patient with only one viable copy of the normal polyGln length htt gene did not develop HD [Ambrose et al. 1994]. Several gain of function hypotheses are described in greater detail in this section.

Compounding the difficulty in identifying the toxic species is the critical issue of establishing the nature of the cellular events that are associated with HD symptoms. Should we be looking for overt cell death, or for more subtle sub-lethal dystrophic events

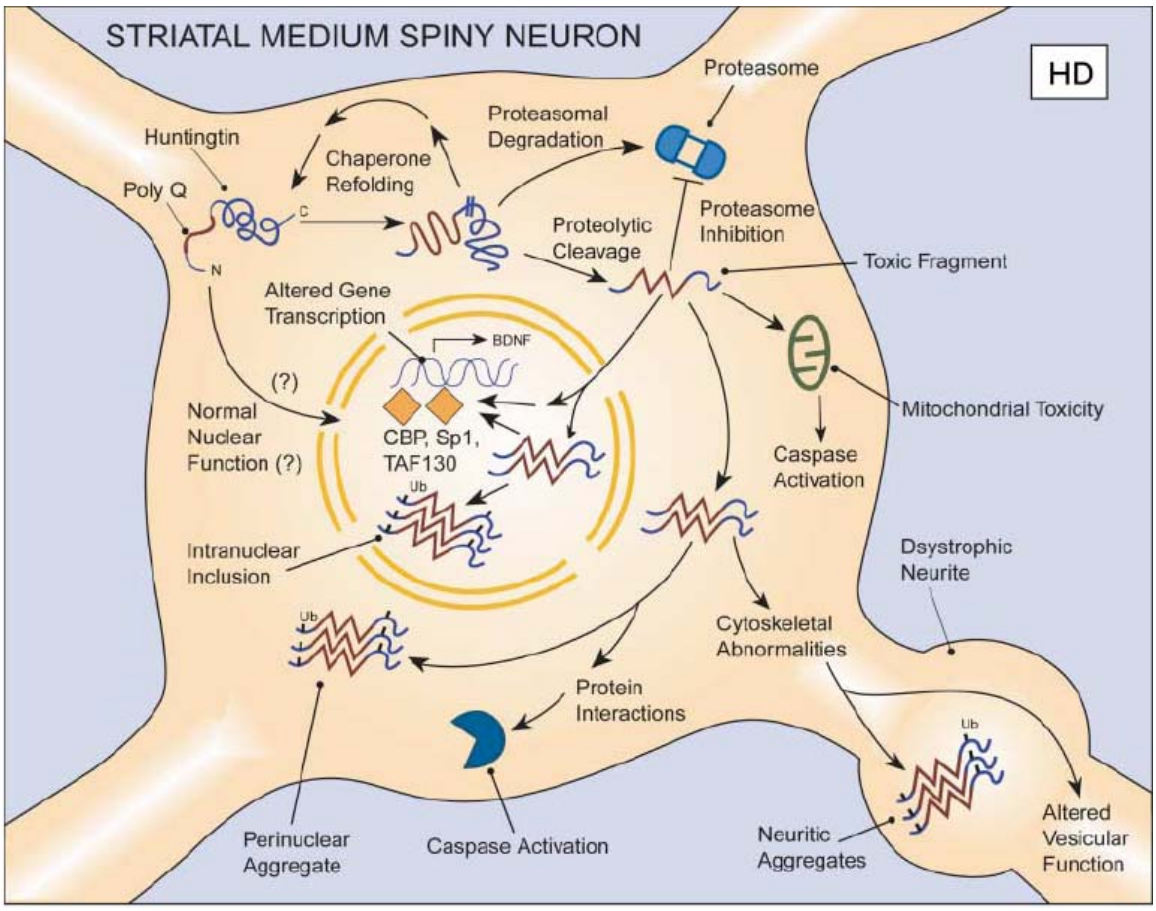

Figure 1.14: Model representing modes of HD cellular pathogenesis. (Taken from [Ross 2004]).

that are more difficult to observe and quantify? The brain atrophy evident at autopsy is a clear indication that cell death occurs during the development of HD, but does this account for early symptoms or is it only an end-stage event? Is the loss of cell mass really due to cell death or to cell shrinkage? Are there earlier events in HD progression, such as synaptic loss and neurite retraction that are responsible for disruptions in neuronal circuitry associated with abnormal motor neuron function? Clearly, identifying and validating the molecular species responsible for HD requires a correct perspective on the abnormal biology behind the disease symptoms and progression, and the lack of certainty on these central questions contributes to our inability to define the key molecular players.

EXPANDED HUNTINGTIN AGGREGATE FORMATION

Many researchers believe that some aspect of polyGln protein misfolding and aggregation is an early, necessary event in HD pathogenesis. It has been shown that directing the aggregate to the nucleus by introducing a nuclear localization signal (NLS) causes cellular toxicity [Cooper et al. 1998; Hackam et al. 1999; Yang et al. 2002]. Furthermore, numerous experiments have demonstrated that a reduction in aggregate burden can rescue neuronal damage [Yamamoto et al. 2000; Kazantsev et al. 2002]. In contrast, several lines of evidence suggest that protein aggregation is not directly linked to disease pathogenesis, in that aggregate burden does not always correlate well with cell death [Cummings and Zoghbi 2000; Tobin and Signer 2000]. It is possible, however, that good correlations are not always observed because the genuinely toxic aggregate species are not observable or quantifiable. Furthermore, it is possible that htt inclusions

offer protection against neurotoxic effects by sequestering smaller, potentially more toxic oligomers [Kopito 2000]. A number of mechanisms of aggregate toxicity have been postulated, and these will be reviewed below. The strong indications of a central, early role for htt aggregates in the disease mechanism argues for a closer look at the nature of the aggregated species in the cell. In addition, regardless of their role in pathogenesis, aggregates are a hallmark of HD and deserve attention on that basis alone.

TOXIC FRAGMENT HYPOTHESIS

One theory regarding the pathogenic mechanism of HD is the "toxic fragment hypothesis", which suggests that following proteolytic processing, full-length mutant htt generates N-terminal fragments that accumulate and aggregate in the nucleus leading to toxicity [DiFiglia, Sapp et al. 1997; Martindale et al. 1998; Saudou et al. 1998]. Full-length htt contains several proteolytic cleavage sites within the first five exons (Figure 1.15) [Li and Li 2004], which are sensitive to caspase-3, calpain, and aspartic endopeptidase cleavage. Caspases are enzymes that play essential roles in apoptosis and inflammation. Calpains are a group of calcium-dependent cysteine proteases. Aspartic endopeptidases are another class of intracellular proteases. Recently, it was shown that mutation of two calpain cleavage sites in mutant htt renders the protein less susceptible to proteolytic cleavage and reduces cell toxicity in an *in vitro* cell culture model [Gafni et al. 2004]. N-terminal mutant htt fragments have been shown to be more toxic in model systems than their full-length protein counterpart [Hackam et al. 1998; Lunkes and Mandel 1998; Martindale et al. 1998; Lunkes et al. 2002]. It has been proposed that the generation of such htt fragments favors the formation and deposition of insoluble

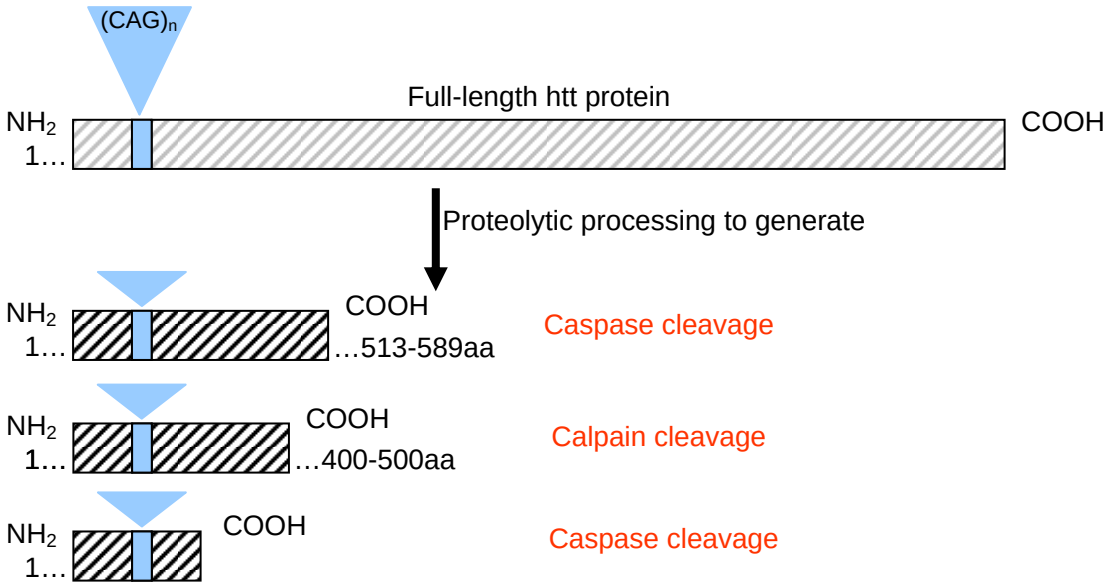

Figure 1.15: Proteolytic processing of full-length mutant huntingtin generates polyGln expanded N-terminal htt fragments.

aggregates in the nucleus [Lunkes and Mandel 1998; Martindale et al. 1998; Hackam et al. 1999; Li et al. 2000]. This hypothesis, as far as it goes, accounts for the localization of aggregates in the nucleus, but does not offer any clues to why aggregates might be toxic. The remaining portions of this section deal with this issue.

TRANSCRIPTIONAL DYSREGULATION / RECRUITMENT-SEQUESTRATION

It is known that expanded htt aggregates can recruit proteins, such as certain transcription factors and co-factors, in a polyGln-mediated manner (See Table 1.5) [Davies, Turmaine et al. 1997; DiFiglia, Sapp et al. 1997; Scherzinger, Lurz et al. 1997; Jiang et al. 2003], thus sequestering them and compromising their ability to function normally. This recruitment and sequestration provides an attractive mechanism for cellular dysfunction. PolyGln-specific sequestration is likely mediated by the ability of amyloid-like polyGln aggregates to highly selectively elongate via recruitment of other polyGln sequences into the growing aggregate [Chen et al. 2001]. This model is the basis of the recruitment-sequestration hypothesis. In the past decade, it has also become increasingly clear that several transcriptional pathways are altered in mouse models of HD as well as patients with Huntington's disease [Cha 2000; Luthi-Carter et al. 2000; Luthi-Carter et al. 2002], and recruitment of transcription factors is one mechanism by which this might occur.

Two well characterized examples where polyGln-containing transcription factors have been shown to be sequestered by htt aggregates will be discussed. In the first example, TATA binding protein (TBP), an essential polyGln containing transcription

Table 1.5: Huntingtin-interacting proteins.

Protein	Possible cellular role	Reference
TBP, CBP, and p300/CBP-associated	Transcription factors. Co-localization with NIIs	[Huang et al. 1998; Boutell et al. 1999; Kazantsev et al. 1999; Steffan et al. 2000; Nucifora et al. 2001]
P53	Transcription factor. Repressed by mutant N-terminal htt	[Steffan et al. 2000]
Nuclear receptor co-repressor and mSin3A	Transcriptional repressor complex. Cellular localization altered in HD brain	[Boutell et al. 1999; Jones 1999]
SP1 and $TAF_{II}130$	Transcriptional activator and co-activator	[Dunah et al. 2002]
BDNF	Neurotrophic factor required for striatal neuronal survival	[Zuccato et al. 2001]
HAP1	Cytoskeletal, microtubule, and vesicle functions	[Li et al. 1995]
HIP1	Cytoskeletal, microtubule, and vesicle functions	[Kalchman et al. 1997; Wanker et al. 1997; Singaraja et al. 2002]
α-Adaptin	Cytoskeletal, microtubule, and vesicle functions	[Faber et al. 1998; Gusella and MacDonald 1998]
Caspase-3	Apoptotic pathway	[Goldberg et al. 1996]
HIP2	Ubiquitin-conjugating enzyme	[Kalchman et al. 1996]
GAPDH	Glycolytic enzyme	[Burke et al. 1996]
Cystathionine β synthase	Amino acid metabolism	[Boutell et al. 1999; Jones 1999]
Calmodulin	Intracellular calcium binding and sensing	[Bao et al. 1996]
HYP A, B, and C	Non-receptor signaling, protein degradation, and pre-mRNA splicing. Interaction enhanced by lengthening of polyGln tract	[Faber et al. 1998; Passani et al. 2000]

factor involved in the separation of double stranded DNA, was found to interact with mutant N-terminal htt in a polyGln-dependent manner and was recruited into the polyglutamine aggregates [Schaffar et al. 2004]. *In vivo*, TBP has also been shown to be present in HD inclusions [Huang et al. 1998].

Secondly, cAMP response element (CRE)-regulated genes have been implicated in HD pathogenesis [Wyttenbach et al. 2001; Sugars et al. 2004]. The cAMP response element-binding protein (CREB) binds the CRE promoter, and upon phosphorylation, recruits the polyGln-containing co-activator CBP. This is an essential process in genetic transcription. It has been shown that CBP can be recruited into polyglutamine aggregates in multiple model systems, as well as in HD patients [Kazantsev et al. 1999; Steffan et al. 2000; Nucifora et al. 2001]. Therefore it is easy to imagine how aberrant interactions with such vital transcription factors can lead to cellular dysfunction. For example, it was demonstrated that mutant N-terminal htt directly interacts with and inhibits the acetyltransferase activity (responsible for histone acetylation) of CBP and p300/CBP-associated factor. Furthermore, the reduction can be reversed by treatment with histone deacetylase (HDAC) inhibitors [Steffan et al. 2001; Bodai et al. 2003]. In an elegant demonstration of the important role of CBP sequestration in cell death, the Ross group showed that recruitment of endogenous CBP into exon1 aggregates killed cells, but that over-expression of a CBP molecule lacking the polyGln stretch protects cells from this recruitment, presumably by being impervious to recruitment and by providing the functions of the recruited endogenous CBP [Nucifora et al. 2001].

Another transcriptional pathway that has been shown to be dysfunctional in HD involves the interaction of normal htt and repressor element 1 transcription factor–neuron-restrictive silencer factor (REST-NRSF) [Boutell et al. 1999; Holbert et al. 2001; Zuccato et al. 2001; Dunah et al. 2002], which is a transcriptional repressor responsible for binding neuron-restrictive silencer elements (NRSEs) in the nucleus. This pathway is implicated in the transcription of neuroprotective proteins such as brain-derived neurotropic factor (BDNF) [Zuccato, Ciammola et al. 2001]. When htt becomes expanded, it fails to bind properly, resulting in the accumulation of REST-NRSF in the nucleus, and the transcriptional repression of genes regulated by NRSEs [Zuccato et al. 2003]. This further supports the hypothesis that mutant htt can interfere and dysregulate normal transcriptional processes leading to pathology and ultimately toxicity.

The recruitment-sequestration mechanism is a favored explanation to describe the interference of mutant htt in various transcriptional processes, where the expanded protein is thought to play a role in recruiting vital proteins from their normal locations and depositing them either in htt inclusions or other abnormal cellular locations thereby rendering them unable to perform their normal functions. It is easy to imagine how these interactions can contribute to cellular dysfunction.

TOXICITY DUE TO COMPROMISING PROTEIN QUALITY CONTROL

Chaperones

The dominating presence of htt inclusion bodies throughout brains of various HD model systems suggests that the aggregated protein somehow escapes the many quality

control systems within a cell. The first of those mechanisms is chaperone proteins. Chaperone proteins are known to assist proteins in folding to their native conformations, help to refold abnormally folded proteins, and to liberate proteins from an aggregated protein in both normal and stress conditions [Hartl 1996]. Many molecular chaperones are also heat shock proteins (Hsps), which are expressed in response to an environmental stress [Lodish 2004]. Two major classes of molecular chaperones are Hsp70 and Hsp40, which jointly act in an ATP-dependent manner to properly fold misfolded proteins [Bett 2006].

Chaperone proteins are often found localized within polyGln aggregates in HD transgenic mice [Jana et al. 2000; Hay et al. 2004] as well as brains of patients with polyGln diseases [Alves-Rodrigues et al. 1998; Cummings et al. 1998; Chai et al. 1999; Schmidt et al. 2002]. These findings indicated that aggregated polyGln proteins were recognized as misfolded, and therefore, much attention was given to understanding the roles of molecular chaperones in the disease process. The two most studied chaperones in HD are Hsp70 and Hsp40. Several studies have been performed in which these two molecular chaperones were overexpressed [Cummings et al. 1998; Warrick et al. 1999; Chan et al. 2000; Jana et al. 2000; Kobayashi et al. 2000; Sittler et al. 2001; Zhou et al. 2001]. The results indicate that the overexpression of the Hsp70 and Hsp40 combination in cell cultures profoundly inhibited polyGln aggregation and that this correlated with a decrease in cellular toxicity [Cummings et al. 1998; Jana et al. 2000; Kobayashi et al. 2000; Sittler et al. 2001; Zhou et al. 2001]. It was also shown that overexpression of

Hsp70 in *Drosophila* suppressed neurodegeneration [Warrick et al. 1999], and the effect was more dramatic when both Hsp70 and Hsp40 were overexpressed [Chai et al. 2001].

Another interesting observation was that Hsp40 and Hsp70, when expressed in cell-free and yeast systems, altered the biochemical properties of mutant polyGln proteins, rendering the aggregates more soluble than previously described as well as delayed the formation of ordered-amyloid fibrils [Muchowski, Schaffar et al. 2000]. Furthermore, addition of the chaperones to *in vitro* polyGln aggregation reaction was only effective when they were added during the lag phase, suggesting that chaperones were most active on earlier forming species rather than the inclusions themselves [Muchowski et al. 2000; Wacker et al. 2004]. Yet further data suggesting the importance of molecular chaperones in the disease mechanism was provided by the Hartl group in 2004. They showed that *in vitro* the Hsp70/Hsp40 combination was effective in inhibiting the negative interactions of expanded htt and TBP [Schaffar et al. 2004]. With the substantial data presented, one can see the importance of molecular chaperones in HD.

Ubiquitin-Proteasome System

The ubiquitin-proteasome system (UPS) is responsible for regulating protein turnover and is vital for many cellular processes, including differentiation, antigen presentation, cell survival, cell cycle control, as well as the elimination of misfolded or damaged proteins [Ciechanover 1994]. The proteasome is barrel-shaped multiprotein complex that is responsible for the breakdown and clearance of short-lived nuclear and cytosolic proteins as well as ubiquitin-tagged misfolded proteins [Ciechanover 2006]. Degradation by the UPS involves many successive steps. First, the misfolded proteins are

tagged for clearance by the covalent attachment of a polyubiquitin chain. This conjugation is ATP-dependent and typically involves three enzymes: ubiquitin-activating enzyme (E1), ubiquitin-conjugating enzyme (E2), and ubiquitin-protein ligase (E3). Together these enzymes compose the ubiquitin ligase system [Hershko and Ciechanover 1998; Taylor et al. 2002]. With the linkage of four or more ubiquitin molecules to the substrate, a recognition signal is generated that allows the substrates to be shuttled to the proteasome, via escort and chaperone proteins, where they are degraded [Hershko and Ciechanover 1992; Jentsch 1992; Richly et al. 2005; Weihl et al. 2006].

HD inclusion bodies have been shown to be ubiquitinated, suggesting that the UPS has targeted the aggregated proteins for degradation [Alves-Rodrigues et al. 1998; Cummings et al. 1998; Chai et al. 1999; Sieradzan et al. 1999; Waelter et al. 2001]. Both Hsp40 and Hsp70 chaperones have been shown to be involved in the clearance of misfolded proteins via the UPS [Bercovich et al. 1997]. However, once the polyGln-containing proteins have appreciably aggregated, they appear to be resistant to degradation by the UPS [Cummings et al. 1999; Verhoef et al. 2002]. It has been suggested that impairment may be a direct result of the misfolded polyGln proteins getting 'trapped' within the proteasome [Jana et al. 2001; Holmberg et al. 2004] or the inability of the proteasome to cleave between successive Gln residues [Goellner and Rechsteiner 2003; Holmberg et al. 2004; Venkatraman et al. 2004], therefore limiting its normal activity. However, data have shown that impairment of the proteasome can occur in the absence of visible aggregates, suggesting other factors, such as the presence soluble, potentially toxic species, also contribute to this impairment [Bennett et al. 2005].

Other supporting evidence for the impairment of the UPS by polyGln aggregates was provided by the Kopito lab, in which they used two non-related aggregating proteins (Q103-GFP and CFTR-GFP) [Bence et al. 2001]. In both instances, they utilized a fluorescence-based measurement for UPS activity, where higher fluorescence intensities indicated a more severe disruption of UPS activity. In each case, protein aggregation led to the accumulation of intracellular ubiquitin and, thus, cell cycle arrest. This impairment yielded an increase in aggregate production, which was suggested, may result in the increase of the ubiquitin conjugates [Mayer et al. 1989] and other UPS substrates that are aberrantly expressed in diseased neurons [Raina et al. 2000]. Therefore, as more protein accumulated, the UPS became more impaired.

Autophagy-Lysosome Pathway

Another commonly proposed mechanism by which aggregate-prone proteins are removed is through the autophagy-lysosome pathway, which is induced by a stress response. Autophagy is a process that involves bulk degradation of the cell's own components through encapsulation and enzymatic processing. There are three primary forms of autophagy: macroautophagy, microautophagy, and chaperone-mediated autophagy. Macroautophagy, typically referred to as autophagy, is the most common form and occurs after an induction signal (often stress) when a flat membrane cistern engulfs a portion of the cytoplasm, forming a double membrane vacuole (autophagosome) [Williams et al. 2006]. After vacuole formation, the autophagosome fuses with a digestive lysosome, which is responsible for the breakdown. Ultimately, the breakdown products are returned to the cytoplasm [Klionsky and Ohsumi 1999;

Stromhaug and Klionsky 2001; Mizushima 2004]. Microautophagy, which has been characterized the least, involves the invagination of the lysosomal membrane to sequester portion of the cytoplasm for degradation [Kim and Klionsky 2000]. Chaperone-mediated autophagy, in contrast to the other two forms, is more selective and involves the direct translocation of cytosolic proteins containing a specific pentapeptide sequence motif to the lysosome [Massey et al. 2004].

Because it was demonstrated that aggregated htt is inefficiently degraded by the UPS [Verhoef et al. 2002], it was proposed that the autophagy-lysosome pathway may be responsible for the clearance of aggregated polyGln proteins [Qin et al. 2003; Ravikumar et al. 2003; Webb et al. 2003; Iwata et al. 2005; Berger et al. 2006; Shibata et al. 2006]. Clearance by this pathway is proportional to polyGln repeat length, and wild-type proteins are less susceptible to autophagy than the mutant form [Ravikumar et al. 2002; Webb et al. 2003; Berger et al. 2006]. It was shown that inhibiting autophagy increased the accumulation of aggregates thereby inhibiting the clearance of mutant htt [Qin et al. 2003; Ravikumar et al. 2004], and enhancing autophagy resulted in the more rapid clearance of both soluble and aggregated species of expanded htt [Williams, Jahreiss et al. 2006].

Aggresomes

When aggregated proteins are unable to be degraded or refolded by the normal quality control mechanisms, the cells can sequester aggregates by a microtubule-mediated process and transport them to a cytoplasmic site near the centrosomes [Johnston et al. 1998; Ross and Poirier 2005]. These structures are referred to as aggresomes.

Clearance of the aggresomes is often accomplished through autophagy. The protein within an aggresome is largely surrounded by a structural protein known as vimentin [Johnston, Ward et al. 1998]. Aggresome formation involves the trafficking of mutant proteins and the rearrangement of intermediate filaments around the perinuclear inclusion [Kopito 2000].

Data suggests that inclusion body formation, containing htt and molecular chaperones, primarily occurs due to this inability to be degraded by the normal protein quality control systems. It has been suggested that these inclusions, aggresomes, which generally have a perinuclear location, are similar in structure to cystic fibrosis transmembrane conductance regulator (CFTR) aggresomes [Johnston, Ward et al. 1998] that occur when the proteasome's degradative capacity is exceeded. Aggregates expressed in transiently transfected cell models of HD have many characteristics reminiscent of aggresomes [Qin et al. 2003]. Several groups have shown that inhibiting microtubule polymerization inhibits the formation of aggresomes [Johnston et al. 1998; Garcia-Mata et al. 1999; Webb et al. 2004]. One interesting possible mechanism of cell dysfunction caused by aggregation involves the normal cellular trafficking of aggregates to the perinuclearly located aggresome [Chang et al. 2006]. Thus, the inability of mitochondria to be correctly trafficked through the neuronal processes along microtubules, which are also involved in shuttling aggregates, could lead to energy starvation at the synapse and synaptic retraction.

Whether or not the aggregates themselves are toxic remains to be answered. However, a substantial amount of evidence has shown that aggregates are both handled

by, and can impair, normal protein quality control mechanisms [Hartl 1996; Cummings et al. 1998; Johnston et al. 1998; Chai et al. 1999; Jana et al. 2001; Waelter et al. 2001; Ravikumar et al. 2002; Verhoef et al. 2002; Qin et al. 2003; Holmberg et al. 2004; Schaffar et al. 2004]. It is therefore important to continue the search for the toxic species and to investigate each of their roles in cellular dysfunction and death.

TOXICITY BY AXONAL TRANSPORT IMPAIRMENT

Another important development in unfolding the mystery of HD pathogenesis, was the discovery that htt localizes with microtubules and synaptic vesicles suggesting a role in vesicle trafficking by axonal transport [Gutekunst et al. 1995; Lee et al. 2004; Webb et al. 2004; Gunawardena and Goldstein 2005; Truant et al. 2006]. Axonal transport is a microtubule-dependent system that is responsible for the movement of various cargo, such as mitrochondria, proteins, lipids, and synaptic vesicles, to and from the cell body [Feany and La Spada 2003; Chang et al. 2006].

Pertinent to this idea, was the detection of two significant cytoskeletal associated proteins that interact with htt, huntingtin-interacting protein (HIP1) and huntingtin-associated protein (HAP1) [Li, Li et al. 1995; Kalchman et al. 1997]. It has been reported that mutant htt binds antagonistically to synaptic vesicles decreasing the association of HAP1 resulting in a decrease in glutamate release in HD mouse brain sections [Li et al. 2003]. It was also shown that HIP1 has a decreased affinity for htt with expanded polyGln suggesting that HIP1 and htt interactions may be crucial for cellular function [Kalchman, Koide et al. 1997]. Data available on both of these interacting proteins

suggest a loss of function mechanism and will not be further addressed in this dissertation.

The presence of htt inclusion bodies are well documented in human HD patients [DiFiglia et al. 1997; Gutekunst et al. 1999] as well as in various other models of HD [Lunkes and Mandel 1998; Hollenbach et al. 1999; Kazantsev et al. 1999; Bates 2002; Rubinsztein 2002; Bates 2003; Feany and La Spada 2003; Marsh et al. 2003; Thompson and Marsh 2003; Gunawardena and Goldstein 2005; Chang et al. 2006]. Often these inclusions are found associated with microtubules [Tukamoto et al. 1997; Muchowski et al. 2002; Trushina et al. 2003; Webb et al. 2004; Iwata et al. 2005; Chang et al. 2006; Truant et al. 2007], suggesting a role for the impairment of axonal transport in HD.

It has been shown that in a *Drosophila model* expressing N-terminal htt fragments, inclusion bodies are formed in axonal processes and organelle accumulation is also present, suggesting a blockage of axonal transport [Gunawardena et al. 2003], which may be a direct result of the presence of the large aggregates and their ability to sequester vital polyGln-containing proteins necessary for axonal transport [Lee et al. 2004]. It was also recently shown, in a primary neuronal culture, that the presence of expanded htt aggregates was responsible for impairing mitochondrial trafficking, causing an accumulation of mitochondria, while aggregate-free sites were unaffected [Chang et al. 2006]. Thus, the concept of impaired axonal transport by the presence of htt inclusions can undoubtedly be imagined.

TOXICITY CAUSED BY EXCITOTOXICITY AND OXIDATIVE STRESS

It has also been suggested that calcium-dependent, glutamate-mediated excitotoxicity plays a pivotal role in HD pathogenesis [Greene and Greenamyre 1996; Tabrizi et al. 1999]. This mechanism will not be described in significant detail. Briefly, this theory proposes that subpopulations of striatal neurons (MSNs) become sensitive to glutamate release due mainly to changes in *N*-methyl-D-aspartate (NMDA) receptors [Freese et al. 1990], which can be correlated to neuronal death [Olney et al. 1971].

There has been a tremendous amount of data that demonstrates mitochondria dysfunction in HD (reviewed in [Lin and Beal 2006]). For example, htt has been shown to be associated with mitochondria in both truncated and full-length mutant htt models [Gutekunst et al. 1998; Panov et al. 2002; Yu et al. 2003; Choo et al. 2004], thus suggesting another impairment of normal cell processes by the presence of these inclusions.

This section has addressed the various mechanisms by which Huntington's disease pathogenesis is thought to occur. Some central questions surrounding HD are whether or not the aggregated proteins are themselves toxic, if the aggregation process is responsible for toxicity, or if early or later cellular events trigger dystrophy. While many theories have been posed, the exact mechanism is still unknown and the toxic species have not been identified. However, the disease mechanism is likely to involve several factors and multiple pathways that ultimately lead to cellular dysfunction and death.

1.4 Model Systems:

OVERVIEW

HD is a late-onset disorder, and therefore, the changes that are observed in the patients' brains are likely representative of late-stage pathological events or in combination with some early-stage pathogenesis. However, the limited availability of pre-symptomatic and early-stage HD patient material has made it difficult to study the exact causes of neurodegeneration *in situ*. Considering HD lesions are localized in the brain, tissue samples can only be feasibly obtained post-mortem. For these reasons, it was important to develop alternative model systems that recapitulate the deleterious effects seen in HD. With the identification in 1993 of the *IT15* gene responsible for HD, it has been possible to create both synthetic and genetic variations of the htt protein product.

Through the years, there have been many model systems created that include virtually every phylum, including *in vitro* synthetic peptide models, cell and yeast models, invertebrate models, and vertebrate models. Although there isn't a perfect model for HD, the hope is that collectively the information gained from each model will provide new insights into the mechanism(s) of disease. The goal of this section will be to provide a summary of the various model systems created and a brief synopsis of the results and limitations associated with each.

IN VITRO MODELS

The use of chemically synthesized polyGln peptides and recombinant fusion proteins have been particularly important models for studying the biochemical, biophysical, and structural characteristics of polyGln-containing proteins [Scherzinger et al. 1997; Chen and Wetzel 2001; Wetzel 2005] because they bypass many complications that can arise due to studying whole animal systems. In synthetic models, various length polyGln peptides can be solubilized by exposure to disaggregating solutions, subjected to ultracentrifugation in order to remove any small oligomeric species, and then resuspended in physiological solutions [Wetzel 2005].

Aggregation kinetics and thermodynamics have been thoroughly studied in these models, and a great deal of knowledge has been acquired about the folding properties of these proteins as well. These accomplishments were made using various techniques, such as ThT and Congo red birefringence, which shed light on the β-sheet structure of the fibrillar protein [Scherzinger et al. 1997; Huang et al. 1998; Chen et al. 2002]. Dynamic light scattering, which increases as particles increase in size and number, has been used to measure the kinetics of aggregation; however, this method is generally used in conjunction with one or more methods due to the problem of larger aggregates dominating the signal [Lomakin et al. 1999].

Another important observation from *in vitro* models is the ability of polyGln proteins to exhibit recruitment-competency [Berthelier et al. 2001; Berthelier and Wetzel 2003]. Data from *in vitro* models reveal that simple polyGln sequences can self-assemble into aggregates and that this process is nucleation-dependent [Chen et al. 2001; Chen et

al. 2002; Ross et al. 2003]. At the same time, studies on larger fragments that include flanking sequences to polyGln indicate more complex aggregation mechanisms that include initial rapid formation of amyloid-like aggregates [Ellisdon, Pearce et al. 2007] or non-amyloid oligomeric aggregates (huntingtin; [Thakur] involving the flanking sequences.

CELL MODELS

There have also been many yeast and mammalian cell models developed that have had great impacts in the HD field. Such models are simpler than animal models but at the same time, compared to in vitro models, allow a better understanding of how the misfolded proteins behave in a more complex mixture of other cellular components.

Yeast model

Saccharomyces cerevisiae has often been used to explore the relationship between polyGln aggregation and toxicity and other cellular components including chaperones. Yeast models are relatively simple to generate and study and do not feature huge cell-to-cell variations of the total proteome as is evident in mammalian cell culture models. Most commonly these yeast models are designed to express variant htt exon 1 constructs. As seen in other eukaryotic systems, the polyGln repeat length is directly correlated to aggregate formation. While yeast cells do not appear to be actually killed by expanded polyGln aggregates, their growth is retarded, and it is in this context that expanded polyGln is said to be toxic in yeast. After some confusion about the yeast strain dependence of this toxic effect, it was shown that Rnq1, a yeast prion, is required for

polyGln aggregation, which directly correlates with cellular toxicity, and that upon deletion of Rnq1, aggregation and toxicity were both suppressed [Meriin et al. 2002]. The overexpression of both Hsp40 and Hsp70 have been found to attenuate polyGln aggregation and alleviate cellular toxicity [Muchowski, Schaffar et al. 2000]. Interestingly, it has also been observed that the molecular chaperone Hsp104 is required for polyGln aggregation [Krobitsch and Lindquist 2000], and upon its deletion, virtually none of the detected protein is found in an aggregated form. A similar counter-intuitive ability of Hsp104 to promote the formation of a yeast prion was described previously [Schirmer and Lindquist 1997].

More recently, the role of the polyGln flanking sequences have been found to have a profound influence on the toxicity in yeast associated with the protein [Dehay and Bertolotti 2006; Duennwald et al. 2006; Duennwald et al. 2006]. Introduction of a htt construct containing the proline-rich region of exon 1 creates morphologically different aggregates, which are generally smaller than the well-described insoluble polyGln aggregates [Dehay and Bertolotti 2006; Duennwald et al. 2006]. Next, deleting this polyproline region slowed aggregate formation [Dehay and Bertolotti 2006]. Also, the deletion of this region created a more insoluble aggregate compared to a construct that includes the polyproline region. Furthermore, yeast expressing the proline flanking sequences in htt exhibited less toxic effects than cells expressing a htt construct lacking the proline-rich region [Dehay and Bertolotti 2006]. The ability of a proline-rich sequence to suppress polyGln aggregation and weaken aggregate structure can also be observed in vitro using simple polyGln peptides (Bhattacharyya et al 2006).

Mammalian cell models

There have been a host of transient and stably transfected mammalian cell culture models developed that constitutively or inducibly overexpress fusion proteins of either truncated or full-length huntingtin DNA constructs (See Table 1.6 for a summary of the various models and the major findings associated with each model) [Lunkes and Mandel 1998; Martindale, Hackam et al. 1998; Saudou, Finkbeiner et al. 1998; Li et al. 1999; Preisinger et al. 1999; Sanchez et al. 1999; Wellington et al. 2000; Apostol et al. 2003; Aiken et al. 2004]. In transient expression models, plasmid DNA is introduced into the cells by various delivery methods, usually via a lipid-mediated carrier, and expression is only detectible for up to one week. This effect is due to the fact that a majority of the DNA introduced to the cells does not make it into the nucleus for transcription. The DNA that manages to get into the nucleus becomes diluted with the dividing cells until it is no longer observable. The transient effect is solely due to the lack of integration of the plasmid DNA into the genome of the dividing cell line.

In contrast, stably transfected models depend on the recombination of a delivered transgene into the model system's genome. This technique involves introducing the plasmid DNA, which spontaneously inserts itself into the genome of the model organism, and selecting for this rare event by the use of drug resistance or a phenotypic alteration. Once incorporation occurs, the transgene will replicate in synchrony with the dividing cell, theoretically creating a stable, long-lasting genotype. Addition of an inducible promoter to a stable transfectant creates a stable genotype in which transgene expression is controlled by the addition or removal of an inducing (suppressing) agent.

Table 1.6: Cellular models of Huntington's disease.

Cell Line	Expression	Htt fragment*	Findings	Reference
Cos-7, SK-N-SH	Transient	Full-length Q21, 72	Wildtype htt protective against mutant htt	[Ho et al. 2001]
Cos-1	Transient	N-terminal fragments Q20-51	Mutant htt aggregate formation dependent on repeat length, concentration, & time	[Scherzinger et al. 1999]
Cos-7, SK-N-SH	Transient	Exon 1 Q23, 53, 74	Mutant htt increased reactive oxygen species	[Wyttenbach et al. 2002]
HEK293	Transient	Exon 1 fragments Q25-103	Cleavage of mutant htt results in N-terminal fragments localization to nucleus: recruitment-sequestration	[Steffan et al. 2000]
HEK293	Stable, inducible	Exon 1 fragments Q20, 51, 83	Mutant htt form detergent-resistant aggresome inclusions. Inhibition of proteasome results in further accumulation	[Waelter et al. 2001]
PC12	Transient	Exon 1 fragments Q25-103	PolyGln aggregates are detergent-resistant, located perinuclear, and interact with other polyGln-containing proteins	[Kazantsev et al. 1999; Preisinger et al. 1999]
PC12	Stable, inducible	Exon 1 Q20, 150	Benign htt diffuse in the cytoplasm; mutant htt diffuse in the nucleus and is susceptible to stress	[Li, Cheng et al. 1999]
PC12	Stable, inducible	Exon 1 Q25, 47, 103 Exon1 fragments Q25, 103	Drug screen coupled with *Drosophila*: disruption of aggregation correlates with reduces neurodegeneration in *Drosophila*	[Apostol, Kazantsev et al. 2003]
PC12	Stable, inducible	Exon 1 Q103	Drug screen showed caspase inhibitors protected against cell death	[Aiken, Tobin et al. 2004]

Table 1.6. Continued

Cell Line	Expression	Htt fragment*	Findings	Reference
PC12, Cos-7	Stable, inducible	Exon 1 Q23, 74	Mutant htt formed cytoprotective aggresomes that are formed via microtubule-dependence	[Webb et al. 2004]
N2a	Transient	N-terminal fragments Q23, 75	Nuclear localization of mutant htt important for toxicity	[Peters et al. 1999]
N2a	Stable, inducible	Exon 1 Q16, 60, 150	Increased polyGln expression = decreased proteasomal processing, mitochondrial membrane, activated caspases	[Jana et al. 2001]
IMR	Transient	Full-length Q82	Mutant htt more resistant to proteolysis than normal. N-terminal cleavage products sequestered by full-length htt	[Dyer and McMurray 2001]
Primary striatal / hippocampal	Transient	Exon 1 Q17, 68	Nuclear localization important for cell death, not aggregation	[Saudou, Finkbeiner et al. 1998]
Primary cortical	Transient	Full-length Q15, 44, 128	Increasing Gln length and truncation = increased toxicity	[Hackam et al. 1998; Martindale et al. 1998]

* N-terminal fragments = various shortened Exon 1 fragments that do not necessarily contain the first 17 amino acids (region preceding Gln stretch). Exon 1 differs from exon 1 fragments in that "fragments" represents truncation after the Gln sequence. Synthetic indicates only the Gln sequence was used. N2a, IMR and SK-N-SH cells are neuroblastomas.

The rat pheochromocytoma cell line, PC12, is one of the most commonly used mammalian cell lines to study neurodegenerative diseases [Warren and Chute 1972; DeLellis et al. 1973; Greene and Tischler 1976; Schubert and Whitlock 1977; Chai et al. 1999; Li et al. 1999; Wyttenbach et al. 2001; Apostol et al. 2003; Aiken et al. 2004]. Like neurons, PC12 cells synthesize and store dopamine and norepinephrine, which are catecholamine neurotransmitters, and upon treatment with nerve growth factor (NGF) can be transformed into a more neuronal-like appearance with long, extended neuritic processes [Greene and Tischler 1976]. The most ideal cell models are those involving the use of primary neuronal cultures; however, these models are not immortal and generally more difficult to maintain.

There has been a great variety in the types of cells studied and the polyGln length transfected. In spite of this variety, common features have emerged. There appears to be a polyGln repeat length dependence for aggregation [Lunkes and Mandel 1998; Kazantsev et al. 1999]; toxicity requires nuclear localization of the aggregate [Saudou et al. 1998; Yang et al. 2002]; and the overexpression of chaperone proteins reduces aggregate burden and/or toxicity [Cummings et al. 1998; Sittler et al. 2001; Firdaus et al. 2006]. However, these findings appear to indicate cell background independence because a number of models have utilized the non-neuronal-like cell lines [Cooper et al. 1998; Zeron et al. 2001; Skinner et al. 2002; Firdaus et al. 2006]. Regardless of the simple eukaryotic model used, yeast or mammalian cells, these systems provide the framework for addressing key questions about disease mechanism.

INVERTEBRATE MODELS

Invertebrate models, such as *Caenorhabditis elegans* (worm) and *Drosophila melanogaster* (fly), are also now being used to study neurodegenerative diseases (See Table 1.7) [Jackson et al. 1998; Satyal et al. 2000; Link 2001; Driscoll and Gerstbrein 2003; Marsh et al. 2003; Marsh and Thompson 2006; Slepko et al. 2006; Brignull et al. 2007]. These models are important because they represent simple multicellular organisms and have a greater rank than *in vitro* systems, yeast, and cell cultures. Both the worm and the fly have been utilized for studying neurodegenerative disorders largely because of their rapid generation times and fully functional nervous systems, which are absent in the above presented models. In both models, many neuronal dysfunction characteristics are exhibited. For instance, in *Drosophila*, a commonly used, easily measured assessment of dysfunction is the degree of climbing activity in a glass tube. Another common endpoint used in neurodegeneration research is the loss of the photoreceptors of the eye in response to expression of disease proteins.

Invertebrate models of HD are created from either truncated or full-length htt constructs. Simple glutamine sequences, without the htt context, have also been explored. In the *Drosophila* models, virtually all the reported systems are placed under the control of the upstream activating sequence (UAS), which does not express until crossed with fly strains that express the yeast transcriptional activator GAL4. GAL4 is present in every cell of the nervous system from embryogenesis forward [Robinow and White 1988]. Jackson's group [Jackson et al. 1998] used gmr, which is another common

Table 1.7: Invertebrate models of Huntington's disease.

Model	Construct	Driver / Promoter	Repeat Size	Target Cells	Mutation phenotype	Reference
Drosophila	UAS polyQ	gmr-GAL4	Q46	Eye retina	Retinal degeneration	[Steffan et al. 2001]
Drosophila	UAS polyQ	Gmr-GAL4	Q27, 108	Eye retina	50% lethal	[Marsh et al. 2000]
Drosophila	Htt exon 1	GMR	Q2, 75, 120	Eye retina	Retinal degeneration	[Jackson, Salecker et al. 1998]
Drosophila	UAS htt exon 1 fragment	gmr-GAL4	Q20, 93	Eye retina	Retinal degeneration / lethality	[Steffan et al. 2001]
C. elegans	GFP polyQ	*unc-54*	Q19, 82	Body wall muscle	Growth retardation	[Satyal et al. 2000]
C. elegans	GFP polyQ	*myo-2*	Q19, 82	Pharyngeal wall muscle	Unreported	[Satyal et al. 2000]
C. elegans	Htt exon 1	*osm-10*	Q2, 23, 95, 150	ASH sensory	Touch response defect	[Faber et al. 1999]
C. elegans	Htt exon 1 fragment	*Mec3*	Q19, 88, 128	Touch receptor neurons	Touch response defect	[Parker et al. 2001]

Abbreviations: Upstream activating sequences (UAS), glass multimer reporter (gmr), green fluorescent protein (GFP), glutamine (Q)

driver for neurodegenerative studies that is expressed in all the cells of the eye [Ellis et al. 1993]. Regardless of the driver used, the most commonly targeted organ for neurodegeneration is the eye. *Drosophila* models have shown striking neuronal degeneration, with apoptotic hallmarks, which are highly correlated with the polyGln repeat length, as well as the identification of chaperones that suppress polyGln-associated toxicity [Jackson et al. 1998; Kazemi-Esfarjani and Benzer 2000]. More recently, it has also been shown that when a Q20 sequence was co-expressed with a Q93 sequence [Slepko et al. 2006], inclusions formed at a much faster rate than when the Q93 was expressed alone. The observed aggregation kinetics correlated well with an increase in toxicity, which was not seen in *Drosophila* expressing only Q20. Furthermore, by day 10 of the experiment, the majority of the aggregates present were found in the nucleus.

PolyGln toxicity has also been evaluated in *C. elegans* by expressing various Gln constructs in the muscle or sensory neurons. As in the fly model, progressive neurodegeneration occurs in a polyGln length-dependent manner; however, toxicity is not observed until a second toxin is introduced [Faber, Alter et al. 1999]. In *C. elegans,* the heat shock response has also been shown to be activated under the stress of expanded Gln proteins. This effect can be alleviated by co-expression of a yeast chaperone Hsp104 [Satyal et al. 2000], which reduces the appearance of polyGln aggregates and the associated developmental delay.

In *C. elegans*, behavioral assays are used to determine dysfunction in a specific neuron [Faber, Alter et al. 1999; Parker, Connolly et al. 2001], where an unhealthy worm is slower to respond to a touch response compared to its healthy counterpart. For

example, worms expressing a 150 Gln repeat formed aggregates that increased as the animal aged, which correlated with the progressive neurodegeneration of sensory neurons [Faber, Alter et al. 1999]. In another example, worms that expressed expanded polyGln repeats exhibited touch insensitivity, whereas worms expressing normal lengths did not possess this characteristic [Parker, Connolly et al. 2001].

The invertebrate models share many of the same features of HD that are observed in the human disease [Marsh et al. 2003; Brignull et al. 2006; Slepko et al. 2006], such as the presence of polyGln aggregates and progressive degeneration. Both *Drosophila* and *C. elegans* models provide excellent systems for combining cellular complexity and behavioral phenotypes.

VERTEBRATE MODELS

Although the aforementioned models are well-studied, have relatively quick generation times, are relatively easy to work with, and are readily available, they still lack the complexity of higher eukaryotic species. Mice and rats share significant homologies with humans, including similar proteomes and basic anatomical features. Furthermore, all mammals share similar nervous, digestive, and circulatory systems, which stresses the importance of developing vertebrate models depicting human disease. Finally, the N-terminal segment of mouse and rat huntingtin is very similar to the human [Barnes et al. 1994; Schmitt et al. 1995], while there is no recognizable exon1 or polyGln sequence in Drosophila huntingtin [Li et al. 1999], and there is no huntingtin homolog at all in C. elegans [NCBI 2007].

Mouse models of HD can be grouped into two different categories 1) the transgenic model, in which a portion of the mutated gene is expressed under the control of various exogenous promoters, including bacterial and yeast artificial chromosomes (BAC and YAC, respectively), and 2) the knock-in / knock-out models, in which an expanded Gln repeat containing huntingtin gene is engineered at the mouse *IT15* locus (See Table 1.8 for a summary) [Sipione and Cattaneo 2001; Bao et al. 2002; Bates 2002; Rubinsztein 2002; Levine et al. 2004].

Hdh is the mouse homolog of the human HD gene and has been shown to share a 91% identity with the human huntingtin protein [Barnes et al. 1994]. A homozygous knock-out of this full-length murine gene results in embryonic lethality [Duyao et al. 1995], which is accompanied by an increase in apoptosis in the embryonic ectoderm [Zeitlin et al. 1995]. These studies demonstrated the importance of htt during development, and also proved that simply the loss of htt function could not account for the neurodegeneration seen in HD. The lack of an HD-like phenotype in knock-out models, is generally interpreted as proof of the expanded polyGln imparting a gain of function activity. Furthermore, an *Hdh* heterozygous knock-out resulted in a normal phenotype, reinforcing this belief [Duyao et al. 1995; Zeitlin et al. 1995].

Transgenic mouse models expressing truncated forms of mutant htt develop a progressive neurological phenotype that includes tremors, NII, hypokinesis, failure to gain weight, abnormal gait, a lack of coordination, limb clasping, and a reduced response to stimuli [Bates 1998; Sipione and Cattaneo 2001]. These mice were constructed to

Table 1.8: Mouse models of Huntington's disease.

Model design (Promoter / gene size/ Gln repeat)	Behavioral disorder	Neuropathology		Reference
		Inclusions	Cell loss	
Transgenic *Hdh* models				
HD promoter; exon 1 R6/2 line: Q20, 115, 150	Onset at 2 mo. Tremors, abnormal gait, learning deficit, hypokinesis, diabetes	NII and NA throughout brain, fewer dendritic spines	Overall atrophy. Fontal cortex, dorsal striatum, and Purkinje cells (late stage)	[Mangiarini et al. 1996]
Mouse prion promoter; First 171 aa. Q16, 44, 82	Onset 5 mo. with Q82. Tremors, abnormal gait, hypokinesis, weight loss, early death	Striatum, cortex, hippocampus, amygdale. Diffuse nuclear accumulation of htt	Overall atrophy. Striatum	[Schilling et al. 1999]
Tet-off (camKIIα-tTA) promoter; exon 1 Q94	Onset in 50% by 2.5 mo. late onset tremor and abnormal gait	Striatum, septum, cortex, hippocampus, reactive astrocytes	Progressive striatal neurodegeneration	[Yamamoto et al. 2000]
HD YAC transgenic. Full-length gene Q18, 46, 72, 128	Onset 3 mo. with Q72, 128. Hyperactive and circling. Hyperkinesis, progressive motor deficit	Striatum	Striatal cell loss, cortical atrophy with Q128	[Hodgson et al. 1999; Slow et al. 2003]
CMV promoter; full-length gene, Q16, 48, 89	Onset 4 mo. with Q48, 89. Circling hyperactivity, end-stage, hypoactivity, and urinary incontinence	Fewer inclusions throughout the brain	20% cell loss in striatum of some animals	[Reddy et al. 1998]
Rat neuron-specific enolase promoter; 3-kb N-terminal fragment, Q18, 48, 100	Onset 3-4 mo. with Q100	Inclusions in Q100, few in Q46; dystrophic neuritis observed	20% cell loss at 8 mo. in some animals	[Laforet et al. 2001]

Table 1.8. Continued

Model design (Promoter / gene size/ Gln repeat)	Behavioral disorder	Neuropathology		Reference
		Inclusions	Cell loss	
Knock-in *Hdh* models				
Endogenous mouse HD gene *Hdh* promoter; Q50, 92, 111	None determined	PolyGln- and age-dependent htt nuclear relocalization at 1.5 mo. Some inclusions >6 mo.	None observed	[Wheeler et al. 1999]
Neo and *Hdh* promoter; Q20, 111	Onset ~2 mo. and show disorders similar to R6/2 mice	Age-dependent htt nuclear relocalization and inclusion	None observed	[White et al. 1997]
Hdh promoter; Q72, 80	Early onset aggressive behavior	Late inclusions, hippocampus, repeat instability in striatum	Long term potentiation impaired	[Shelbourne et al. 1999]
Hdh promoter; Q71, 94	None determined	Striatal cell swelling in response to NMDA	Smaller striatal cells, NMDA sensitivity	[Levine et al. 1999]
Hdh promoter; full-length gene, Q80, 150	Onset 6 mo. Q150 homozygote, 15 mo. heterozygote. Motor task deficits, abnormal gait, hypoactivity	NII Q150 mainly in striatum. Htt nuclear relocalization	Reactive gliosis	[Lin et al. 2001]

express much larger CAG repeats than are actually seen in late-onset Huntington's disease. The life span is also shortened compared to transgenic mice expressing full-length mutant htt [Bates 2002]. As is the case for the human disease, the mechanism(s) responsible for the phenotype are unknown.

Knock-in models are an improvement over previous transgenic models because Gln repeats can be precisely inserted into the endogenous mouse HD gene and expression is controlled by the mouse's own promoter. This is in contrast to the random transgene incorporation into the mouse germline. Mild and very late onset neuronal phenotypes have been observed in these knock-in mice; phenotypes are more severe in homozygotes [Sipione and Cattaneo 2001].

Knock-in mice are more similar to the human disease than the other transgenic mice expressing the truncated or full-length protein in that the expression levels are more comparable to those of wildtype and affected tissues are more widespread in the brain and peripheral tissues [Sipione and Cattaneo 2001]. This is due, in part to inheriting the normal control elements that are associated with expressing the species specific gene under the mouse promoter. A progressive neuronal phenotype and selective neurodegeneration is also observed in transgenics (including knock-ins) expressing the mutant full-length protein [Bates 1998].

There are many similarities among these various murine models and the human disease. For example, a great deal of CAG repeat instability is observed both in different vertebrate models and in humans. The largest degree of expansion, within the human brain, was noted in the caudate and putamen, while the smallest repeats were in the

cerebellum [Telenius et al. 1994]. CAG instability was also observed in a couple of the knock-in models [Shelbourne et al. 1999; Wheeler et al. 1999] and in the R6 transgenic models [Bates et al. 1997; Mangiarini et al. 1997]. Many of these models have been reported to exhibit progressive phenotypes [Mangiarini et al. 1996; Reddy et al. 1998; Hodgson et al. 1999; Schilling et al. 1999; Laforet et al. 2001; Lin et al. 2001], but the majority of this type of characterization has been performed on the R6/2 mice [Carter et al. 1999; Lione et al. 1999].

The propensity to form polyGln-containing inclusions is a hallmark of HD in humans [DiFiglia et al. 1997; Becher et al. 1998; Gutekunst et al. 1999] that is also found in many of the vertebrate models. PolyGln aggregate pathology similar to the inclusions observed in humans has been described in every HD mouse model [Mangiarini et al. 1996; White et al. 1997; Reddy et al. 1998; Hodgson et al. 1999; Schilling et al. 1999; Shelbourne et al. 1999; Wheeler et al. 1999; Yamamoto et al. 2000; Laforet et al. 2001; Lin et al. 2001; Levine et al. 2004]; however, the precise role of these aggregates in HD pathogenesis is still unclear.

Although there are many questions still unanswered, several important discoveries about the molecular basis of HD have been acquired from each of these model systems.

CHAPTER 2

PROJECT RATIONALE AND SUMMARY

The most common of a family of trinucleotide repeat neurodegenerative disorders, Huntington's disease is an autosomal dominant disease caused by a glutamine expansion in the N-terminus of the gene encoding the huntingtin protein [Bates 2002]. The expanded polyGln itself is thought to be responsible for the pathogenesis of the disease. Indeed, the severity of the disease increases with the length of the polyGln repeat. As in all these trinucleotide repeat diseases, the expansion of the polyGln tract induces misfolding of the protein, which then forms insoluble cytoplasmic and/or nuclear aggregates within affected neurons [Davies, Turmaine et al. 1997; Scherzinger, Lurz et al. 1997]. The length of the polyGln sequence (~35 Glns) associated with disease is very similar for most of these disorders and correlates well with the length-dependent aggregation properties observed *in vitro* [Harper and Newcombe 1992; Evert, Wullner et al. 2000]. Recent experiments using cell systems support the idea that polyGln aggregates are cytotoxic due to their ability to recruit other critical cellular proteins, via their own polyGln components [Davies, Turmaine et al. 1997; McCampbell et al. 2000; Nucifora et al. 2001]. In addition, it has been shown in another CAG repeat disease that some neuronal aggregates, which are not polyGln-rich, are capable of recruiting polyGln proteins [Takahashi et al. 2001]. On the other hand, it has also been postulated that the formation of large, insoluble aggregates is a defense mechanism that has the beneficial effect of sequestering smaller, more cytotoxic misfolded protein aggregates, thereby

rendering them harmless [Klement et al. 1998; Saudou, Finkbeiner et al. 1998]. These seemingly contradictory findings demonstrate that the aggregation phenomenon is complex and may involve multiple discrete or interdependent pathways featuring different misfolded and aggregated states with unique physical and biological properties.

To help distinguish different aggregated states, we have developed a cell-based method capable of identifying intracellular aggregates based on whether or not they are able to actively recruit biotinylated-monomeric Q_{28} peptide. This method was initially developed using transiently transfected cell models in which various lengths of htt-polyGln-green fluorescent protein (GFP) fusion constructs were introduced via liposome-mediated delivery. The optimized biotinyl-polyGln system was then applied to a more robust and reproducible model of stably-transfected PC12 cells capable of inducible expression of htt with different polyGln repeat lengths. In these inducible cell models, punctate areas were visible with the polyGln recruitment stain but not by the GFP fluorescence typically used to discern aggregates in such models. The actively recruiting species were designated aggregation foci (AF) [Osmand 2004; Osmand, Berthelier et al. 2006]. For reasons not entirely understood, these htt-inducible cells do not exhibit cell toxicity due to the presence of expanded polyGln htt molecules [Apostol, Kazantsev et al. 2003], in contrast to some other models [Li, Cheng et al. 1999; Aiken, Tobin et al. 2004]. This intrinsic property of the cell line has provided a unique opportunity to dissect the aggregation process without the complication of cell death.

The goal of this dissertation research was to: (a) develop a method for identifying and validating the polyGln recruitment-competency within a cellular model of htt

overexpression; (b) optimize the cells for htt-polyGln-GFP expression; (c) characterize and investigate the potential role(s) of each of the various observed aggregated states in aggregate propagation by examining their functionality and structure over time; and (d) study the roles of various cellular functions in the formation and flux of AF and other aggregates. The majority of this characterization was completed using immunofluorescence microscopy to monitor the appearance and disappearance of AF and htt-polyGln-GFP aggregates in a time-dependent manner. Further biochemical characterization was achieved by isolating and examining a series of cell fractions that contained the htt-polyGln-GFP proteins of interest. Each fraction was examined for its reactivity with anti-GFP and 1C2-binding (anti-polyglutamine) antibodies using Western blot assays. An attempt was also made to functionally characterize each fraction for their abilities to support *in vitro* polyglutamine elongation using a microtiter plate assay [Berthelier et al. 2001].

Finally, two compounds directed at specific cellular processes were investigated for their ability to alter the aggregate formation pathway(s), which will be discussed in Chapter 7. These compounds exhibit specific effects on AF and htt-polyGln-GFP aggregates in the inducible cell system. These data suggest several possible modes for aggregate formation in cells, which are addressed in greater detail in the Discussion and Conclusions sections in Chapter 9. Taken together, the data obtained from these studies and the protocols that have been developed can be used to dissect the basic principle of htt aggregation *in vivo* and provide a platform to identify and quantitatively evaluate novel therapeutic interventions to treat patients with this devastating human condition.

CHAPTER 3

MATERIALS AND METHODS

3.1 Polyglutamine Constructs and Synthetic Peptides:

HTT DNA CONSTRUCTS

The DNA constructs used for all experiments were a generous gift from Alex Kazantsev at the Center for Aging and Neurodegeneration, Massachusetts General Hospital, Charlestown, MA. The original DNA constructs used were all truncated htt exon-1-polyGln-GFP fusions (htt-Q_n-GFP) [Kazantsev et al. 1999; Preisinger et al. 1999; Michalik et al. 2001]. Exon-1 of the HD gene contains the CAG repeat region, which is translated into a polyGln stretch within the huntingtin protein. For a number of reasons, the exon-1 fragment of htt, rather than the full-length molecule, is frequently used as a model system for studying outcomes of expanded polyGln expression. Truncated htt constructs were initially used because it has been shown in a mouse model that the HD inclusions contain processed N-terminal htt fragments [Martindale, Hackam et al. 1998], and that these fragments were more toxic than the mutant full-length protein [Hackam et al. 1998; Lunkes and Mandel 1998]. More recently, N-terminal fragment models have been further validated with evidence that caspase release of an N-terminal portion of htt is likely to be a critical step in the disease mechanism [Sawa et al. 2005; Maglione et al. 2006].

The truncated constructs were composed of the first 17 amino acids (aa) of htt exon 1, followed by the Gln repeat expansion with alternating CAG/CAA for added stability [Michalik et al. 2001], and an in frame fusion with GFP at the C-terminus of truncated htt exon 1 (htt-Q_n-GFP, Q25, 47, 65, and 103) (see Figure 3.1B).

Complete htt exon 1 GFP constructs were used to create a stable htt-inducible cell line (generously supplied by Leslie Thompson at the University of California, Irvin, and Aleksey Kazantsev at Massachusetts General Institute for Neurodegenerative Disease [Apostol, Kazantsev et al. 2003]), which will be discussed in detail in Section 3.2. These constructs also contained the first 17 aa of huntingtin exon 1, the Gln repeat stretch, the polyproline region, and the GFP tag, as indicated in Figure 3.1A. Cells containing these constructs were available in 25, 47, and 103 Gln repeat lengths. The cells expressing complete htt exon 1 constructs will be designated as 25QP, 47QP, and 103QP. Also for the htt-inducible cells, we had one cell line expressing a truncated form of htt exon 1 (Figure 3.1B). This cell line will be referred to as Q103.

POLYGLUTAMINE PEPTIDE PREPARATION

Synthetic polyGln peptides were utilized for the polyGln-recruitment stain (Section 3.3) and as control samples for the polyGln microtiter plate elongation assay (Section 3.7), see Figure 3.1C. All peptides were prepared by custom solid-phase synthesis from the Keck Biotechnology Center at Yale University (http://info.med.yale.edu/wmkeck). The polyGln sequences were flanked by pairs of lysine (Lys or K) residues to enhance solubility by conferring a net positive charge on the

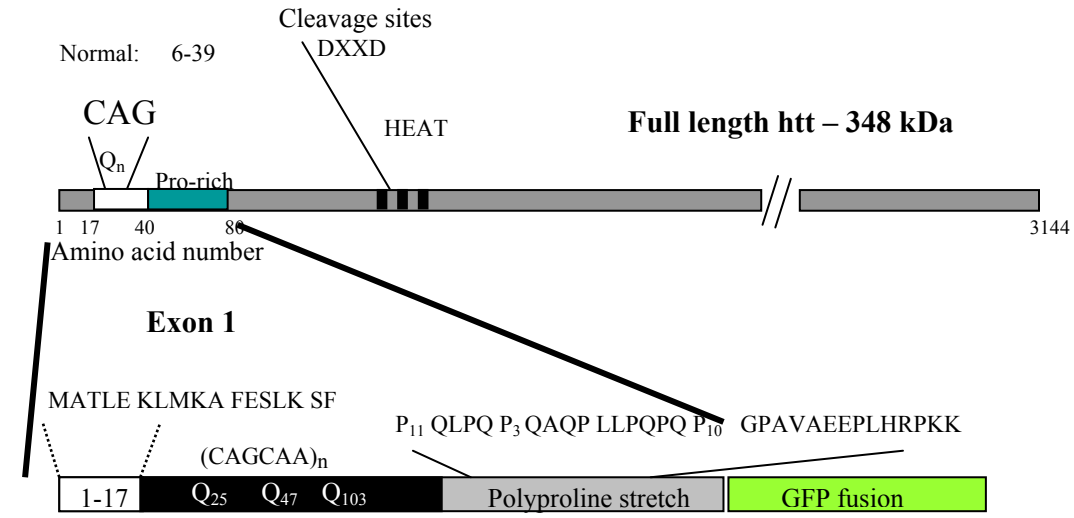

(A) Complete exon 1 constructs: 25QP, 47QP, and 103QP

(B) Truncated exon 1 constructs: Q25, Q47, Q65, and Q103

(C) Synthetic polyGln peptides: $K_2Q_{47}K_2$ and biotin-PEG-$K_2Q_{28}K_2$

Figure 3.1: PolyGln constructs and peptide sequences. *(A) Complete htt exon 1 constructs. (B) Truncated htt exon 1 constructs. (C) Synthetic polyGln peptides.*

peptide at a neutral pH [Chen and Wetzel 2001]. We utilized biotinylated peptides as well, which were created by an N-terminal derivatization during the synthesis. The biotinylated peptide was enhanced by the addition of a polyethylene glycol (PEG) spacer between the biotin moiety and the polyGln peptide [Osmand, Berthelier et al. 2006]. Peptides were purified by disaggregation and HPLC [Berthelier et al. 2001; Chen and Wetzel 2001], and stored at -80°C in 1- or 5-ml aliquot stock solutions in extension buffer (1X phosphate buffered saline (PBS) and 0.01% Tween® 20) with 5% dimethyl sulfoxide (DMSO) or PBS alone.

Solubilization and Disaggregation of Peptides

Peptides were dissolved at 0.5mg/ml in a 1:1 mixture of trifluoroacetic acid (TFA, #28901, Pierce, Rockford, IL) and 1,1,1,3,3,3-hexafluoro-2-propanol (HFIP, #52517, Sigma-Aldrich, St. Louis, MO) for 24 hour. The solvents were evaporated in a fume hood under a stream of argon and further lyophilized under a vacuum for one hour. The peptide residue was resuspended in an equal volume of cold water, adjusted to pH 3.0 by TFA, and allowed to dissolve for at least 15 minutes at 4°C. The sample was then subjected to ultracentrifugation at 100,000xg overnight at 4°C to remove any aggregate contaminants. All but the bottom 10% of the supernatant was carefully removed and stored at 4°C while the exact peptide concentration was determined by reverse-phase high-performance liquid chromatography (RP-HPLC, Hewlett-Packard, Palo Alto, CA) fitted with a Zorbax SB-C3 column. Biotinylated-PEG-K_2-Q_{28}-K_2 peptides were diluted to a final concentration of 500nM in extension buffer, aliquoted, flash frozen, and stored at -80°C.

A more complete description of the disaggregation protocol has been published [O'Nuallain et al. 2006].

Preparation of Polyglutamine Aggregates

$K_2Q_{47}K_2$ peptides were subjected to the above disaggregation protocol; after which, the concentration was adjusted to 10μM (44μg/ml) in 1X PBS. The peptide solution was then incubated at 37°C for 24 hours, snap frozen, and subjected to an additional 24 hour incubation at -20°C [Berthelier, Hamilton et al. 2001]. Aggregates were aliquoted, snap frozen, and stored at -80°C.

3.2 Cell Culture and Treatment:

MAINTENANCE

PC12 Cells

Two cell lines, PC12 and SH-SY5Y cells, were utilized for the transient expression model systems. Rat pheochromoctyoma (PC12) cells are an adherent cell line that were established in the 1970s to provide a model system that displayed neuronal characteristics but was easier to work with than primary neuronal cultures [Warren and Chute 1972; Greene and Tischler 1976]. For these reasons, PC12 cells are commonly used as mammalian cells to study neurodegenerative diseases [Li, Cheng et al. 1999; Apostol, Kazantsev et al. 2003; Aiken, Tobin et al. 2004]. PC12 cells were graciously

donated by Erik Schweitzer in the Department of Physiological Science and Neurology at the Brain Research Institute, University of California, Los Angeles, CA.

PC12 cultures were maintained in Dulbecco's Modification of Eagle's Medium (DMEM) supplemented with 5% fetal bovine serum (FBS), 5% horse serum (HS), and penicillin/streptomycin antibiotics (complete growth medium). Media and supplements were purchased from MediaTech, Inc. (Herndon, VA), Hyclone, (Logan, UT), and Calbiochem (San Diego, CA) unless otherwise noted. All cells were grown at 37°C in 5.0% carbon dioxide (CO_2) and at 98% relative humidity. The media was changed every third day, and the cultures were passaged weekly.

SH-SY5Y Cells

To create an even more physiologically relevant mammalian culture, a human neuroblastoma cell line, SH-SY5Y (American Type Culture Collection (ATCC) – #CRL-2266, Manassas, VA) was used. These cells are a third generation clone that was established from the parental SK-N-SH cells. Although SH-SY5Y cells grow as a mixture of adherent and floating cells, they can be differentiated with 10μM retinoic acid (RA) to generate a more adherent phenotype. Like the PC12 cells, SH-SY5Y cells exhibit many neuronal characteristics. These cells, irrespective of differentiation, actively produce many neurotransmitters that are found in the normal human brain. Although SH-SY5Y cells are less commonly used than PC12 cells (probably because they are more difficult to maintain) there have been several reports of their use in neurodegenerative disease research [Grierson et al. 2001; Ho, Carmichael et al. 2001; Wyttenbach, Sauvageot et al. 2002; Olivieri et al. 2003]. SH-SY5Y cells were cultured in a 1:1

mixture of DMEM and Ham's F12 Medium supplemented with 10% FBS and penicillin/streptomycin antibiotics.

Stable, htt-inducible PC12 Cells

We also had available several htt-inducible PC12 cell models that expressed various polyGln lengths (25QP, 47QP, 103QP, and Q103; detailed in Section 3.1) [Apostol, Kazantsev et al. 2003]. Protein expression within these cells was controlled by an ecdysone-inducible promoter and was regulated by Ponasterone (#H101-01, Invitrogen, Carlsbad, CA), an insect steroid. The htt-inducible PC12 cells were cultured in DMEM supplemented with 10% HS, 5% FBS, 15mM HEPES (4-(2-hydroxyethyl)-1-piperazineethanesulfonic acid) buffer, and antibiotics. Dilution cloning on these cells will be discussed in the next subsection.

The ecdysone-inducible mammalian expression systems were created using a co-transfection of a vector (pVgRXR) containing a heterodimer receptor that would bind to a hybrid ecdysone response element and a vector containing the cDNA of interest (pIND) (see Figure 3.2). In the presence of the inducing agent (Ponasterone), a stable transfectant can be established. Selection for this stably incorporated transgene was maintained with concurrent treatment of 100µg/ml G418 (#11811-023, Invitrogen) and 200µg/ml Zeocin (#R250-01, Invitrogen) antibiotics. These cells maintain their stability for at least 1.5 years when stored in liquid nitrogen; furthermore, the transgene is stable up to passage 25 once reconstituted.

The day prior to transfection, induction or differentiation (in the case of SH-SY5Y cells), cells were seeded onto poly-D-lysine coated glass coverslips and allowed to

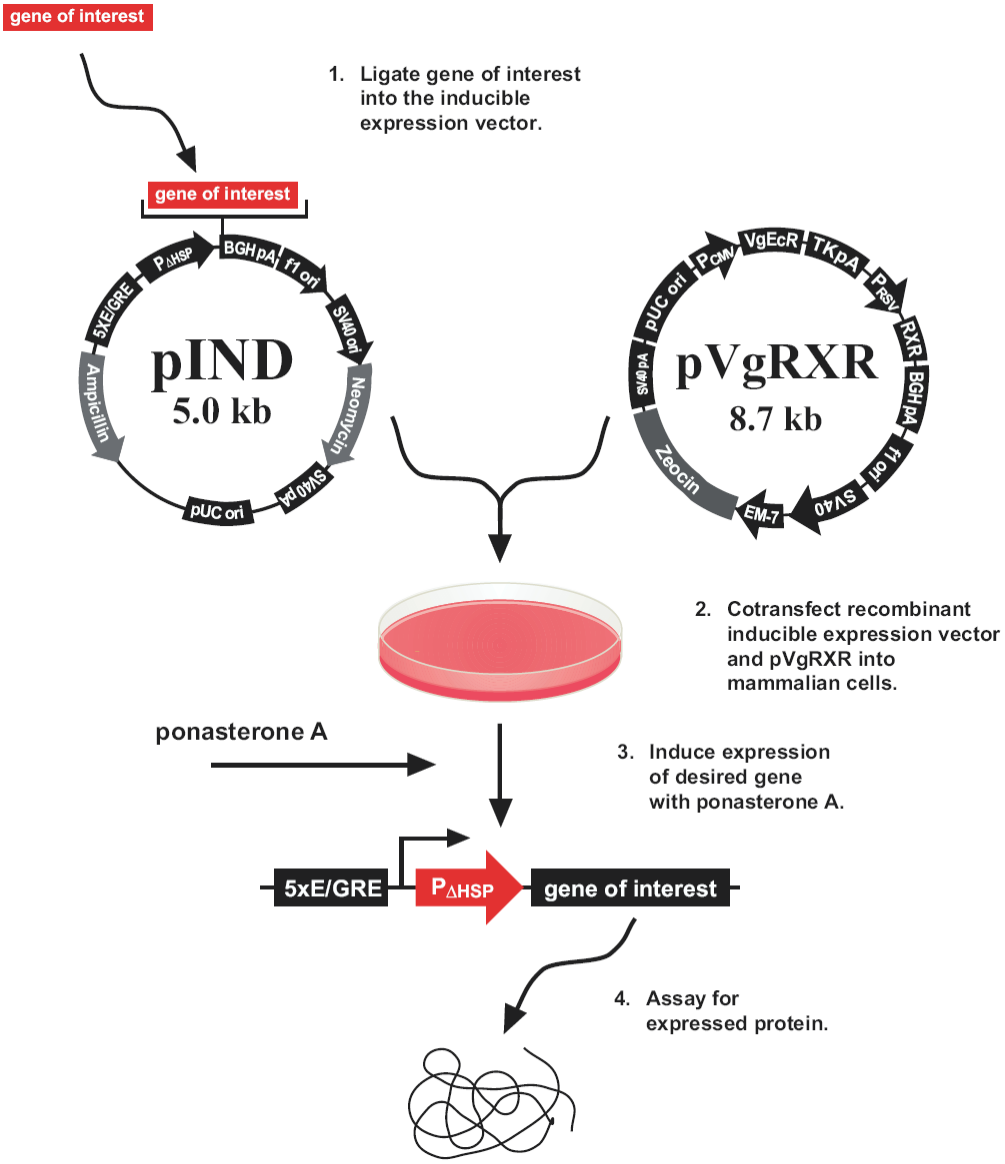

Figure 3.2: Ecdysone-inducible mammalian expression system. This is a schematic representation of how the htt-inducible cells were generated (Taken from [Invitrogen 2002]).

adhere for a minimum of 16 hours. PC12 cells were plated at a density of 150,000 cells/ cm^2 in either 6-, 12-, or 24-well microplates. SH-SY5Y cells were seeded at 50,000 cells/cm^2 density in 24-well microplates. SH-SY5Y cells were differentiated with 10μM RA for seven days prior to transfection. Htt-inducible PC12 cells were plated at a density of 50,000 or 100,000 cells/cm^2, depending on the length of time in culture, into a 24-well microplate.

DILUTION CLONING

We received four htt-inducible PC12 cell lines: 25QP, 47QP, 103QP, and Q103. Although all these cells were expressing the selectable marker, they were not uniform cell lines. In general, only a small percentage of these cells exhibited good expression of the transgene, as indicated by GFP fluorescence. To obtain a more uniform cell line, it was necessary to subclone. As received from the Thompson lab, only the Q103 cells had been subjected to subcloning and hence were enriched for a high percentage of htt-polyGln-GFP expressing cells. These cells had been subcloned, pooled, and flow sorted (MoFlo cell sorter, Cytomation, Fort Collins, CO) [Apostol, Kazantsev et al. 2003]. The other three cell lines were not of very high clonal integrity and needed to be enriched.

Dilution cloning, or subcloning, is a process by which a polyclonal cell population is serially diluted until a population of one or two cells has been achieved. This population, a subclone, is then plated and allowed to reach confluency. Ideally during cellular division, the characteristics of the original one or two cells will be passed on to the next generation of cells. By performing this technique, one should be able to achieve a fairly homogenous monoclonal population of cells.

Dilution cloning was performed as described in "Culture of Animal Cells. A Manual of Basic Technique" [Freshney 1987]. Cells were treated with Cellstripper (#25-056-CI, MediaTech) to detach the culture. Cells were resuspended in complete growth media (described in Section 3.2), counted, and serially diluted to achieve approximately one cell/100µl of media (10 cells/1ml of media). Once the correct dilution had been found, 100µl/well of cells were plated into 96-well plates and cultured until ~80% confluency had been achieved.

When the cells had reached this confluency, the cultures were detached and divided between a well in a 96-well microtiter plate and a well in a 24-well plate. The sample in the 24-well plate was maintained for continual growth. The sample in the 96-well plate was subjected to induction with 5µM ponasterone, and htt-polyGln-GFP expression was monitored for several days beginning 24 hours post-induction. Clones were chosen based on their percent GFP expression, and presumably percent htt-polyGln expression. The highest percentage of expressing cells was chosen as the most optimal clones.

Ideally, to match the Q103 cells, the samples should have also been flow sorted, which would have allowed for an even purer population of cells. This was not possible; however, even without the use of a flow cytometer, we were able to achieve a high clonal integrity with our cell lines.

TRANSFECTION

PC12 and RA differentiated SH-SY5Y cells were transiently transfected with the htt-Q_n-GFP constructs using the liposome-mediated LipofectAMINE PLUS™ reagent

(#18324-012 and 11514-015, Invitrogen), according to manufacturer's instructions. In this method of transfection a cationic lipid is mixed with the DNA to produce a positively charged liposome. The net positive charge of the liposome/DNA complex is attracted to the negatively charged plasma membrane. Upon their fusion, the liposome becomes engulfed by the cell where the DNA is then deposited and travels to the nucleus. It is unclear the exact mechanism that allows the DNA to cross the nuclear membrane [Felgner et al. 1987].

The day prior to transfection, PC12 cells were plated on poly-D-lysine coated glass coverslips at a density of 150,000 cells/cm^2. SH-SY5Y cells were plated at a density of 50,000 cells/cm^2 and differentiated for seven days with 10μM retinoic acid. In both cell lines, the DNA was complexed with the PLUS reagent at a ratio of 2μg DNA to 10μL PLUS reagent in 100μl of serum- and antibiotic-free media for 15 minutes at room temperature. During incubation, 10μl of LipofectAMINE reagent was diluted in 100μl of serum- and antibiotic-free media. The two mixtures were then combined and incubated for an additional 15 minutes at room temperature. Complete media was replaced by serum- and antibiotic-free media in each well prior to the addition of the liposome/DNA complexes. After the 15 minutes of incubation, the liposome/DNA complexes were gently mixed into each well and incubated at 37°C in 5% CO_2 for 5 hours; after which, fresh media containing twice the normal serum was added to each well. Coverslips were removed at 16, 24, 48, and 72 hours post-transfection, fixed and permeabilized (Section 3.2), and subjected to the polyGln-recruitment stain discussed in Section 3.3.

INDUCTION

At least 16 hours prior to induction, stable, htt-inducible PC12 cells were detached, counted, and plated at a density of 50,000 – 100,000 cells/cm^2 on poly-D-lysine coated glass coverslips located in 24-well microplates. Just prior to the addition of inducing agent, the growth media was exchanged for 1ml/well of fresh complete growth media. To each well, 5μM ponasterone (stock = 1.1mM in absolute, ethanol) was added. Cells were maintained under constant induction for 16, 24, 48, 72, 96, 120, 144, or 168 hours, with the induction media being changed every day. At each time point, the cells were fixed and permeabilized (Section 3.2) and subjected to the polyGln-recruitment stain discussed in Section 3.3.

Compound Treatment

In experiments where stable htt-inducible cells were treated with inhibitory compounds, the compounds were introduced simultaneously with the ponasterone. Curcumin has been shown to be an effective for its anti-inflammatory, anti-oxidant, anti-tumor, and most importantly, anti-amyloid compound [Kelloff et al. 1996; Lim et al. 2005; Yang et al. 2005]. The stock solution of curcumin was prepared at a concentration of 10mM in absolute ethanol. The day of induction curcumin was diluted into complete growth media to concentrations of 0.1, 1, or 10μM. Cells were treated for 24 hours; after which, they were fixed, permeabilized (Section 3.2), and subjected to the polyGln-recruitment stain (Section 3.3).

Two antimitotic compounds were also tested: nocodazole and demecolcine. These compounds have been shown to depolymerize microtubules [Luduena and Roach 1991; Nishiyama and Fujii 1992; Wang et al. 1998]. Demecolcine was dissolved in absolute ethanol to a concentration of 10mg/ml (27mM) then further diluted in ethanol to 2µg/ml. Prior to induction and compound treatment, dilutions were made in complete growth media to the final concentrations of 50, 200, 400, and 1000ng/ml. Treatment was continued for 24 hours then the cells were fixed, permeabilized, and stained for polyGln-recruitment competency and cell nuclei (Section 3.3).

Nocodazole was resuspended in ethanol to a concentration of 10mg/ml (33mM) and further diluted to 2µg/ml in ethanol. Before the cells were treated, dilutions were again made in complete growth media to concentrations of 50 and 400ng/ml. Cells were fixed, permeabilized, and stained with 100µg/ml Hoechst 33342 (stock solution was 10mg/ml diluted in water, #H-3570, Molecular Probes, Eugene, OR) for 30 minutes at 37°C. Hoechst fluorescent dye is a nucleic acid specific reagent that exhibits blue fluorescence upon excitation.

FIXATION AND PERMEABILIZATION OF COVERSLIPS

At the specified time points, coverslips with the attached transfected or induced cells were subjected to fixation and permeabilization. The process of fixation halts the life processes taking place within the culture; thereby preserving a snapshot of the culture for microscopic analysis. Permeabilization is necessary to gain access into the intracellular structures.

There are two widely accepted protocols for the fixation and permeabilization of cell cultures: 1) subquential treatments with acetone and methanol and 2) the use of a cross-linking reagent, such as paraformaldehyde, followed by a detergent permeabilization [Melan and Sluder 1992; Allan 2000]. Each method has been reported to stabilize both soluble and insoluble proteins in their native cellular locations [Melan and Sluder 1992].

In initial transient transfection experiments, coverslips were washed with 1X PBS, immediately fixed in acetone for 10 minutes, and allowed to air-dry overnight. The coverslips were permeabilized the following day by incubating in cold methanol (100%) for 5 minutes; after which, the coverslips were washed in Tris-buffered saline containing 0.01% Tween® 20 (TBST). This method, however, proved inefficient in our system due to the leaching of the GFP from the cellular cytoplasm [Kalejta et al. 1999]. All data shown were therefore obtained from cells fixed using a paraformaldehyde solution and permeabilized using 0.2% Triton® X-100 detergent.

Coverslips were washed with 1X PBS and fixed for 15 minutes at room temperature with Cytofix buffer (#554655, BD Biosciences, Rockville, MD), a neutral pH-buffered solution containing 4% paraformaldehyde. The coverslips were washed again with 1X PBS and permeabilized with cold 0.2% Triton® X-100 for 5 minutes. After permeabilization, the coverslips were washed with 1X TBST and subjected to the polyGln-recruitment stain detailed in Section 3.3.

3.3 Polyglutamine-recruitment Stain:

Upon fixation and permeabilization, the coverslips were subjected to the polyGln-recruitment stain (Figure 3.3), which relies on the specific ability of amyloid-like polyGln proteins to recruit biotinylated Q_{28} monomeric protein. After each addition or incubation, the coverslips were washed extensively with 1X TBST. Prior to incubation with the biotinylated monomer, coverslips were blocked with streptavidin / biotin (#SP2002, Vector Laboratories, Burlingame, CA) to eliminate any non-specific biotin binding. Briefly, cells were incubated with cold (4°C) streptavidin for 15 minutes followed by 15 minutes of incubation with cold (4°C) biotin.

After the blocking step was complete, cells were incubated with 100nM of biotinylated Q_{28} monomer (stock solution was 500nM) for 2 hours at room temperature. Several incubation times and temperatures were explored; however, the 2 hour, room temperature incubation provided the most consistent results with the lowest background. The coverslips were then incubated with 100µg/ml Hoechst 33342 (Molecular Probes) for 30 minutes at 37°C, washed, then incubated with a 1:200 dilution of a red streptavidin-conjugated Alexa Fluor® 594 (stock solution was 2mg/ml, #S-32356, Molecular Probes) for 1 hour at room temperature. This dye was used for the detection of the incorporated biotinylated monomer. Coverslips were washed exhaustively with 1X TBST followed by an extensive wash with distilled water to remove any salt precipitation from the previous buffer.

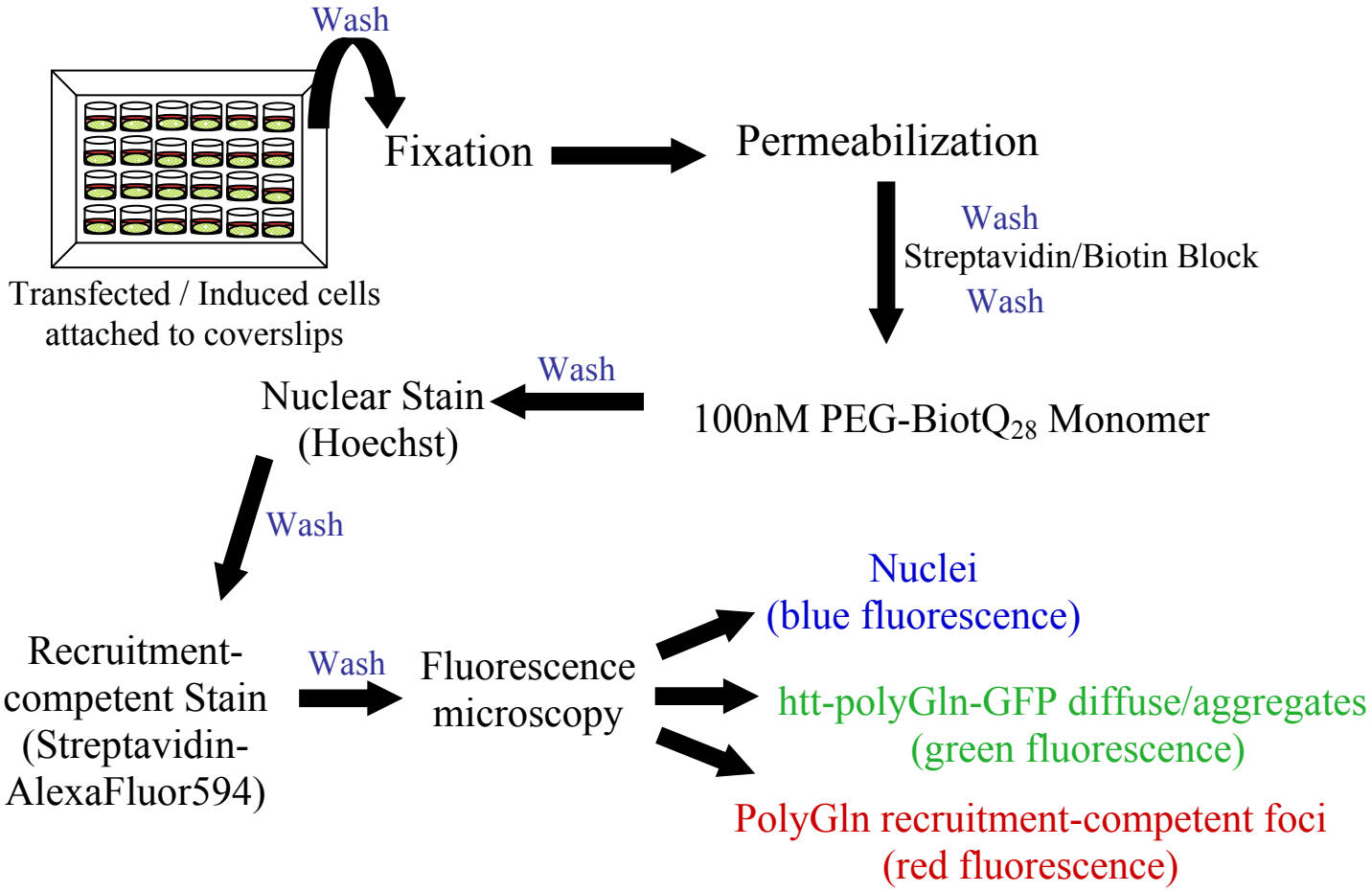

Figure 3.3: Schematic representation of polyGln-recruitment staining protocol. Transfected / induced cells were removed at various time points and subjected to the above staining protocol. Blue fluorescence represented cell nuclei (stained with Hoechst), green fluorescence was indicative of htt-polyGln-GFP expression, and red fluorescence represented polyGln recruitment-competent foci.

Coverslips were mounted onto slides with the cell-side up using an aqueous fluorescent mounting medium (#S3023, DakoCytomation, Carpinteria, CA), and a cover glass was applied for microscopic analysis. Green fluorescence was indicative of the htt-polyGln-GFP fusion constructs, blue fluorescence represented cell nuclei, and red fluorescence corresponded to polyGln recruitment-positive regions.

3.4 Microscopy and Flow Cytometry:

IMMUNOFLUORESCENCE MICROSCOPY

Images were obtained using a Leica DMRB fluorescent microscope equipped with a SPOT RT color camera (Diagnostic Instruments, Inc., Sterling Heights, MI) and SPOT Advanced, version 3.5.2 imaging software (Diagnostic Instruments). Data was analyzed using *Image-Pro Plus* software (Windows version 4.5, Media Cybernetics, Inc., Silver Springs, MD) or Adobe Photoshop 5.5 (San Jose, CA). The microscope was fitted with a brightfield differential interference contrast (DIC) analyzer, a DAPI/blue fluorescent protein (BFP) filter (excitation 360/40nm, emission 460/50nm, with a bandwidth 400nm), a Texas red filter (excitation 560/40nm, emission 630/60nm, bandwidth 595nm), and a FITC/GFP filter (excitation 480/30nm, emission 535/40nm, bandwidth 505nm). DIC microscopy utilizes the contrast between background and specimen to generate an image of the unstained structures. The DIC analyzer was used in conjunction with all experiments to observe overall cell morphology.

FLOW CYTOMETRY

Transient transfection efficiencies were initially confirmed using a FACScan (Becton-Dickinson, San Jose CA). Htt-Q_n-GFP expression was monitored by the excitation of the GFP fusions at 488nm (FL-1, 530nm emission). At least 10,000 events were collected for each sample. Data was analyzed using Cell Quest software version 1.2 (Becton-Dickinson).

3.5 MTS Reduction Assay:

Cell viability was determined using the CellTiter 96® AQ_{ueous} One Solution Cell Proliferation Assay (#G3580, Promega, Madison, WI) according to manufacturer's instructions. CellTiter 96® is a colorimetric assay that contains a tetrazolium compound MTS (3-(4,5-demethylthiazol-2-yl)-5-(3-carboxymethoxyphenyl)-2-(4-sulphophenyl)-2H-tetrazolium) and PES (phenazine ethosulfate, an electron coupling reagent), which is converted to water-soluble formazan by NADH- or NADPH-, presumably. The formazan product can then be quantified by measuring the absorbance at 490nm. Absorbance is directly proportional to the number of viable cells [Promega 2005]. MTS reduction is generally considered to be an indication of the health of cell mitochondria [Gschwind 1997]. When used previously to observe the response of PC12 cells to polyGln aggregates, MTS reduction gave a read-out entirely in agreement with other assays for cell viability, eg., lactate dehydrogenase release and propidium iodide exclusion [Yang et al. 2002].

Briefly, cells were detached, counted and seeded into 96-well microplates at least 16 hours prior to induction and/or compound treatment. Cells were induced with 5µM ponasterone as previously described (Section 3.2, Cell Culture and Treatment, Induction). At the appropriate time point, the inducing medium was exchanged for 100µl of complete growth medium/well. To each well, 20µl of CellTiter 96® AQ_{ueous} One Solution reagent was added, and the plate was incubated at 37°C for 4 hours. After incubation, absorbance readings were taken at 490nm on a Synergy™ HT multi-detection microplate reader (BioTek Instruments, Inc., Winooski, VT). Data were analyzed using Microsoft Excel 2000 (Microsoft Corporation).

3.6 Preparation and Fractionation of Cell Lysates:

PREPARATION OF CELL LYSATES

There are two common techniques for the lysis of cells: 1) physical means or 2) the use of detergents. Lysis by physical means employs a method that physically ruptures the cell membrane. Sonication, freeze/thawing, and grinding are a few examples of physical lysis. There are some drawbacks associated with this technique. Often during physical disruption, a localized heating may occur, which can lead to the denaturation or aggregation of cellular proteins[Alberts 1994]. Another problem is the lack of consistency with making lysates. Cells are not homogenous and will therefore dissociate at various rates. Because of this, there is little control over the rate and extent of cellular components being disrupted[Alberts 1994].

The other means of lysing a cell is by the use of detergents. Detergents disrupt the lipid barrier surrounding the cells by solubilizing the proteins and interfering with the interactions that hold them together. This type of lysis is generally milder than physical disruption. However, detergent lysis is often used in conjunction with sonication for a more complete means of releasing cellular proteins. There are several detergents available: ionic, zwitterionic, and nonionic. The latter two types are less denaturing than the ionic detergents, which tend to destroy protein activity. Various detergents have been shown to have different capabilities of dissolving aggregates. For example, SDS (sodium dodecyl sulfate) treatment has been shown inefficient at dissolving late-stage fibrillar htt aggregates [Davies et al. 1997; DiFiglia et al. 1997; Kazantsev et al. 1999]; whereas, early forming htt exon-1 aggregates have been found susceptible to treatment with the detergent [Poirier, Li et al. 2002]. Although there are no formal guidelines for choosing the proper detergent for studying aggregates, we tried to choose a detergent that has not been shown to have solubilizing effects on polyGln aggregates.

We chose to use detergent lysis followed by sonication in order to release the cellular proteins. Triton® X-100 is a nonionic detergent that is commonly used for the isolation of proteins [Barbero et al. 1984]. Triton® X-100 was chosen largely because it was also used we used during our polyGln recruitment stain. Cell lysates were prepared from htt-inducible cells using a balanced salt solution containing the following constituents: 150mM sodium chloride (NaCl), 0.1% Triton® X-100, 50mM Tris, 50mM HEPES, 1mM EDTA (ethylenediamine tetraacetic acid), and a cocktail of inhibitors of various classes of proteases (#P8340, Sigma-Aldrich). The addition of protease inhibitors

was necessary to prevent the unwanted proteolytic degradation of the sample [Roskams 2002].

At specified time points that correlated with the microscopic data, i.e., 24-72 hours post-induction, cells were detached, counted, and disrupted using the lysis buffer. Cell lysates were prepared at a density of ~$2.0x10^7$ cells/200µl of lysis buffer. Whole cell lysates were sonicated for 20 seconds and divided into two portions, one of which was retained for analysis at a later time. The other portion was subjected to fractionation by either centrifugation or gel filtration. Lysates were prepared, snap frozen, and stored at -80°C for future analysis. Protein concentrations were determined using the Coomassie Plus – Better Bradford Assay (#23236, Pierce, Rockford, IL).

FRACTIONATION BY GEL FILTRATION

Two separate methods were used to isolate the observed polyGln species: 1) size exclusion chromatography (gel filtration) and 2) differential centrifugation. Gel filtration is used to separate proteins based on their size, where larger proteins elute faster than smaller proteins.

Q103 lysate samples were sonicated briefly, and 200µl (~8mg/ml) of the total sample was loaded onto a Sephacryl® S500HR resin (#S500HR-100ML, Sigma-Aldrich). The same buffer used for cell lysis was also used for protein elution. Fractions were collected immediately and until triple the bed volume (10ml) had been achieved. A total of 67 fractions were collected in 500µl volumes each. After the fractions had been collected, absorbance readings at 280nm (wavelength specific for proteins) and protein concentrations were obtained for each sample.

FRACTIONATION BY DIFFERENTIAL CENTRIFUGATION

Differential centrifugation relies on the fact that there are many proteins with different masses within the cell suspension that will separate at different rates. For this reason whole cell lysates (W) were subjected to two centrifugation speeds: a slower speed to pull down the larger particles and a higher speed to collect the smaller aggregated species (refer to Figure 3.4). The samples were briefly sonicated and centrifuged at 15,000xg for 30 minutes at 4°C. The supernatant (S1) was transferred to a new tube, and the pellet was washed twice with lysis buffer. The combined washes and supernatant (S1) from the first centrifugation was subjected to a 100,000xg spin for 30 min at 4°C. Both the pellet from the 15,000xg (P1w) and the pellet from the 100,000xg (P2) were resuspended, separately, in lysis buffer. Protein concentration was determined on each fraction (W, P1w, P2, and S2 – final supernatant fraction) before further analysis. Our hypothesis was that the P1w fraction would contain the largest aggregates; the P2 fraction would contain the smaller, nuclear aggregates and aggregation foci; and the S2 fraction would contain monomeric protein. Fractionation by differential centrifugation provided a good way for separating the large aggregates from the smaller aggregates and monomeric protein. Several wash steps had to be introduced in order to release the sticky proteins from cellular debris. However, this method proved useful for the crude separation of proteins.

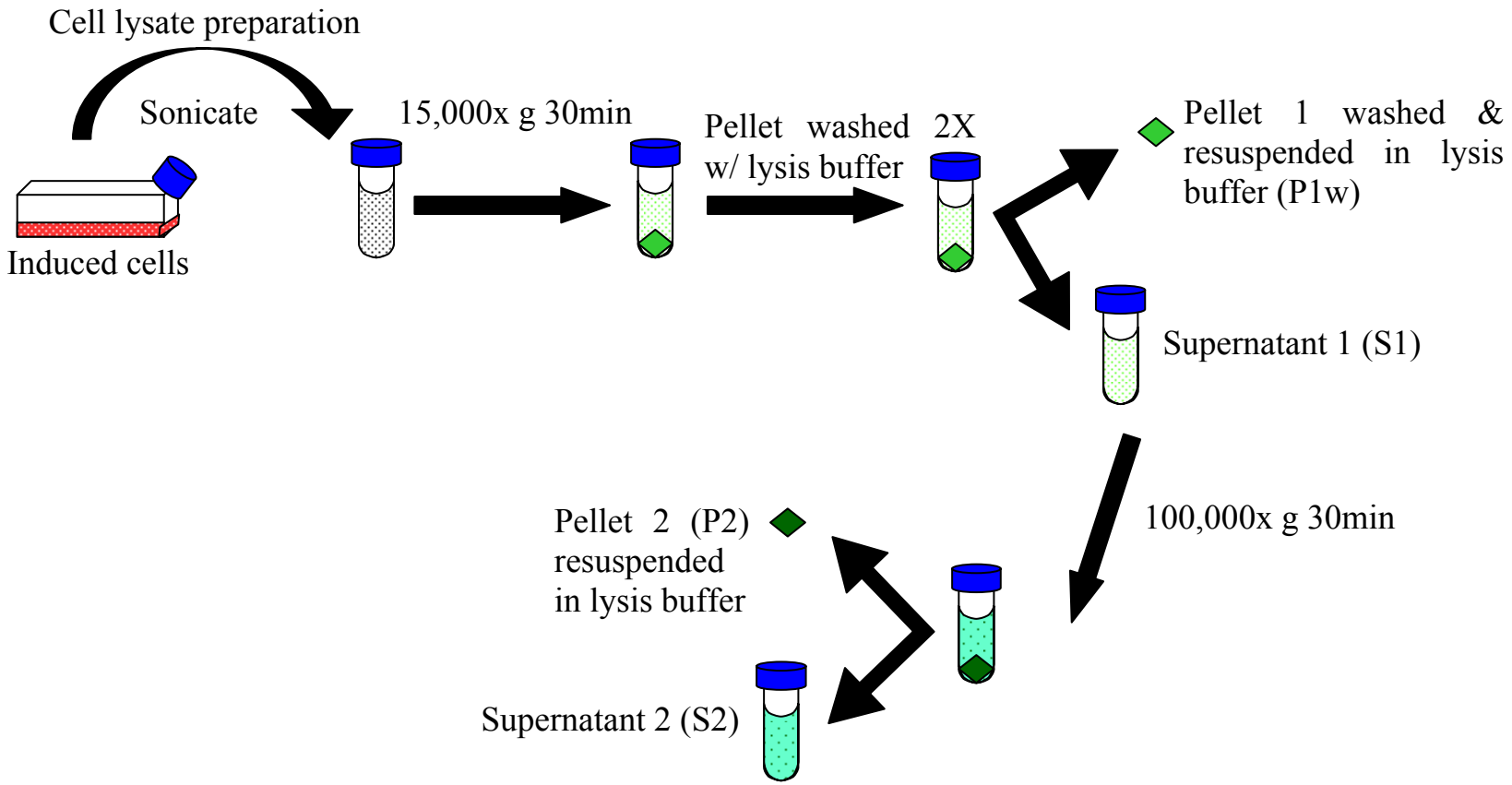

Figure 3.4: Schematic representation of polyGln aggregate isolation protocol by differential centrifugation. Cell lysates are prepared from cells 24-72h post-induction. The lysates were subjected to a medium and low speed centrifugation step. Both pellet (P1w and P2 – aggregated species) and supernatant (S2 – monomeric species) fractions were analyzed for protein content**.**

3.7 Protein Gel Electrophoresis and Western Blot Analysis:

PROTEIN GEL ELECTROPHORESIS

The fractionated cell lysates were then subjected to protein gel electrophoresis (a technique used for separating proteins according to their net charge: smaller proteins migrate faster than large ones) and Western blot analysis. Commonly, protein separation is performed on polyacrylamide gels [Laemmli 1970]. Proteins are often found in complexes or aggregated states. When the goal of an experiment is to study individual proteins or gain information about the non-aggregated state, it is important to denature the protein prior to loading the sample onto the gel. SDS is an ionic detergent that is commonly used for this purpose. SDS treatment abolishes the effects of any differences in shape, so proteins are separated solely on their masses.

Two gels were loaded with equal amounts of material (~9µg/well prepared from ~$2x10^7$ cells) were loaded into a 10-well pre-cast NuPAGE® (polyacrylamide gel electrophoresis) 4-12% Bis-Tris gel from Invitrogen Corporation (#NP0321BOX) and subjected to electrophoresis under denaturing conditions (according to manufacturer's instructions). After which, one gel was stained with Coomassie Blue (a protein specific dye) and the proteins from the other gel were electrotransferred onto 0.2µm nitrocellulose membranes (#LC2000, Invitrogen) using the XCell II Blot Module (#E19051, Invitrogen). Transfer of the proteins took ~2 hours at 35 Volts.

WESTERN BLOT ANALYSIS

Nitrocellulose membranes containing the cell lysate proteins were analyzed for their reactivities to anti-GFP (#sc-8334, Santa Cruz Biotechnology, Santa Cruz, CA) and 1C2 (#MAB1574, Chemicon, Temecula, CA) (anti-polyglutamine) antibodies. Briefly, each membrane was blocked with 1% Casein (in TBST) for 1h and exposed to either the 1C2 or anti-GFP antibody at a 1:1,500 or 1:150 dilution, respectively, for 1 hour at room temperature. The membranes were washed with 1X TBST and then exposed to a horseradish peroxidase (HRP) conjugated goat-anti-mouse or rabbit secondary antibody (depending on the primary antibody) at a 1:10,000 dilution (Jackson Laboratories, Bar Harbor, ME) for 1 hour. After thoroughly washing the membranes with 1X TBST, Luminol (#sc-2048, Santa Cruz), a chemiluminescent product, was used to detect 1C2 and anti-GFP reactive protein bands. The membranes were exposed to autoradiography film and developed using Kodak supplies.

3.8 Microtiter Plate Extension Assay:

Centrifuged fractions of htt-inducible cell lysates were examined for their ability to support polyGln recruitment as measured by the microtiter plate polyGln extension assay [Berthelier, Hamilton et al. 2001]. Cell lysate material (~9µg/well) was coated into the wells of a 96-well plate and allowed to air dry overnight at 37°C. As a positive control for polyGln extension, synthetic $K_2Q_{47}K_2$ aggregates (80ng/well) were also immobilized in the microplates. The plates were thoroughly washed with extension buffer (1X PBS with 0.01% Tween® 20) and blocked for 1 hour in a 0.3% Gelatin solution. The

plates were again washed and incubated with 100µl/well of either extension buffer (negative control) or 100nM biotinylated Q_{28} monomer (the same concentration as used in the microscopy experiments) for 1-3 hours.

After monomer incubation, the plates were washed then incubated with 100µl/well of a 100ng/ml streptavidin-labeled Europium (Eu) solution (0.5% bovine serum albumin (BSA)) for 1 hour. The plate was again washed, and europium released by the addition of 100µl/well of an enhancement solution (#1244-105, PerkinElmer, Waltham, MA). Eu-incorporation was measured by time-resolved fluorescence in a Victor^2 1420 Multi-label Counter (EG&G Wallac, Gaithersburg, MD). Europium counts were converted to femtomoles using a determined standard curve.

CHAPTER 4

FLUORESCENCE METHODS FOR AGGREGATE DETECTION

4.1 Rationale:

It is well documented that polyGln aggregates are present in HD disease tissue, and in various models of HD and other CAG repeat diseases [DiFiglia et al. 1997; Ross 1997; Lunkes and Mandel 1998; Hackam et al. 1999; Kazantsev et al. 1999; Bates 2002; Marsh et al. 2003]; however, it is unclear the precise role they play in the disease mechanism. There have been much evidence supporting a toxic role of the aggregates themselves [Cooper et al. 1998; Hackam et al. 1999; Yamamoto et al. 2000; Kazantsev et al. 2002; Yang et al. 2002]; conversely, there is also speculation that the aggregates are not directly linked to toxicity [Cummings and Zoghbi 2000; Tobin and Signer 2000]. It has also been proposed that aggregates represent an end stage in an aggregation process with multiple steps [Ross and Poirier 2005]. This is suggestive that early events, including the formation of misfolded monomers [Weissmann 2005; Nagai et al. 2007] or soluble oligomeric/protofibrillar intermediates [Poirier et al. 2002; Bucciantini et al. 2004; Katsuno et al. 2004; Wacker et al. 2004; Mukai et al. 2005] accelerated by the expansion of the polyGln sequence, may actually be responsible for cellular toxicity. Nevertheless, there is not an agreement on which species actually exist in the cell and which are toxic; furthermore, it is also not known whether the intermediate species are "on-" or "off-pathway" in aggregate formation.

In vitro, polyGln proteins have been shown to form a host of aggregate types with different sizes, shapes, and functional characteristics [Wetzel 2006]. Among these, amyloid-like fibrils are highly ordered structures that are capable of growth by monomer addition [Lomakin et al. 1996; Lomakin et al. 1997; Berthelier et al. 2001; Chen et al. 2002; Collins et al. 2004; O'Nuallain et al. 2005]. Smaller polyGln aggregates were more potent, on a weight basis, than larger aggregates at recruiting biotinyl-monomer [Chen, Berthelier et al. 2001]. Currently, aggregate detection methods are not optimal and often rely on the fluorescence associated with fusion proteins for identification or antibodies that recognize the presence of polyGln sequences. Methods such as these may not be sufficient to recognize every aggregated species that might be present and may not be specific enough to distinguish among aggregate types and to detect the most toxic species. Therefore, much attention has been given to the need for more sensitive detection methods, which should help reveal the aggregation pathway.

In vitro discoveries in our lab [Berthelier et al. 2001; Chen et al. 2001; Chen et al. 2002] led to the development of a highly sensitive stain that recognizes areas active in recruiting free polyGln monomer [Osmand, Berthelier et al. 2006], allowing for the first time a functional staining method for better characterizing aggregated species. Initially, this stain was developed using HD patient and animal brain tissue, but its success in these settings raised the possibility that such an assay may also be beneficial in characterizing aggregates in cell culture. The polyGln recruitment stain was adapted and applied to various cell culture models. In this chapter, we will discuss the optimization of the new detection method, the problems and limitations of the technique, and the caveats of the microscopic evaluations.

In our cell models, htt-polyGln expression was monitored by the presence of a GFP-fusion tag. The GFP fluorescence yields two expression patterns: diffuse and punctate. Diffuse fluorescence, in such models, is assumed to be representative of monomeric species [Lunkes and Mandel 1998; Preisinger et al. 1999; Apostol et al. 2003], and punctate fluorescence is always used synonymously with the term "aggregate" [Fink 1998; Johnston, Ward et al. 1998; Lunkes and Mandel 1998; Garcia-Mata et al. 1999; Kazantsev, Preisinger et al. 1999; Preisinger, Jordan et al. 1999; Apostol, Kazantsev et al. 2003]. It must not be overlooked that punctate centers of fluorescence may also represent a collection of monomers trapped in an organelle, such as a lysosome, proteasome, or aggresome. However, for the purposes of this dissertation, this terminology will be adopted; therefore, "diffuse fluorescence" and "monomer" will be used interchangeably, as will "punctate fluorescence" and "aggregate". As will be seen later, this usage is validated by our experimental results. Aggregation foci (AF), which were identified using the new functional stain, are punctate sites found within the cell that actively recruit externally added polyGln monomer. AF and polyGln recruitment-competency will be used equivalently.

4.2 Detection by Fluorescence:

As mentioned above, the AF stain was originally developed in using HD patient and animal autopsied brains [Osmand, Berthelier et al. 2006]. This method was modified for the use in cell cultures (see Section 3.3). One modification to the original protocol was the method of detection. The preferred method for visualizing AF in cell cultures was fluorescence. Some major reasons for this was because our protein of interest already

had a fluorescent tag associated with it, and the use of fluorescence allowed for the ability to incorporate multiple colors (theoretically, as many as four) within the same experiment. For our experimental purposes, three fluorescent labels were utilized: 1) green – expressed upon transfection / induction of htt-polyGln-GFP fusion proteins, 2) blue – Hoechst dye used to stain the cell nuclei, and 3) red – streptavidin-conjugated Alexa Fluor® 594 dye used to detect biotinylated polyGln monomer (see Section 3.3). These three fluorescent labels were chosen for their different absorption properties, which made it possible for the simultaneous detection of multiple events / species (Figure 4.1).

4.3 Determination of the Correct Incubation Conditions:

The polyGln recruitment stain was optimized primarily in the transiently transfected cell models expressing htt-Q_{47}-GFP constructs. Various concentrations of biotinylated polyGln monomer (10nM, 50nM, 100nM, and 500nM) were incubated with fixed and permeabilized cells for 16 hours at room temperature (Section 3.3). The concentration that gave the most consistent results and the best fluorescence signal, while keeping the background to a minimum, was 100nM. After the optimal concentration had been decided, incubation times (1 hour – 16 hours) and temperatures (room temperature, 4°C, and 37°C) were varied. Incubation at room temperature provided the best signal-to-noise ratio, while incubation at 37°C provided excessive background, presumably due to the self-aggregation of the monomer. Irrespective of temperature below 25°C, incubation for 16 hours with the biotinylated monomer provided the best conditions for visualizing AF. These conditions were double-

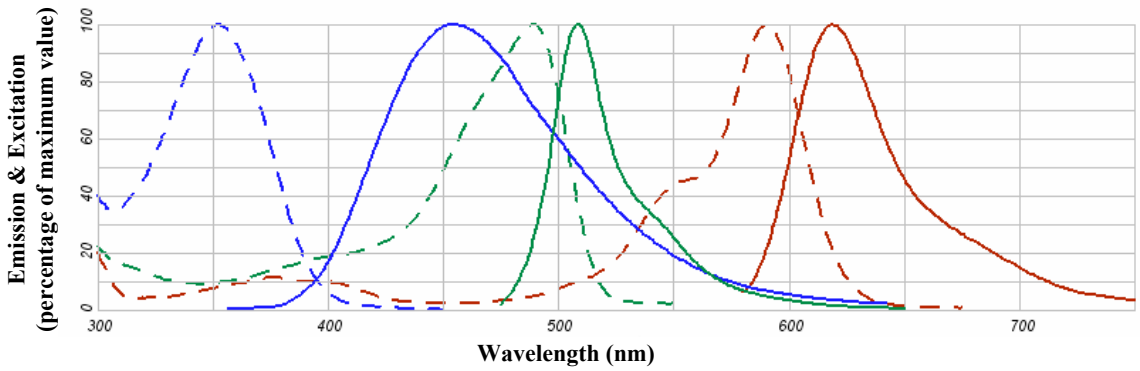

Figure 4.1: Absorption spectra of fluorescent dyes used for detection. Dashed lines represent the excitation spectra, while solid lines represent the emission spectra. Blue color is for Hoechst dye, green color is for GFP fusion proteins, and red color is for Alexa Fluor 594® streptavidin-conjugated dye. (Created using Spectra Viewer from Molecular Probes – http://probes.invitrogen.com/servlets/spectraviewer?fileid1=11005p72).

checked with the stably transfected PC12 cells, and polyGln recruitment competency was slightly diminished after prolonged incubation (16 hours) with 100nM of the biotinylated monomer; therefore, the protocol was modified such that incubation with 100nM biotinylated polyGln monomer was carried out at room temperature for 2 hours prior to staining (Figure 3.3). Figure 4.2 shows the optimal conditions for both the transiently transfected cells and the stably transfected PC12 cells.

4.4 Image Exposure Time Variations:

When working with different fluorescence entities, one problem that is often encountered is the various camera exposure times that are required for each fluorescent dye and for varying degrees of fluorescent intensities using the same fluorochrome. An example of the latter is the situation in which both monomer and aggregate were present within the same microscopic field. Monomeric expression had much less fluorescence intensity than an aggregated structure. This is probably due to the concentration of the protein at any one location or the compact folding of the htt- polyGln-GFP protein, which presumably brings many GFP into close proximity creating a much more intense object.

In order to collect interpretable data, two exposure times of the green image where taken so that both types of species could be more properly characterized (Figure 4.3). The first exposure was taken at 500 milliseconds (msec) to capture the diffuse entities, while the second image was exposed using the automatic / default exposure time (< 1 msec). Images taken from both exposure times are necessary so that all species can be accounted for. Exposure times for red images also had to be modified from the normal default settings of the camera. All red images were photographed first in the series and

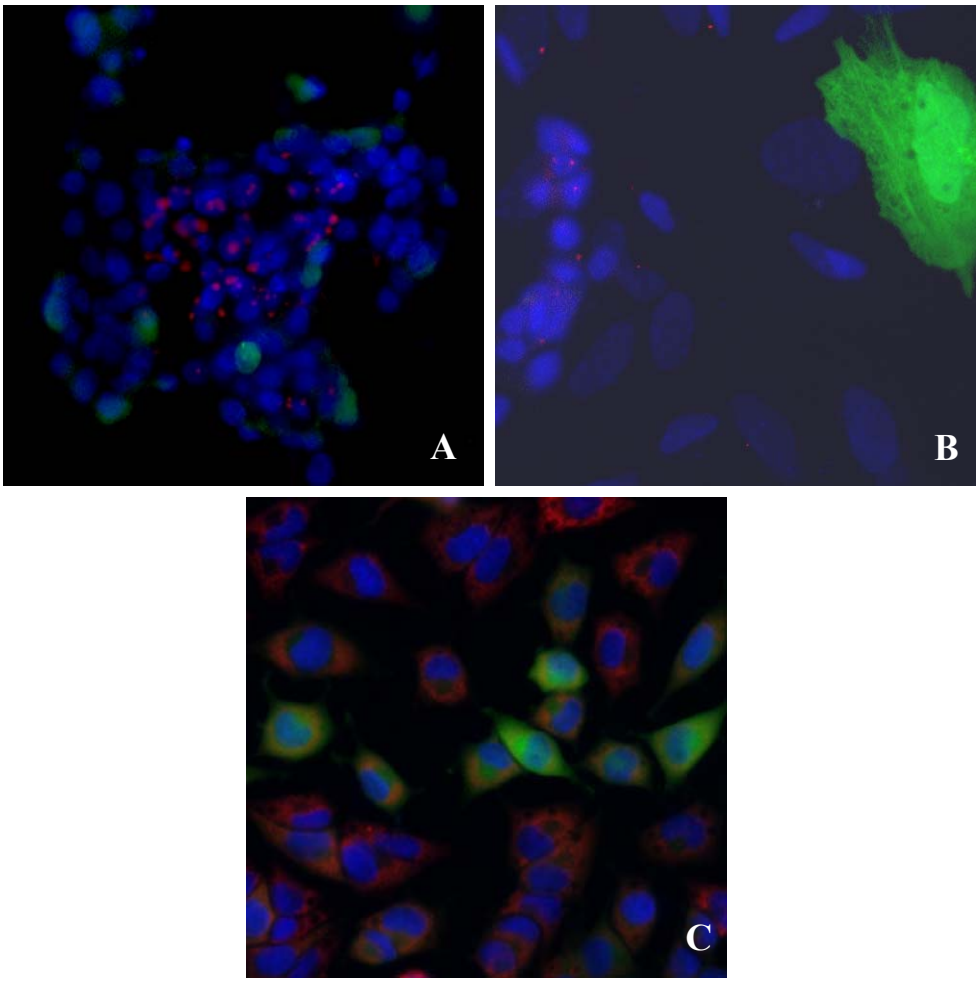

Figure 4.2: Optimal AF staining conditions in a transient and stable htt exon-1 cell models. *(A) Transiently transfected PC12 cells expressing htt-Q_{47}-GFP constructs. (B) SH-SY5Y cells transiently transfected with htt-Q_{47}-GFP constructs.* 100nM biotinylated monomer was incubated for 16 hours at room temperature before staining in each of the transient models. *(C) Stable 47QP PC12 cells.* 100nM biotinylated monomer was incubated for 2 hours at room temperature prior to staining. Fluorescence color is blue for cell nuclei, green for htt-polyGln-GFP proteins, and red for AF.

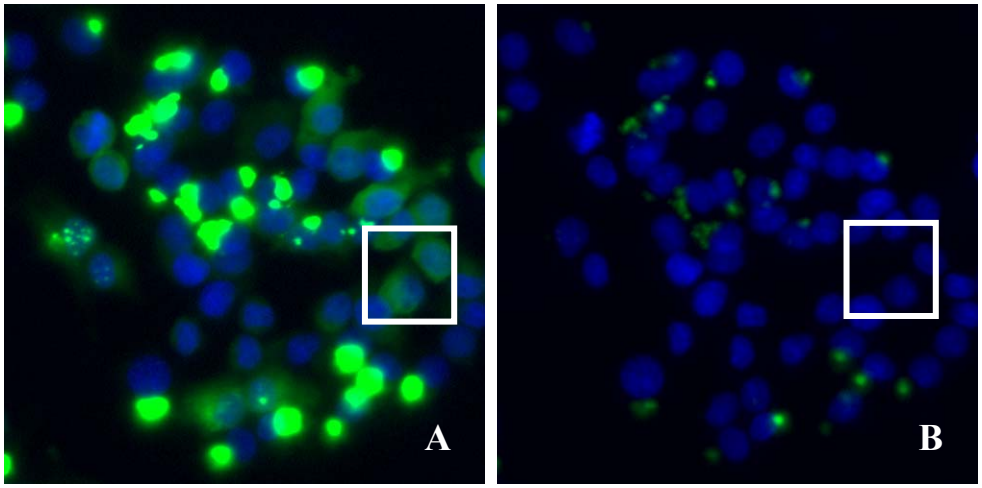

Figure 4.3: Various exposure times needed to photograph different fluorescence entities. Both images are of the same field of stable 103Q cells 24 hours post-induction. *(A) 500 msec exposure time. (B) <1 msec exposure time.* Blue color is cell nuclei and green color is htt-polyGln-GFP protein. The white box shows that diffuse protein was photographed only when the longer exposure time (A) was utilized, which caused the aggregated species to be overexposed. Therefore, two exposures of such images were necessary to account for all species present.

captured at a 1 second exposure time to account for the diminished fluorescence intensity and the photobleaching of the Alexa Fluor 594® dye. Blue images were exposed to the camera using the default settings and were the last fluorescence images taken in the series because of the high stability of the fluorochrome.

Development and optimization of the AF stain allowed, for the first time in cell cultures, the observation of a class of aggregates capable of further growth by monomer addition, as is especially evident in Figure 4.2C. This new technique promised to be very beneficial in characterizing multiple aggregated species and their roles in the aggregation pathway.

4.5 Fluorescence Microscopy Caveats:

As will be shown later, we identified a number of morphological forms of htt exon-1 in our cell models, including dispersed fluorescence normally interpreted as monomeric protein, as well as several different types of aggregates. It is appropriate in this discussion of the fluorescence microscopy to include some caveats and rationales for some of the assumptions we make in the interpretation of our microscopy data.

There were limitations to the types of analysis that could be performed using a two dimensional imaging system. For example, subcellular localization of the protein (nuclear/cytoplasmic or co-localization) could not be irrefutably confirmed. In many images presented throughout this dissertation, there will be an apparent co-localization of the different polyGln species. The only thing that can be said for certain is that, in the case of co-localization, the two species, were in the same cellular location (Z-plane), and without the use of a three dimensional imaging system, such as confocal microscopy, we

could not exclude the possibility that the two species were, perhaps, independent and not co-localized. The same is true for the question of nuclear vs. cytoplasmic localization. The appearance of nuclear accumulation may actually be cytoplasmic accumulation located in the volume above or below the nucleus. More images will be presented throughout this dissertation that appear to exhibit co-localization or nuclear distribution, but when interpreting the data, one cannot must consider the alternative interpretations. This problem is more difficult to resolve in the case of determining with certainty whether aggregates are in the nucleus. In contrast, when a cell contains a limited number of punctuate green objects, and the only red objects observed are found to exactly co-localize with them, it seems unlikely that these objects are not truly co-localized; however, the possibility remains that they are distinct.

Another limitation of the imaging method is the question of whether diffuse green fluorescence is actually indicative of monomer. As stated earlier, a diffuse staining pattern, like as observed in our cells, is often interpreted as monomeric species [Lunkes and Mandel 1998; Preisinger et al. 1999; Apostol et al. 2003]. However, in our experiments at least, the "diffuse green" areas often have a speckled appearance and don't always provide a uniform distribution. It might thus be argued that the granular appearance of these "diffuse green" areas might arise from a field of microaggregates (or htt-polyGln-GFP in organelles/lysomes/proteasomes) rather than monomeric protein. However, this granular appearance most likely is a consequence of the camera exposure time needed to capture the diffuse pattern (Section 4.4). This question could not be addressed by fluorescence microscopy – at least not with the available equipment – but instead was addressed by other, biochemical experiments (presented in Chapter 8).

CHAPTER 5

DEVELOPMENT AND EVALUATION OF CELL MODELS EXPRESSING HTT EXON-1 CONSTRUCTS

5.1 Rationale:

Implementation and optimization of the AF stain were explored in two types of cell models: transient and stable. Transient models were explored first, as the most straightforward approach, while stable, htt-inducible models were utilized in later experiments and were found to be the superior model system. In this chapter, we will discuss the development of each of these cell model systems (transient and stable) expressing htt exon-1 constructs, the limitations, and the problems encountered along the way.

5.2 Transient Cell Models Expressing Htt Exon-1:

For these experiments, PC12 and SH-SY5Y cells were transiently transfected with truncated htt exon-1 constructs expressing Q25, 47, 65, and 103 (as described in Sections 3.1 and 3.2). Protein expression was monitored by virtue of the GFP tag associated with the htt exon-1 constructs and was calculated at 24 hours post-transfection. Therefore, no matter the expression pattern, diffuse, punctate, or AF, the images were scored the same: expression or no expression. Total htt-polyGln expression was similar for each cell line (Figure 5.1) and aggregation occurred in a polyGln length-dependent manner (Figure 5.2). Data obtained from the flow cytometer was a measure of cells

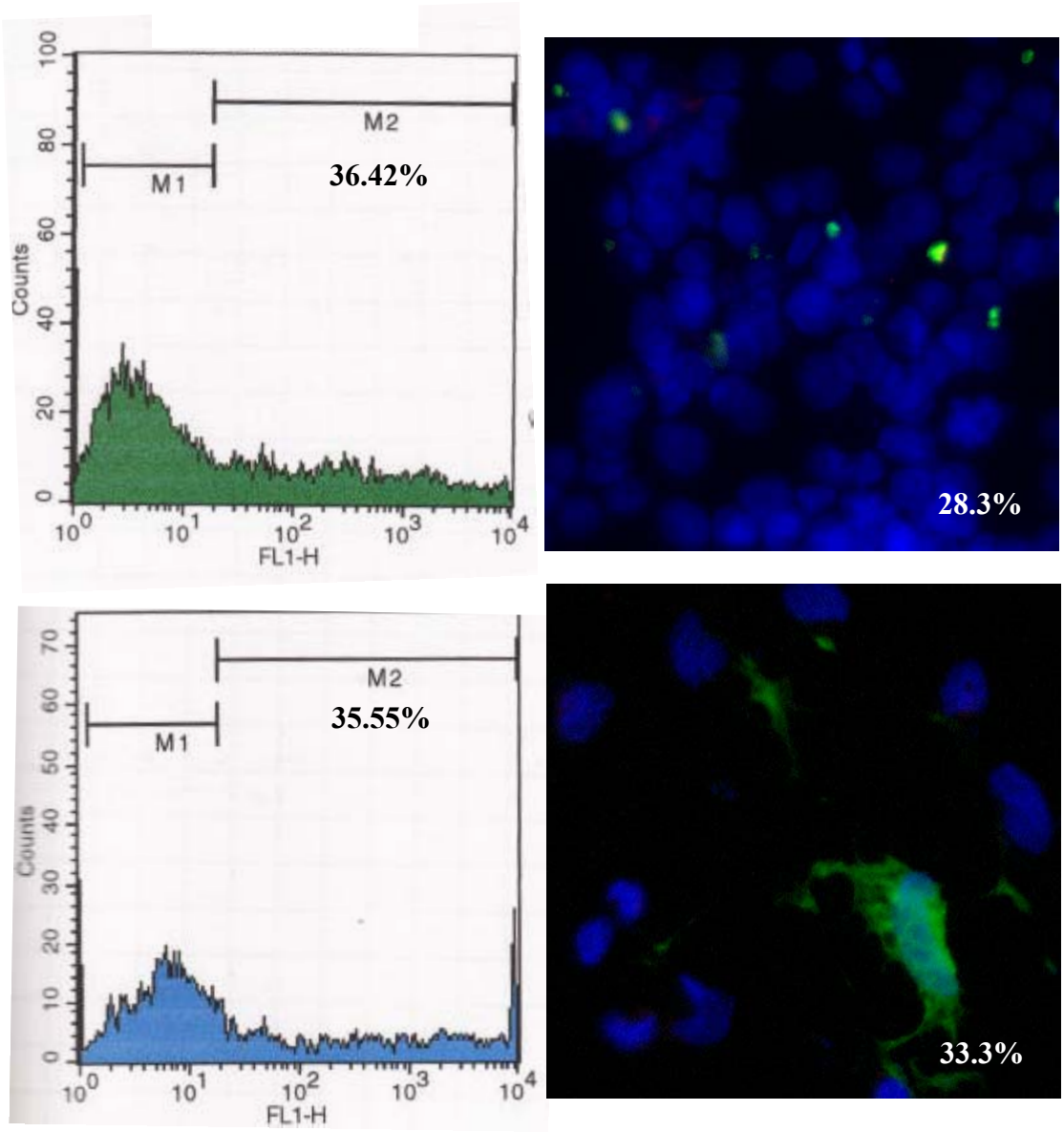

Figure 5.1: PolyGln expression was similar by flow cytometry and immunofluorescence. Flow cytometry data are shown in the left panels. M2 represents polyGln expression. Right panels are fluorescence microscopy images: blue – nuclei, green – htt-polyGln-GFP. Top row is data from PC12 cells transiently transfected with htt-Q65-GFP at 24 hours post-transfection. Bottom row is SH-SY5Y cells transiently transfected with htt-Q47-GFP at 24 hours post-transfection.

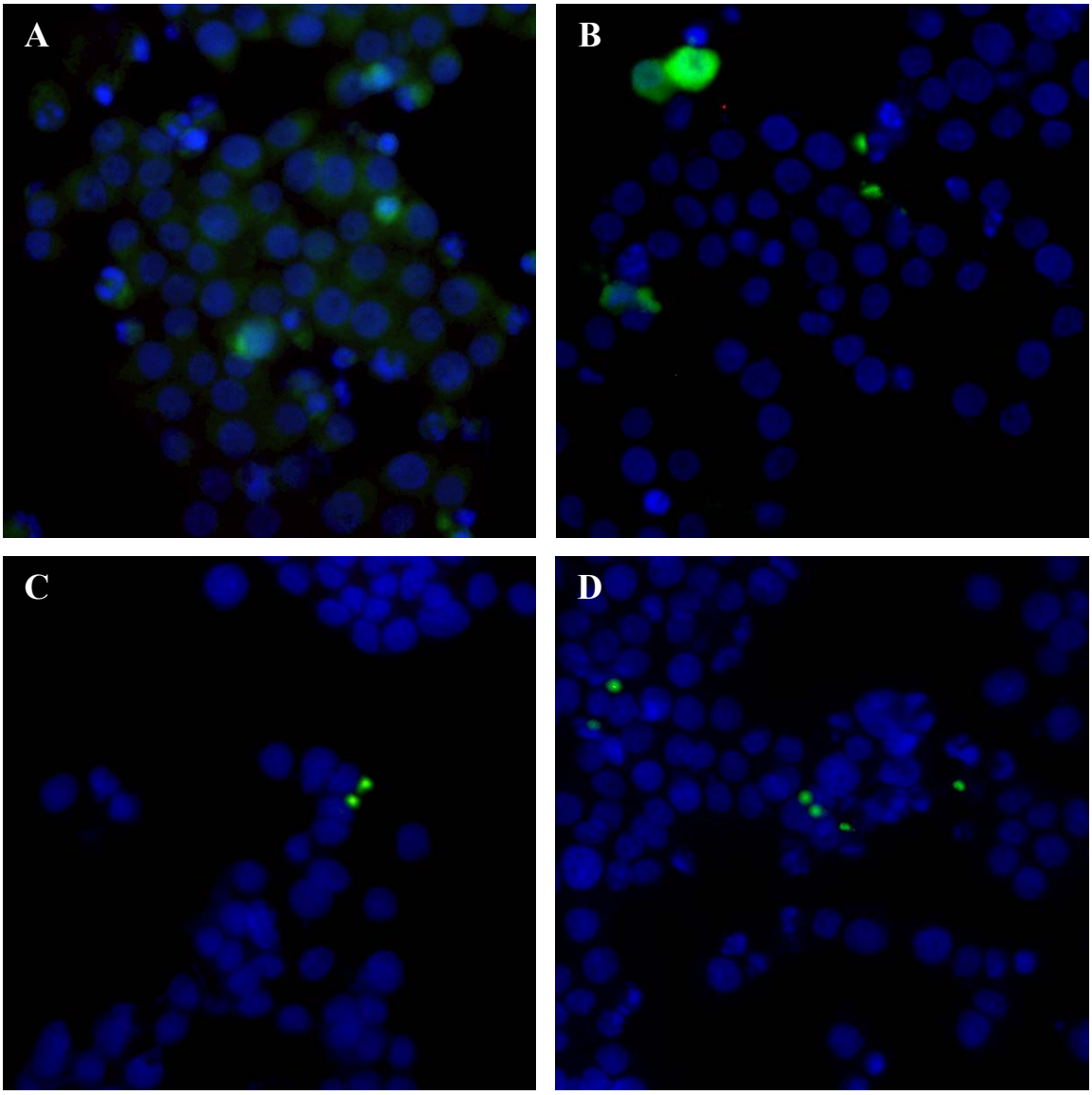

Figure 5.2: Aggregation occurs in a polyGln-length dependent manner. PC12 cells were transiently transfected for 24 hours with various lengths of htt-polyGln-GFP constructs. *(A) Q25, (B) Q47, (C) Q65, (D) Q103.* Fluorescence color is blue for cell nuclei and green for GFP fusion constructs. Cells were exposed to the AF staining procedure as well but exhibit no red AF above background. Aggregation was faster when cells expressed longer polyGln repeats.

exhibiting GFP fluorescence and did not necessarily reflect any species that exhibited AF, while microscopic measurements were calculated by counting cells that exhibited all types of htt-polyGln fluorescence (red and/or green) and dividing by the total number of cells in the microscopic field.

For microscopic experiments, SH-SY5Y cells were differentiated in order to aid in cellular attachment. However, experiments involving PC12 cells were performed without differentiation because the cells did not possess the same detachment properties that were observed with SH-SY5Y cells (Section 3.2). Figures 5.3 and 5.4 show a temporal progression of polyGln expression in transiently transfected PC12 and SH-SY5Y cells, respectively.

Cells expressing htt exon-1-Q25-GFP exhibited a faint, diffuse green fluorescence throughout the cytoplasm (PC12 and SH-SY5Y cells) and/or the nucleus (SH-SY5Y cells) at all time points studied and never showed any aggregation foci. In contrast, cells transfected with htt exon-1-Q47, 65, or 103-GFP produced two types of aggregates (Figure 5.5). One class consisted of punctate green-fluorescent aggregates that developed by 24 hours and whose numbers correlate with polyGln-repeat length (Figure 5.6). These aggregates were primarily located just outside the cell nucleus (perinuclear) in the PC12 cells with some apparent localization in the nucleus for SH-SY5Y cells. The second class of aggregates were recruitment-competent but at the same time not observable by GFP fluorescence. These were more evident in cells expressing htt exon-1-Q47 and Q65-GFP, and tended to form at early time points (Figure 5.6). Aggregates that exhibited GFP fluorescence appeared to be coincident with AF at early time points (Figures 5.3 – 5.6), but, as the cells aged, less co-localization was observed.

Figure 5.3: Transiently transfected PC12 cells expressing various polyGln-length constructs. Blue – nuclei, Green – htt exon-1-Qn-GFP, Red – aggregation foci. **(a)** Columns from left to right represent the various lengths of polyGln constructs expressed in PC12 cells. Rows from top to bottom show the temporal progression of polyGln expression from 16 hours to 72 hours post-transfection. A magnification for observing specific detail will be provided for pictures of particular interest. For example, at 16 hours and 12 hours post-transfection with htt-Q47-GFP and htt-Q65-GFP, respectively, a class of aggregates form that are recruitment-positive but do not exhibit green fluorescence **(b)**. GFP aggregates are often found superimposed on AF in the same focal plane, yielding a yellow color mix which represent co-localization, as shown in cells transfected with htt-Q65-GFP for 24 hours **(c)**.

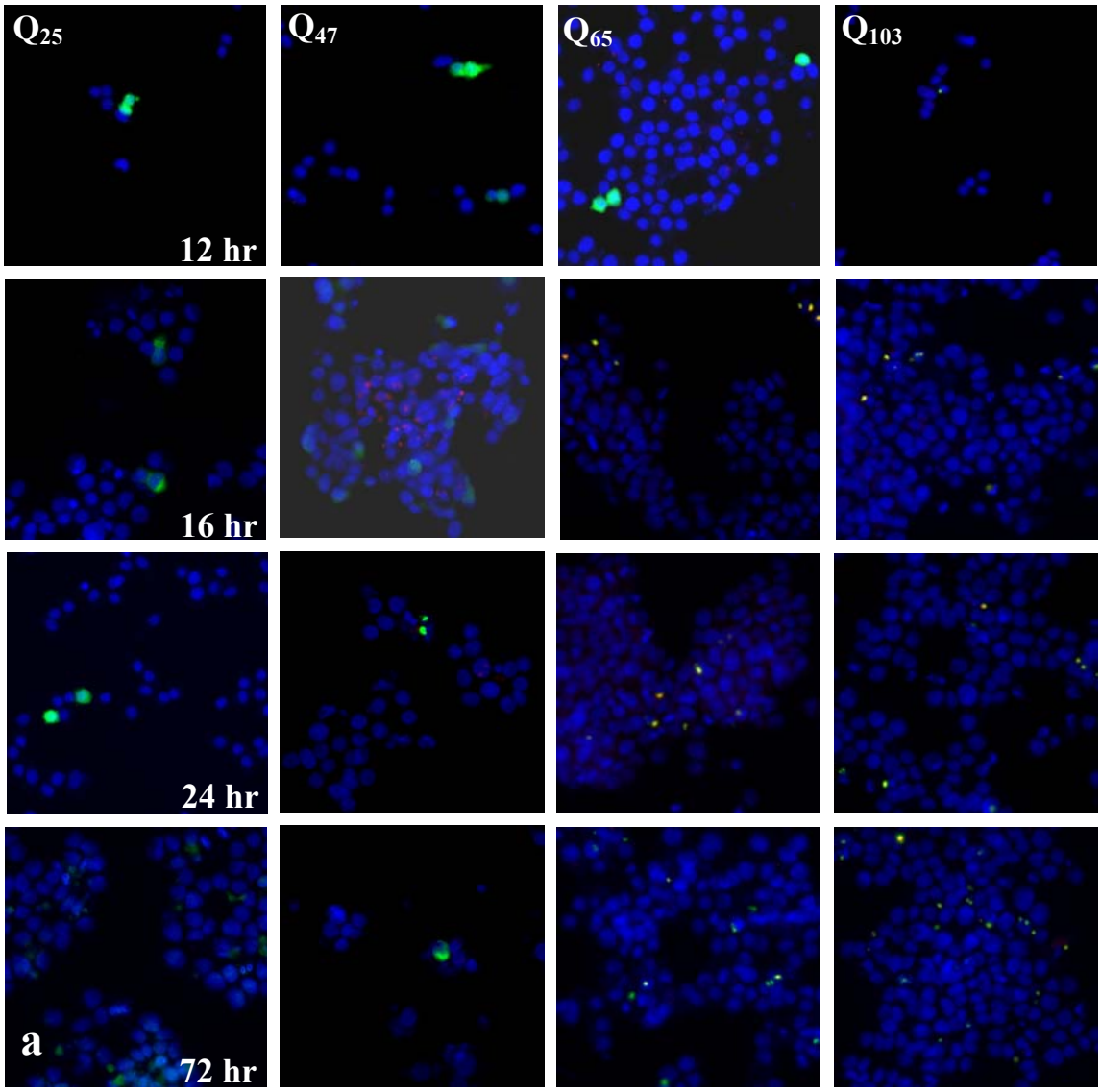

Figure 5.3. Continued.

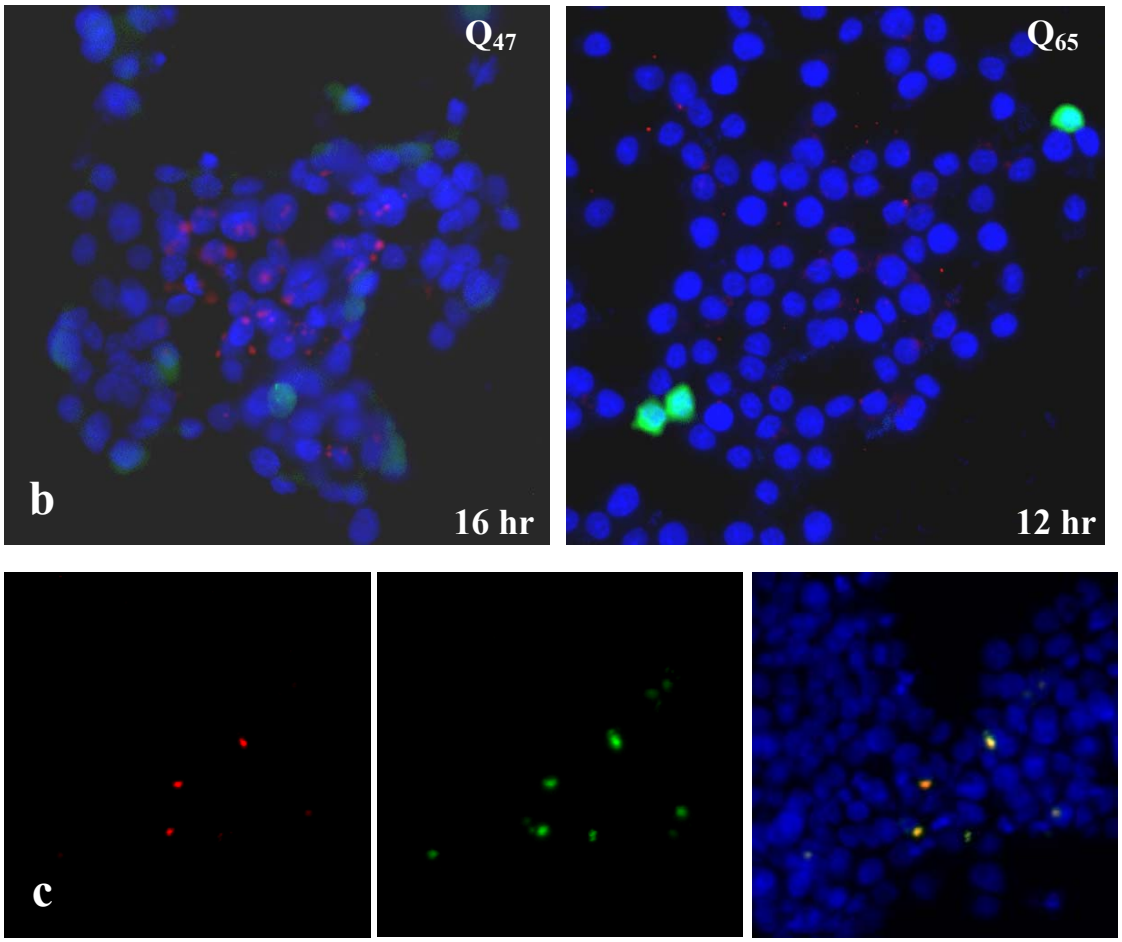

Figure 5.3. Continued.

Figure 5.4: Transiently transfected retinoic acid differentiated SH-SY5Y expressing various htt exon-1-Qn-GFP constructs. Blue – nuclei, Green – htt exon-1-Qn-GFP, Red – aggregation foci. **(a)** Columns from left to right show the different polyGln lengths expressed in cells. Rows from top to bottom show the time-dependent manner of polyGln expression. At 24 hours post-induction, SH-SY5Y cells transitioned from a mostly adherent cell line to a mostly floating cell line. A magnification for observing specific detail will be provided for pictures of particular interest. At 12 and 16 hours post-transfection with htt-Q47-GFP AF were the predominant species **(b)**. GFP aggregates are often found in the same focal plane as AF, which represent co-localization, as shown in cells transfected with htt-Q65-GFP for 16 hours **(c)**

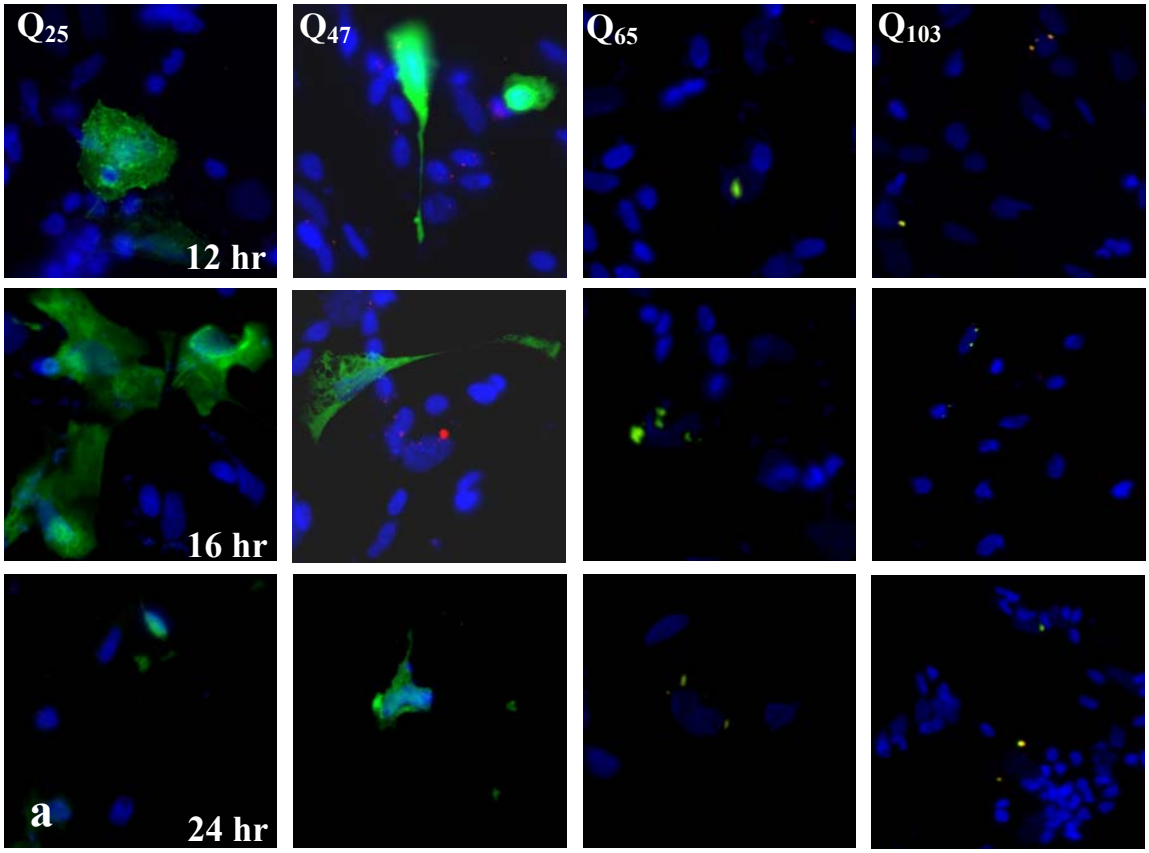

Figure 5.4. Continued.

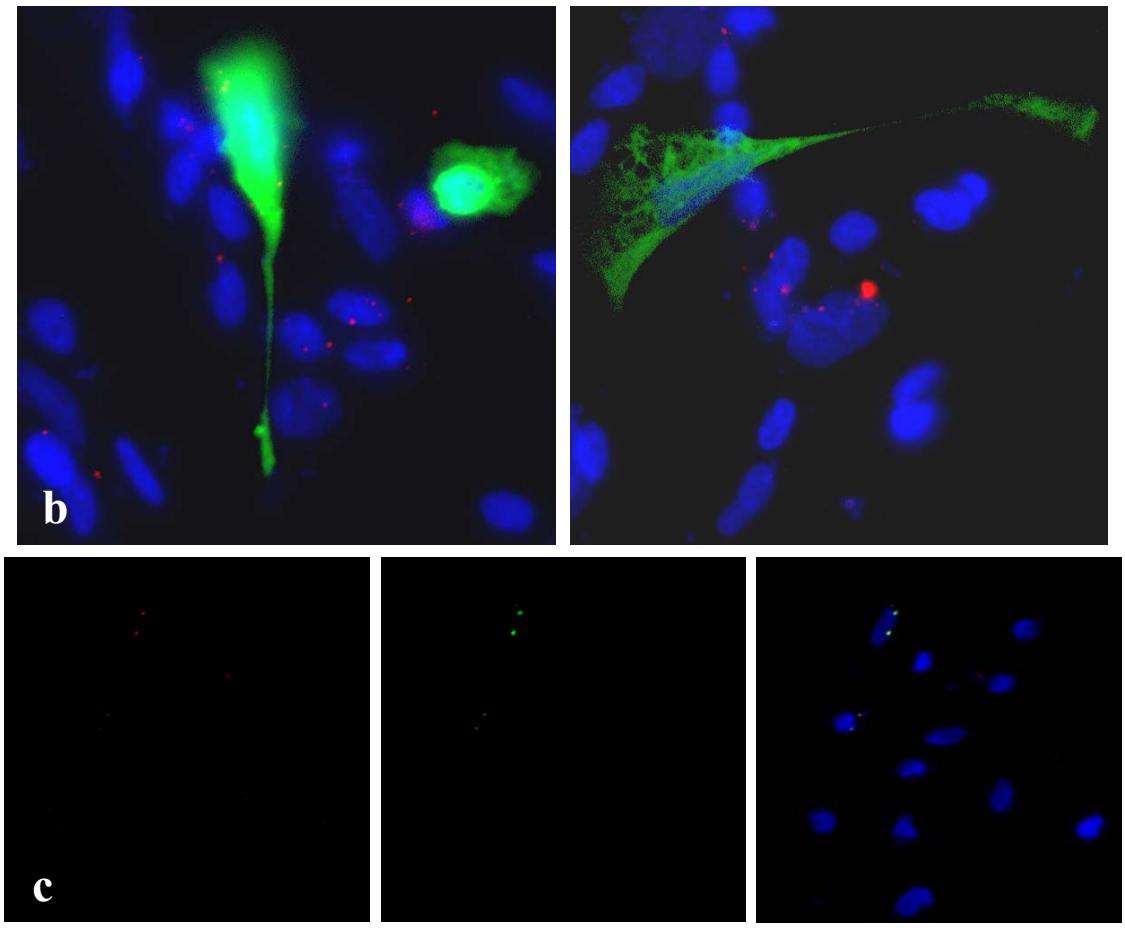

Figure 5.4. Continued.

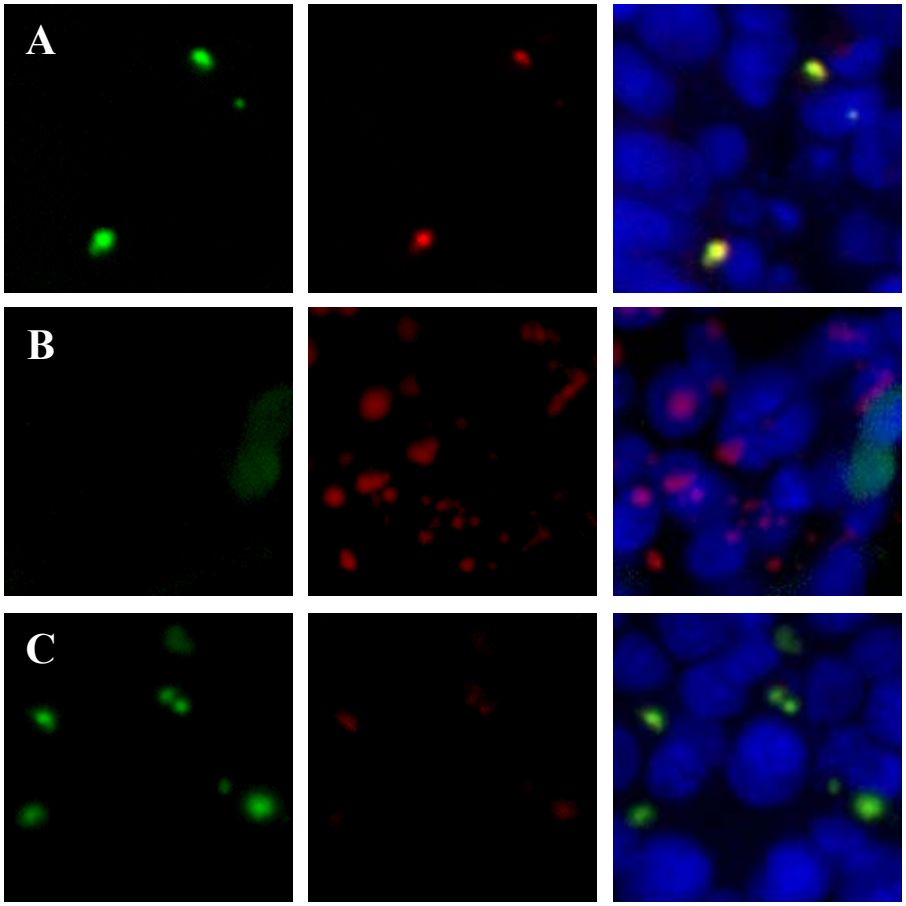

Figure 5.5: Aggregated species observed in transiently transfected PC12 cells. *(A) htt-Q103-GFP at 16 hours post-transfection. (B) htt-Q47-GFP at 16 hours post-transfection. (C) htt-Q103-GFP at 72 hours post-transfection.* Blue – cell nuclei, green – htt-polyGln-GFP constructs, red – AF.

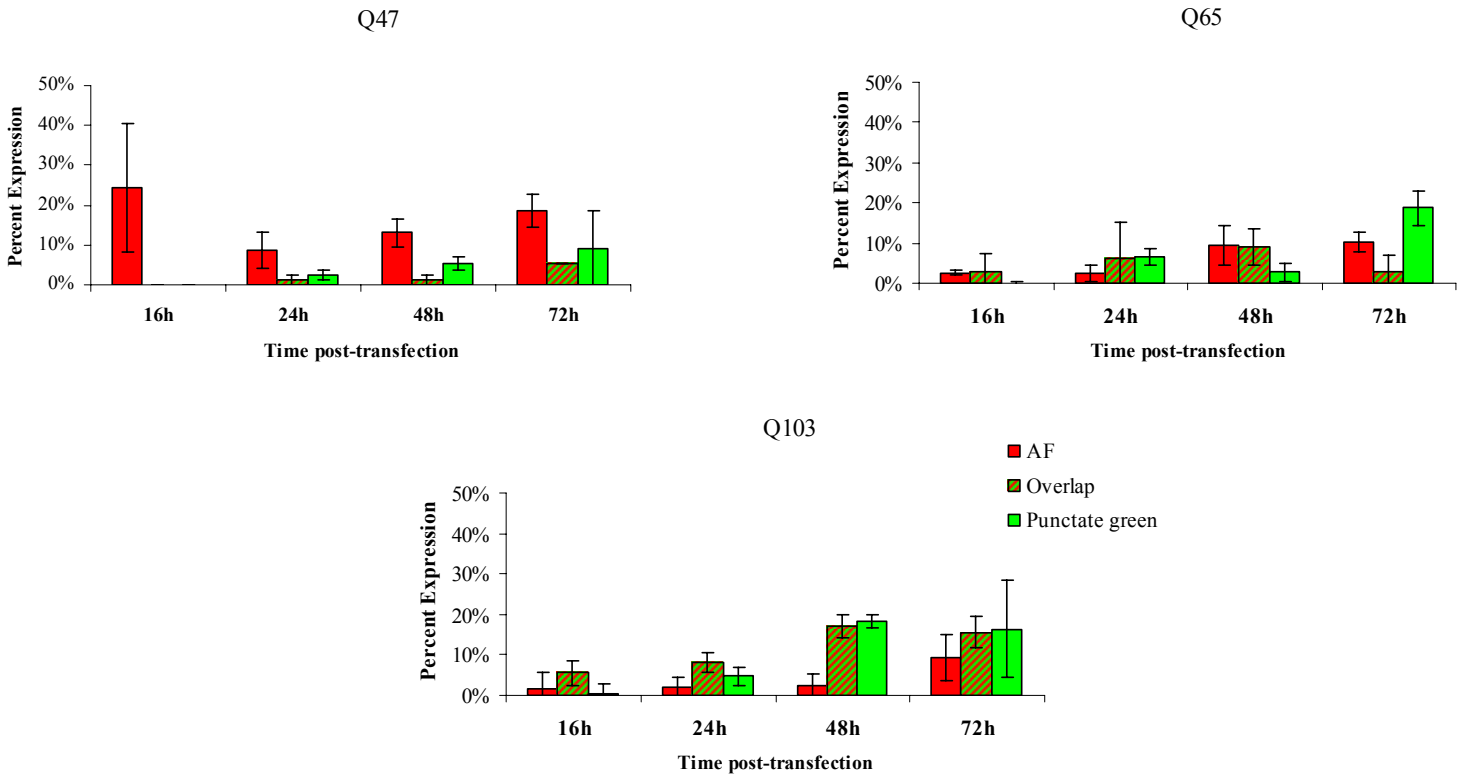

Figure 5.6: Percentage of cells exhibiting different polyGln expression patterns in transiently transfected PC12 cells. Data were obtained from microscopy images. At least two independent fields were counted within a single experiment. No AF or punctate green aggregates were observed in cells expressing htt-Q25-GFP constructs (data not shown). Red bars represent AF, green bars represent punctate htt-polyGln-GFP aggregates, red/green stripped bars indicate the aggregates that exhibit both green and red species.

Interestingly, PC12 and SH-SY5Y cells expressing htt exon-1-Q47 exhibited an abundant population of AF at 16 hours post-transfection, prior to the formation of punctate polyGln aggregates detected by GFP fluorescence (Figures 5.3, 5.4, and 5.6). AF diminished with increasing transfection times as the larger, GFP polyGln aggregates became more abundant. The implications of the timing of appearance of these two classes of aggregate will be considered in a later chapter.

As expected, cells expressing the hyperexpanded htt exon-1-Q103-GFP construct were more aggressive in the formation of polyGln aggregates. Interestingly, there was a mixture of both recruitment-competent and recruitment-inert GFP-positive aggregates (Figure 5.6). The small number of AF observed only briefly exhibited coincidence with the punctate polyGln aggregates. At later stages of cell growth, green fluorescent aggregates inefficient at polyGln recruitment became more dominant.

We observed inconsistencies in the expression patterns for both cell lines in multiple experiments, irrespective of the polyGln length (Figure 5.7). For example, one experiment would yield polyGln expression of 35%, while another experiment (following the same protocol) would yield an expression of 18%. These data were again confirmed by flow cytometry (Figure 5.8). The inconsistencies observed did not appear to correlate with the passage number of the cells before transfection.

Regardless of the cell line, htt exon-1-Qn-GFP protein expression was never more than 35% at 24 hours post-transfection, and cells with aggregation foci numbered far less than that (21% maximal expression), and these upper limits placed a number of

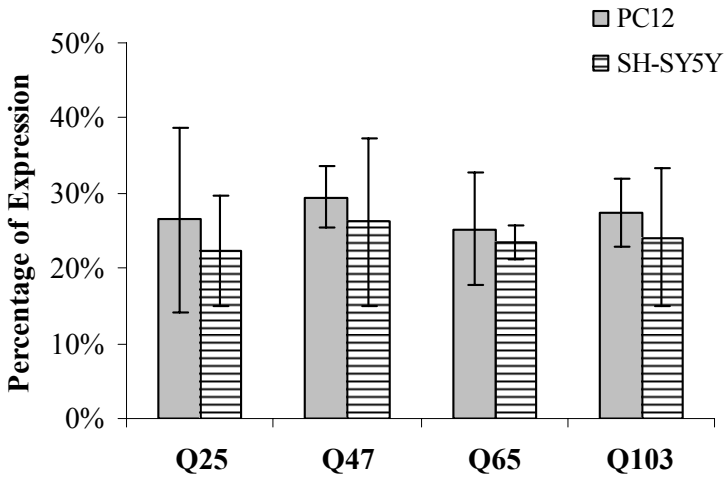

Figure 5.7: Inconsistencies observed in percentage of polyGln expression. Data was obtained from at least 4 independent experiments. PolyGln expression was calculated at 24 hours post-transfection as the percentage of cells expressing any detectible form of htt exon1: diffuse green, punctuate green, or red AF. This total expression figure was never more than 35%, and the numbers varied, in most cases, by at least 10%.

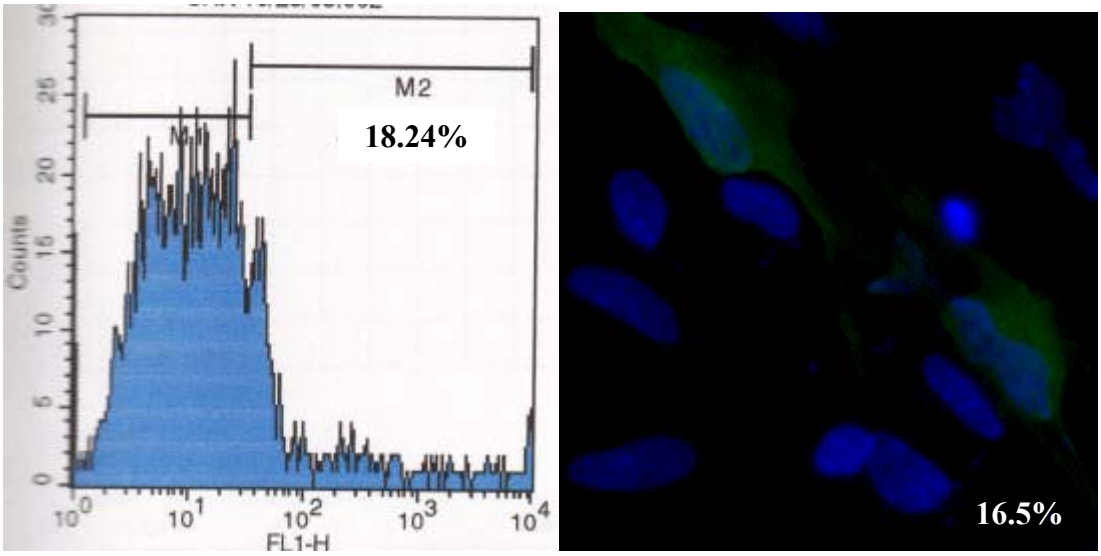

Figure 5.8: Transfection efficiency varied between experiments. SH-SY5Y cells were transiently transfected for 24 hours with htt-Q47-GFP. Left panel: flow cytometry. Right panel: immunofluorescence, blue – nuclei, green – htt-polyGln-GFP. Expression levels decreased from 35% as is shown in Figure 5.1.

restrictions on the kinds of experiments we could do and the kinds of interpretations we could make. With such low expression levels and the transient time frame in which AF were present; characterization of the various aggregates would have been challenging and not very fruitful. For example, in a cell population expressing only a handful of aggregates, as is evident in Figures 5.2 – 5.4, it is very difficult to make global interpretations from extracts of the entire population, especially when this population of cells is the minority. The above limitations led us to investigate an alternative model involving stably transfected cells engineered for inducible expression, described next.

5.3 Stable PC12 Model Expressing Various Htt Exon-1 Constructs:

Although the work on the transient protein expression systems provided the groundwork for the dissertation research, the majority of the experiments and the most exciting data were obtained from PC12 cells stably transfected for inducible expression of htt exon-1 (see Sections 3.1 and 3.2). This section will provide the details pertaining to the creation a viable cell model system that exhibited a high percentage of polyGln expressing cells and the troubleshooting that was addressed along the way.

For these experiments, stable PC12 cells expressing complete htt exon-1 constructs (Gln repeats: 25, 47, and 103) and truncated htt exon-1 fragments (Q103) were induced for 24 hours, as described in Section 3.2, to determine the initial polyGln expression levels in each of the cell lines. As with the transient models, polyGln expression was monitored by following the green fluorescence of the attached GFP molecule. Given that we found an excellent correlation between the quantitative flow cytometry data and qualitative immunofluorescence images in all our transient expression

experiments (Figures 5.1 and 5.8), in subsequent experiments only the microscopy data was used to determine levels of expression. As received from the Thompson lab, the 25QP and 103QP cells had initial GFP expression levels of ~32%, while the 47QP cells had a beginning expression level of ~22%. Q103 cells, on the contrary, exhibited a high number of cells the expressed htt-polyGln-GFP (~65%).

Considering the relatively low percentages of protein expression in the cells expressing the complete htt exon-1 constructs, these three cell lines were subcloned with selection for high htt-GFP expression (Figure 5.9 for representative) (see Section 3.2) [Freshney 1987]. After the cells had been subcloned, percent expression increased to ~56% in each cell line. While the 25QP and 103QP cell lines after subcloning maintained these expression levels, a stability issue arose with the cell line expressing the physiologically relevant Gln repeat (47QP). Following a freeze/thaw cycle of the 47QP cells, polyGln expression reverted back to the observed basal expression levels of ~22% (Figure 5.10). Furthermore, the intensity at which the polyGln species were observed in the subcloned cells prior to the freeze/thaw cycle was vastly superior to those seen afterwards. Repeated attempts at subcloning the parental 47QP cells did not yield satisfactory results. Finally, our collaborators kindly supplied a new parental vial of cells from an earlier passage and a separate clone. Upon subcloning these cells, we were able to achieve and maintain 47QP cells that exhibited high clonal integrity for exon-1 production, irrespective of the amount of times they were subjected to freezing and thawing (Figure 5.11).

Considering polyGln expression was stabilized after receiving the new vial of parental 47QP cells, the problem we encountered using the original lot of cells was

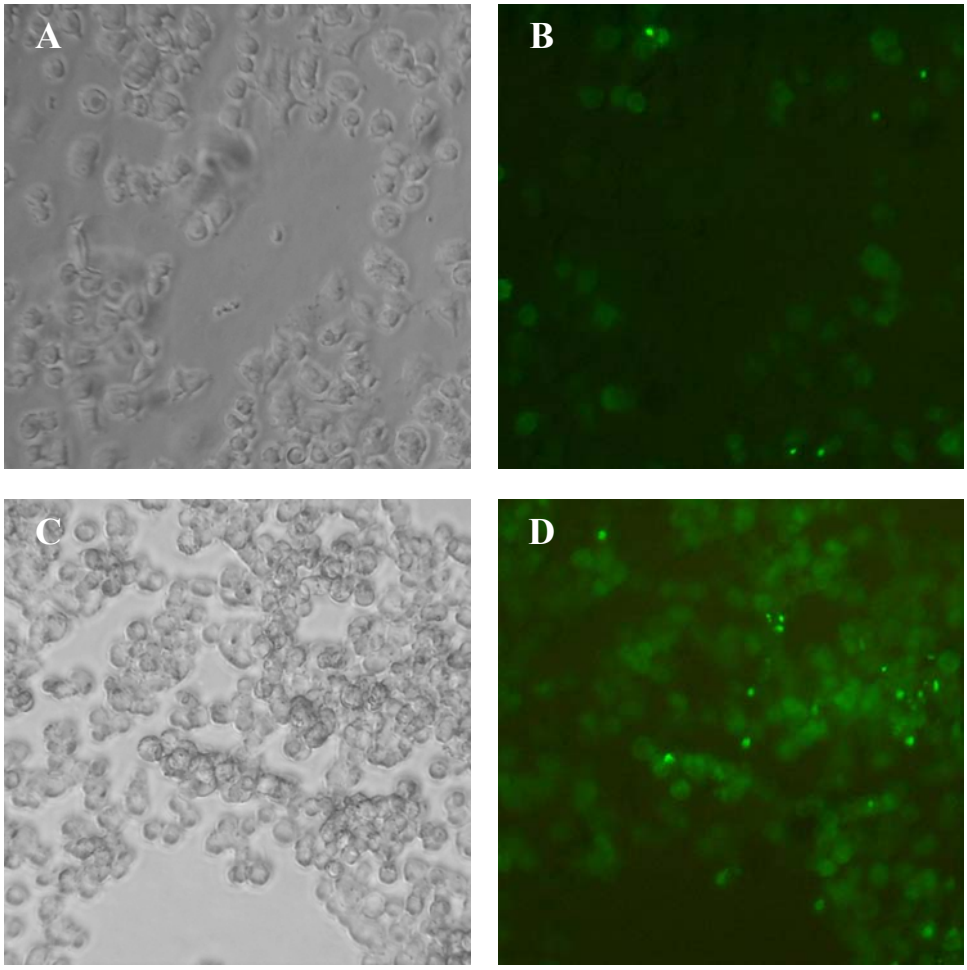

Figure 5.9: Representative sample of cells before and after clonal dilution. Top panel: 103QP cells prior to enrichment. Bottom panel: 103QP cells after selection for a high percentage of htt-polyGln-GFP expressing cells. (A & C) Phase contrast microscopy image. (B & D) Fluorescence images taken using a FITC filter.

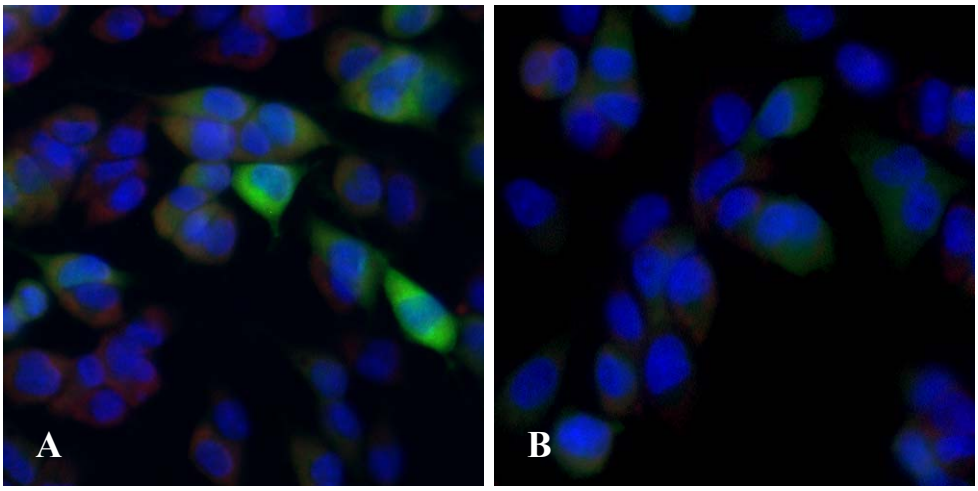

Figure 5.10: Stable PC12 cells expressing 47QP were unable to maintain high clonal integrity once subjected to a freeze/thaw cycle. *(A) Cells were photographed at 48 hours post-induction and exhibited ~56% htt-polyGln-GFP prior to being frozen. (B) Cells were thawed and induced for 48 hours. Expression levels dropped to ~20% after the cultures had been thawed.* Blue – nuclei, green – htt-polyGln-GFP, red – AF.

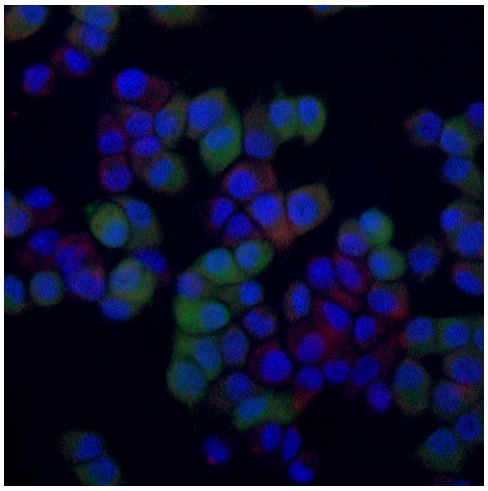

Figure 5.11: New 47QP parental cell line generated stable expression after repeated freeze/thaw cycles. Photograph was taken 48 hours post-induction. Blue – nuclei, green – htt-polyGln-GFP, red – AF.

probably due to poor stability of the inserted transgene into that particular parental clone. Obtaining a different clone of the 47QP parental cells appeared to resolve the problem, and additional subcloning provided a population with high clonal integrity that was unaltered by successive freeze/thaw cycles.

Other complications arose during experiments with the stable PC12 cells. A reoccurring obstacle that was addressed in many ways but was never quite resolved was the issue of cell detachment. Irrespective of the incorporated htt construct and inducing agent, each cell line had a tendency to lift from the coverslips on which the cells were grown. As mentioned with the transient cell lines (Section 3.2), this phenomenon limited cell numbers at later growth points and introduced the possibility that selective detachment might skew results. Several steps were taken to address this issue including the use of poly-D-lysine, a common attachment factor used in cell culture, as a coating agent. Another change that was integrated into the protocol was the use of the pH buffering agent HEPES. While these efforts yielded some improvement, the most useful change was to the seeding density of the cells. These cells had a very quick doubling time (32-36 hours). Once the cultures became slightly overgrown, the cells began to detach; this may be due to a depletion of nutrients in the culture medium, but detachment seemed to occur regardless of how often the media was changed. In any case, decreasing the density at which the cells were plated provided the most beneficial results and decreased the detachment rate, which was especially evident in the later time points. Prior to these changes, an estimated 50% of the plated cells lifted from the coverslips; however, after the changes were incorporated, we estimated that <10% of the culture had detached. We also examined the detached cells, and found that the cells that had lifted from the

coverslips were a mixed population of cells that expressed the GFP transgene and those that did not. Thus, the detachment problem was not a direct effect of the incorporated htt transgene, and it is clear that detachment is not an indication of polyGln-dependent cell death or dystrophy.

One of the biggest obstacles encountered was the inability to view polyGln recruitment via live cell microscopy. A drawback to the current staining technique is that in order for the cells to take up free monomeric peptide, the cells must be permeabilized. For this reason, there was no feasible way to view polyGln incorporation in real-time. In principle, this might be done by co-expression of an appropriately tagged short polyGln substrate, analogous to our biotinylated polyGln peptide; however, the problem of peptide uptake would have still been present.

PRESENCE OF INDUCIBLE-HTT DOES NOT CAUSE CYTOTOXICITY

Many cell models have shown reduced viability when cells express an expanded polyGln protein [Lunkes and Mandel 1998; Chai et al. 1999; Li, Cheng et al. 1999; Wyttenbach et al. 2001; Yang et al. 2002; Aiken, Tobin et al. 2004], while other groups have found contradictory results [Ding et al. 2002; Apostol et al. 2003; Webb, Ravikumar et al. 2004]. Prior to aggregate characterization (discussed in Chapter 6), we wanted to confirm whether or not the htt constructs were causing cell death. As discussed earlier, while cell death might in some sense validate these cells as a valid model for HD, the loss of cells and their contents during the experiment – and before analysis – would clearly have complicated the interpretation of data. Microscopically, it did not appear that the

presence of the htt insert was causing cell death. However, it was imperative to determine whether or not this was true.

We performed an MTS reduction assay (Section 3.4) to determine the number of proliferating cells within each induced culture at 24 hours post-induction. We found that, irrespective of the polyGln length insert, overt cytotoxicity was not detected ($p>0.2$, Figure 5.12). As is evident by the absorbance values in Figure 5.12, each cell line was plated at different seeding densities. Regardless of the plating density, polyGln expression had no effect on cell viability.

It has been shown that, for reasons not entirely understood, these particular cell lines are not susceptible to polyGln-induced cytotoxicity [Apostol, Kazantsev et al. 2003], and our data were consistent with these results. Recently, Apostol and colleagues performed gene expression profiling on this particular cell line and showed that genes, such as HSP27 and 70, involved in pro-survival pathways were significantly upregulated [Apostol et al. 2006], providing a possible reason why these cells do not die even with nuclear aggregates present.

We were successfully able to subclone three of the four received stable cell lines. The fourth did not need further enrichment because they were initially obtained at an already high clonal integrity. Each cell line provided consistent expression levels from experiment to experiment, and the protein abundance (~60%) was far superior to that of the transient models (~30%). These data will be presented in the next chapter. The use of an inducible system was also beneficial because it provided more control of the experimental timeline, i.e. the experiment could be conducted for longer times. The majority of the stable cell lines were designed to produce complete htt exon-1 proteins,

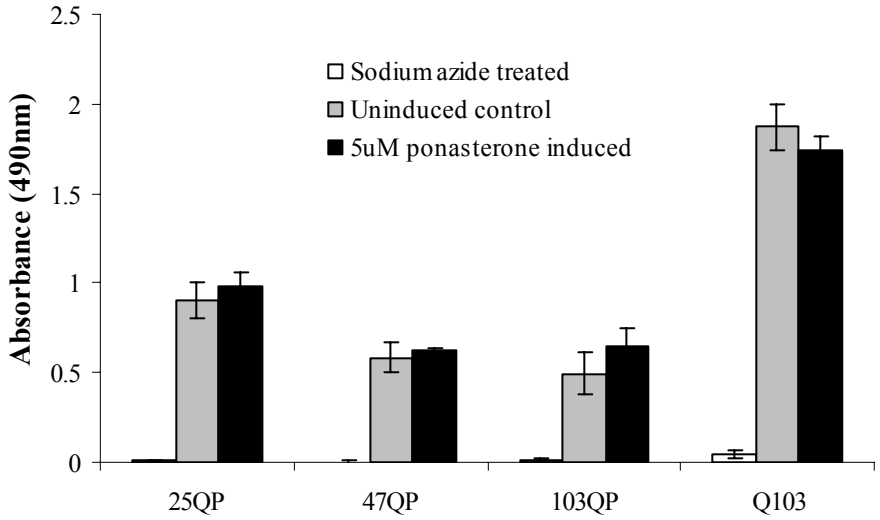

Figure 5.12: Polyglutamine expression does not cause cell death. Each cell line was plated at different seeding densities: 25QP cells were plated at a density of ~100,000 cells/cm^2; 47QP and 103QP cells were plated at a density of ~60,000 cells/cm^2; and Q103 cells were plated at a density of ~200,000 cells/cm^2. A cell proliferation assay (MTS reduction) was performed to measure the number of viable cells. Although there were slight fluctuations in the number of measurable cells, no significant change was observed when uninduced controls were compared to the induced samples.

which provided more physiological relevance than the truncated models lacking the proline rich C-terminus. It has been well documented that the presence of a proline-rich sequence following polyglutamine in huntingtin significantly decreases the rate of aggregate formation [Bhattacharyya, Thakur et al. 2006; Dehay and Bertolotti 2006]. Inclusion of the proline-rich segment not only made the cell model more relevant to the disease situation, it also slowed down at least some aggregation reactions, providing an opportunity to observe the cells prior to the development of polyGln aggregates and to monitor the aggregation pathway (discussed in Chapter 6). This was in contrast to our transient transfection models in which aggregates developed very rapidly, making it difficult to dissect precursor-product relationships. The fact that the cells did not exhibit cytotoxicity was also an advantage because that allowed us to focus strictly on the aggregation pathway without complicating the interpretation with cellular demise.

CHAPTER 6

CHARACTERIZATION OF POLYGLUTAMINE AGGREGATES IN STABLE PC12 CELLS EXPRESSING HTT EXON-1 CONSTRUCTS

6.1 Nomenclature for Identified PolyGln Species:

With the detection of multiple polyGln species in the stable, htt-inducible PC12 cells (to be discussed later in the chapter), a simple nomenclature is clearly required. During this section we will establish a nomenclature for the observed polyGln species, which will be used throughout the remaining dissertation.

The species identified were categorized into four major divisions (Figure 6.1): 1) Diffuse, monomeric protein (designated Monomer, M), 2) Aggregation foci, which were recruitment-competent, diffusely scattered throughout the cytoplasm, and did not demonstrate green fluorescence (designated $Green^{-}\ Red_{(Cytoplasm)}^{+}$, $G^{-}R_{C}^{+}$), 3) Aggregates that showed GFP formation but did not exhibit recruitment-capabilities (designated $Green^{+}\ Red^{-}$, $G^{+}R^{-}$), and 4) Aggregates that were large enough to be visualized via their GFP component but also exhibited polyGln recruitment (designated $G^{+}R_{C}^{+}$), which represented only a small percentage of the observed species and were observed only in the cytoplasm.

Furthermore, the class that was designated $G^{+}R^{-}$ was found in two different cellular locations: the majority was perinuclear (designated G_C for cytoplasmic localization, Figure 6.1C), while ~5% were nuclear (designated G_N for nuclear

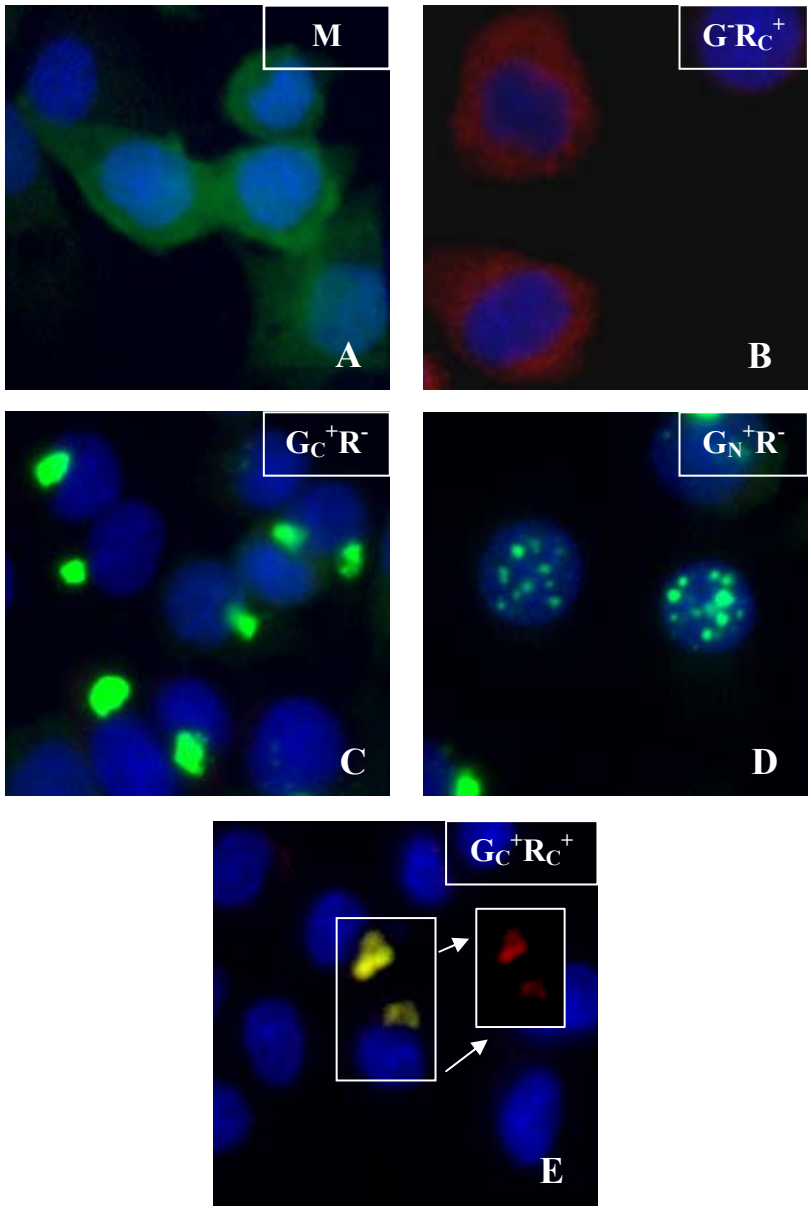

Figure 6.1: Distinct polyGln species identified within stable PC12 cells expressing htt-inducible proteins. *(A) Diffuse monomeric protein.* M, green fluorescent protein was found diffusely scattered throughout the cytoplasm of most cells. Diffuse staining was also found in some cell nuclei during later time points. *(B) Aggregation foci*. $G^-R_C^+$, polyGln recruitment competent centers that were not detectable by the GFP component. *(C) PolyGln aggregates that did not exhibit recruitment-competency located in the cytoplasm.* $G_C^+R^-$. *(D) Nuclear aggregates that were recruitment-inert.* $G_N^+R^-$. *(E) Perinuclear aggregates that were also capable of polyGln recruitment.* $G_C^+R_C^+$, these structures were only visualized in the 103QP cells at early time points. White inset shows that AF were coincident with GFP aggregates. Blue – nuclei, Greene – htt-polyGln-GFP, Red – AF.

localization, Figure 6.1D). Perinuclear aggregates are commonly defined as an aggregated structure that is found in the cytoplasm close to the nucleus or associated with the nuclear membrane [Kazantsev, Preisinger et al. 1999]. These structures are also generally quite large and even, in some instances, appear to distort the shape of the nucleus. In the case of the stable PC12 cells, perinuclear aggregates were often 1/5 or greater the size of the cell nucleus and were easily visualized by their fluorescent tag. Nuclear aggregates, on the other hand, have been described to be much smaller and are located inside the cell nucleus [Kazantsev, Preisinger et al. 1999] but can also be observed via their fluorescent label.

The remaining chapters of the dissertation will adopt this nomenclature and will present experiments specifically designed to provide insights into a key question that plagues HD research: Are these small, recruitment-competent aggregates that occur early in development precursors to the larger, recruitment-inert, GFP-positive aggregates, or do they form via separate, parallel assembly pathways?

6.2 Microscopic Observations:

This section will present the findings of the data obtained using the stable PC12 cells expressing htt exon-1 constructs of varying polyGln repeat lengths (25QP, 47QP, 103QP, and Q103, described in Chapter 3). At least three polyGln species were visualized during the seven days in which the replicating cells were monitored by fluorescence microscopy (see Figures 6.2 and Figure 6.3). With respect to GFP fluorescence, cells expressing 25QP and 47QP exhibited only diffuse green, indicative of

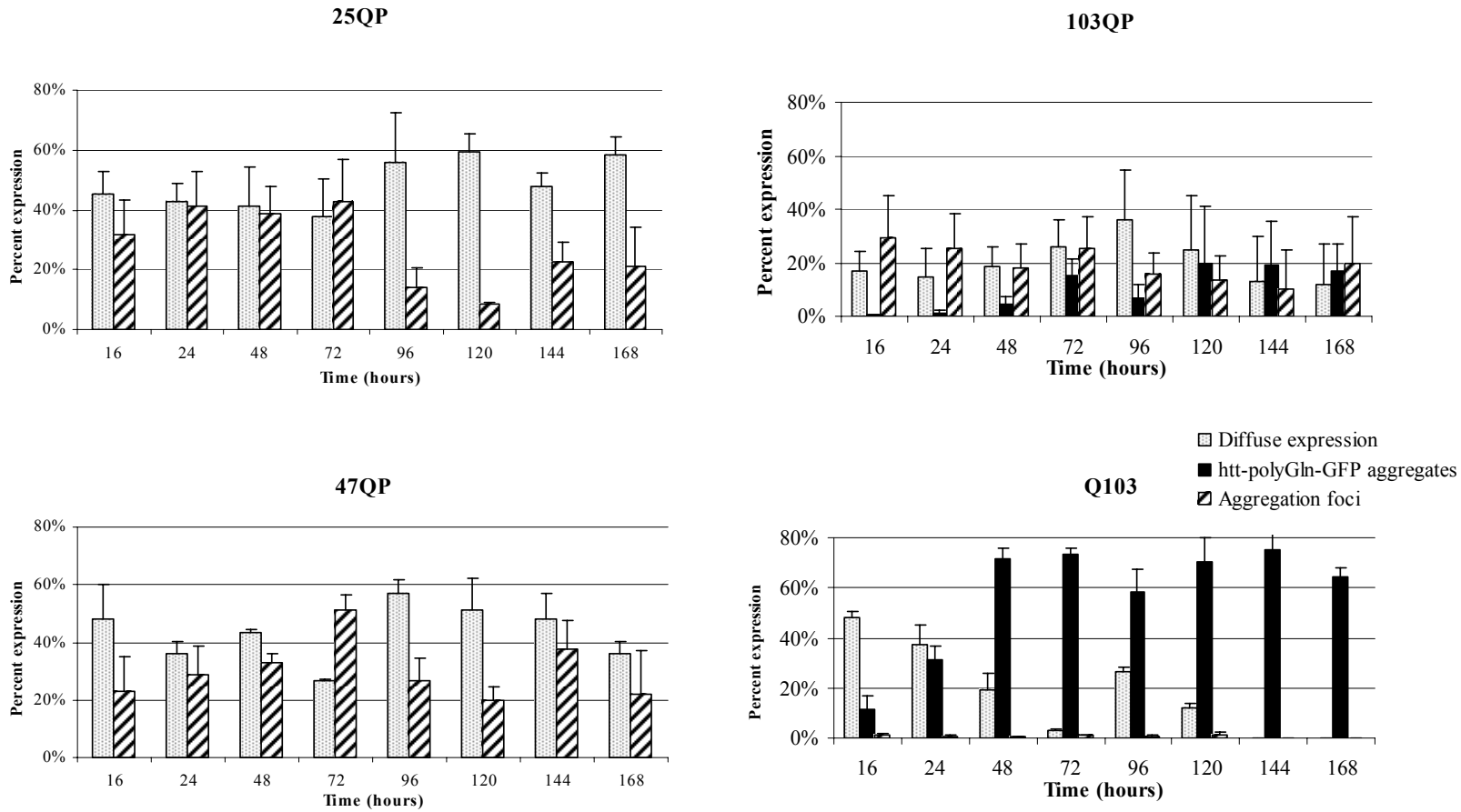

Figure 6.2: Percentage of polyglutamine expression within huntingtin-inducible PC12 cells. Data were collected from at least two separate experiments. For each time point, cells were counted from three or more independent fields. The data are expressed as the percentage of total cells that exhibited either htt monomer ( ), htt-polyGln-GFP aggregates ( ), or aggregation foci ( ). Data shown are from 16-168 hr. post-induction.

Figure 6.3: Kinetic study of polyglutamine formation in huntingtin-inducible, stable PC12 cells and uninduced controls. Fluorescent color is blue for cell nuclei, green for GFP fusion constructs, and red for aggregation foci. Time labels indicate hours post-induction. **(a)** First panel: Untreated control PC12 cells. Second panel: Cells expressing 25QP. Third panel: Cells expressing 47QP. **(b)** First panel: Cells expressing 103QP. Second panel: Cells expressing Q103. In each panel, the left column represents images taken by modified differential interference contrast (DIC) microscopy. The last column in each panel represents the red, green, and blue merged image. Where present, the middle column(s) show a merger of only the red and green images, where the detail of AF and htt colocalization may be more easily observed. In part b of the figure, two exposures of the same image were taken. The second image was taken at a longer exposure so that the monomeric species could be photographed (Section 4.3). In the 103QP cells, where htt aggregates were also recruitment-competent, insets (solid white boxes) are included showing the red image prior to the merger with the green image. Details of each image can be observed at a higher magnification. **(c)** Diffuse fluorescence and AF were the only species observed with 25QP and 47QP cells. Displayed images were taken at 24 hours post-induction. **(d)** Punctate aggregates were present in cells expressing both complete and truncated htt exon-1 constructs. Images were photographed at 24 hours post-induction. The amount of htt-polyGln-GFP aggregates increased with longer induction times (Figure 6.2).

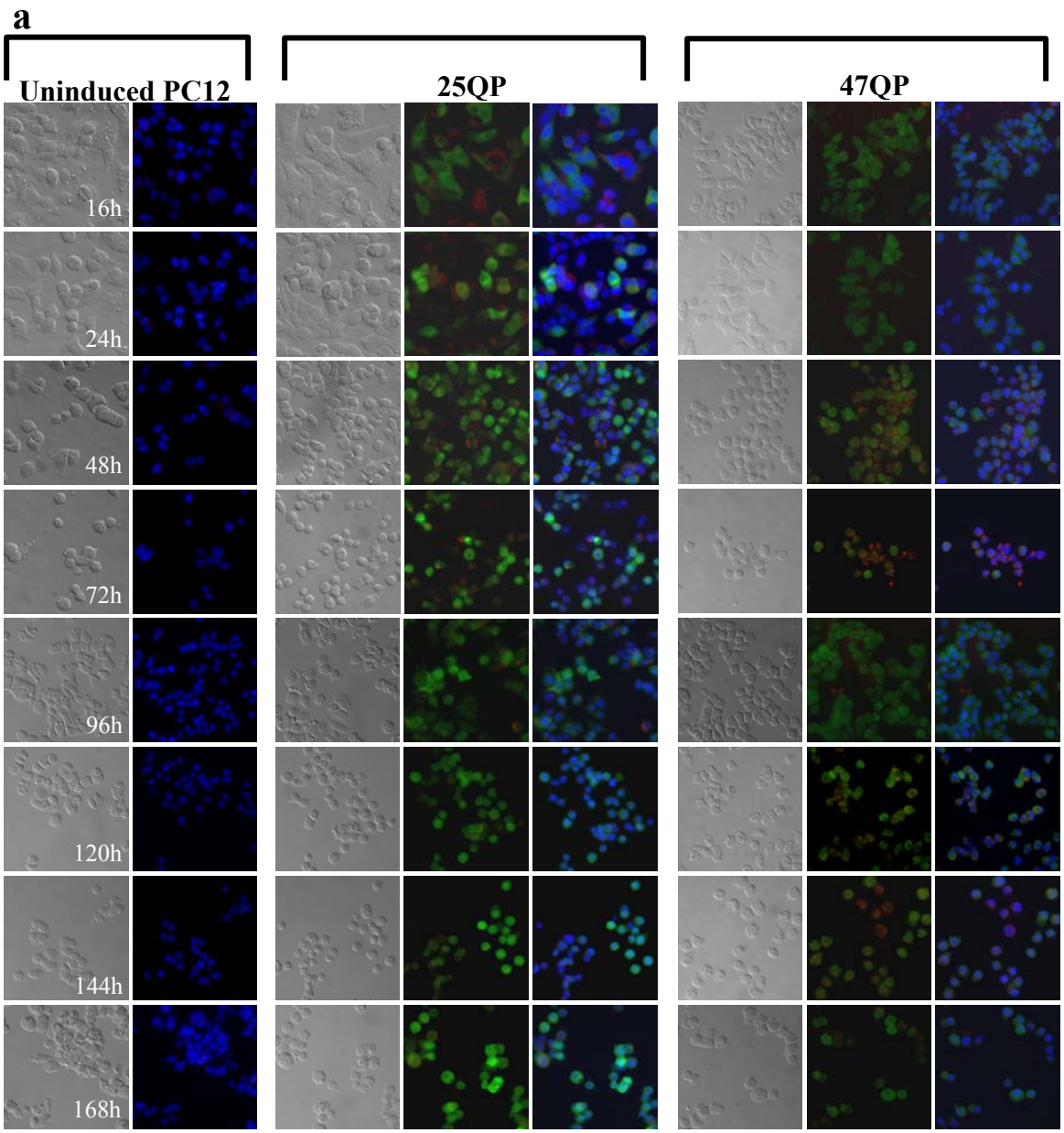

Figure 6.3. Continued.

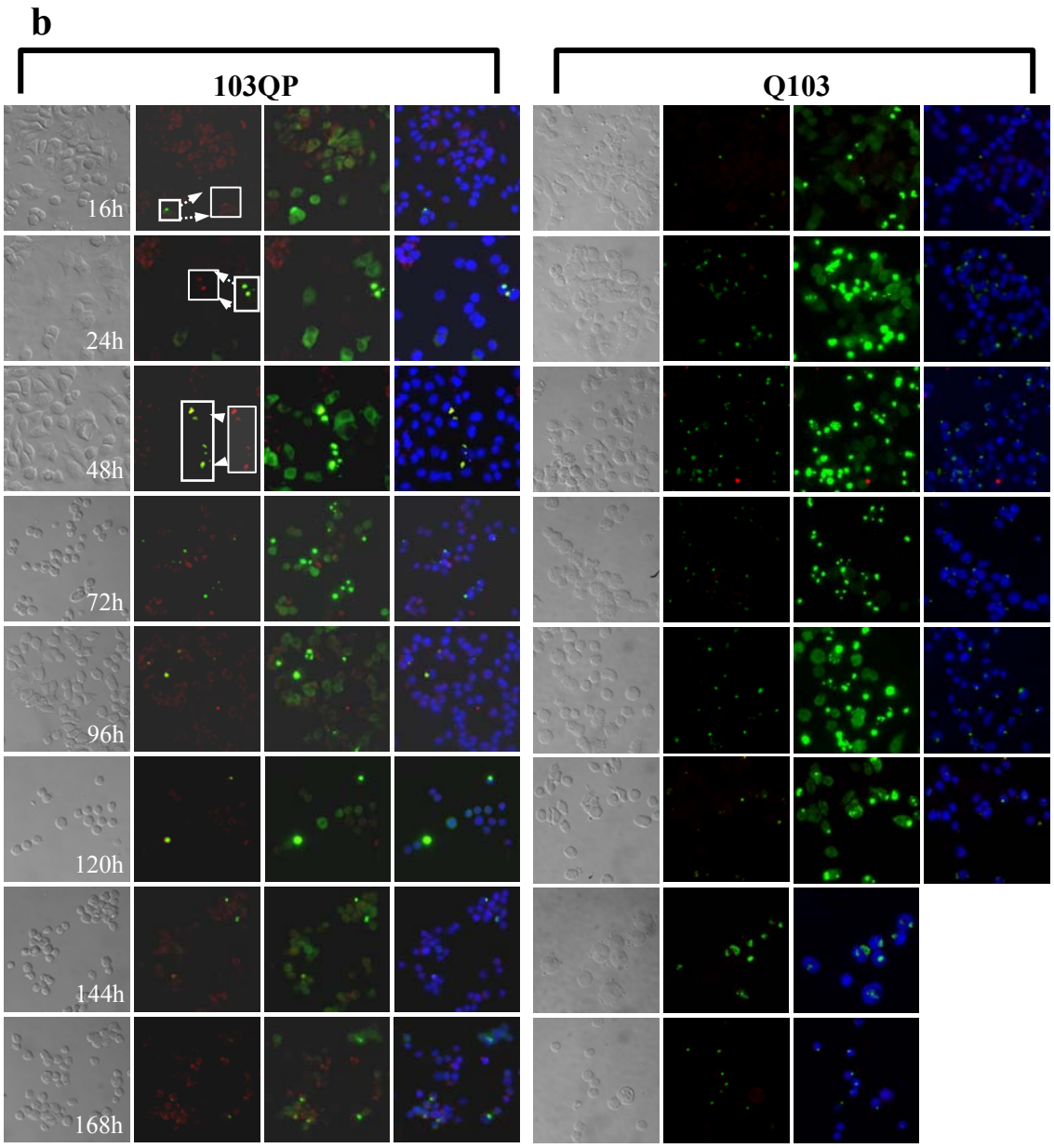

Figure 6.3. Continued.

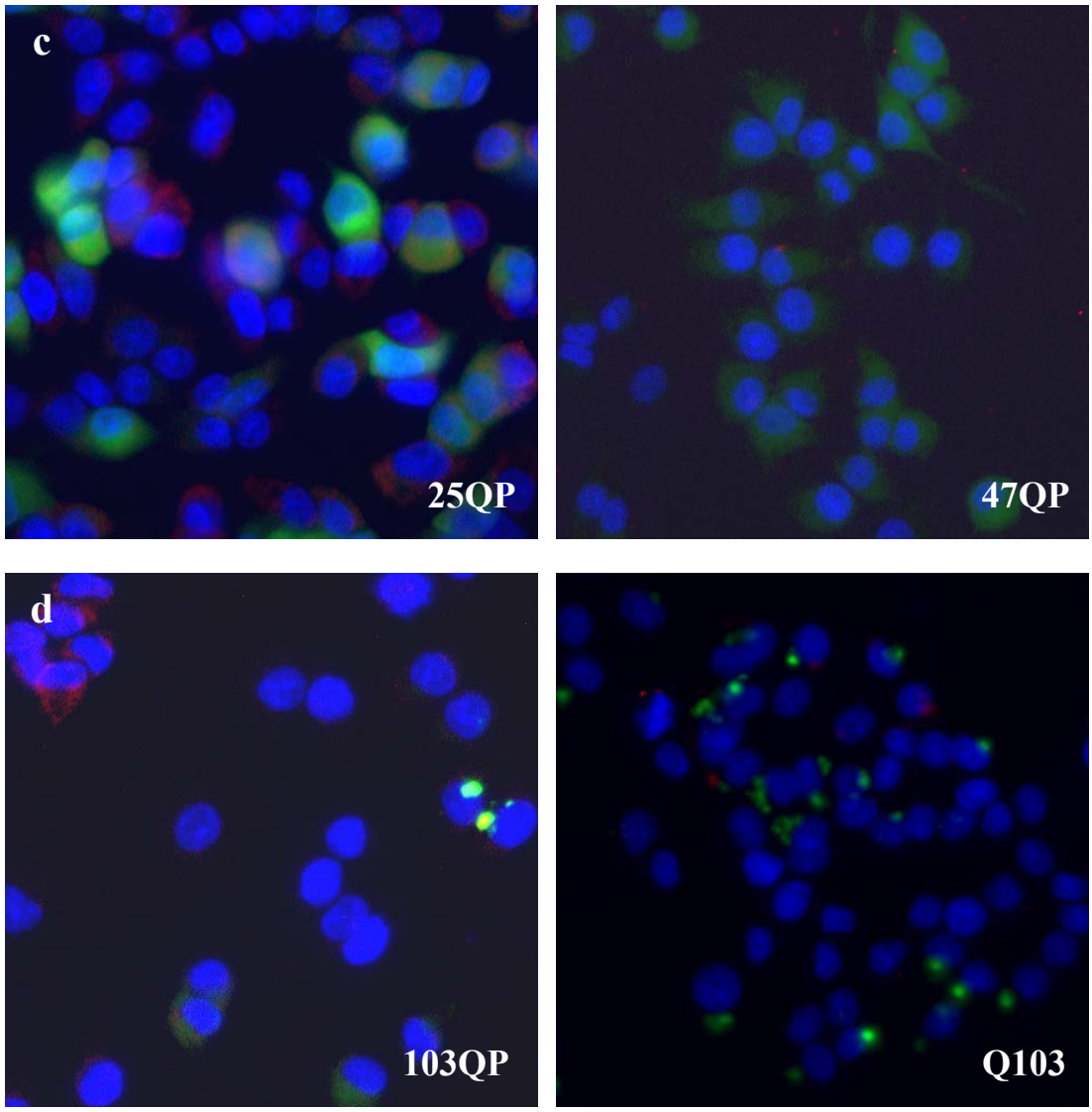

Figure 6.3. Continued.

presumably monomeric htt expression (Figure 6.3c), throughout the seven day experiment; whereas cells expressing 103QP and Q103 developed punctate green htt (presumably aggregates) early in development that increased in number as the cells aged and divided (Figures 6.2 and 6.3d). In addition to green fluorescent species, a third species, AF (red fluorescence), was present only in cell lines expressing intact htt exon-1 including the Pro-rich segment and were not observed (<3%) in Q103 cells that expressed truncated htt exon-1 (Figures 6.2 and 6.3c-d).

All three cell lines expressing complete htt exon-1 constructs exhibited steady M expression over the initial 72 hours (Figure 6.2). In all three cell lines, this expression peaked at peaked at 96 hours. While 25QP cells maintained this high M expression out to 168 hrs, diffuse expression dropped somewhat after 96 hrs for the 47QP and 103QP cells. All three cell lines also exhibited steady levels of cells expressing $G^-R_C^+$ over the first 72 hrs, after which the percentage of cells with $G^-R_C^+$ declined, generally by about a factor of 2. Of these three cell lines expressing complete exon1 constructs, only the 103QP cells exhibited any significant formation of punctate green bodies; these increased in number from 24 to 120 hrs, after which levels remained fairly steady.

In contrast, Q103 cells expressing a construct lacking the proline-rich region exhibited a rapid decline in M expression from 16 to 72 hours, with a commensurate rapid rise in punctate green bodies over the same time period. By 144 hrs over 70% of cells had punctate green bodies and no cells exhibited diffuse GFP staining. Significantly, only a very low percentage (<3%) of $G^-R_C^+$ were observed at any time point.

All cell lines exhibited very good homogeneity of expression, a reflection of their being products of rigorous subcloning procedures as well as an indication of the stability of their gene insertions. Thus, by 48 hrs, the Q103 cell line exhibited 94% of cells with some manifestation of htt exon-1 expression. By 96 hrs, 47QP and 103QP reached maximal expression of 84 and 66%, respectively. The 25QP cell line reached maximal expression at 24 hrs, with 84% of cells exhibiting expression of the transgene.

The AF expression patterns in the QP cell lines is especially interesting in several respects. First, the conventional view is that cells expressing htt exon-1 with normal length polyGln do not make significant aggregates, and indeed this is the case if aggregation is only detected as punctate green bodies. However, using the recruitment stain we observe significant $G^-R_C^+$ formation even at early time points and even in 25QP cells. Second, in 103QP cells, $G^-R_C^+$ form early while punctate green bodies form later, suggesting a possible precursor-product relationship. Interestingly, at early time points in these 103QP cells, AF co-localize with punctate GFP bodies (Figure 6.4); while at later times, fewer punctate green bodies contain $G^-R_C^+$ (Figure 6.5); this also suggests a precursor-product relationship where AF develop first. The Q103 cells are also consistent with a progression of AF to punctate GFP bodies; since removal of the proline rich sequence is expected to lead to more aggressive aggregation (more than triple the number of $G_{C/N}^+R^-$ species, see Figure 6.2), AF may progress so rapidly to punctate GFP bodies that few $G^-R_C^+$ are ever detected. However, these data alone were not sufficient to rule out the possibility that they were forming via alternate assembly pathways. These results will be considered further in the last chapter.

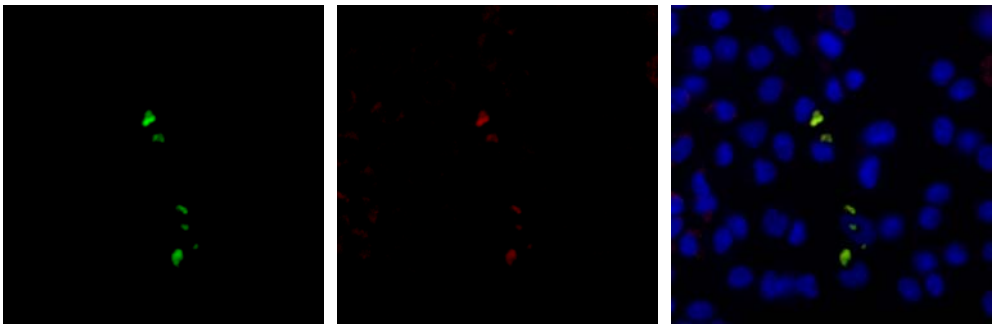

Figure 6.4: $G_C^+R_C^+$ aggregates appear to co-localize with $G^-R_C^+$ in cells expressing 103QP. Blue – cell nuclei, green – htt-polyGln-GFP fusions, red – $G^-R_C^+$. The first and second panels show the separate images taken with the green and red filter sets, respectively. The third panel shows a merger of the images including the cell nuclei. Images were taken at 48 hours post-induction of cells expressing 103QP constructs.

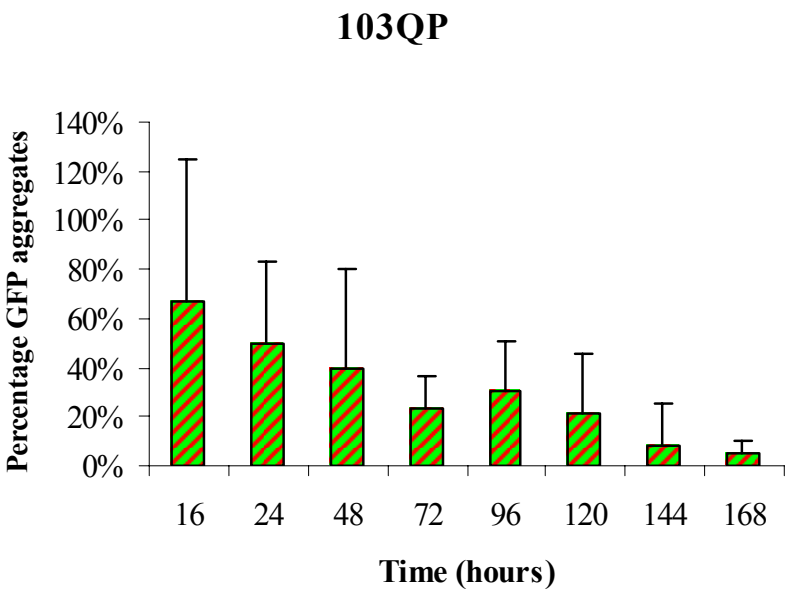

Figure 6.5: Co-localization of $G^-R_C^+$ and $G_C^+R_C^+$ aggregates in cells expressing 103QP diminished with time. PolyGln aggregates measurable by their GFP fluorescence were counted and scored for their apparent coincidence with AF. Data were collected from at least five non-overlapping fields in two independent experiments. Data is expressed as percentage of GFP aggregates that were coincident with AF. Earlier time points demonstrated a higher percentage of error due to the presence of fewer polyGln aggregates.

Another intriguing observation was noted in cells expressing Q103. These cells exhibited small $G_N^{+-}R^-$ aggregates (Figure 6.6), which were not seen with any other cell line. Figure 6.7 shows that the percentage of cells that contained nuclear aggregates were far less than those that contained the larger $G_C^+R^-$ aggregates. Why does this cell line uniquely produce nuclear aggregates? One possibility is that the proline rich segment is a nuclear export signal, so that when it is present it strongly counter-balances some intrinsic ability of htt exon-1 to enter the nucleus. Another possibility is that there is always some cycling of htt exon-1 through the nucleus, which however normally does not lead to accumulation because of a stronger export signal. However, with Q103, rapid aggregation within the nucleus traps the exon-1. Other explanations are possible. Previously it was shown that when recruitment-positive polyGln aggregates are delivered to the nuclei of PC12 cells, they rapidly die [Yang, Dunlap et al. 2002]. Presumably the $G_N^+R^-$ aggregates observed here are not toxic because they are not recruitment positive (i.e., are not $G^-R_C^+$).

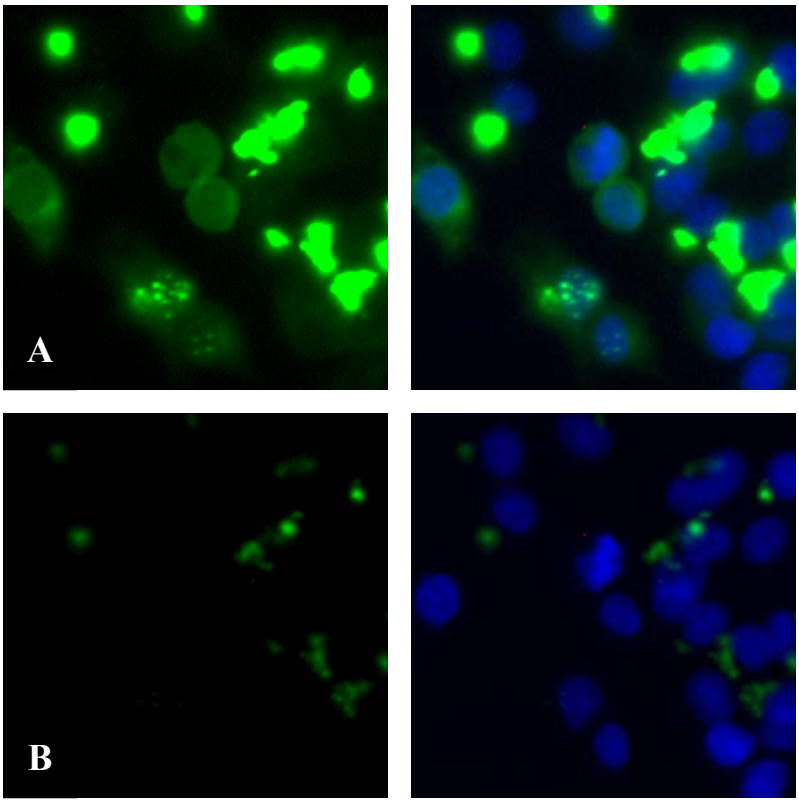

Figure 6.6: Cells expressing Q103 exhibited $G_N^+R^-$ aggregates. Images were obtained at 24 hours post induction. The left column represents green images (htt-polyGln-GFP fusions), while the right column represents a merger of the image with the blue (nuclei). Both top and bottom pictures are the same microscopic field. **(A)** Images were taken at a longer exposure time to photograph diffuse and nuclear entities (500msec). **(B)** Photographs acquired at a shorter exposure.

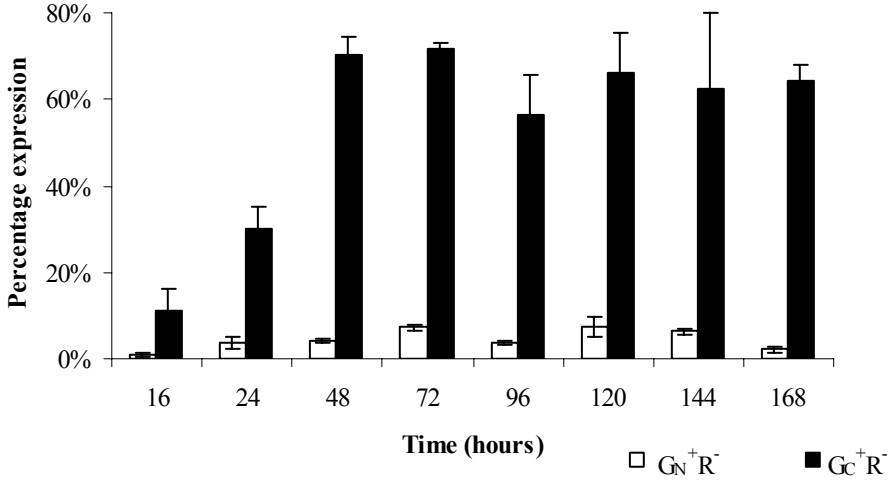

Figure 6.7: $G_N^+R^-$ aggregates were observed but were less abundant than $G_C^+R^-$ aggregates in cells expressing Q103 constructs. Data were obtained from two separate experiments and from at least 3 independent microscopic fields. Data are expressed as percentage of cells expressing either $G_N^+R^-$ or $G_C^+R^-$ aggregates.

CHAPTER 7

MECHANISTIC STUDIES OF AGGREGATE FORMATION

7.1 Rationale:

We were successful in identifying multiple polyGln species within stable PC12 cells that are inducible for htt expression. Identification of two of those species, $G^-R_C^+$ and $G_C^+R_C^+$, relied solely upon the development and implementation of a stain that is based upon the ability of aggregated polyGln proteins to recruit free monomeric polyGln [Berthelier et al. 2001; Chen et al. 2001; Chen et al. 2002; Osmand et al. 2006]. This characteristic is similar to other amyloid diseases, in which a proposed mechanism of fibril growth is facilitated by monomer addition [Lomakin et al. 1996; Lomakin et al. 1997; Collins et al. 2004; O'Nuallain et al. 2005]. With the identification of the various species, the next logical step was to undertake the challenge of discerning each of their roles in the aggregation process. This question was addressed in two manners: 1) utilizing a compound that has been shown to inhibit amyloid formation *in vivo* [Yang, Lim et al. 2005] and 2) using other compounds to alter cellular processes that have been implicated in aggregation [Johnston et al. 1998; Webb et al. 2004; Ross and Poirier 2005; Chang et al. 2006].

7.2 Curcumin Inhibits $G^-R_C^+$ Species in a Dose-dependent Manner:

Curcumin, the main ingredient in the Indian curry spice tumeric, has been used therapeutically for its anti-inflammatory, anti-oxidant, and anti-amyloid properties [Lim

et al. 2005; Yang et al. 2005]. Curcumin is a low molecular weight compound that has a favorable toxicity profile and is currently being investigated as a potential chemotherapeutic agent for cancer [Kelloff, Boone et al. 1996]. Curcumin has been found effective at inhibiting the formation of Aβ fibrils at concentrations ranging from 0.5μM-8μM. Recently, curcumin was also shown to reduce aggregate formation and ameliorate rearing deficits in an HD mouse model [Zhu 2006]. Because of the possibility that curcumin might selectively inhibit amyloid formation, and not other aggregation reactions, we chose to treat our stable PC12 cells with curcumin and to monitor any effects on the aggregation pathway.

To monitor the effects of curcumin on aggregate formation, we chose to use the htt-inducible cells expressing 25QP and 47QP, a benign polyGln length and a disease-relevant polyGln length, respectively. *In vivo,* the most common Gln repeat length is ~42 (Figure 1.12). These particular cell lines exhibited diffuse monomeric staining and never displayed punctuate GFP-positive aggregates within a one week time frame. However, ~40% of the population expressed $G^{-}R_{C}^{+}$ species (Figure 6.2) at any given time. The question we wanted to answer was if curcumin inhibited or accelerated the production of AF.

Cells were plated and maintained under the same conditions as previously described (Section 3.2). 25QP and 47QP cells were induced with 5μM Ponasterone and simultaneously treated with 0.1, 1, or 10μM of curcumin (10mM stock in ethanol) for 24 hours. After one day of incubation with the compound and inducing agent, the cells were fixed, permeabilized, and subjected to the AF stain (Section 3.3).

As shown in Figures 7.1 and 7.2, curcumin treatment decreased the formation of $G^-R_C^+$ in both 25QP and 47QP cells by >40% at all concentrations tested ($p \leq 0.02$), while not appreciably altering the M expression. This effect was dose-dependent, with 10μM curcumin (the highest concentration tested) showing a 75% reduction in AF, $p \leq 0.003$ (Figure 7.2). While shifting the balance of AF in the cultures, there was no alternate build up of GFP-positive aggregates as one might expect based on other data using other polyphenolic compounds (Figure 7.3A) [Mazzulli et al. 2006; Berthelier unpublished data]. Our lab has shown *in vitro* that the treatment of Q50 synthetic aggregates with catechols modifies polyGln aggregate morphology so that the aggregate appears more truncated than an untreated fibril (Figure 7.3B) and are incapable of extension in a polyGln elongation assay (Section 3.8) [Berthelier unpublished data]. These data support other *in vivo* findings where catechols were found to be inhibitors of α-synuclein aggregation while facilitating the formation of oligomeric intermediates [Mazzulli et al. 2006]. Furthermore, curcumin is similar in structure to CR in that both have charged poles and are symmetrical with a hydrophobic spacer. CR has been shown to inhibit the oligomerization of polyGln in cell cultures as well as had beneficial effects when administered to mice [Sanchez et al. 2003]. Also important to note is that no visual cytotoxic response was induced by curcumin treatment. For this reason, a cell proliferation assay was not performed. Implications of these results will be discussed in Chapter 9 of the dissertation.

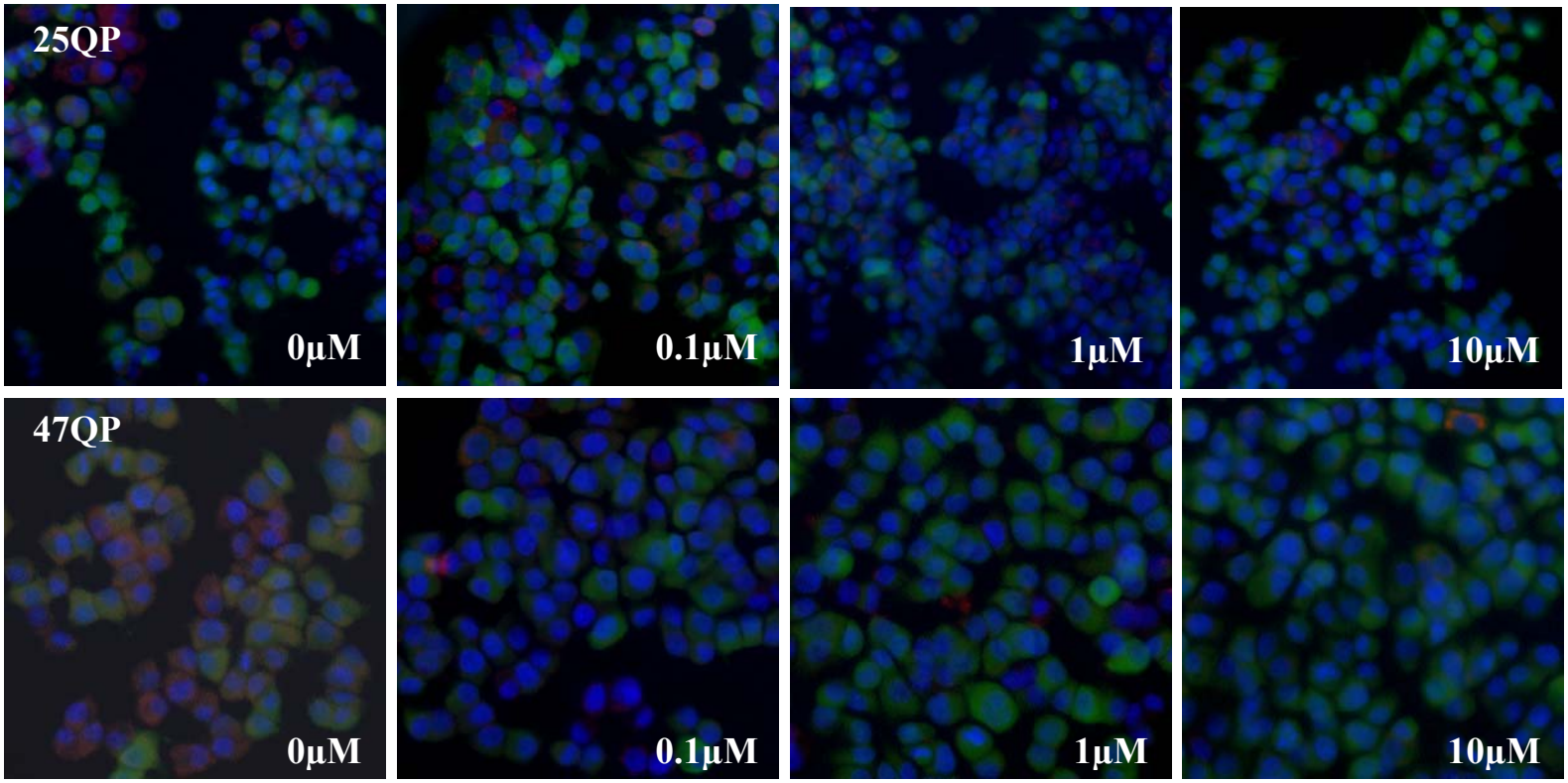

Figure 7.1: Effects of curcumin on aggregation foci in 25 QP and 47QP cells. Cells were simultaneously exposed to the curcumin and inducing agent for 24 hours. Top row: 25QP cells. Bottom row: 47QP cells. From left to right cells were treated with 0, 0.1, 1, or 10μM curcumin. Fluorescence colors: blue – cell nuclei, green – htt-polyGln-GFP fusion protein, red – aggregation foci.

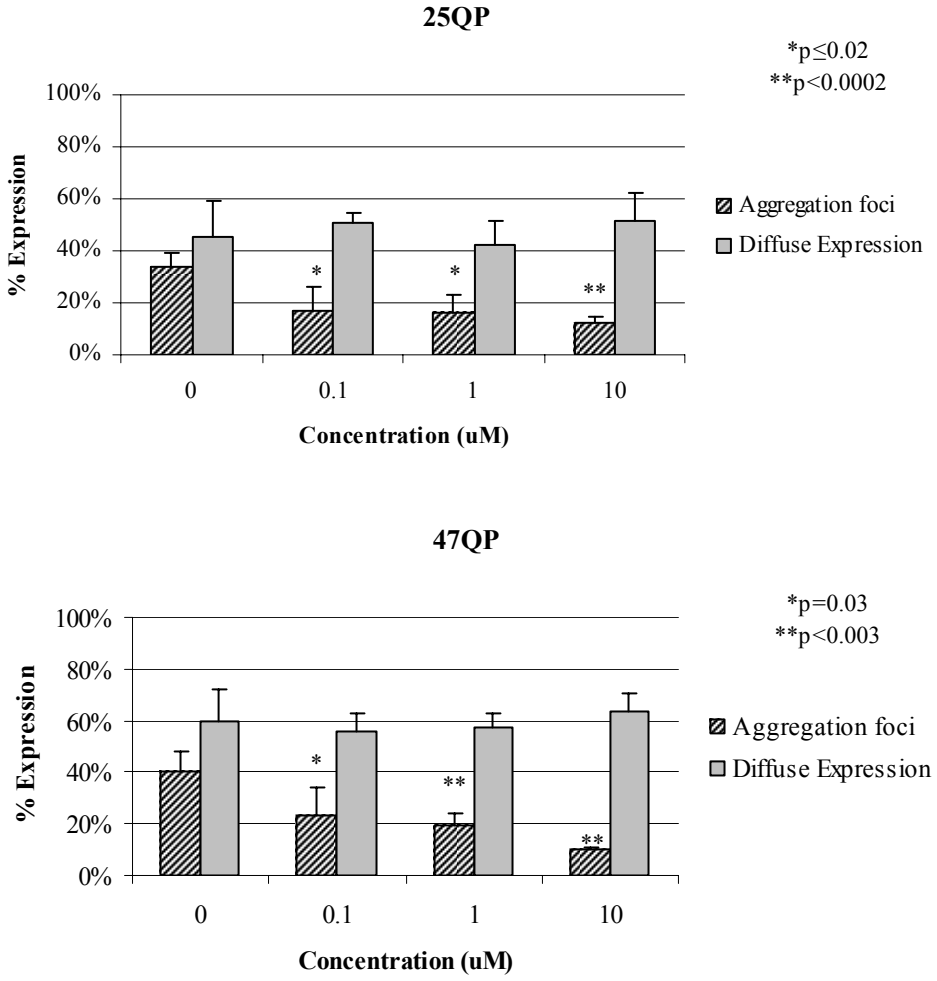

Figure 7.2: Curcumin inhibited $G^-R_C^+$ in a dose-dependent fashion. Cells were plated at a density of 100,000 cells/cm^2 16-24 hours prior to the addition of ponasterone and curcumin. Results are calculated from four independent fields within a single experiment. More than 100 cells per field were counted. Data are expressed as percentage of cells expressing either species. An unpaired Student's t-test was used to calculate the p values.

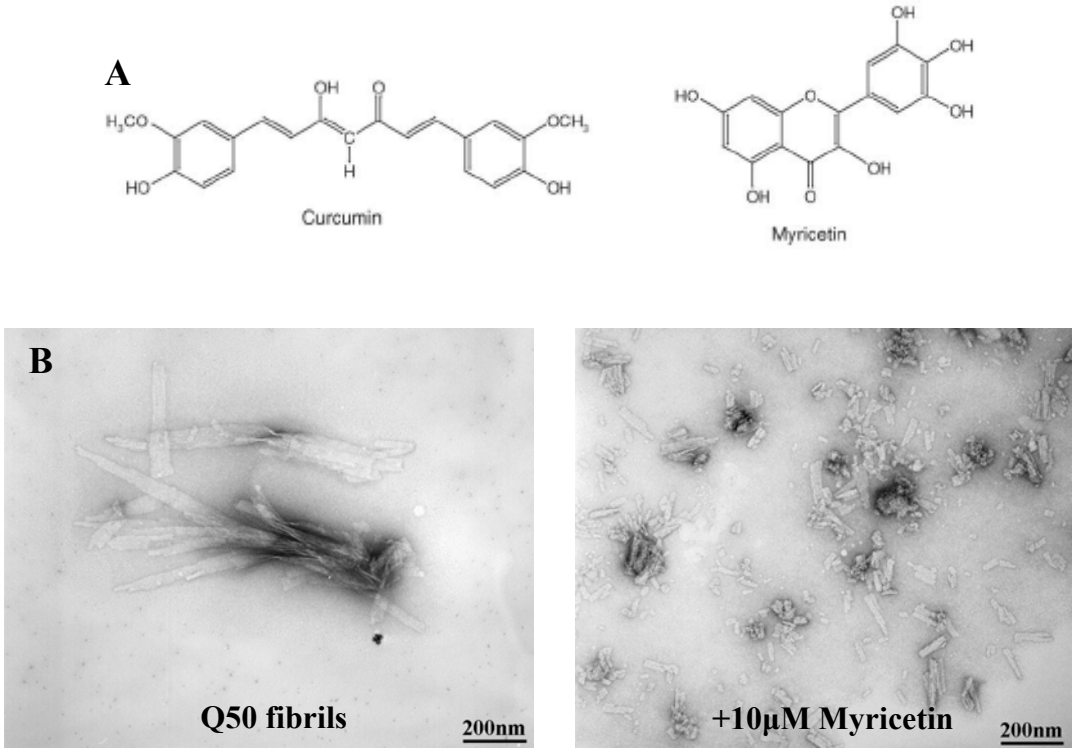

Figure 7.3: Curcumin is similar to Myricetin, which alters aggregate morphology. *(A) Curcumin and Myricetin are antioxidants that contain phenol groups. (B) Q50 synthetic fibrils untreated or treated with 10μM Myricetin.* Myricetin alters aggregate morphology. [Berthelier unpublished data]

7.3 Demecolcine inhibits $G_C^+R^-$ Species:

Since similar anti-amyloid effects of curcumin are seen in vitro, the role of curcumin in the above experiments is probably to attack the biophysical mechanism of aggregate assembly as it would occur in a simple in vitro experiment. Another approach would be to test a compound that interferes with a cellular mechanism potentially involved in modulating protein aggregation.

Therefore we now describe experiments in which cells were treated with a compound known to disrupt a vital cellular mechanism, i.e., microtubules, that are critical in aggresome formation [Johnston et al. 1998; Webb et al. 2004; Ross and Poirier 2005; Chang et al. 2006]. Aggresome formation is initiated in response to a cellular stress response, such as the overexpression of an insoluble, misfolded protein. Aggresomes are also characterized by perinuclear, large aggregates reminiscent of those seen in the Q103 expressing PC12 cells. It has been well documented that aggresome formation can be inhibited by disrupting microtubule polymerization [Johnston et al. 1998; Garcia-Mata et al. 1999; Dul et al. 2001; Webb et al. 2004]. It was, therefore, important to examine the possibility that $G_C^+R^-$ structures might be aggresomes and whether treating the culture with a microtubule disrupting compound might alter aggregate formation.

Demecolcine is a compound known to synchronize the cell cycle and interfere with microtubule polymerization [Luduena and Roach 1991; Nishiyama and Fujii 1992; Sherwood et al. 1994; Wang et al. 1998; Dul et al. 2001; Knockaert et al. 2002]. At the same time, demecolcine has not been shown to exhibit any remarkable effects on other biochemical events within the cell [Nishiyama and Fujii 1992].

DETERMINATION OF THE APPROPRIATE COMPOUND CONCENTRATION

Htt-inducible cells expressing Q103, which make aggregates very aggressively, were chosen to test the effects of the compound because of the abundance of perinuclear $G_c^+R^-$ species in these cells. The assumption was that this cell line would display the most measurable amount of inhibition if these aggregates were formed via a microtubule-dependent mechanism. Q103 cells and the 25QP control cells were subjected to the same induction protocol as previously described (Section 3.2) with the simultaneous addition of demecolcine for 24 hours. Percentage of htt-polyGln was calculated based on the number of cells expressing GFP-positive monomers and/or aggregates. The data were obtained by assessing a minimum of 200 total cells within five non-overlapping microscopic fields.

Based on the literature, a variety of compound concentrations (70ng/ml (190nM)-400ng/ml (1.1μM)) have been shown effective at inhibiting aggresome formation [Sherwood et al. 1994; Dul et al. 2001; Knockaert et al. 2002]. For this reason, it was important to establish an effective inhibitory dose in our inducible cell system. We tested demecolcine in a concentration range of 0ng/ml-1,000ng/ml.

Based on an examination of diffuse staining, polyGln monomer expression (M) in 25QP cells was unaffected by the compound treatment (Figure 7.4A), suggesting the compounds did not interfere with the normal protein production within the cells. Without demecolcine treatment, Q103 cells yielded ~38% $G_C^+R^-$ species and ~5% $G_N^+R^-$ species (Figure 7.3B). However, upon compound treatment, there was a significant reduction in the percentage of cells that expressed the $G_C^+R^-$ species (decrease from 38% to <10%). In

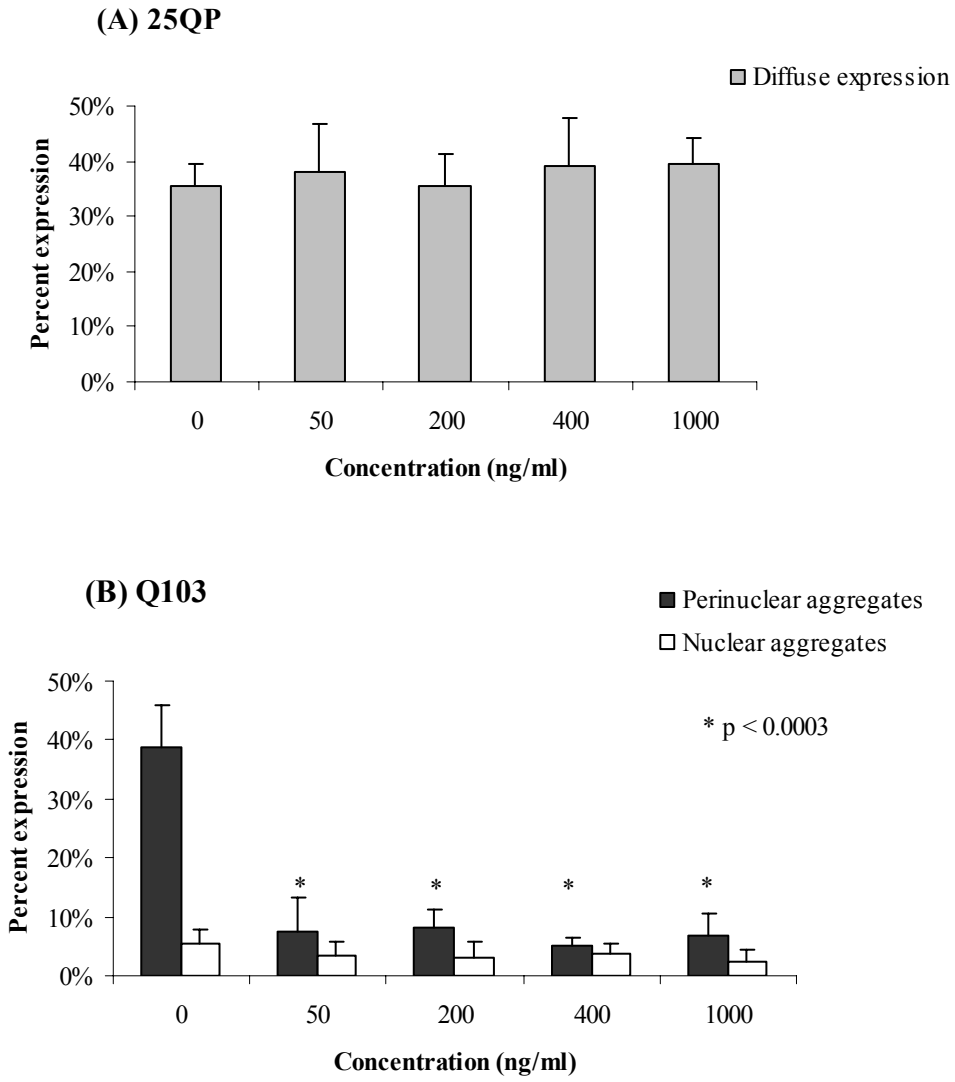

Figure 7.4: Effects of demecolcine on M and $G_C^+R^-$ expression. 25QP and Q103 cells were treated with various concentrations of demecolcine. *(A) Monomeric expression was relatively unaffected by compound treatment, as indicated in 25QP cells. (B)Percentage of Q103 cells that expressed $G_C^+R^-$ or $G_N^+R^-$ species.* $G_N^+R^-$ species were relatively unaffected by demecolcine treatment; however, $G_C^+R^-$ species were dramatically reduced. Percent expression was calculated based on the number of GFP-positive cells/total cell number. At least 200 cells in five non-overlapping fields were counted.

contrast, there was no statistically significant difference in the number of cells expressing $G_N^+R^-$ species (Figure 7.4B).

The effects we observed appeared to be dose-independent at the concentrations that we tested: 50ng/ml had the same significant $G_C^+R^-$ reduction as the 1,000ng/ml dose (Figure 7.4B). Figure 7.5 shows a representative image of Q103 cells prior to demecolcine treatment and an image after 24 hours treatment with 50ng/ml demecolcine.

7.4 Use of the PolyGln-recruitment Stain on Demecolcine Treated Cells:

Initial experiments indicated that demecolcine treatment mediated a significant reduction in $G_C^+R^-$ aggregates; however, it was uncertain whether the compound had any effect on the $G_C^+R_C^+$ or $G^-R_C^+$ species. In order to test the effects of demecolcine on each of the polyGln species, all htt-inducible cells (25QP, 47QP, 103QP, and Q103) were treated with 50ng/ml demecolcine; after which, they were subjected to the polyGln-recruitment stain (Section 3.3) (Figure 7.6).

The results revealed that upon demecolcine treatment, the observed polyGln species (M, $G_C^+R^+$, and $G^-R_C^+$) in 25QP, 47QP, and 103QP cells were relatively unaffected (Figure 7.7). In 47QP cells, M species remained at ~50% expression while $G^-R_C^+$ species were representative of ~30% of the expressing cells. In 103QP cells, ~25% of the polyGln expressing cells were M and another ~20% expressed the $G^-R_C^+$ species. Perinuclear GFP-positive aggregates ($G_C^+R_C^{-/+}$) appeared unaffected in this particular cell line.

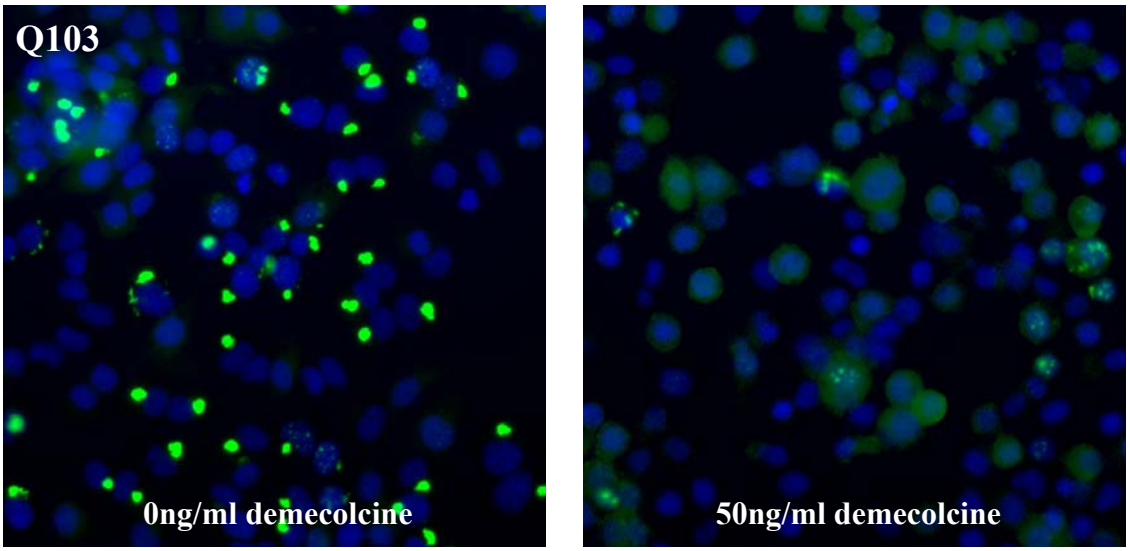

Figure 7.5: Treatment with demecolcine effects $G_C^+R^-$ species in Q103 cells. Cells were treated with 0ng/ml demecolcine and 50ng/ml demecolcine for 24 hours. Compound treatment significantly reduced the percentage of cells that expressed $G_C^+R^-$ but not $G_N^+R^-$**.** Blue – cell nuclei, Green – polyGln-GFP fusion constructs. These images are of cells that were not subjected to the AF stain; therefore, no red fluorescence should be observed.

Figure 7.6: Microscopic observations of the effects of demecolcine on htt-polyGln species. Fluorescence color is blue for cell nuclei, green for GFP fusion constructs, and red for aggregation foci. In each panel, the left column represents images taken by modified DIC microscopy. The last column in each panel represents the red, green, and blue merged image. The middle columns show a merger of the red and green images, where the detail of AF and htt colocalization may be more easily observed. The top rows of the cell lines are representative of untreated cells, while the bottom rows show cells treated with 50ng/ml demecolcine for 24 hours.

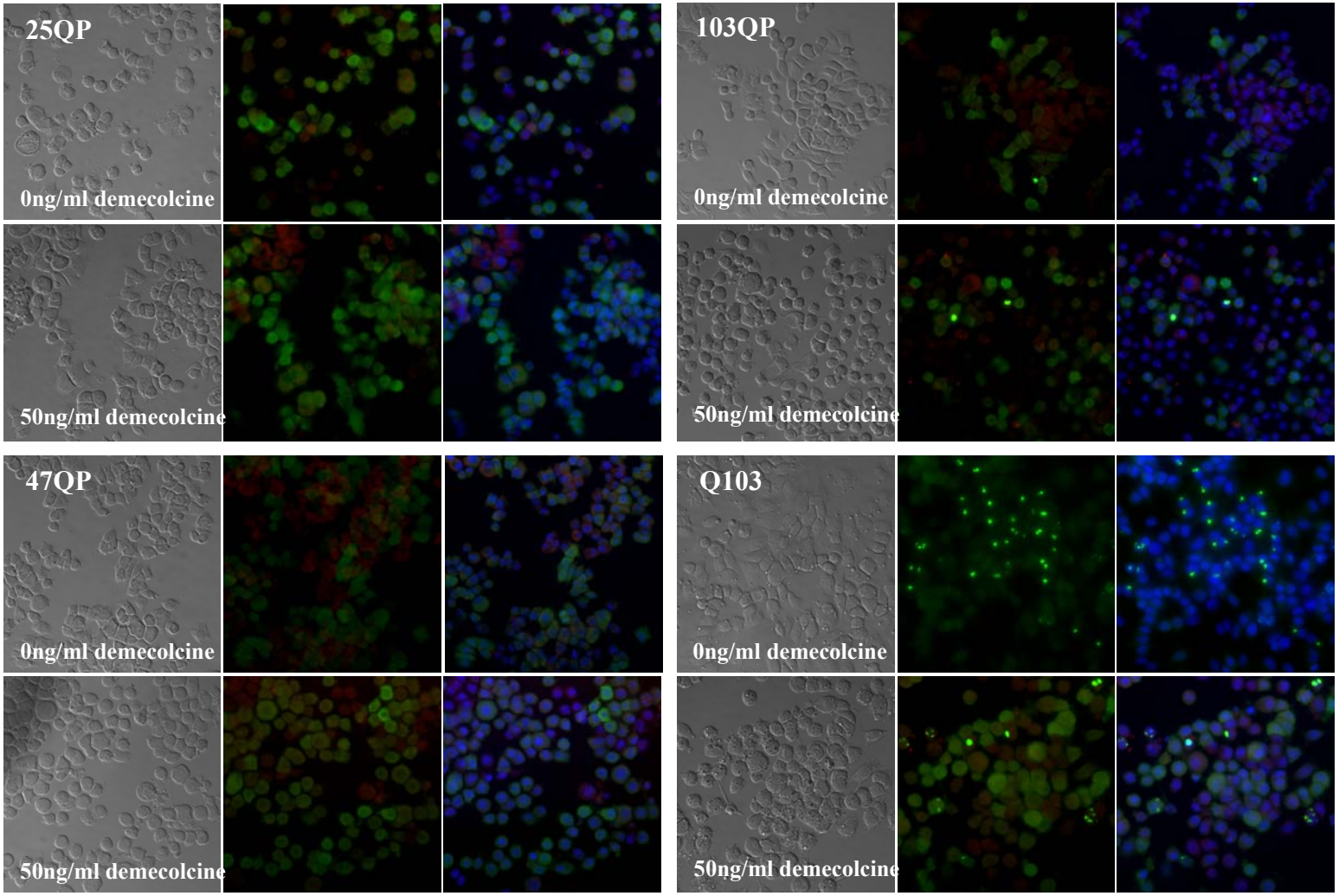
25QP
0ng/ml demecolcine
50ng/ml demecolcine
103QP
0ng/ml demecolcine
50ng/ml demecolcine
47QP
0ng/ml demecolcine
50ng/ml demecolcine
Q103
0ng/ml demecolcine
50ng/ml demecolcine

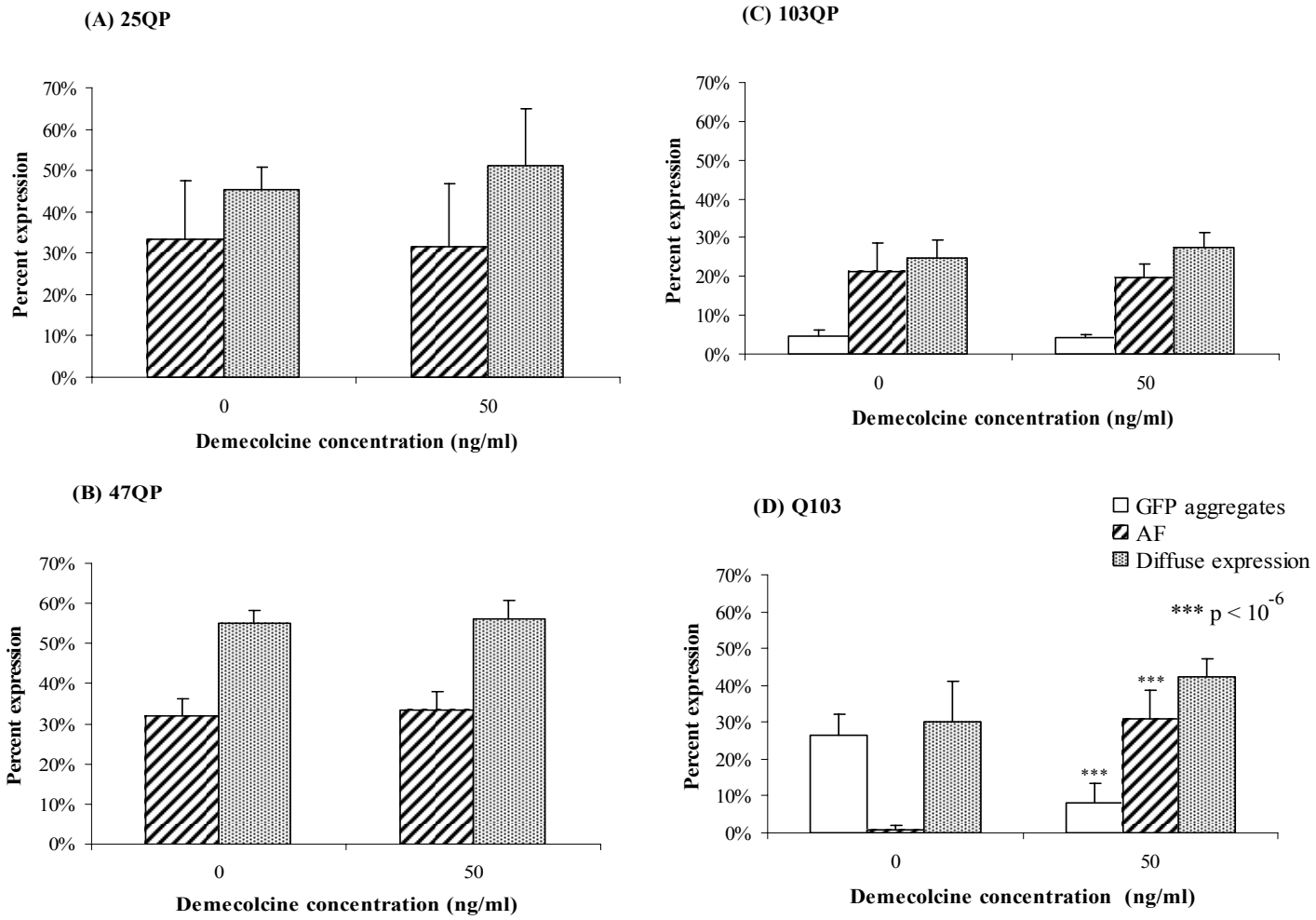

Figure 7.7: Percentage of expression of the various polyGln species after demecolcine treatment. Data were collected from a minimum of five independent fields. The data are expressed as the percentage of total cells that exhibited either diffuse expression (▩), GFP aggregates (□), or AF (▨). Data shown are 24 hours post-induction and compound treatment.

In contrast to the modest effects of demecolcine treatment of the various full length exon-1 ("QP") constructs, we observed a remarkable demecolcine effect in the Q103 cell line. These cells normally aggregate very robustly yet fail to exhibit any AF. In the presence of demecolcine, there was a significant knockdown in the number of $G_C^+R^-$ species by 75% (Figure 7.7D), yet, as shown previously, $G_N^+R^-$ species were relatively unaffected (Figure 7.4B). Interestingly, we observed that in addition to a reduction in the $G_C^+R^-$ species, the $G^-R_C^+$ species was remarkably increased (from 1% to 30% (Figure 6.2)). The total htt-polyGln protein expression (M, $G_C^+R^-$, $G_N^+R^-$, $G^-R_C^+$), however, was relatively unchanged.

Demecolcine treatment did not have a profound effect on any of the cells expressing the complete htt exon-1 and was only effective in altering the polyGln expression profile in cells expressing the truncated htt exon-1 fragment. The implications of these data will be discussed in Chapter 9.

EFFECTS OF DEMECOLCINE ON CELL PROLIFERATION

Microscopic examination of demecolcine treated cells revealed the presence of some (<10%) apoptotic cells (condensed or fragmented nuclei and cytoplasmic blebbing); however, the observed amounts did not appear to be considerable. To be certain, a cell proliferation assay was performed as described in Section 3.5 on all htt-inducible cell lines (25QP, 47QP, 103QP, and Q103). The results indicated that the effects of demecolcine mimicked the observed microscopic data, with the exception of the 25QP cells (Figure 7.8). In this case, the microscopic data suggested only a slight reduction in viability of demecolcine treated cells (Figure 7.9), but an MTS reduction assay showed

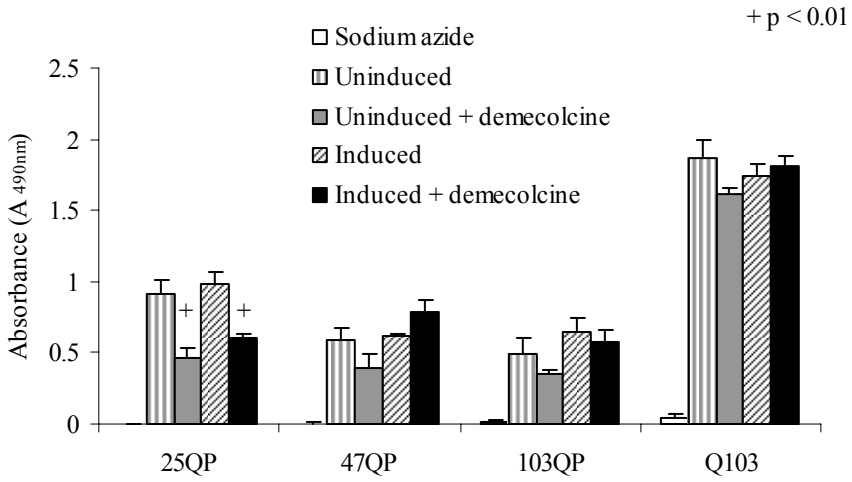

Figure 7.8: Effects of demecolcine on cell proliferation. Cells were plated at various densities: 25QP cells were plated at a density of ~100,000 cells/cm^2; 47QP and 103QP cells were plated at a density of ~60,000 cells/cm^2; and Q103 cells were plated at a density of ~200,000 cells/cm^2. A cell proliferation assay (MTS reduction) was performed to measure the number of viable cells. The number of viable cells is directly correlated to the absorbance readings.

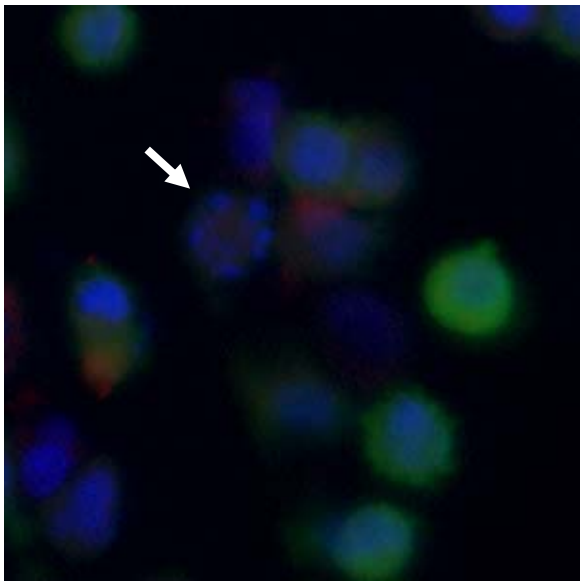

Figure 7.9: Minimal apoptotic bodies were observed in 25QP cells treated with demecolcine. These results were in contrast to the MTS reduction assay (Figure 7.8). Blue – nuclei, green – htt-polyGln-GFP, red – AF.

that demecolcine treatment significantly reduced the number of 25QP viable cells ($p < 0.01$) (Figure 7.8).

The reasons for the conflicting results are not clear; however, the simplest explanation may be that when the cell proliferation assay was performed, there was an uneven distribution of the cells such that fewer 25QP demecolcine treated cells were plated than the untreated counterparts, which is consistent with the design of the assay (absorbance signal is directly proportional to the number of viable cells present). Also, considering demecoline arrests cellular division [Luduena and Roach 1991; Nishiyama and Fujii 1992], some cell death is inevitable. An alternative rationale would be that this particular subclone of the cell line was more susceptible to apoptotic induction (possibly due to the randomness of transgene insertion) than a different subclone of the same cell line. These hypotheses were not tested due to time constraints; however, additional work should be performed to better understand this occurrence.

The positive effects seen on demecolcine treatment suggests the operation of microtubule-dependent processes in the intracellular aggregation of these truncated exon-1 proteins. M and $G_N^+R^-$ species were unaffected by this treatment, while $G^-R_C^+$ and $G_C^+R^-$ species were only affected in cells expressing truncated htt exon 1 fragments lacking the proline-rich region. These results suggest that there are multiple aggregate assembly pathways and that factors in the cellular environment may govern the rates at which aggregates are formed. The implications of these results will be discussed later.

7.5 Effects of Nocodazole on Aggregate Formation:

We wanted to confirm the observed effects of demecolcine are really attributable to its microtubule-depolymerizing activity by also testing another compound (nocodazole) also shown to be an effective microtubule-depolymerizing agent [Johnston, Ward et al. 1998; Shimohata et al. 2002; Webb, Ravikumar et al. 2004]. The major mechanistic difference between the two compounds is that the effects of demecolcine are reported to be irreversible, while removal of nocodazole treatment allows restoration of microtubule formation [DeBrabander 1981; Zieve 1984]. Since reversibility might provide some unique advantages in our experiments, we also investigated nocodazole.

Like with demecolcine, a range of effective nocodazole doses have been reported (100ng/ml (330nM) – 200ng/ml (650nM)) [Shimohata et al. 2002; Webb et al. 2004]. Therefore, we treated Q103 cells with doses ranging from 50ng/ml-400ng/ml (Figure 7.10). Treatment with nocodazole (400ng/ml) for 24 hours was effective at reducing $G_C^+R^-$ species (Figure 7.11); however, we also observed a drastic reduction in the number of attached cells, indicating that this concentration was detrimental to the cells in our system. Because of the loss of cells observed with nocodazole and the dramatically higher concentration needed to achieve aggregate inhibition, we terminated this line of experiments.

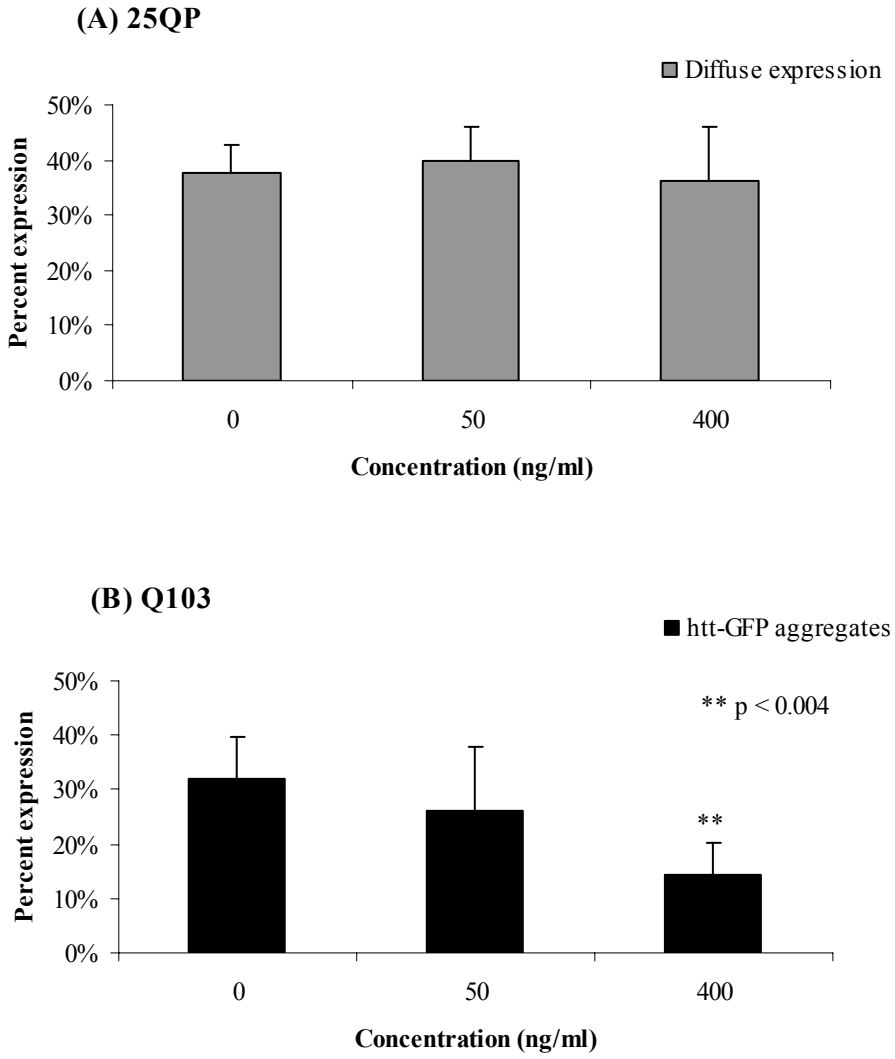

Figure 7.10: Nocodazole reduced $G_C^+R^-$ aggregates at a concentration of 400ng/ml. 25QP and Q103 cells were treated with various concentrations of nocodazole for 24 hours. *(A) Monomeric expression was relatively unaffected by compound treatment, as indicated in 25QP cells. (B)Percentage of Q103 cells that expressed htt-GFP aggregates.* $G_C^+R^-$ species were dramatically reduced. Percent expression was calculated based on the number of GFP-positive cells/total cell number. At least 120 cells in five non-overlapping fields were counted.

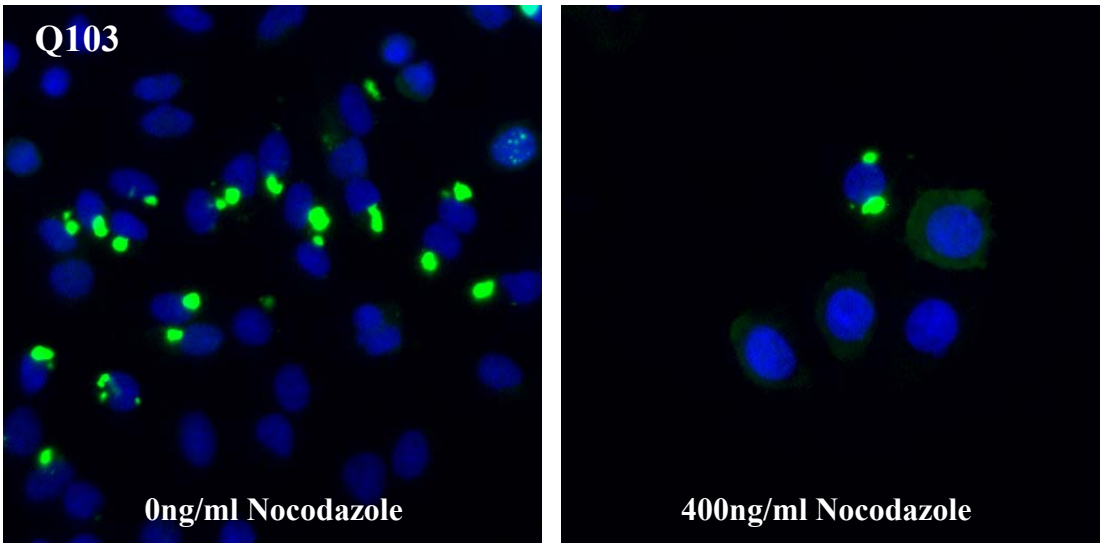

Figure 7.11: Nocodazole effectively inhibited $G_C^+R^-$ species in Q103 cells but caused a loss of cells. Blue – nuclei, green – htt-GFP fusion proteins. AF stain was not applied to these cells; therefore, there was no red fluorescence to monitor.

CHAPTER 8

BIOCHEMICAL CHARACTERIZATION OF OBSERVED POLYGLUTAMINE PHENOTYPES

8.1 Rationale:

Considering a number of polyGln species have been identified in the PC12 cell system, and some of these species were affected by compound treatment, the next logical step was to try to gain some biochemical information about each class that corroborated the microscopic observations. These measurements were necessary to address some key questions that we were unable to address with the microscopic data: such as, 1) whether the observed diffuse expression pattern actually represents monomer or microaggregate structures, 2) whether it was possible to physically separate the observed species, and 3) to obtain functional data, for example that might allow us to determine which species is the most active in recruiting biotinylated polyGln monomer *in vitro*. In the long run, the ability to prepare enriched cellular aggregate fractions might allow further studies, for example to determine the non-htt-exon-1 components of these fractions.

In recent years, several groups have shown that multiple aggregated forms of polyGln-containing proteins exist [Poirier, Li et al. 2002; Ellisdon, Thomas et al. 2006; Wanderer and Morton 2007]. A considerable amount of effort has been spent trying to isolate polyGln aggregates and learn more about their biochemical makeup [Scherzinger et al. 1999; Steffan et al. 2000; Suhr et al. 2001; Webb et al. 2004; Chow et al. 2006;

Cong et al. 2006; Schilling et al. 2007]. Many isolation techniques have been explored. For example, the most common isolation approach has been to utilize centrifugation [Scherzinger, Sittler et al. 1999; Steffan, Kazantsev et al. 2000; Suhr et al. 2001; Webb, Ravikumar et al. 2004; Schilling et al. 2007], while others have used size exclusion chromatography [Cong et al. 2006], and immunoaffinity purification (purification by using an antibody to the protein or to the fusion tag) [Chow et al. 2006]. Each method was successful in the crude isolation of polyGln proteins with affinity tags proving especially effective. This chapter will discuss the methods we evaluated for isolating the various classes as well as the gamut of other techniques utilized to gain more information about the observed species.

8.2 Cell Lysis:

Whole cell lysates of each cell line were prepared at 24-72 hours post-induction as described in Section 3.6. Briefly, cells were collected by centrifugation, resuspended in the isotonic lysis buffer containing Triton® X-100, vortexed, and sonicated resulting in disruption of the cellular material. Cell lysates were then fractioned (via gel filtration or differential centrifugation) and examined for the presence of the polyGln proteins of interest by virtue of Western blot analysis and reactivity to anti-GFP (Santa Cruz Biotechnology) and 1C2 (Chemicon) (anti-polyglutamine) antibodies.

8.3 Gel Filtration:

We began our efforts to fractionate cell lysates using size exclusion chromatography (gel filtration). For these studies, Q103 cells (24 hours post-induction), which produced a high percentage of cells expressing $G_C^+R^-$ and some M, were subjected to this technique (Section 3.6). Each gel filtration fraction collected was tested for the presence of polyGln-containing proteins and reactivity with an anti-GFP antibody (data not shown). 1C2 and anti-GFP reactivities were only detected in fractions that were collected within 7-9 ml (less than one column bed volume). Interestingly and contradicting our original hypothesis, we found no detectable protein (polyGln or otherwise) in the void volume, suggesting that only soluble, low molecular weight polyGln species were being isolated. From these results, three alternative hypotheses were formed: 1) the lysis buffer that we used to extract the proteins was solubilizing the aggregates, 2) the large aggregates were getting trapped in the gel filtration column, or 3) there are no aggregates in these cells (i.e., the punctuate green staining does not indicate aggregated material).

To address the first concern, preformed synthetic aggregates, which have been shown to be SDS-resistant [Chen and Wetzel 2001], were treated with the lysis buffer and subjected to SDS PAGE as described in Section 3.7. Synthetic and recombinant exon-1 polyGln aggregates have been shown to be similar to late-stage htt aggregates [Cooper, Schilling et al. 1998; Kazantsev, Preisinger et al. 1999; Chen, Berthelier et al. 2001] in that they are SDS-resistant. Lysis treatment did not alter the SDS solubility of the $K_2Q_{47}K_2$ aggregates. These aggregates remained insoluble and did not enter into the

gel (Figure 8.1). Although this experiment was important to conduct, perhaps it did not fully resolve the question. The purpose of conducting such biochemical experiments was to learn more about the nature of all the aggregates and other polyGln species within the cell culture. By only testing the lysis buffer with very stable, end-stage polyGln aggregates, the possibility cannot be excluded that less stable, early aggregates might be dissociated by the lysis buffer.

The second concern was addressed, by sampling the top of the column for 1C2 reactive proteins. A small portion of lysis buffer and the column bed (500µl) was removed by a pipette, homogenized, and subjected to the SDS-PAGE protocol (Section 3.7). One set of the SDS gels were stained with Coomassie Blue, while the other set was transferred to a nitrocellulose membrane and subjected to the Western blot protocol using the 1C2 antibody (Section 3.7). In support of the hypothesis that polyGln aggregates did not enter the column, the Coomassie stained gels exhibited a small amount of protein was associated with the top of the column (Figure 8.2). However, this protein appeared to not be related to the transgene product, since it was negative in Western blots using the 1C2 antibody. The source of the Coomassie-positive, 1C2-negative material was not clear. It could have represented non-htt-exon-1 related high MW proteins from the cell. Failure to detect polyGln aggregates might also be explained by a failure of the "aggregated" protein to transfer to the membrane. To test this, the gel after electrotransfer was stained with Coomassie and found to exhibit no residual protein staining, consistent with complete protein transfer (data not shown).

Thus, clear results on the gel filtration fractionation of cells shown by fluorescence microscopy to contain aggregates were unattainable. Proteins containing

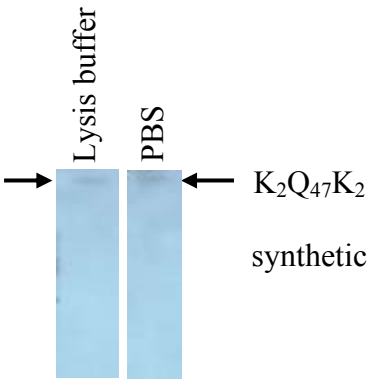

Figure 8.1: Lysis buffer does not affect SDS-resistance in $K_2Q_{47}K_2$ synthetic aggregates. Aggregates were subjected to SDS treatment, gel electrophoresis, and Western blot analysis with 1C2 antibody. Irrespective of treatment, the preformed aggregates did not migrate into the gel but remained at the top of the well, as indicated by the black arrows.

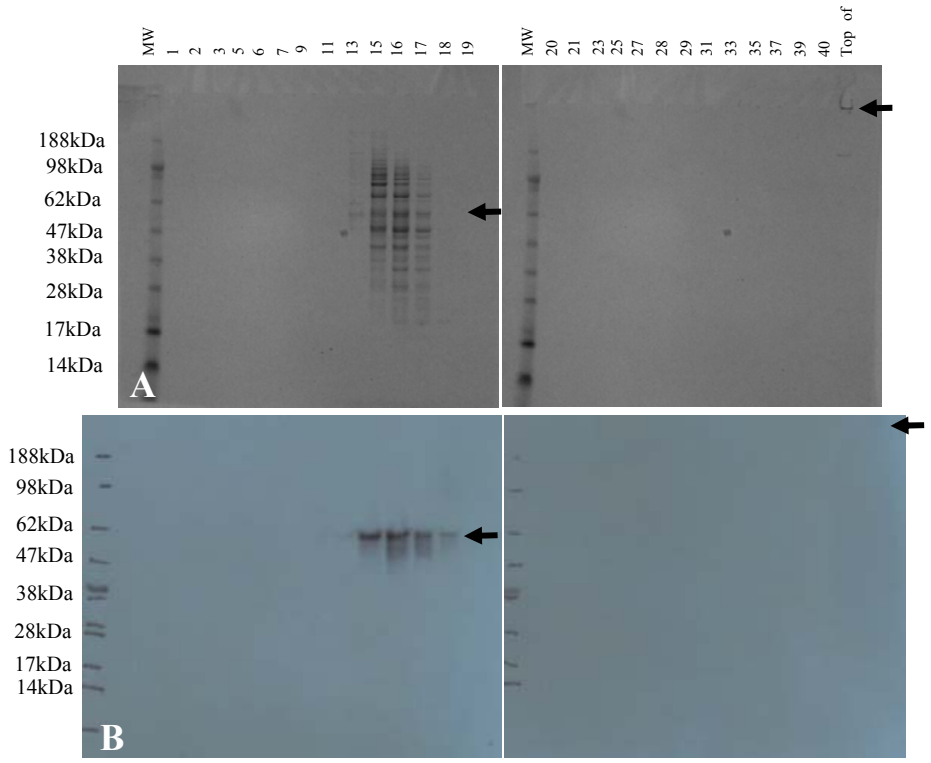

Figure 8.2: Material at the top of a gel filtration column was 1C2-negative. *(A) Q103 fractions subjected to SDS-PAGE and stained with Coomassie blue. (B) 1C2 reactivity of transferred gel.* While there was Coomassie staining in the top of the gel, usually suggestive of aggregates, they were not reactive with an anti-expanded polyGln antibody.

extended polyglutamine stretches are inherently known to be very sticky molecules, which might account for loss of protein. Alternatively, the chosen method of evaluating the top of the column could have been better designed. Since, for whatever reasons, isolation of the polyGln species by gel filtration was unsuccessful, we investigated an alternative approach at fractionation: centrifugation.

8.4 Differential Centrifugation:

Cell lysates prepared as described in Section 3.6 were fractionated by the differential centrifugation protocol shown in Figure 3.4. Four fractions were analyzed from each cell line 24-72 hours post-induction: 1) whole cell lysate (W), 2) washed pellet from 15,000xg spin (P1w), 3) pellet from 100,000xg spin (P2), and 4) supernatant from 100,000xg spin (S2). The hypothesis was that P1w should contain the large $G_C^+R_C^{-/+}$ species, P2 should contain the relatively small $G_N^+R^-$ and $G^-R_C^+$ species, and S2 should contain M species. Each fraction was subjected to electrophoresis under denaturing conditions (Section 3.7) after which the proteins were electrotransferred to a nitrocellulose membrane where they were probed for their reactivities with anti-GFP and 1C2 antibodies (Section 3.7). Positive antibody binding was detected using chemiluminescence.

Initial experiments were performed to confirm that the GFP aggregates were indeed co-localized with polyGln. GFP has been shown to self-aggregate (a rare occurrence) in the presence of small peptides [Link et al. 2006], these aggregates maintain there fluorescence. Therefore, we needed to be certain that the observed fluorescence was not due to the proteolytic cleavage of GFP from htt exon-1, which then

self-aggregated. Cell lysates from Q103 cells were tested for this occurrence. Microscopically, these cells expressed an abundant population of cells with $G_C^+R^-$ aggregates. Western blot analysis revealed that there was an overwhelming 1C2 anti-polyGln reactivity co-localizing with the anti-GFP antibody (Figure 8.3), suggesting that no measurable proteolysis of the construct occurred prior to aggregation.

Next, the question of whether the observed diffuse fluorescence was due to monomeric species or microaggregates was addressed. This question was most cleanly addressed with the 25QP cells. At 24 hours post-induction, 25QP cells have been shown by fluorescence microscopy to have 40% of the cells expressing M and 40% of the cells expressing $G^-R_C^+$ aggregates, with no cells expressing G^+R^- aggregates (Figure 6.2). Western blot analysis of lysate centrifugation fractions of these cells supported the fluorescence microscopy in showing the htt exon-1 immunoactivity to be associated only with the high speed centrifugation supernatant (presumably M) and pellet (presumably $G^-R_C^+$). The S2 fraction from the 25QP cells showed a high reactivity with both the 1C2 and anti-GFP antibodies (Figure 8.4), suggesting that the observed diffuse green staining pattern was due to intact (monomeric) GFP-htt-exon1 fusion proteins. The fact that there was a quantitative difference between the gel and microscopy results for 25QP cells may be due to the inefficient pelleting of the small $G^-R_C^+$ aggregates. At the same time, there seems to be no reason to expect quantitative agreement, given that the scoring of the microscopy was not based on molar measurements.

While the possibility that some of the diffuse green in these and other cells may be due to SDS-stable microaggregates cannot be eliminated, the results in Figure 8.4 suggest that the bulk of diffuse staining is really due to M. Microscopic examinations from other

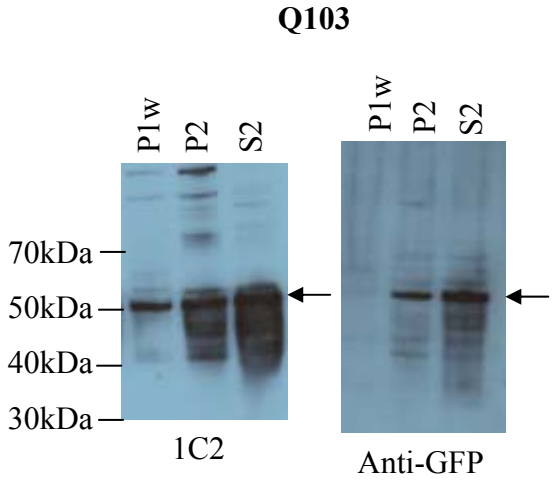

Figure 8.3: Representative autoradiograms that show 1C2 and anti-GFP co-reactivity. Q103 cell lysate samples (24h) showed that the only GFP detected runs at a MW consistent with that of the full length exon1-GFP fusion. Abbreviations: P1w – washed pellet from low speed centrifugation, P2 – pellet from high speed centrifugation, S2 - supernatant

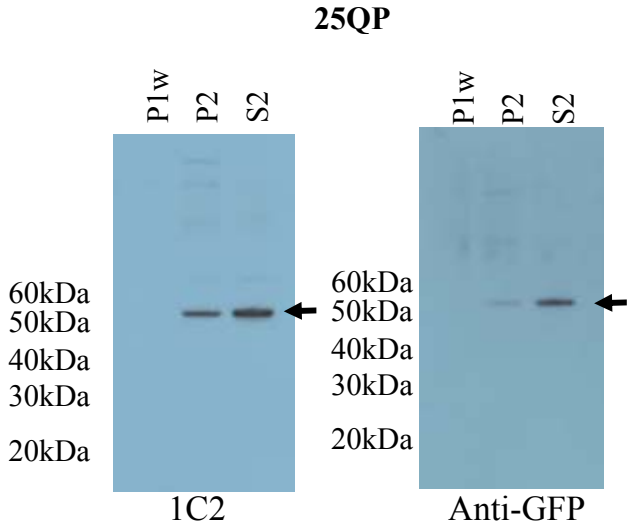

Figure 8.4: Autoradiograms of 25QP cells lysates 24 hours post-induction. The predominant 1C2 and anti-GFP reactive bands are found in the S2 fraction; however, there was also some GFP reactivity found in the P2 fraction. Abbreviations: P1w – washed pellet from low speed centrifugation, P2 – pellet from high speed centrifugation, S2 - supernatant

groups are consistent with the idea that the diffuse staining pattern is representative of monomeric species [Lunkes and Mandel 1998; Preisinger et al. 1999; Apostol et al. 2003]. In this thesis, we will be assuming that diffuse staining comes exclusively from monomers. Parenthetically, we also cannot formally exclude the possibility that monomer might sometimes migrate in more dense centrifugation fractions due to association with cellular membranes/debris.

Microscopically, the appearance and disappearance of the different polyGln species with increasing induction times were able to be monitored. We, therefore, wanted to examine whether or not we could develop a better understanding of the nature of these species by analyzing cell fractions. Cell fractionation studies focused on the time period 24-72 hours post induction, mainly because of the significant changes observed in the 103QP and Q103 cells during this time frame. At each time point in these fractions, the most reactive gel band (according to the Western blot analysis) was, as expected, our expressed htt-polyGln-GFP constructs, which can be observed between 45-55kDa depending on the polyGln repeat length[1]. Figure 8.5 shows a representative 1C2 blot from each of the cell line lysates at 48 hours post-induction. In the Q103 blot, it is important to note that non-transformed PC12 cells as well as uninduced control samples were also assayed. The uninduced controls had some slight reactivity with the 1C2 antibody that corresponded to our positive bands in the induced samples. This was not unexpected

[1]In these gels, there is a consistent discrepancy between the calculated molecular weights and the observed molecular weights of the polyGln containing proteins (Table 8.1). These differences are routinely seen in SDS gels of polyGln proteins by our group and by others, and can be accounted for by some not-well-understood interaction between polyGln and polyacrylamide producing aberrant mobility of polyGln proteins in SDS-PAGE.

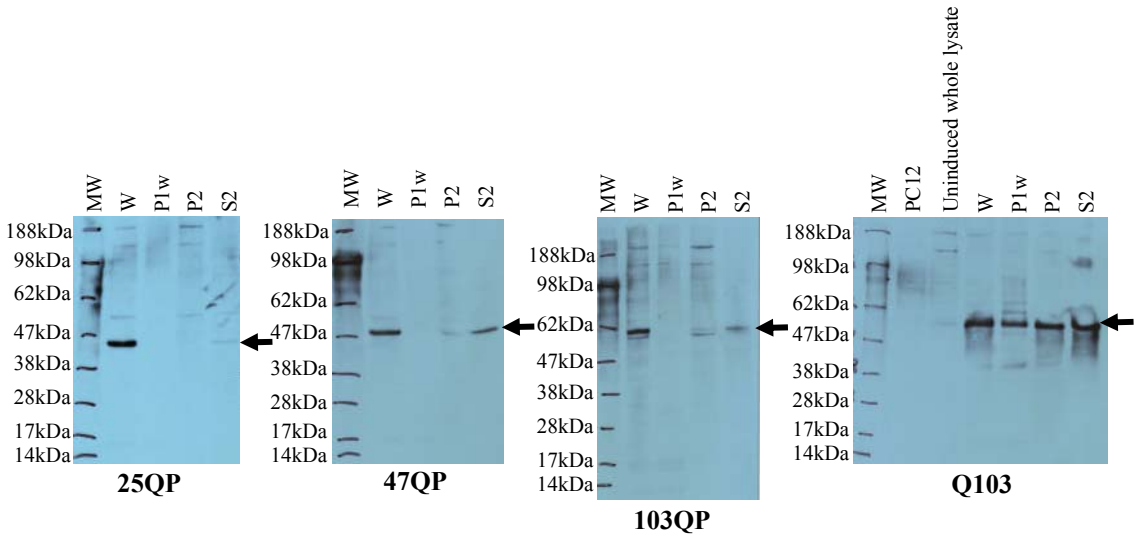

Figure 8.5: 1C2 Western blot analysis of all cell line lysates at 48 hours post-induction. Lysates were fractionated by differential centrifugation. The htt-polyGln-GFP construct of interest is denoted by a black arrow.

Table 8.1: Approximate molecular weights of polyglutamine proteins and fragments.

Protein fragment	Calculated MW (kDa)	Observed MW (kDa) (±4kDa)
25QP	37.4	46
47QP	40	49
103QP	46.8	59
Q103	43	54
Free GFP	25.9	--
Free N1-17	2	--
Free C-Exon 1	6.5	--

because it has been shown [Apostol, Kazantsev et al. 2003] that these cells do have some "leaky" expression of the transgene.

Each cell line was examined independently for correlations between the microscopy data and the cell fractionation data. Densitometry analysis was performed on each 1C2 Western blot. Protein abundance was calculated for each major fraction. The numbers obtained from the P1w, P2, and S2 fractions are expressed as percentages of total gel staining material, and therefore sum to 100%. In contrast, the microscopy data was normally expressed as the percentage of cells containing each manifestation of htt exon-1. Since 10-30% of cells generally exhibit no expression of the transgene, the data were normalized to 100% in order to put the microscopy data on an equal footing for comparisons.

As mentioned previously, cells expressing 25QP exhibited a population expressing an equal mixture (±10%) of about 40% diffuse protein and 40% AF, which was relatively unchanged over the 24-72 hours period (Figure 8.6A). Densitometry analysis of the 1C2 Western blots revealed a similar trend, with fractions representing the soluble protein remaining at ~60% and the P2 fraction, which we interpret as AF, remaining at ~40% (Figure 8.6B) during the 3 time points.

Cells expressing 47QP produced similar data to 25QP cells (Figure 8.7). Both microscopic results and densitometry analysis revealed 40% expression of AF or P2 and 60% expression of diffuse or S2 at the 24 hour and 48 hour time points. There was, however, a slight discrepancy at 72 hours post-induction. Microscopic analysis showed that 60% of the cells were expressing AF and 40% of the cells were expressing monomer, whereas densitometry analysis revealed 5% of the protein was found in the P1w fraction

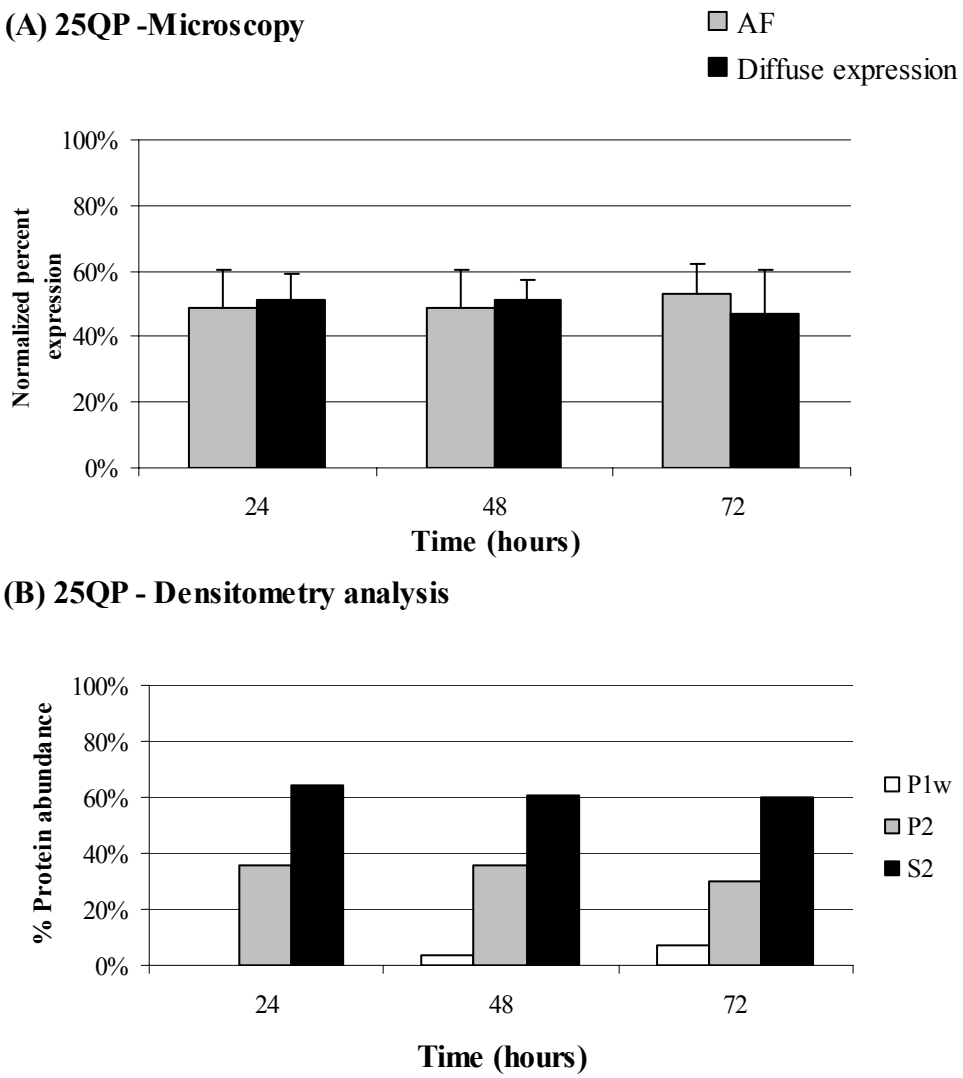

Figure 8.6: Microscopic and densitometry comparison of 25QP cells. *(A) Microscopic analysis of 25QP cells from 24-72 hours post-induction.* Percentage of cells expressing each species was normalized to 100% expression. *(B) Densitometry analysis of 25QP cell lysate fractions from 24-72 hours post-induction.* P1w- washed pellet from 15,000xg, P2 – pellet from 100,000xg, S2 – supernatant.

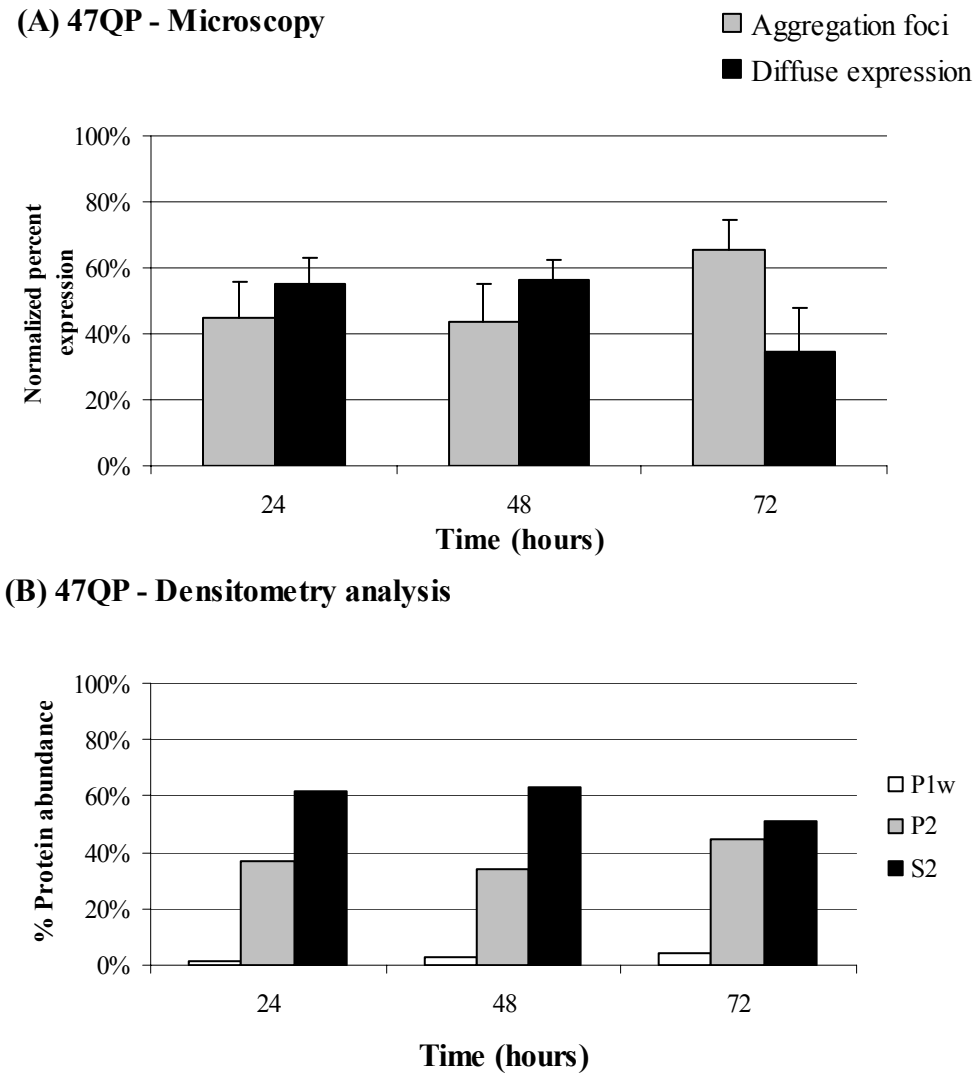

Figure 8.7: Microscopic and densitometry comparison of 47QP cells. *(A) Microscopic analysis of 47QP cells from 24-72 hours post-induction.* Percentage of cells expressing each species was normalized to 100% expression. *(B) Densitometry analysis of 47QP cell lysate fractions from 24-72 hours post-induction.* P1w- washed pellet from 15,000xg, P2 – pellet from 100,000xg, S2 – supernatant.

(normally associated with larger aggregates), 45% of the protein was found in the P2 fraction, and 50% of the protein was found in the S2 fraction. The small portion of material pelleting at low centrifugation speed found in these cells may be due to some aggregates not detected in the microscopy, or to M that is physically associated with cell debris and was not dislodged by washing.

103QP cells, which exhibited all the observed polyGln species, appear to be a more complex situation (Figure 8.8). At the 24 hour time point, it appeared that the major species by microscopic examination were $G^-R_C^+$. According to the densitometry data at this same time, the P2 fraction also represented the most abundant species. At 48 hours, the microscopic and densitometry analyses correlate fairly well, with 10% of the protein being large aggregates, 40% being smaller aggregated material, and ~50% of the protein being monomeric. By 72 hours, however, there was a small disagreement between the two data sets. Microscopically, we saw that 20% of the population had large $G_C^+R_C^+$ aggregates; however, the densitometry analysis revealed the P1w fraction represented only ~10% of the protein abundance. It is possible that the larger aggregates may be partially broken down by the detergent treatment used to prepare the lysate (see below). Even considering the slight disagreement at 72 hrs, the match between the centrifugation data and the microscopy data is striking.

Finally, microscopy showed that in Q103 cells there is a time-dependent increase in $G_C^+R^-$ species that we interpret as large exon-1 aggregates (Figure 8.9A). Consistent with this, densitometry of the 1C2 stained gel on Q103 cells shows a corresponding time-dependent increase in the P1w fraction that was expect to contain large aggregates (Figure

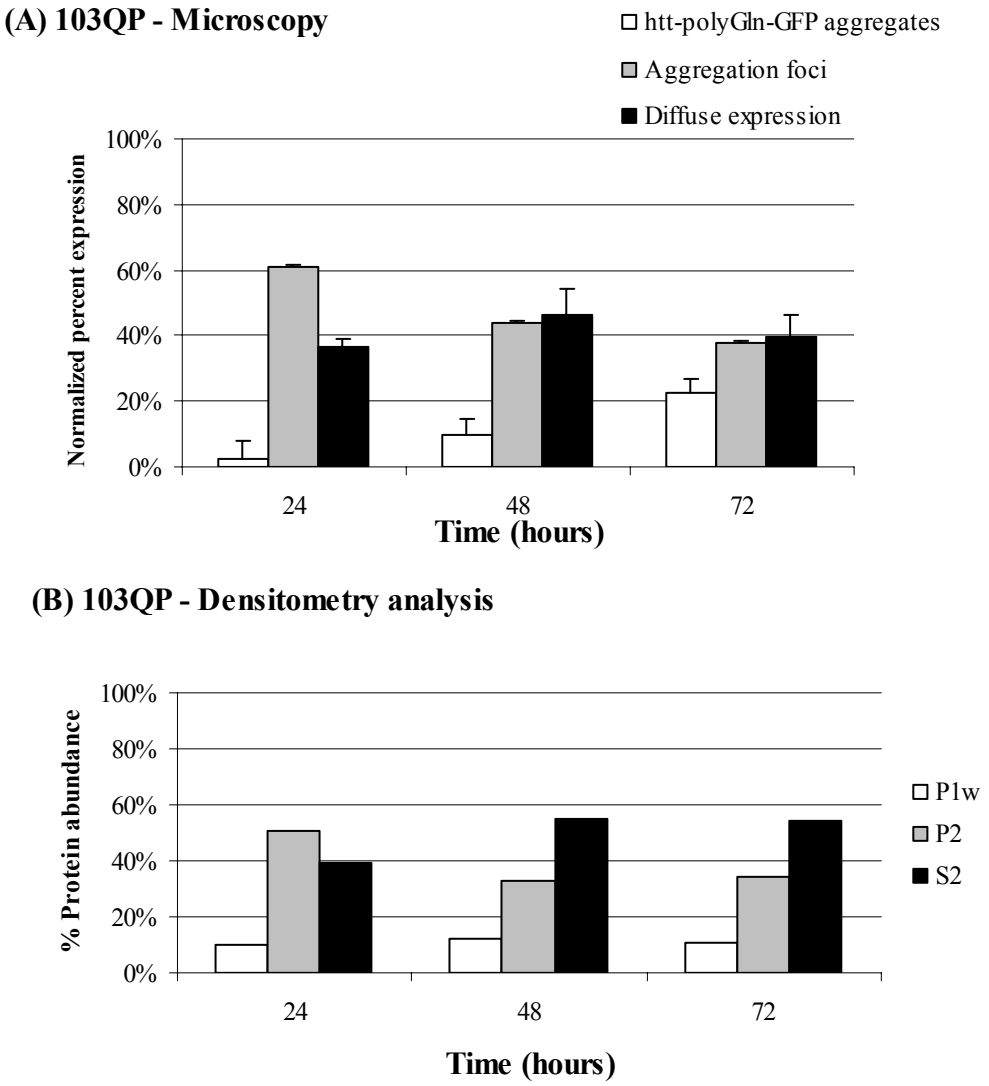

Figure 8.8: Microscopic and densitometry comparison of 103QP cells. *(A) Microscopic analysis of 103QP cells from 24-72 hours post-induction.* Percentage of cells expressing each species was normalized to 100% expression. *(B) Densitometry analysis of 103QP cell lysate fractions from 24-72 hours post-induction.* P1w- washed pellet from 15,000xg, P2 – pellet from 100,000xg, S2 – supernatant.

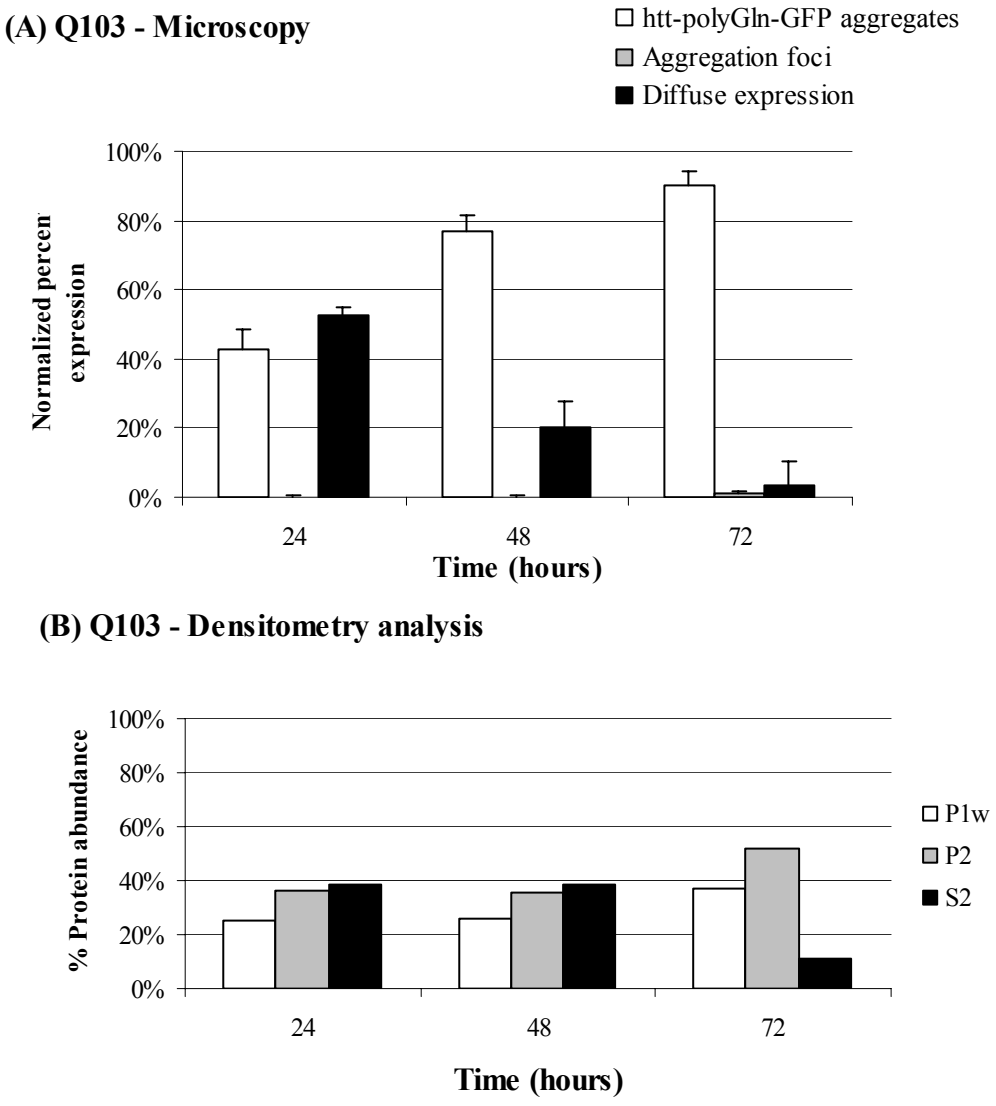

Figure 8.9: Microscopic and densitometry comparison of Q103 cells. *(A) Microscopic analysis of Q103 cells from 24-72 hours post-induction.* Percentage of cells expressing each species was normalized to 100% expression. *(B) Densitometry analysis of Q103 cell lysate fractions from 24-72 hours post-induction.* P1w- washed pellet from 15,000xg, P2 – pellet from 100,000xg, S2 – supernatant.

8.9B). However, inconsistent with the microscopic data is the relative abundance in which this species was found. The microscopy data revealed an increase from 40% $G_C^+R^-$ species to >80% $G_C^+R^-$ species from 24-72 hours; however, the densitometry data showed only an increase from 20% to 40% in the P1w fraction. Additionally, while the densitometry data shows that 40% or greater of the protein population was collected in the P2 fraction, microscopy found none of the $G^-R_C^+$ species in these cells that, in the "QP" series of cells discussed above, consistently correspond to material in the P2 (high speed) pellet fraction. Some of this more-difficult-to-pellet material may derive from the relatively small $G_N^+R^-$ species (<10%) observed by microscopy at these times (Figure 6.7). We hypothesize that the remainder of the material in the P2 fraction is from small aggregates generated by the lysis procedure from labile $G^-R_C^+$ species.

Overall, the cell fractionation data agrees remarkably well with the fluorescence microscopy. These data comparisons can be used to address another important question concerning the interpretation of the fluorescence microscopy data, the issue of whether perinuclear, punctate, green fluorescent bodies are really composed of aggregates of htt exon-1. As stated in Chapter 4, researchers often assume that punctate inclusions represent aggregated protein, and in fact use the terms interchangeably [Fink 1998; Johnston et al. 1998; Lunkes and Mandel 1998; Garcia-Mata et al. 1999; Preisinger et al. 1999; Apostol et al. 2003]. However, given the presence in the cell of a number of kinds of organelles, it is formally possible that punctate fluorescence might sometimes be due to the organization of monomers within a membranous compartment. The Western blot analysis revealed at this same time point that ~10% of the 1C2-positive population was found in the soluble fraction (Figure 8.8B), which was in remarkable agreement with the microscope data that revealed

that ~5% of the cells contained diffuse staining interpreted as "monomeric" species (Figure 8.8A). If most of the $G_{C/N}^{+}R^{-}$ species were collections of monomers, much more material would have been seen in the S2 fraction. We think these results justify our working assumption, shared with most of the field, that punctate inclusions represent some kind of aggregated material.

Some minor difficulties were encountered in the Western blot analysis. While polyGln-positive bands always were mirrored by a GFP-reactive band, the latter was often of a much lower intensity. This was especially evident in lysates produced from cells 24-72 hours post-induction (Figure 8.10). This problem was addressed by testing two different GFP antibodies: a rabbit polyclonal and a mouse monoclonal antibody. Although we used both antibodies at the lowest dilution suggested (1:150), the antibodies still failed to produce an intensity equal to that of the 1C2 antibody, even at extended exposure time (data not shown). There are several possible reasons for the reduced sensitivity: 1) the primary antibodies were not matched in their efficiencies, 2) the secondary antibodies (which were different for the rabbit and mouse derived primaries) could have also had different relative affinity, and 3) the GFP binding sites were either less accessible than polyGln binding sites or may not have been present due to some protein degradation. A proper GFP-positive control was never tested, so without this piece of data, we cannot be certain why we experienced less intense GFP-reactive bands. Importantly, the lower intensity of the anti-GFP bands cannot be interpreted as an indication that some of the polyGln-containing proteins may have lost their GFP. If that were the case, some of the 1C2 reactive bands would have been detected at lower MWs.

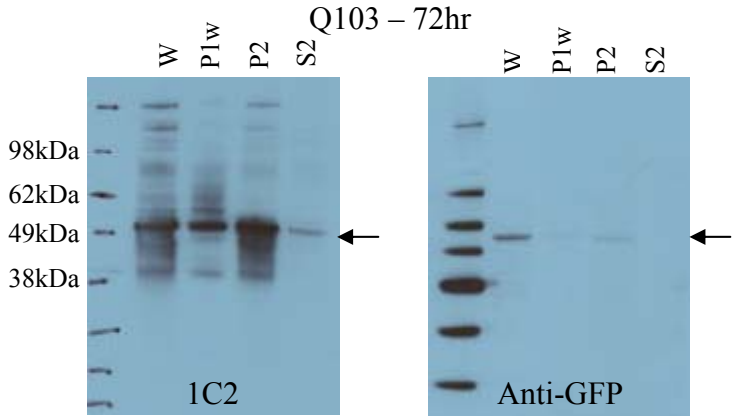

Figure 8.10: GFP antibody was not as sensitive as the 1C2 antibody. Regardless of antibody dilution or exposure time of the membrane to the x-ray film, the anti-GFP antibody was not as effective in recognizing the GFP-tagged proteins as the 1C2 antibody. Abbreviations: W – whole cell lysate, P1w – pellet from 15,000xg, P2 – pellet from 100,000xg, S2 – supernatant.

DEMECOLCINE TREATED CELLS

Biochemical data was also obtained from stable cells treated with demecolcine. As described in Chapter 7, the immunofluorescence data revealed that demecolcine had little effect on 25QP, 47QP, and 103QP cells (Figures 7.5 and 7.6), but had a major effect on Q103 cells. In view of this, fractionation studies were conducted on Q103 and 25QP cell lysates. Cell lysates corresponding to 24 hour incubation with or without demecolcine treatment were subjected to SDS-PAGE and Western blot analysis using the protocol previously described in Section 3.7.

Analysis of 25QP cells with and without exposure to 50ng/ml demecolcine gave cell fractionation results that not only agreed with the previous microscopy results in showing no effect of demecolcine, but also exhibited remarkable quantitative agreement with the microscopy analysis (Figure 8.11).

Analysis of demecolcine-treated Q103 cells also showed very good agreement between the two measurement techniques. In the demecolcine treated cells, the relative amounts of material in the M, $G_C^-R^+$, and $G_C^+R^-$ species by microscopy were closely matched by the amounts of material in the S2, P2, and P1w fractions (Figure 8.12). It is interesting that there was a poorer agreement in the untreated cells. As discussed previously, this can be explained if the perinuclear $G_C^+R^-$ aggregates were somewhat unstable, breaking apart into smaller aggregates and monomer under lysis conditions. The better agreement of the demecolcine-treated cells may be due to the presence of a substantial fraction of $G_C^-R^+$ in these cells; as highly stable, mature amyloid fibrils, these

(A) 25QP - Microscopy

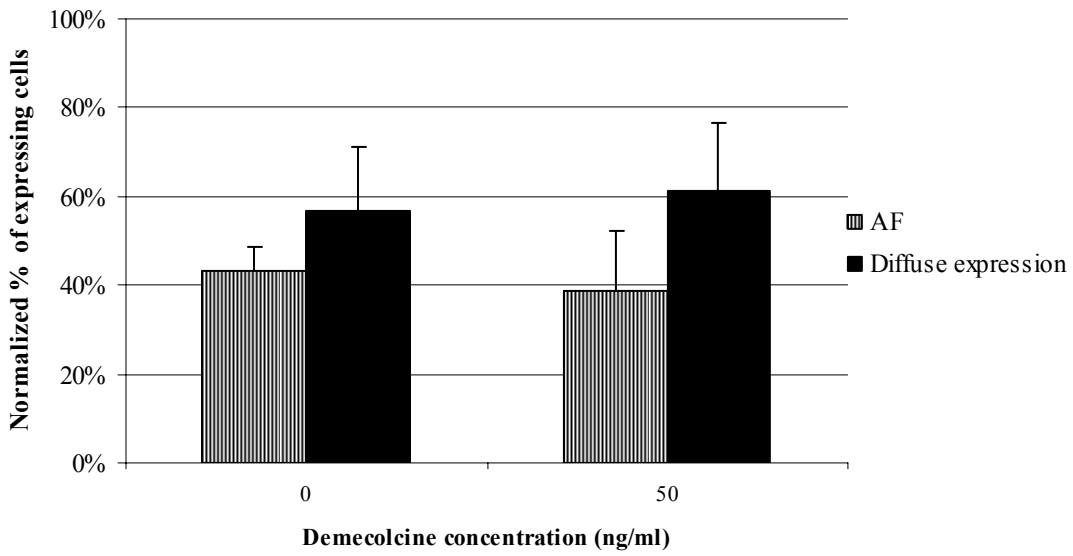

(B) 25QP - Densitometry analysis

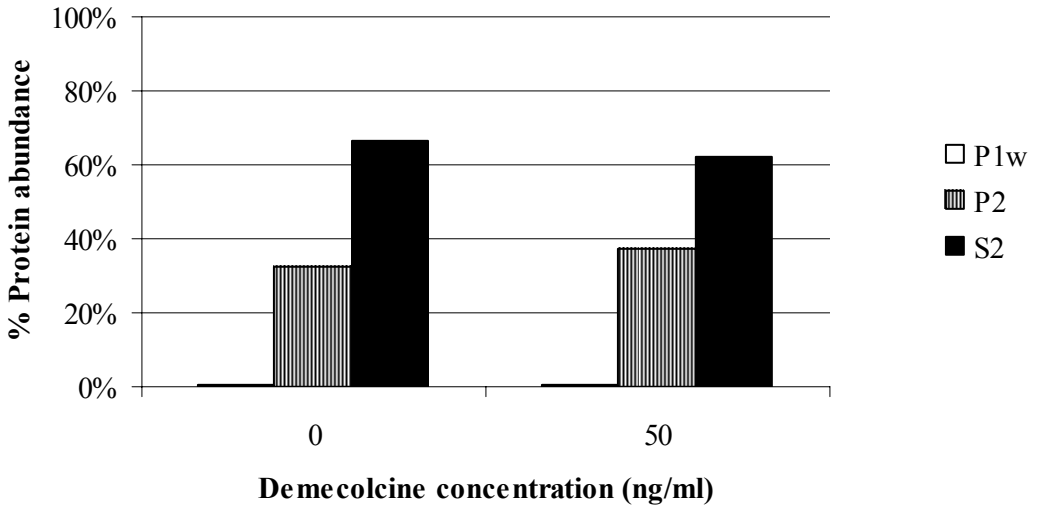

Figure 8.11: Microscopic and densitometry comparison of 25QP cells treated with demecolcine. *(A) Microscopic analysis of 25QP cells treated with 0 or 50ng/ml demecolcine.* Percentage of cells expressing each species was normalized to 100% expression. *(B) Densitometry analysis of 25QP cell lysate fractions treated with 0 or 50ng/ml demecolcine.* P1w- washed pellet from 15,000xg, P2 – pellet from 100,000xg, S2 – supernatant.

(A) Q103 -Microscopy

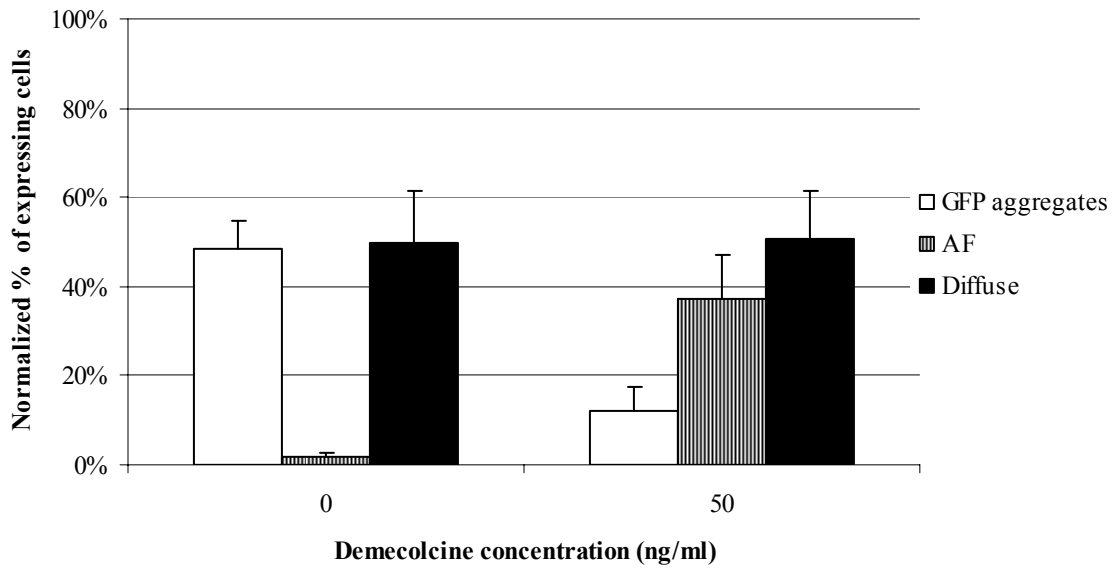

(B) Q103 - Densitometry analysis

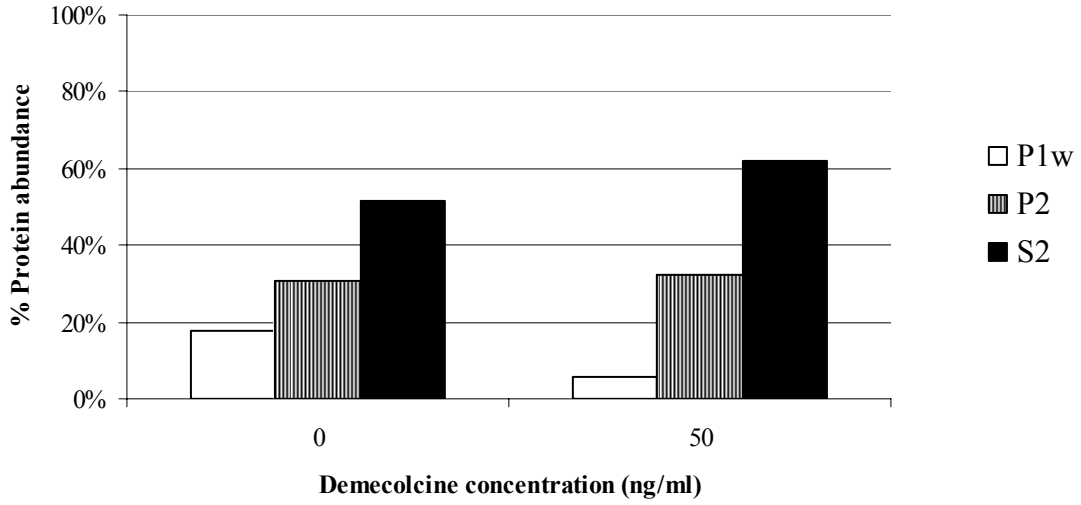

Figure 8.12: Microscopic and densitometry comparison of Q103 cells treated with demecolcine. *(A) Microscopic analysis of Q103 cells treated with 0 or 50ng/ml demecolcine.* Percentage of cells expressing each species was normalized to 100% expression. *(B) Densitometry analysis of Q103 cell lysate fractions treated with 0 or 50ng/ml demecolcine.* P1w- washed pellet from 15,000xg, P2 – pellet from 100,000xg, S2 – supernatant.

aggregates were expected to withstand the lysis conditions and hence retained an appropriately sized signal in the Western blot analysis of the P2 fraction.

8.5 Microtiter Plate Extension Assay of Various Polyglutamine Lengths:

In a functional assay, the centrifuged fractions were examined for their ability to seed the fibrillogenesis of polyglutamine peptides. A modified protocol of a microtiter plate polyGln extension assay (Section 3.8) that was previously designed in our lab [Berthelier, Hamilton et al. 2001] was used. Immobilized cell lysate material and preformed synthetic $K_2Q_{47}K_2$ aggregates (positive control for polyGln elongation) were incubated with 100nM biotinylated polyGln monomer (the same as used in the microscopy experiments) for a determined amount of time. After which, the plates were washed and incubated with a streptavidin-labeled Europium (Eu) solution. Eu-incorporation was then measured by time-resolved fluorescence and converted to femtomoles using a determined standard curve.

Experiments were performed on 103QP cell lysate material from the 48 hour time point. The reason for choosing this polyGln length and time point was because at 48 hours post-induction, multiple polyGln species (M, $G_C^+R^-$, $G_C^+R_C^+$, and $G^-R_C^+$) were observed by immunofluorescence, including the AF fraction that is the only material we expected to be positive in this assay. Logically this appeared to be the best cell line for optimizing the elongation assay. Multiple experiments, however, yielded only inconclusive and inconsistent results (data not shown), which were not a consequence of

experimental technique as was evident by the consistent positive recruitment of our positive control (data not shown).

The lack of reproducibility in the experimental data may be due to the fact that the starting material was cell lysates. In general, cell lysates contain many contaminants such as lipids, cell and nuclear membranes, and other cellular proteins, all of which might interfere with the assay (although controls in which untransformed cell lysates were added to control polyGln aggregates, to see if they affected elongation activity, were not done). Another problem with cell lysates is that, because they are not homogenous, aggregates may not dry in a monolayer when they are plated, such that superficial cell debris material may mask potential polyGln binding sites.

For each assay, equivalent amounts of material were plated per well; however, this amount did not actually reflect the amount of polyGln-containing proteins that was immobilized. It simply represented the total protein that was plated. This is yet another problem with the assay as it stands. While a great deal of time was spent attempting to optimize this procedure, the data produced from these experiments were equivocal. Nonetheless, these efforts should provide a good foundation for future work using this assay on cell lysates.

One suggestion for improving the microplate assay would be to improve the cell lysate preparation. By introducing a purification step, such as immunoprecipitation with 1C2 antibody (which would remove any non-polyGln containing or associated proteins from the mixture), or by the use of a density gradient for protein separation, one might expected a better outcome for the elongation assay. However, even if conditions were

optimal, there is still the question of quantity regarding polyGln recruitment-competent proteins within the lysate. Fluorescence microscopy and Western blotting are very sensitive techniques, and we have no independent estimate of how much protein is being made in these cells on a molar or weight basis. Therefore, although these cell lines were of high clonal integrity, it is possible that the quantities of aggregates are simply too low to give a positive result in the microplate assay. As mentioned previously, it is also possible that other cellular factors, associated with the aggregates upon cell disruption, inhibit the aggregates' ability to stick to the plates or their ability to bind monomer.

Despite the pitfalls along the way, we identified a method (differential centrifugation) that was effective for the crude separation of the polyGln species. Taken together, these biochemical experiments clarified a number of uncertainties about the true natures of the species observed in fluorescence microscopy, providing a critical foundation for the interpretation of this data. The knowledge acquired from the biochemical characterization has provided important details on the larger GFP-positive aggregates and insights about the aggregation pathway of Huntington's disease. Finally, these results have provided a solid basis for future attempts at the chemical characterization of these polyGln species.

CHAPTER 9

DISCUSSION AND CONCLUSIONS

9.1 Possible Aggregation Mechanisms:

Experimentation with the stable cell lines led to the identification of several polyGln species (M, $G^-R_C^+$, $G_C^+R_C^+$, $G_C^+R^-$, and $G_N^+R^-$) some of which were recruitment-competent and others that were recruitment-inert. These species could be found either in isolation or within the same microscopic field, and in some instances even within the same cell. The identification of multiple aggregated polyGln species corroborated other findings from *in vitro* experiments with isolated protein that such structures do exist [Poirier, Li et al. 2002; Wacker et al. 2004; Mukai et al. 2005; Thakur unpublished data]. There are many possibilities for how the assembly pathways of the various species are intertwined (Figure 9.1). One possible mechanism is that AF are online intermediates in GFP inclusion formation (Figure 9.1A), while another possibility is that, conversely, recruitment-inert GFP inclusions are precursors to amyloid-like AF (Figure 9.1C). A third mechanism is that the two species are formed via kinetically competing pathways (Figure 9.1B). In this chapter we will discuss those possible modes of aggregation and speculate on the implications of these various models. We will then review some of our experimental work, namely the response of htt exon1 expression patterns to certain compounds and to sequence variation within htt exon1, and discuss the results in the context of these models.

Figure 9.1: Possible modes of polyglutamine aggregation. M - diffuse, monomeric protein; $G^-R_C^+$ - aggregation foci; $G_{C/N}^+R^-$ - aggregates that showed cytosolic or nuclear GFP formation but did not exhibit recruitment-capabilities; $G_C^+R_C^+$ - aggregates that were large enough to be visualized via their GFP component but also exhibited polyGln recruitment (only observed in the cytoplasm). This schematic represents possible pathways for polyGln aggregation. Part A shows all proposed models without picture representation, where Part B provides visual aides. Models A-C address possible aggregation mechanisms for cytoplasmic species. Model A proposes a linear relationship where aggregation foci ($G^-R_C^+$) are precursors to mature polyGln aggregates ($G_{C/N}^+R^-$) [Osmand 2004]. Model B suggests a competitive pathway for $G^-R_C^+$ and $G_{C/N}^+R^-$ formation. The rapid conversion of M → $G_C^+R^-$ appears to be a reversible process governed by the lack of aggregate stability. Model C represents a linear pathway, based on *in vitro* data, where recruitment-inert aggregates occur prior to the formation of recruitment-positive fibrils [Thakur unpublished data]. Schematics D-F parallel models A-C with the inclusion of $G_N^+R^-$ species being on a separate assembly mechanism (observation from treatment with demecolcine).

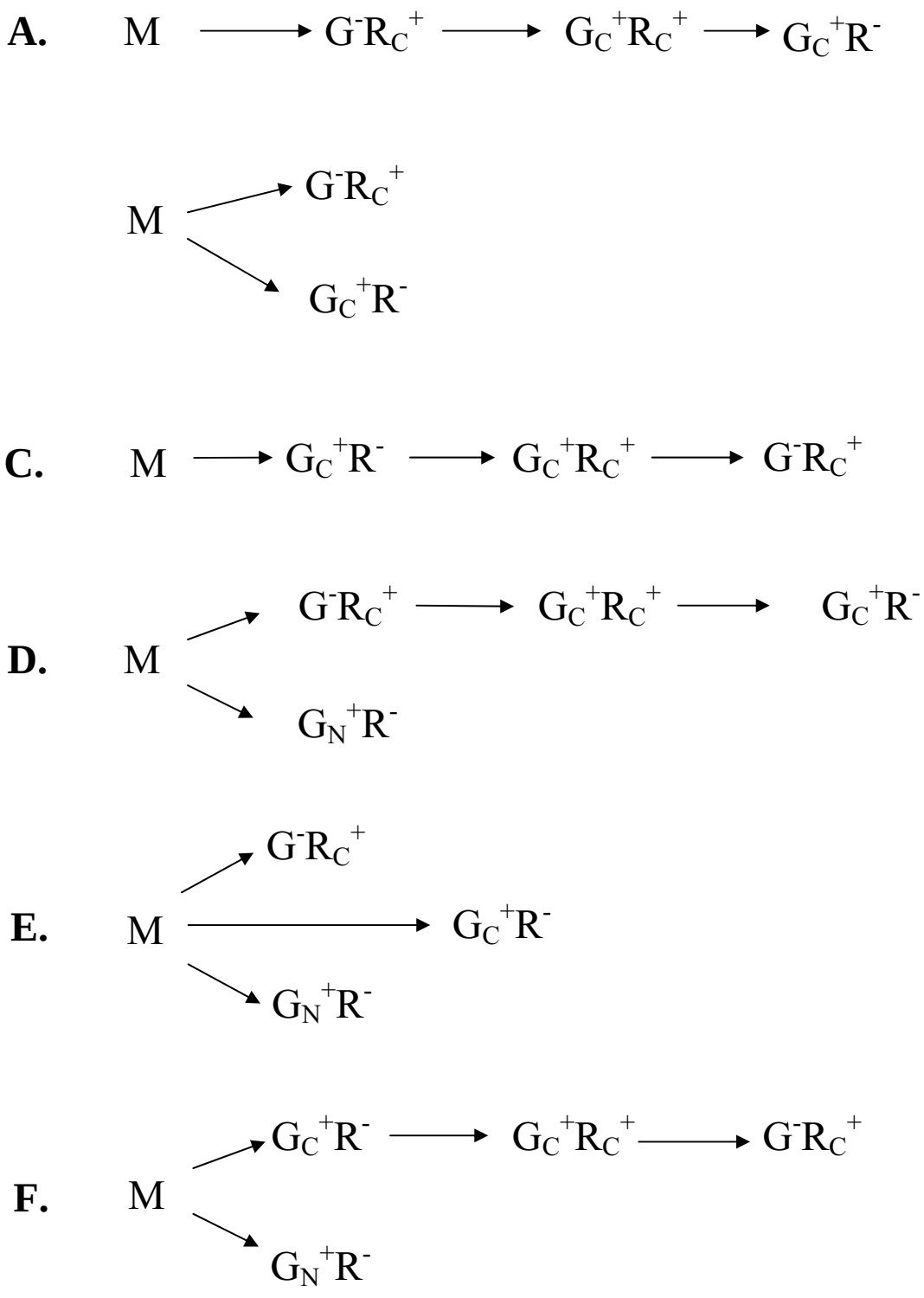

Figure 9.1A. Continued.

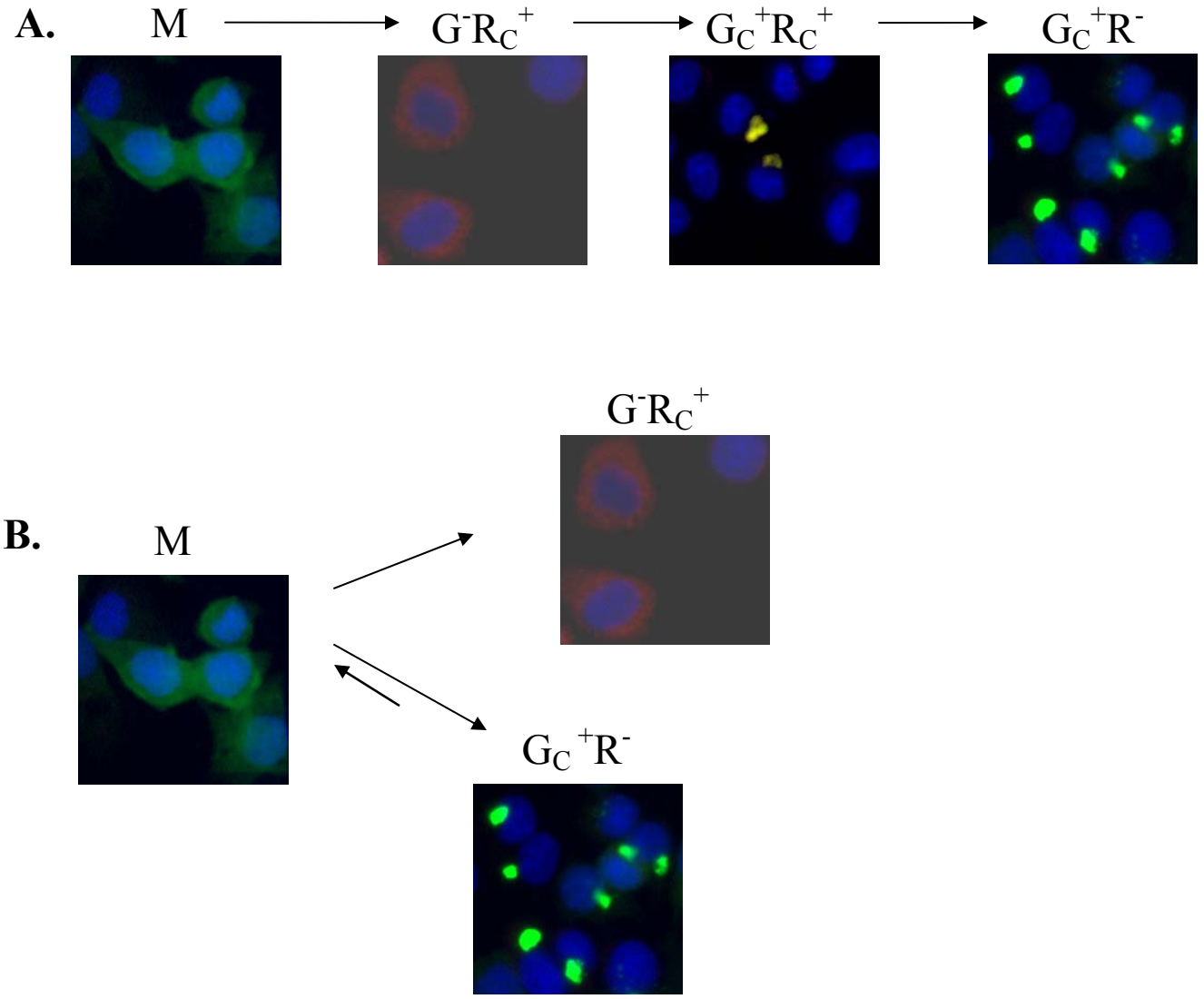

Figure 9.1B. Continued.

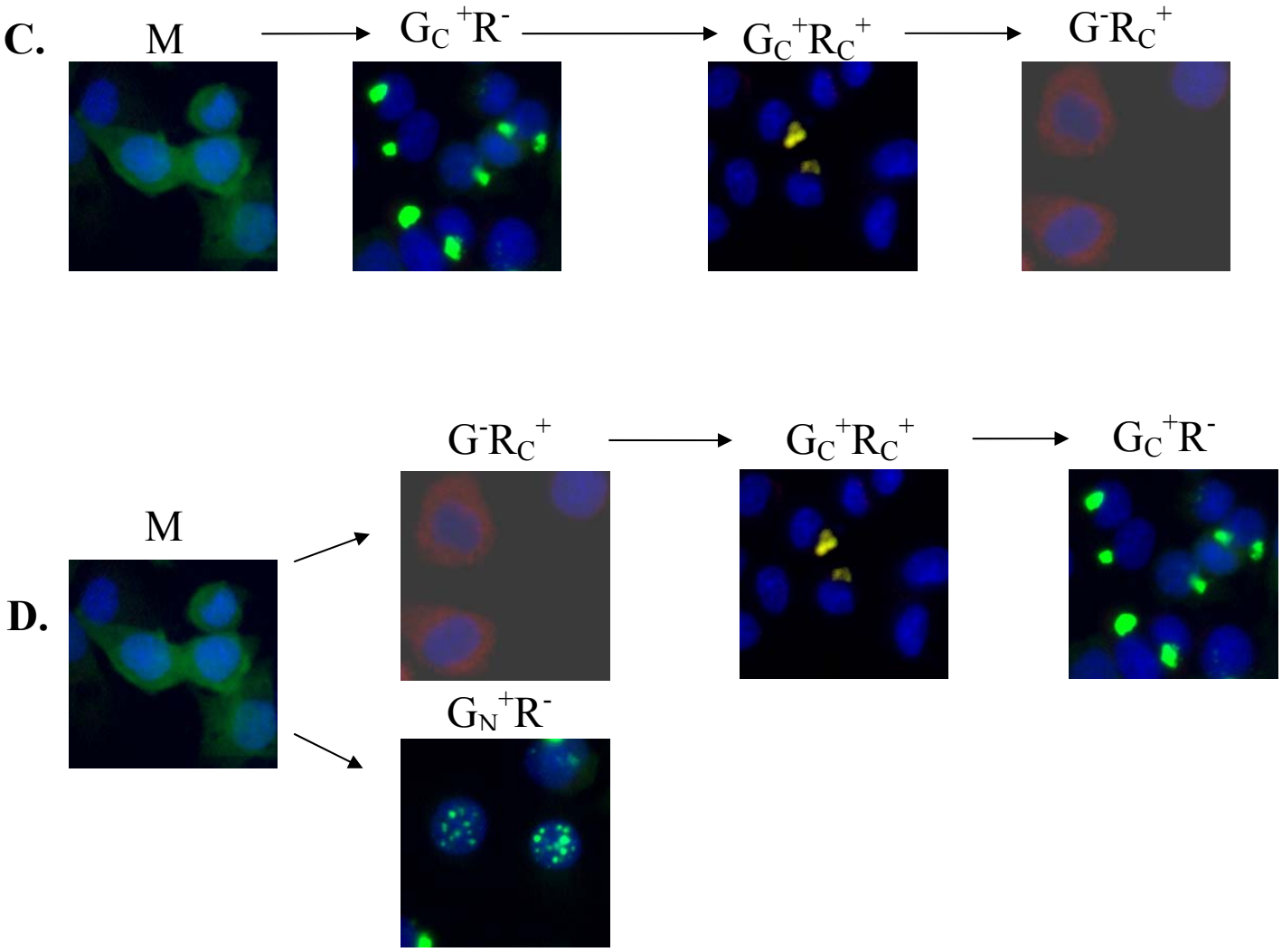

Figure 9.1B. Continued.

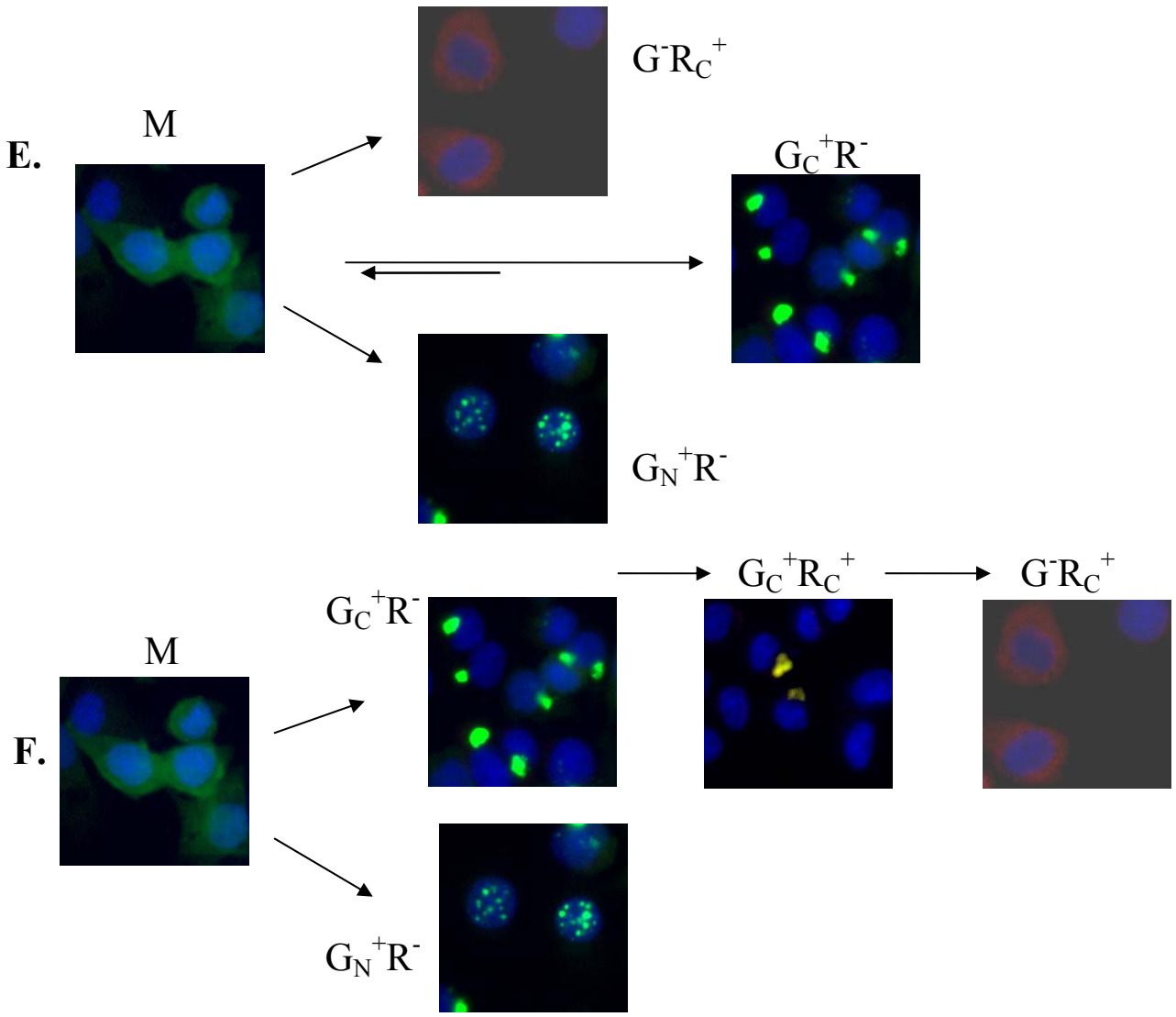

Figure 9.1B. Continued.

Why are AF not always green? During many of the experiments, AF were detected in species that did not exhibit detectible GFP fluorescence. There are several possible interpretations of this counterintuitive finding. One hypothesis is that AF did not accumulate enough mass to be visualized by their GFP fluorescence. The fluorescence yield of AF on a mass basis is expected to be determined by (a) the number of biotinylated polyGln monomers residing on each aggregate after staining, (b) the number of dye molecules per streptavidin, and (c) the quantum yield of the dye. It may be that this produces a fluorescence yield, per htt exon1 molecule in the aggregate, that is substantially brighter than the yield of the GFP associated with each exon1 molecule. Another possibility is that AF are composed largely of htt-exon-1 constructs that have lost all or part of their GFP component due to intracellular proteolysis (not consistent, however, with the SDS gel data). A third, related possibility is that, although AF retain the GFP component of the htt exon1 fusion, the GFP has lost its fluorescence due to its becoming unfolded during the amyloid formation process intrinsic to AF formation. While it would be interesting to know the reason for the poor GFP fluorescence of AF, this property does not impact any of the key interpretations of this data discussed here.

9.2 Effects of Curcumin Treatment on the Aggregation Pathway:

The effects of curcumin were explored in cells expressing a benign polyGln repeat length (25QP) and a physiologically relevant polyGln repeat length (47QP). Each of these cell lines, in the absence of curcumin, produced an abundant mix of M protein

and $G^-R_C^+$ aggregates. Curcumin treatment inhibited the formation of $G^-R_C^+$ in a dose-dependent fashion, while only slightly altering the percentage of cells producing M.

Other experiments suggest that curcumin is specifically an anti-amyloid inhibitor, rather than being non-specific [Frautschy et al. 2001; Nakagami et al. 2002; Lim, Jin et al. 2005; Yang, Lim et al. 2005]. Because of their strong ability to grow by monomer addition, a property unique among aggregates to amyloid and amyloid-like fibrils, we think that $G^-R_C^+$ aggregates are amyloid in nature. The ability of curcumin to effectively knock down $G^-R_C^+$ production in cells is consistent with their expected amyloid-like structure. While it is clear from our results that curcumin down-regulates AF in cells, it could be that this is a result, not of the inhibition of their formation from M, but rather a result of altering the aggregate morphology to interfere with its ability to recruit, or in fact to simply bind to AF and directly inhibit their recruitment of M in the AF stain.

Curcumin treatment was only investigated in cells expressing 25QP and 47QP, which never exhibited any $G_C^+R^-$ aggregates. These experiments simply address the relationship of M and AF, and therefore, do not specifically address the central question of whether AF and GFP-positive aggregates are on linear or competing pathways.

9.3 Effects of Demecolcine Treatment on the Aggregation Pathway:

The central meaning of the data presented in this dissertation can best be considered by focusing attention on stable PC12 cells expressing Q103. These cells very rapidly formed punctate, predominantly cytoplasmic, GFP-positive inclusions, resulting in a corresponding decrease in cells with other forms of htt exon1 (Figure 6.2). By 144

hours post-induction, >70% of the cell population exhibited $G_{C/N}^{+}R^{-}$ aggregates with no cells exhibiting detectable M species. Furthermore, AF were present in less than 1% of the cells.

We examined the effects of two modifications with Q103-producing cells. The first set of modifications of Q103 producing cells involves the addition of cell-pathway modifying compounds to the cells in culture. Because $G_C^{+}R^{-}$ aggregates resemble perinuclear aggresomes that require microtubules for their formation [Johnston et al. 1998; Webb et al. 2004], we treated Q103-producing cells with the microtubule-disrupting agent demecolcine. Demecolcine treatment significantly changed the aggregation pattern in cells in both expected and unexpected ways. First, as expected, drug treatment almost completely eliminated $G_C^{+}R^{-}$ aggregates in cells. Second, as expected, this resulted in cells harboring greatly increased amounts of M and smaller aggregates. Surprisingly, however, the smaller aggregates turn out to be $G^{-}R_C^{+}$ aggregates (AF) rather than smaller versions of $G_C^{+}R^{-}$ aggregates (Figure 7.7).

The fact that demecolcine-treated Q103 producing cells contain essentially no $G_C^{+}R^{-}$ aggregates, but large amounts of both M and $G^{-}R_C^{+}$ aggregates, has profound implications for intracellular aggregation mechanisms. Here we consider, in turn, the aggregation mechanisms outlined in Figure 9.1 A-C. If one of the pathways (A or C) containing $G_C^{+}R^{-}$ and $G^{-}R_C^{+}$ in a precursor-product relationship represents the correct assembly mechanism, then demecolcine treatment should have had different effects than what was observed. Pathway A posits that M is converted entirely to $G^{-}R_C^{+}$, which subsequently are converted to $G_C^{+}R^{-}$, presumably by virtue of being collected into

aggresomes. (This mechanism doesn't explain why simple collecting AF into aggresomes should allow them to acquire GFP fluorescence while at the same time losing recruitment ability.) According to this mechanism, the blocking of $G_C^+R^-$ formation by demecolcine should lead to an accumulation of 100% of the htt exon-1 material in $G^-R_C^+$. Since $G^-R_C^+$ represent very stable, polyGln-core amyloid fibrils [Berthelier et al. 2001; Chen et al. 2001], it is very unlikely that, once formed, any significant amount of these $G^-R_C^+$ aggregates will dissociate to M within the cell.

Pathway C posits that M is first efficiently converted to $G_C^+R^-$, which subsequently are converted directly into $G^-R_C^+$. As in pathway A, there seems to be no simple way under this mechanism to explain the formation of M in response to demecolcine treatment. If $G_C^+R^-$ are the initial aggregates – formed from M as mediated by the microtubule network, and if they are also obligate intermediates in the formation of $G^-R_C^+$, one would expect disruption of the microtubule network by demecolcine to lead to a complete reversal of aggregation to regenerate 100% M.

The only mechanism that seems to be capable of producing, in response to demecolcine elimination of $G_C^+R^-$, a mixture of both M and $G^-R_C^+$ aggregates, is pathway B. In this mechanism, in Q103 cells, formation of $G_C^+R^-$ aggregates is so rapid that the more slowly developing $G^-R_C^+$ aggregates do not form; in the competition for M, $G^-R_C^+$ aggregates lose. However, if the stabilization of $G_C^+R^-$ within aggresomes is blocked by demecolcine treatment, monomers persist and partially convert to $G^-R_C^+$, now no longer in competition with $G_C^+R^-$.

The poor stability of the $G_C^+R^-$ aggregates implicit in this analysis is consistent both with the literature [Muchowski et al. 2000; Muchowski et al. 2002] and with the cell fractionation experimental results described in Chapter 8 and highlighted in Figures 8.9 and 8.12. As discussed in Chapter 1, growth of htt exon-1 aggregates in vitro leads to two classes of aggregates – those that are soluble by SDS-treatment and those that are not [Muchowski, Schaffar et al. 2000]. Growth in the presence of some molecular chaperones increases the fraction of SDS-soluble aggregates, suggesting that these are the earliest formed in the assembly pathway. Only the amyloid-like end products of htt exon-1 aggregation are SDS-stable [Cooper et al. 1998; Kazantsev et al. 1999; Chen et al. 2001]. In our cell fractionation experiments (Figures 8.9 and 8.12), disrupting Q103 cells rich in $G_C^+R^-$ aggregates was sufficient to render about half of the htt exon1 material incapable of being sedimented by a high-speed centrifugation step (and hence, we assume, monomeric).

The affects of demecolcine were examined in the other stable cells as well. Compound treatment did not alter the aggregate balance in any of these cells, which suggested that the polyproline stretch modulated the types of aggregates being produced.

9.3 PolyGln Flanking Sequences Influence Aggregation:

The second modification was contained within the construct itself and consisted of a direct examination of the role of the proline-rich region neighboring the polyGln sequence of htt exon-1. While the 103QP cells expressed intact exon-1, including the

proline-rich segment, the Q103 cells expressed htt exon-1 constructs lacking this flanking sequence.

It has been consistently shown that polyGln flanking sequences have profound effects on polyGln aggregation kinetics [Bhattacharyya, Thakur et al. 2006], aggregation mechanism [Ellisdon, Thomas et al. 2006], protein stability [Bhattacharyya, Thakur et al. 2006], toxicity [Dehay and Bertolotti 2006], and subcellular localization [Rockabrand, Slepko et al. 2007]. *In vitro,* it has also been shown that various lengths of synthetic polyGln lacking any other htt sequences, always produce aggregates, at all stages of the aggregate assembly reaction, that are fibril-like and recruitment-competent [Chen, Berthelier et al. 2001; Chen et al. 2002; Thakur and Wetzel 2002; Yang, Dunlap et al. 2002]. When peptides including a proline-rich sequence following polyGln are examined, the aggregation kinetics are slowed and the aggregates formed appear to be less stable [Bhattacharyya, Thakur et al. 2006]. This effect is also observed in peptides also containing the N-terminal 17 amino acids of htt, even though this sequence alone radically affects the aggregation mechanism. Thus, in contrast to simple polyGln peptides, when the first 17 amino acids of the huntingtin protein are included along with polyGln, these peptides result in much more rapid aggregation kinetics than for a comparable polyGln sequence and lead to an initial aggregated product that is neither fibril-like nor recruitment-competent (thus resembling protofibrils/oligomers); with recruitment-competent, amyloid-like fibrils forming later in the aggregation reaction [Thakur unpublished data]. When a proline rich sequence is included in the peptide containing both polyGln and the N-terminal 17 amino acids, the initial aggregation rate

significantly decreases, but the assembly mechanism, including various non-fibrillar early intermediates, is retained[2] [Thakur unpublished data]. Thus, regardless of the aggregation mechanism and the nature of the aggregated products, addition of a proline-rich sequence on the C-terminal side of the polyGln consistently slows aggregation.

Consistent with these *in vitro* findings, our data demonstrate that the presence of flanking oligoproline sequences significantly decreases the rate at which $G_C^+R^-$ aggregates form. Rather than simply leading to a buildup of diffuse GFP monomers in cells, however, the ability of the proline-rich sequence to inhibit formation of $G_C^+R^-$ aggregates surprisingly leads to the accumulation of substantial levels of $G^-R_C^+$ aggregates (AF) that are not detected in cells expressing oligoproline-minus htt exon-1. Information we acquired from cells expressing 103QP suggest that $G^-R_C^+$ and $G_C^+R^-$ are on parallel assembly pathways (Figure 9.1B) and that the presence of polyproline affects the formation of GFP-positive inclusions while not altering the formation of AF. If the species were on a linear pathway, where AF were precursors to $G_C^+R^-$ aggregates, then one would expect that the presence of oligoproline would, indeed, slow down the aggregation reaction, and fewer GFP inclusions would be observed, which is consistent with Mechanism A. However, one would also expect that if this model were true, then eventually, all the $G^-R_C^+$ aggregates would be converted to $G_C^+R^-$ aggregates. Our data show that while aggregation does occur more slowly in the absence of proline and that

---

[2]While we did not specifically address the importance of the first 17 aa of htt, it has been shown that this sequence can act as a cytoplasmic retention signal even in the presence of a nuclear localization signal [Seffan, J.S., et al. 2004]. Our findings that the aggregated species were predominantly found in the cytoplasm are supported by these data.

GFP-positive aggregates become more abundant with increasing time (Figure 6.2), AF levels remained constant (~20%) throughout the time course, which would be inconsistent with Mechanism A.

As in Mechanism A, Mechanism C would also be inconsistent with our findings that the presence of polyproline slows down the aggregation mechanism. In this case, if Mechanism C were viable, then $G^-R_C^+$ aggregates would form much later than the initial times at which they were observed (Figure 6.2), and there would be an early abundance of $G_C^+R^-$ aggregates, which would more slowly convert to $G^-R_C^+$ aggregates.

Therefore, the mechanism that seems the most possible is Mechanism B, where $G^-R_C^+$ and $G_C^+R^-$ are on competing pathways, producing a more diverse mixture of polyGln species.

9.4 Role of Nuclear Aggregates in the htt Exon-1 Aggregation Pathway:

The data we gathered from the treatment of Q103 cells with demecolcine also brought forth the possibility that the two forms of recruitment-inert aggregates ($G_N^+R^-$ and $G_C^+R^-$) were on separate, competing pathways (Figure 9.1D-F). While demecolcine treatment significantly reduced $G_C^+R^-$, the compound treatment did not significantly affect $G_N^+R^-$ species (Figure 7.4B), suggesting that $G_N^+R^-$ aggregates formed via an assembly pathway that did not involve microtubules. While nuclear aggregation appeared to occur independently of compound treatment, $G_N^+R^-$ aggregate formation was proline-dependent. Nuclear aggregates were never seen in cells expressing complete exon-1 and were only apparent in cells expressing Q103. Presumably monomeric protein gained

access to the nucleus by an unspecified means where it then aggregated. It is unclear why the nuclear aggregated species never exhibited recruitment-competency. However, one possibility is that cells that formed recruitment-positive aggregates in the nucleus died and were never visualized.

It is has been shown that nuclear penetration is necessary for cell death to occur [Cooper et al. 1998; Hackam et al. 1998; Yang et al. 2002]. In most of these cases, the nuclear aggregates are amyloid-like and are, therefore, recruitment-competent [Yang, Dunlap et al. 2002]. Cells expressing truncated htt exon-1 fragments were the only cells that generated $G_N^+R^-$ species; however, no nuclear AF were ever seen. These results are consistent with published findings that nuclear amyloid aggregates are extremely cytotoxic, and may thus explain why our cells did not exhibit toxicity.

9.5 Current Detection Methods May Ignore Important Indicators of Cell Dystrophy:

In HD, there is a lack of correlation between polyGln inclusions and cell death [Gutekunst, Li et al. 1999], suggesting that there may be other unreported species responsible for cellular demise. Our model directly addresses this important question lingering over HD research. The presence of AF in cells expressing 25QP demonstrate that studies focusing strictly on the larger polyGln inclusions are not comprehensive in their aggregate analysis. Often, AF form in the absence of GFP-positive inclusions and may provide a better correlation with cell dystrophy in the human disease. Similarly, we have shown that inclusions can be recruitment-positive or recruitment-inert. Previous attempts to correlate cell death to inclusions did not take this characteristic into account.

9.6 Future Directions:

While these data have provided many insights into the aggregation pathway, there are many questions still unanswered and hypotheses incompletely proved. For example, an important hypothesis coming out of this work is that the large, perinuclear $G_C^+R^-$ aggregates are detergent-soluble and/or labile to mechanical stress. This hypothesis emerges from the comparison of fluorescence microscopy data with cell fractionation data, as summarized in Figures 8.9 and 8.12. The hypothesis is also consistent with the apparent ability of microtubule disruption to block formation of, or destabilize, $G_C^+R^-$. Thus, providing more experimental support for this hypothesis would strengthen many of the conclusions of this thesis. To further test this hypothesis, we would propose to prepare cell lysates of demecolcine treated and untreated cells in the absence of detergent. If the aggregates were indeed denatured by the presence of the detergent, then cells disrupted in the absence of detergent should exhibit less monomer and more aggregate, and perhaps more easily pelleted aggregates. This set of experiments would provide a new set of biochemical data that may reflect the severe aggregate burden that we see microscopically.

Results from our biochemical data have demonstrated that our method of cell lysis in conjunction with differential centrifugation was sufficient for the crude preparation of various protein fractions. It is, however, imperative to improve upon this method so that the nature of each polyGln species can be more closely examined. As alluded to earlier (Chapter 8), the introduction of an immunoprecipitation step prior to fractionation would provide a much cleaner sample. For example, if the whole cell lysate material were

immunoprecipitated with the 1C2 antibody, then the fractions would be rich in polyGln-containing proteins. Then there are a host of experiments that could be conducted with the purified material. For example, to address the critical question of which, if any, of the species could further support fibril growth *in vitro*. One would expect that the only species capable of this feat would be AF. It would also, then, be possible to examine the samples by EM. This would provide more information about the amyloidogenic properties the species actually possess. Alternately, one could also examine whether or not the large aggregates freely dissociate to monomer.

Finally, the most definitive experiment to gain information regarding whether the various species are formed "on-" or "off-pathway" would be to design an experiment where live-cell imaging could be performed to monitor the formation or dissociation of the various types of aggregates. In order to conduct such an experiment, one would need to design a fluorochrome-labeled (preferably one of the stable red variants that are offered from Molecular Probes) polyGln peptide of benign length that could be introduced to the cells and detected by microscopy. Entry of biotinylated monomer into the cell with our current AF staining method, as mentioned earlier, is dependent upon the permeabilization of fixed cell material. Fixation and permeabilization, while useful for many applications, does indeed kill the cell. There are, however, cell permeabilzing agents (saponin) that can be used to introduce temporary pores in cell membranes without killing the cell cultures, thus allowing aggregate formation to be studied in real-time. The information gained from such experiments would provide direct evidence of the interactions of M, $G_C^+R^-$, and $G^-R_C^+$ species.

9.7 Conclusions:

In summary, we were successful in developing a novel polyGln stain that relies on the recruitment-capabilities of polyGln sequences. This stain combines a functional assay and a visual means for detecting recruitment-positive entities, which were not always detected by normal polyGln staining methods. We were able to optimize an existing stable, htt-inducible PC12 model for maximum protein expression in which we implemented our polyGln-recruitment stain.

With the aid of our polyGln-recruitment stain, we were able to identify several phenotypically distinct polyGln aggregates. We successfully tested the effects of two compounds on their ability to modulate aggregation. One compound had a profound effect on AF while the other compound significantly reduced $G_C^+R^-$ aggregates.

Our data have also shown that polyGln flanking sequences play important roles in altering aggregation kinetics and protein stability. While the mechanism of polyGln aggregation is still a mystery, our data suggest that $G_C^+R^-$, $G_N^+R^-$, and $G^-R_C^+$ aggregates form via alternate assembly pathways (Figure 9.1E). Further experimentation is needed to determine which, if any of these species represent the toxic entity responsible for HD pathogenesis.

Our data support a model of polyGln aggregation which defines three competitive pathways that result in AF, large, perikaryal inclusions, and amorphous nuclear microaggregates.

LIST OF REFERENCES

Aiken, C. T., et al. (2004). "A cell-based screen for drugs to treat Huntington's disease." Neurobiol Dis **16**(3): 546-55.

Alberts, B., Bray, D., Lewis, J., Raff, M., Roberts, K., and Watson, J.D. (1994). Fractionation of Cells and Analysis of Their Molecules. Molecular Biology of the Cell. New York, Garland Publishing**:** 162-177.

Alves-Rodrigues, A., et al. (1998). "Ubiquitin, cellular inclusions and their role in neurodegeneration." Trends Neurosci **21**(12): 516-20.

Ambrose, C. M., et al. (1994). "Structure and expression of the Huntington's disease gene: evidence against simple inactivation due to an expanded CAG repeat." Somat Cell Mol Genet **20**(1): 27-38.

Apostol, B. L., et al. (2006). "Mutant huntingtin alters MAPK signaling pathways in PC12 and striatal cells: ERK1/2 protects against mutant huntingtin-associated toxicity." Hum Mol Genet **15**(2): 273-85.

Apostol, B. L., et al. (2003). "A cell-based assay for aggregation inhibitors as therapeutics of polyglutamine-repeat disease and validation in Drosophila." Proc Natl Acad Sci U S A **100**(10): 5950-5.

Bao, J., et al. (1996). "Expansion of polyglutamine repeat in huntingtin leads to abnormal protein interactions involving calmodulin." Proc Natl Acad Sci U S A **93**(10): 5037-42.

Barbero, M. C., et al. (1984). "Effect of the nonionic detergent Triton X-100 on mitochondrial succinate-oxidizing enzymes." Arch Biochem Biophys **228**(2): 560-8.

Barnes, G. T., et al. (1994). "Mouse Huntington's disease gene homolog (Hdh)." Somat Cell Mol Genet **20**(2): 87-97.

Bates, G. P., et al. (1997). "Transgenic models of Huntington's disease." Hum. Mol. Genet. **6**(10): 1633-1637.

Bates, G. P., Wanker, E.E., and Davies, S.W. (1998). Murine Models of Huntington's Disease. Genetic Instabilities and Hereditary Neurological Diseases. R. D. a. W. Wells, S.T. San Diego, Academic Press**:** 355-367.

Bates, G. P. a. B., C. (2002). The polyglutamine diseases. Huntington's Disease. G. P. Bates, Harper, P.S., and Jones, L. New York, Oxford University Press**:** 429-472.

Bates, G. P. a. M., P.S.J. (2002). Mouse Models of Huntington's Disease. Huntington's Disease. G. P. Bates, Harper,P.S., and Jones,L. New York, Oxford University Press**:** 387-428.

Bennett, E. J., et al. (2005). "Global impairment of the ubiquitin-proteasome system by nuclear or cytoplasmic protein aggregates precedes inclusion body formation." Mol Cell **17**(3): 351-65.

Berson, J. F., et al. (2003). "Proprotein convertase cleavage liberates a fibrillogenic fragment of a resident glycoprotein to initiate melanosome biogenesis." J Cell Biol **161**(3): 521-33.

Berthelier, V., et al. (2001). "A microtiter plate assay for polyglutamine aggregate extension." Anal Biochem **295**(2): 227-36.

Berthelier, V. a. W., R. (unpublished data).

Bett, J. S., Bates, G.P., and Hockly, E. (2006). Molecular Pathogenesis and Therapeutic Targets in Huntington's Disease. Genetic Instabilities and Neurological Diseases. R. D. a. A. Wells, T. . San Diego, Academic Press**:** 223-250.

Bhattacharyya, A., et al. (2006). "Oligoproline effects on polyglutamine conformation and aggregation." J Mol Biol **355**(3): 524-35.

Bhattacharyya, A. M., et al. (2005). "Polyglutamine aggregation nucleation: thermodynamics of a highly unfavorable protein folding reaction." Proc Natl Acad Sci U S A **102**(43): 15400-5.

Boutell, J. M., et al. (1999). "Aberrant interactions of transcriptional repressor proteins with the Huntington's disease gene product, huntingtin." Hum Mol Genet **8**(9): 1647-55.

Burke, J. R., et al. (1996). "Huntingtin and DRPLA proteins selectively interact with the enzyme GAPDH." Nat Med **2**(3): 347-50.

Cattaneo, E., et al. (2001). "Loss of normal huntingtin function: new developments in Huntington's disease research." Trends Neurosci **24**(3): 182-8.

Cha, J. H. and L. S. t. Dure (1994). "Trinucleotide repeats in neurologic diseases: an hypothesis concerning the pathogenesis of Huntington's disease, Kennedy's disease, and spinocerebellar ataxia type I." Life Sci **54**(20): 1459-64.

Chai, Y., et al. (1999). "Evidence for proteasome involvement in polyglutamine disease: localization to nuclear inclusions in SCA3/MJD and suppression of polyglutamine aggregation in vitro." Hum Mol Genet **8**(4): 673-82.

Chai, Y., et al. (2001). "The role of protein composition in specifying nuclear inclusion formation in polyglutamine disease." J Biol Chem **276**(48): 44889-97.

Chapman, M. R., et al. (2002). "Role of Escherichia coli curli operons in directing amyloid fiber formation." Science **295**(5556): 851-5.

Chen, S., et al. (2002). "Amyloid-like features of polyglutamine aggregates and their assembly kinetics." Biochemistry **41**(23): 7391-9.

Chen, S., et al. (2001). "Polyglutamine aggregation behavior in vitro supports a recruitment mechanism of cytotoxicity." J Mol Biol **311**(1): 173-82.

Chen, S. and R. Wetzel (2001). "Solubilization and disaggregation of polyglutamine peptides." Protein Sci **10**(4): 887-91.

Cheng, I. H., et al. (2007). "Accelerating amyloid-beta fibrillization reduces oligomer levels and functional deficits in Alzheimer disease mouse models." J Biol Chem.

Chiti, F. and C. M. Dobson (2006). "Protein misfolding, functional amyloid, and human disease." Annu Rev Biochem **75**: 333-66.

Chow, M. K., et al. (2006). "Purification of polyglutamine proteins." Methods Enzymol **413**: 1-19.

Cicchetti, F., et al. (2000). "Chemical anatomy of striatal interneurons in normal individuals and in patients with Huntington's disease." Brain Res Brain Res Rev **34**(1-2): 80-101.

Ciechanover, A. (1994). "The ubiquitin-proteasome proteolytic pathway." Cell **79**(1): 13-21.

Ciechanover, A. (2006). "The ubiquitin proteolytic system: from a vague idea, through basic mechanisms, and onto human diseases and drug targeting." Neurology **66**(2 Suppl 1): S7-19.

Collins, S. R., et al. (2004). "Mechanism of prion propagation: amyloid growth occurs by monomer addition." PLoS Biol **2**(10): e321.

Cong, S. Y., et al. (2006). "Small N-terminal mutant huntingtin fragments, but not wild type, are mainly present in monomeric form: Implications for pathogenesis." Exp Neurol **199**(2): 257-64.

Conway, K. A., et al. (2000). "Fibrils formed in vitro from alpha-synuclein and two mutant forms linked to Parkinson's disease are typical amyloid." Biochemistry **39**(10): 2552-63.

Cooper, J. K., et al. (1998). "Truncated N-terminal fragments of huntingtin with expanded glutamine repeats form nuclear and cytoplasmic aggregates in cell culture." Hum. Mol. Genet. **7**(5): 783-790.

Cummings, C. J. and H. Y. Zoghbi (2000). "Fourteen and counting: unraveling trinucleotide repeat diseases." Hum Mol Genet **9**(6): 909-16.

Cummings, C. J. and H. Y. Zoghbi (2000). "Trinucleotide repeats: mechanisms and pathophysiology." Annu Rev Genomics Hum Genet **1**: 281-328.

Davies, S. W., et al. (1997). "Formation of neuronal intranuclear inclusions underlies the neurological dysfunction in mice transgenic for the HD mutation." Cell **90**(3): 537-48.

de la Monte, S. M., et al. (1988). "Morphometric demonstration of atrophic changes in the cerebral cortex, white matter, and neostriatum in Huntington's disease." J Neuropathol Exp Neurol **47**(5): 516-25.

Dehay, B. and A. Bertolotti (2006). "Critical Role of the Proline-rich Region in Huntingtin for Aggregation and Cytotoxicity in Yeast." J. Biol. Chem. **281**(47): 35608-35615.

DiFiglia, M., et al. (1997). "Aggregation of huntingtin in neuronal intranuclear inclusions and dystrophic neurites in brain." Science **277**(5334): 1990-3.

Ding, Q., et al. (2002). "Polyglutamine expansion, protein aggregation, proteasome activity, and neural survival." J Biol Chem **277**(16): 13935-42.

Dul, J. L., et al. (2001). "Hsp70 and antifibrillogenic peptides promote degradation and inhibit intracellular aggregation of amyloidogenic light chains." J Cell Biol **152**(4): 705-16.

Duyao, M., et al. (1993). "Trinucleotide repeat length instability and age of onset in Huntington's disease." Nat Genet **4**(4): 387-92.

Ellis, M. C., et al. (1993). "Expression of Drosophila glass protein and evidence for negative regulation of its activity in non-neuronal cells by another DNA-binding protein." Development **119**(3): 855-65.

Ellisdon, A. M., et al. (2007). "Mechanisms of Ataxin-3 Misfolding and Fibril Formation: Kinetic Analysis of a Disease-associated Polyglutamine Protein." J Mol Biol **368**(2): 595-605.

Ellisdon, A. M., et al. (2006). "The two-stage pathway of ataxin-3 fibrillogenesis involves a polyglutamine-independent step." J Biol Chem **281**(25): 16888-96.

Evert, B. O., et al. (2000). "Cell death in polyglutamine diseases." Cell Tissue Res **301**(1): 189-204.
Faber, P. W., et al. (1999). "Polyglutamine-mediated dysfunction and apoptotic death of a Caenorhabditis elegans sensory neuron." Proc Natl Acad Sci U S A **96**(1): 179-84.
Fandrich, M. and C. M. Dobson (2002). "The behaviour of polyamino acids reveals an inverse side chain effect in amyloid structure formation." Embo J **21**(21): 5682-90.
Felgner, P. L., et al. (1987). "Lipofection: a highly efficient, lipid-mediated DNA-transfection procedure." Proc Natl Acad Sci U S A **84**(21): 7413-7.
Ferrone, F. (1999). "Analysis of protein aggregation kinetics." Methods Enzymol **309**: 256-74.
Fink, A. L. (1998). "Protein aggregation: folding aggregates, inclusion bodies and amyloid." Fold Des **3**(1): R9-23.
Fischbeck, K. H. (2001). "Polyglutamine expansion neurodegenerative disease." Brain Res Bull **56**(3-4): 161-3.
Forno, L. a. N., R. (1979). "Ultrastructure of the neostriatum in Huntington's and Parkinson's disease." Adv Neurol **23**: 123-135.
Frautschy, S. A., et al. (2001). "Phenolic anti-inflammatory antioxidant reversal of Abeta-induced cognitive deficits and neuropathology." Neurobiol Aging **22**(6): 993-1005.
Freese, A., et al. (1990). "Characterization and mechanism of glutamate neurotoxicity in primary striatal cultures." Brain Res **521**(1-2): 254-64.
Freshney, R. I. (1987). Culture of Animal Cells. A Manual of Basic Technique. New York, Wiley-Liss.
Gafni, J., et al. (2004). "Inhibition of calpain cleavage of huntingtin reduces toxicity: accumulation of calpain/caspase fragments in the nucleus." J Biol Chem **279**(19): 20211-20.
Garcia-Mata, R., et al. (1999). "Characterization and dynamics of aggresome formation by a cytosolic GFP-chimera." J Cell Biol **146**(6): 1239-54.
Gosal, W. S., et al. (2005). "Competing pathways determine fibril morphology in the self-assembly of beta2-microglobulin into amyloid." J Mol Biol **351**(4): 850-64.
Greene, J. G. and J. T. Greenamyre (1996). "Bioenergetics and glutamate excitotoxicity." Prog Neurobiol **48**(6): 613-34.
Greene, L. A. and A. S. Tischler (1976). "Establishment of a noradrenergic clonal line of rat adrenal pheochromocytoma cells which respond to nerve growth factor." Proc Natl Acad Sci U S A **73**(7): 2424-8.
Grierson, A. J., et al. (2001). "Androgen induced cell death in SHSY5Y neuroblastoma cells expressing wild-type and spinal bulbar muscular atrophy mutant androgen receptors." Biochim Biophys Acta **1536**(1): 13-20.
Group, T. H. s. D. C. R. (1993). "A novel gene containing a trinucleotide repeat that is expanded and unstable on Huntington's disease chromosomes." Cell **72**(6): 971-83.

Gschwind, M. a. H., G. (1997). Detection of apoptosis or necrosis death in neuronal cells by morphological, biochemical and molecular analysis. Neuromethods: Apoptosis Techniques and Protocols. New York. Humana Press: 13-32.

Gunawardena, S., et al. (2003). "Disruption of axonal transport by loss of huntingtin or expression of pathogenic polyQ proteins in Drosophila." Neuron **40**(1): 25-40.

Gusella, J. F. and M. E. MacDonald (2000). "Molecular genetics: unmasking polyglutamine triggers in neurodegenerative disease." Nat Rev Neurosci **1**(2): 109-15.

Gusella, J. F., et al. (1983). "A polymorphic DNA marker genetically linked to Huntington's disease." Nature **306**(5940): 234-8.

Gutekunst, C. A., et al. (1999). "Nuclear and neuropil aggregates in Huntington's disease: relationship to neuropathology." J Neurosci **19**(7): 2522-34.

Gutekunst, C. A., Norflus, F., and Hersch, S.M. (2002). The neuropathology of Huntington's disease. Huntington's Disease. G. Bates, Harper, P.S., and Jones, L. New York, Oxford University Press**:** 251-275.

Hackam, A. S., et al. (1998). "The influence of huntingtin protein size on nuclear localization and cellular toxicity." J Cell Biol **141**(5): 1097-105.

Haggqvist, B., et al. (1999). "Medin: an integral fragment of aortic smooth muscle cell-produced lactadherin forms the most common human amyloid." Proc Natl Acad Sci U S A **96**(15): 8669-74.

Harper, P. S. (2002). The epidemiology of Huntington's disease. Huntington's Disease. G. P. Bates, Harper, P.S., and Jones, L. New York, Oxford University Press**:** 159-197.

Harper, P. S. and R. G. Newcombe (1992). "Age at onset and life table risks in genetic counselling for Huntington's disease." J Med Genet **29**(4): 239-42.

Hartl, F. U. (1996). "Molecular chaperones in cellular protein folding." Nature **381**(6583): 571-9.

Higham, C. E., et al. (2000). "Preparation of synthetic human islet amyloid polypeptide (IAPP) in a stable conformation to enable study of conversion to amyloid-like fibrils." FEBS Lett **470**(1): 55-60.

Ho, L. W., et al. (2001). "The molecular biology of Huntington's disease." Psychol Med **31**(1): 3-14.

Huntington, G. (1872). "On chorea." Med. Surg. Rep. **26**: 320-321.

Invitrogen (2002). Ecdysone-Inducible Mammalian Expression System. An inducible gene expression system for mammalian cells using the ecdysone analog, ponasterone A. Technical bulletin, Invitrogen Life Technologies. **Version H**.

Ionescu-Zanetti, C., et al. (1999). "Monitoring the assembly of Ig light-chain amyloid fibrils by atomic force microscopy." Proc Natl Acad Sci U S A **96**(23): 13175-9.

Jackson, G. R., et al. (1998). "Polyglutamine-expanded human huntingtin transgenes induce degeneration of Drosophila photoreceptor neurons." Neuron **21**(3): 633-42.

Jiang, H., et al. (2003). "Cell death triggered by polyglutamine-expanded huntingtin in a neuronal cell line is associated with degradation of CREB-binding protein." Hum Mol Genet **12**(1): 1-12.

Jimenez, J. L., et al. (2002). "The protofilament structure of insulin amyloid fibrils." Proc Natl Acad Sci U S A **99**(14): 9196-201.
Johnston, J. A., et al. (1998). "Aggresomes: a cellular response to misfolded proteins." J Cell Biol **143**(7): 1883-98.
Jones, A. L. (1999). "The localization and interactions of huntingtin." Philos Trans R Soc Lond B Biol Sci **354**(1386): 1021-7.
Kalchman, M. A., et al. (1996). "Huntingtin is ubiquitinated and interacts with a specific ubiquitin-conjugating enzyme." J Biol Chem **271**(32): 19385-94.
Kalchman, M. A., et al. (1997). "HIP1, a human homologue of S. cerevisiae Sla2p, interacts with membrane-associated huntingtin in the brain." Nat Genet **16**(1): 44-53.
Kalejta, R. F., et al. (1999). "An integral membrane green fluorescent protein marker, Us9-GFP, is quantitatively retained in cells during propidium iodide-based cell cycle analysis by flow cytometry." Exp Cell Res **248**(1): 322-8.
Karpuj, M. V., et al. (1999). "Transglutaminase aggregates huntingtin into nonamyloidogenic polymers, and its enzymatic activity increases in Huntington's disease brain nuclei." Proc Natl Acad Sci U S A **96**(13): 7388-93.
Kayed, R., et al. (2003). "Common structure of soluble amyloid oligomers implies common mechanism of pathogenesis." Science **300**(5618): 486-9.
Kazantsev, A., et al. (1999). "Insoluble detergent-resistant aggregates form between pathological and nonpathological lengths of polyglutamine in mammalian cells." Proc Natl Acad Sci U S A **96**(20): 11404-9.
Kelloff, G. J., et al. (1996). "New agents for cancer chemoprevention." J Cell Biochem Suppl **26**: 1-28.
Kheterpal, I., et al. (2003). "Abeta protofibrils possess a stable core structure resistant to hydrogen exchange." Biochemistry **42**(48): 14092-8.
Kim, J. and D. J. Klionsky (2000). "Autophagy, cytoplasm-to-vacuole targeting pathway, and pexophagy in yeast and mammalian cells." Annu Rev Biochem **69**: 303-42.
Klement, I. A., et al. (1998). "Ataxin-1 nuclear localization and aggregation: role in polyglutamine-induced disease in SCA1 transgenic mice." Cell **95**(1): 41-53.
Klockgether, T. and B. Evert (1998). "Genes involved in hereditary ataxias." Trends Neurosci **21**(9): 413-8.
Knockaert, M., et al. (2002). "p42/p44 MAPKs are intracellular targets of the CDK inhibitor purvalanol." Oncogene **21**(42): 6413-24.
Kodali, R. and R. Wetzel (2007). "Polymorphism in the intermediates and products of amyloid assembly." Curr Opin Struct Biol **17**(1): 48-57.
Kopito, R. R. (2000). "Aggresomes, inclusion bodies and protein aggregation." Trends Cell Biol **10**(12): 524-30.
Krobitsch, S. and S. Lindquist (2000). "Aggregation of huntingtin in yeast varies with the length of the polyglutamine expansion and the expression of chaperone proteins." Proc Natl Acad Sci U S A **97**(4): 1589-94.
Kuemmerle, S., et al. (1999). "Huntington aggregates may not predict neuronal death in Huntington's disease." Ann Neurol **46**(6): 842-9.
Laemmli, U. K. (1970). Nature **227**: 680.

Lambert, M. P., et al. (1998). "Diffusible, nonfibrillar ligands derived from Abeta1-42 are potent central nervous system neurotoxins." Proc Natl Acad Sci U S A **95**(11): 6448-53.

Lee, W.-C. M., et al. (2004). "Cytoplasmic aggregates trap polyglutamine-containing proteins and block axonal transport in a Drosophila model of Huntington's disease." PNAS **101**(9): 3224-3229.

Li, H., et al. (2003). "Abnormal association of mutant huntingtin with synaptic vesicles inhibits glutamate release." Hum Mol Genet **12**(16): 2021-30.

Li, S.-H., et al. (1999). "Cellular Defects and Altered Gene Expression in PC12 Cells Stably Expressing Mutant Huntingtin." J. Neurosci. **19**(13): 5159-5172.

Li, S. H. and X. J. Li (2004). "Huntingtin-protein interactions and the pathogenesis of Huntington's disease." Trends Genet **20**(3): 146-54.

Li, X. J., et al. (1995). "A huntingtin-associated protein enriched in brain with implications for pathology." Nature **378**(6555): 398-402.

Li, Z., et al. (1999). "A putative Drosophila homolog of the Huntington's disease gene." Hum Mol Genet **8**(9): 1807-15.

Lim, C. S., et al. (2005). "Antioxidant and antiinflammatory activities of xanthorrhizol in hippocampal neurons and primary cultured microglia." J Neurosci Res **82**(6): 831-8.

Lin, M. T. and M. F. Beal (2006). "Mitochondrial dysfunction and oxidative stress in neurodegenerative diseases." Nature **443**(7113): 787-95.

Link, C. D., et al. (2006). "Conversion of green fluorescent protein into a toxic, aggregation-prone protein by C-terminal addition of a short peptide." J Biol Chem **281**(3): 1808-16.

Lodish, H., Berk,A., Matsudaira,P., Kaiser,C.A., Krieger,M., Scott,M.P., Zipursky,S.L., and Darnell,J. (2004). Molecular Cell Biology. New York, W.H. Freeman and Company.

Lomakin, A., et al. (1999). "Monitoring protein assembly using quasielastic light scattering spectroscopy." Methods Enzymol **309**: 429-59.

Luduena, R. F. and M. C. Roach (1991). "Tubulin sulfhydryl groups as probes and targets for antimitotic and antimicrotubule agents." Pharmacol Ther **49**(1-2): 133-52.

Lunkes, A. and J. L. Mandel (1998). "A cellular model that recapitulates major pathogenic steps of Huntington's disease." Hum Mol Genet **7**(9): 1355-61.

MacDonald, M. (personal communication). Distribution of HD CAG repeat lengths on normal and HD chromosomes.

Maglione, V., et al. (2006). "Huntingtin fragmentation and increased caspase 3, 8 and 9 activities in lymphoblasts with heterozygous and homozygous Huntington's disease mutation." Mech Ageing Dev **127**(2): 213-6.

Mangiarini, L., et al. (1997). "Instability of highly expanded CAG repeats in mice transgenic for the Huntington's disease mutation." Nat Genet **15**(2): 197-200.

Mangiarini, L., et al. (1996). "Exon 1 of the HD gene with an expanded CAG repeat is sufficient to cause a progressive neurological phenotype in transgenic mice." Cell **87**(3): 493-506.

Marsh, J. L., et al. (2000). "Expanded polyglutamine peptides alone are intrinsically cytotoxic and cause neurodegeneration in Drosophila." Hum Mol Genet **9**(1): 13-25.
Martindale, D., et al. (1998). "Length of huntingtin and its polyglutamine tract influences localization and frequency of intracellular aggregates." Nat Genet **18**(2): 150-4.
Massey, A., et al. (2004). "Pathophysiology of chaperone-mediated autophagy." Int J Biochem Cell Biol **36**(12): 2420-34.
Mayer, R. J., et al. (1989). "Intermediate filaments and ubiquitin: a new thread in the understanding of chronic neurodegenerative diseases." Prog Clin Biol Res **317**: 809-18.
Mazzulli, J. R., et al. (2006). "Cytosolic catechols inhibit alpha-synuclein aggregation and facilitate the formation of intracellular soluble oligomeric intermediates." J Neurosci **26**(39): 10068-78.
McCampbell, A., et al. (2000). "CREB-binding protein sequestration by expanded polyglutamine." Hum Mol Genet **9**(14): 2197-202.
McGowan, D. P., et al. (2000). "Amyloid-like inclusions in Huntington's disease." Neuroscience **100**(4): 677-80.
Melan, M. A. and G. Sluder (1992). "Redistribution and differential extraction of soluble proteins in permeabilized cultured cells. Implications for immunofluorescence microscopy." J Cell Sci **101 (Pt 4)**: 731-43.
Michalik, A., et al. (2001). "Method to introduce stable, expanded, polyglutamine-encoding CAG/CAA trinucleotide repeats into CAG repeat-containing genes." Biotechniques **31**(2): 250-2, 254.
Modler, A. J., et al. (2004). "Polymerization of proteins into amyloid protofibrils shares common critical oligomeric states but differs in the mechanisms of their formation." Amyloid **11**(4): 215-31.
Muchowski, P. J., et al. (2000). "Hsp70 and hsp40 chaperones can inhibit self-assembly of polyglutamine proteins into amyloid-like fibrils." Proc Natl Acad Sci U S A **97**(14): 7841-6.
Mukai, H., et al. (2005). "Formation of morphologically similar globular aggregates from diverse aggregation-prone proteins in mammalian cells." Proc Natl Acad Sci U S A **102**(31): 10887-92.
Myers, R. H., et al. (1989). "Homozygote for Huntington disease." Am J Hum Genet **45**(4): 615-8.
Myers, R. H., Marans, K.S., and MacDonald, M.E. (1998). Huntington's Disease. Genetic Instabilities and Hereditary Neurological Diseases. R. D. Wells, Warren, S.T., and Sarmiento, M. San Diego, Academic Press**:** 301-318.
Myers, R. H., et al. (1988). "Clinical and neuropathologic assessment of severity in Huntington's disease." Neurology **38**(3): 341-7.
Nagai, Y., et al. (2007). "A toxic monomeric conformer of the polyglutamine protein." Nat Struct Mol Biol **14**(4): 332-40.
Nakagami, Y., et al. (2002). "A novel beta-sheet breaker, RS-0406, reverses amyloid beta-induced cytotoxicity and impairment of long-term potentiation in vitro." Br J Pharmacol **137**(5): 676-82.

NCBI (2007). NCBI database, http://www.ncbi.nlm.nih.gov/.
Nelson, R., et al. (2005). "Structure of the cross-beta spine of amyloid-like fibrils." Nature **435**(7043): 773-8.
Nelson, S. R., et al. (1991). "Isolation and characterization of the integral glycosaminoglycan constituents of human amyloid A and monoclonal light-chain amyloid fibrils." Biochem J **275 (Pt 1)**: 67-73.
Nishiyama, I. and T. Fujii (1992). "Laminin-induced process outgrowth from isolated fetal rat C-cells." Exp Cell Res **198**(2): 214-20.
Nucifora, F. C., Jr., et al. (2001). "Interference by huntingtin and atrophin-1 with cbp-mediated transcription leading to cellular toxicity." Science **291**(5512): 2423-8.
O'Nuallain, B., et al. (2006). "Kinetics and thermodynamics of amyloid assembly using a high-performance liquid chromatography-based sedimentation assay." Methods Enzymol **413**: 34-74.
Olivieri, G., et al. (2003). "Beta-amyloid modulates tyrosine kinase B receptor expression in SHSY5Y neuroblastoma cells: influence of the antioxidant melatonin." Neuroscience **120**(3): 659-65.
Olney, J. W., et al. (1971). "Cytotoxic effects of acidic and sulphur containing amino acids on the infant mouse central nervous system." Exp Brain Res **14**(1): 61-76.
Osherovich, L. Z., et al. (2004). "Dissection and design of yeast prions." PLoS Biol **2**(4): E86.
Osmand, A., Berthelier,V., Wetzel,R., Hickey,M., Menalled,L., von Hoersten,S., Slow,E., and Hayden,M. (2004). Polyglutamine Recruitment Sites and Polyglutamine Aggregates Overlap in HD and in Animal Models. Society for Neuroscience, Washington, DC.
Osmand, A. P., et al. (2006). "Imaging polyglutamine deposits in brain tissue." Methods Enzymol **412**: 106-22.
Parker, J. A., et al. (2001). "Expanded polyglutamines in Caenorhabditis elegans cause axonal abnormalities and severe dysfunction of PLM mechanosensory neurons without cell death." Proc Natl Acad Sci U S A **98**(23): 13318-23.
Paulson, H. L. and K. H. Fischbeck (1996). "Trinucleotide repeats in neurogenetic disorders." Annu Rev Neurosci **19**: 79-107.
Pepys, M. B. (2006). "Amyloidosis." Annu Rev Med **57**: 223-41.
Pepys, M. B., et al. (1994). "Human serum amyloid P component is an invariant constituent of amyloid deposits and has a uniquely homogeneous glycostructure." Proc Natl Acad Sci U S A **91**(12): 5602-6.
Perutz, M. F., et al. (2002). "Amyloid fibers are water-filled nanotubes." Proc Natl Acad Sci U S A **99**(8): 5591-5.
Perutz, M. F., et al. (1994). "Glutamine repeats as polar zippers: their possible role in inherited neurodegenerative diseases." Proc Natl Acad Sci U S A **91**(12): 5355-8.
Peters, M. F., et al. (1999). "Nuclear targeting of mutant Huntingtin increases toxicity." Mol Cell Neurosci **14**(2): 121-8.
Plakoutsi, G., et al. (2005). "Evidence for a mechanism of amyloid formation involving molecular reorganisation within native-like precursor aggregates." J Mol Biol **351**(4): 910-22.

Poirier, M. A., et al. (2002). "Huntingtin spheroids and protofibrils as precursors in polyglutamine fibrilization." J Biol Chem **277**(43): 41032-7.
Preisinger, E., et al. (1999). "Evidence for a recruitment and sequestration mechanism in Huntington's disease." Philos Trans R Soc Lond B Biol Sci **354**(1386): 1029-34.
Promega (2005). CellTiter96$^{(R)}$ AQ_{ueous} One Solution Cell Proliferation Assay. Technical Bulletin. Madison, WI, Promega.
Puchtler, H., Sweat,F., and Levine,M. (1962). "On the binding of Congo red by amyloid." J Histochem Cytochem **10**: 355-364.
Qin, Z.-H., et al. (2003). "Autophagy regulates the processing of amino terminal huntingtin fragments." Hum. Mol. Genet. **12**(24): 3231-3244.
Quintas, A., et al. (2001). "Tetramer dissociation and monomer partial unfolding precedes protofibril formation in amyloidogenic transthyretin variants." J Biol Chem **276**(29): 27207-13.
Raina, A. K., et al. (2000). "Abortive oncogeny and cell cycle-mediated events in Alzheimer disease." Prog Cell Cycle Res **4**: 235-42.
Reddy, P. H., et al. (1998). "Behavioural abnormalities and selective neuronal loss in HD transgenic mice expressing mutated full-length HD cDNA." Nat Genet **20**(2): 198-202.
Robinow, S. and K. White (1988). "The locus elav of Drosophila melanogaster is expressed in neurons at all developmental stages." Dev Biol **126**(2): 294-303.
Rockabrand, E., et al. (2007). "The first 17 amino acids of Huntingtin modulate its sub-cellular localization, aggregation and effects on calcium homeostasis." Hum. Mol. Genet. **16**(1): 61-77.
Roskams, J. a. R., L., Ed. (2002). Lab Ref: A Handbook of Recipes, Reagents, and Other Reference Tools for Use at the Bench. New York, Cold Springs Harbor Laboratory Press.
Ross, C. A. (1997). "Intranuclear neuronal inclusions: a common pathogenic mechanism for glutamine-repeat neurodegenerative diseases?" Neuron **19**(6): 1147-50.
Ross, C. A. (2004). "Huntington's disease: new paths to pathogenesis." Cell **118**(1): 4-7.
Ross, C. A. and M. A. Poirier (2005). "Opinion: What is the role of protein aggregation in neurodegeneration?" Nat Rev Mol Cell Biol **6**(11): 891-8.
Ross, C. A., et al. (2003). "Polyglutamine fibrillogenesis: the pathway unfolds." Proc Natl Acad Sci U S A **100**(1): 1-3.
Sanchez, I., et al. (2003). "Pivotal role of oligomerization in expanded polyglutamine neurodegenerative disorders." Nature **421**(6921): 373-9.
Sanchez, I., et al. (1999). "Caspase-8 is required for cell death induced by expanded polyglutamine repeats." Neuron **22**(3): 623-33.
Saudou, F., et al. (1998). "Huntingtin acts in the nucleus to induce apoptosis but death does not correlate with the formation of intranuclear inclusions." Cell **95**(1): 55-66.
Sawa, A., et al. (2005). "Huntingtin is cleaved by caspases in the cytoplasm and translocated to the nucleus via perinuclear sites in Huntington's disease patient lymphoblasts." Neurobiol Dis **20**(2): 267-74.

Schaffar, G., et al. (2004). "Cellular toxicity of polyglutamine expansion proteins: mechanism of transcription factor deactivation." Mol Cell **15**(1): 95-105.
Scherzinger, E., et al. (1997). "Huntingtin-encoded polyglutamine expansions form amyloid-like protein aggregates in vitro and in vivo." Cell **90**(3): 549-58.
Scherzinger, E., et al. (1999). "Self-assembly of polyglutamine-containing huntingtin fragments into amyloid-like fibrils: implications for Huntington's disease pathology." Proc Natl Acad Sci U S A **96**(8): 4604-9.
Schilling, G., et al. (2007). "Characterization of huntingtin pathologic fragments in human Huntington disease, transgenic mice, and cell models." J Neuropathol Exp Neurol **66**(4): 313-20.
Schirmer, E. C. and S. Lindquist (1997). "Interactions of the chaperone Hsp104 with yeast Sup35 and mammalian PrP." Proc Natl Acad Sci U S A **94**(25): 13932-7.
Shelbourne, P. F., et al. (1999). "A Huntington's disease CAG expansion at the murine Hdh locus is unstable and associated with behavioural abnormalities in mice." Hum Mol Genet **8**(5): 763-74.
Sherwood, S. W., et al. (1994). "Induction of apoptosis by the anti-tubulin drug colcemid: relationship of mitotic checkpoint control to the induction of apoptosis in HeLa S3 cells." Exp Cell Res **215**(2): 373-9.
Shimohata, T., et al. (2002). "Expanded polyglutamine stretches form an 'aggresome'." Neurosci Lett **323**(3): 215-8.
Shivaprasad, S. and R. Wetzel (2004). "An intersheet packing interaction in A beta fibrils mapped by disulfide cross-linking." Biochemistry **43**(49): 15310-7.
Sieradzan, K. A., et al. (1999). "Huntington's disease intranuclear inclusions contain truncated, ubiquitinated huntingtin protein." Exp Neurol **156**(1): 92-9.
Sipione, S. and E. Cattaneo (2001). "Modeling Huntington's disease in cells, flies, and mice." Mol Neurobiol **23**(1): 21-51.
Slepko, N., et al. (2006). "Normal-repeat-length polyglutamine peptides accelerate aggregation nucleation and cytotoxicity of expanded polyglutamine proteins." Proc Natl Acad Sci U S A **103**(39): 14367-72.
Steffan, J. S., et al. (2000). "The Huntington's disease protein interacts with p53 and CREB-binding protein and represses transcription." Proc Natl Acad Sci U S A **97**(12): 6763-8.
Suhr, S. T., et al. (2001). "Identities of sequestered proteins in aggregates from cells with induced polyglutamine expression." J Cell Biol **153**(2): 283-94.
Sunde, M., et al. (1997). "Common core structure of amyloid fibrils by synchrotron X-ray diffraction." J Mol Biol **273**(3): 729-39.
Tabrizi, S. J., et al. (1999). "Biochemical abnormalities and excitotoxicity in Huntington's disease brain." Ann Neurol **45**(1): 25-32.
Takahashi, J., et al. (2001). "Recruitment of nonexpanded polyglutamine proteins to intranuclear aggregates in neuronal intranuclear hyaline inclusion disease." J Neuropathol Exp Neurol **60**(4): 369-76.
Terry, R. D., et al. (1991). "Physical basis of cognitive alterations in Alzheimer's disease: synapse loss is the major correlate of cognitive impairment." Ann Neurol **30**(4): 572-80.

Thakur, A., Jayaraman, M., Thakur, M., and Wetzel, R. (unpublished data).
Thakur, A. K. and R. Wetzel (2002). "Mutational analysis of the structural organization of polyglutamine aggregates." Proc Natl Acad Sci U S A **99**(26): 17014-9.
Tobin, A. J. and E. R. Signer (2000). "Huntington's disease: the challenge for cell biologists." Trends Cell Biol **10**(12): 531-6.
Tompkins, M. M. and W. D. Hill (1997). "Contribution of somal Lewy bodies to neuronal death." Brain Res **775**(1-2): 24-9.
Trinh, C. H., et al. (2002). "Crystal structure of monomeric human beta-2-microglobulin reveals clues to its amyloidogenic properties." Proc Natl Acad Sci U S A **99**(15): 9771-6.
Trottier, Y., et al. (1995). "Polyglutamine expansion as a pathological epitope in Huntington's disease and four dominant cerebellar ataxias." Nature **378**(6555): 403-6.
Tycko, R. (2006). "Molecular structure of amyloid fibrils: insights from solid-state NMR." Q Rev Biophys **39**(1): 1-55.
Verhoef, L. G., et al. (2002). "Aggregate formation inhibits proteasomal degradation of polyglutamine proteins." Hum Mol Genet **11**(22): 2689-700.
Vonsattel, J. P., et al. (1985). "Neuropathological classification of Huntington's disease." J Neuropathol Exp Neurol **44**(6): 559-77.
Wacker, J. L., et al. (2004). "Hsp70 and Hsp40 attenuate formation of spherical and annular polyglutamine oligomers by partitioning monomer." Nat Struct Mol Biol **11**(12): 1215-22.
Waelter, S., et al. (2001). "Accumulation of mutant huntingtin fragments in aggresome-like inclusion bodies as a result of insufficient protein degradation." Mol Biol Cell **12**(5): 1393-407.
Wanderer, J. and A. J. Morton (2007). "Differential morphology and composition of inclusions in the R6/2 mouse and PC12 cell models of Huntington's disease." Histochem Cell Biol **127**(5): 473-84.
Wang, T. H., et al. (1998). "Microtubule-interfering agents activate c-Jun N-terminal kinase/stress-activated protein kinase through both Ras and apoptosis signal-regulating kinase pathways." J Biol Chem **273**(9): 4928-36.
Warren, S. and R. N. Chute (1972). "Pheochromocytoma." Cancer **29**(2): 327-31.
Warrick, J. M., et al. (1999). "Suppression of polyglutamine-mediated neurodegeneration in Drosophila by the molecular chaperone HSP70." Nat Genet **23**(4): 425-8.
Webb, J. L., et al. (2004). "Microtubule disruption inhibits autophagosome-lysosome fusion: implications for studying the roles of aggresomes in polyglutamine diseases." Int J Biochem Cell Biol **36**(12): 2541-50.
Weissmann, C. (2005). "Birth of a prion: spontaneous generation revisited." Cell **122**(2): 165-8.
Wellington, C. L., et al. (2000). "Inhibiting caspase cleavage of huntingtin reduces toxicity and aggregate formation in neuronal and nonneuronal cells." J Biol Chem **275**(26): 19831-8.

Wetzel, R. (2005). Protein Folding and Aggregatoin in the Expanded Polyglutamine Repeat Diseases. The Protein Folding Handbook, Part II. J. a. K. Buchner, T. Weinheim, Wiley-VCH**:** 1170-1214.

Wetzel, R. (2006). Chemical and Physical Properties of Polyglutamine Repeat Sequences. Genetic Instabilities and Neurological Diseases. T. a. W. Ashizawa, R.D. San Diego, Academic Press**:** 517-536.

Wexler, N. S., et al. (1987). "Homozygotes for Huntington's disease." Nature **326**(6109): 194-7.

Wheeler, V. C., et al. (1999). "Length-dependent gametic CAG repeat instability in the Huntington's disease knock-in mouse." Hum Mol Genet **8**(1): 115-22.

White, J. K., et al. (1997). "Huntingtin is required for neurogenesis and is not impaired by the Huntington's disease CAG expansion." Nat Genet **17**(4): 404-10.

Williams, A., et al. (2006). "Aggregate-prone proteins are cleared from the cytosol by autophagy: therapeutic implications." Curr Top Dev Biol **76**: 89-101.

Wilmot, G. R. a. W., S.T. (1998). A new mutational basis for disease. Genetic Instabilities and Hereditary Neurological Diseases. R. D. Wells, Warren, S.T., and Sarmiento, M. San Diego, Academic Press**:** 3-12.

Wood, S. J., et al. (1996). "Physical, morphological and functional differences between ph 5.8 and 7.4 aggregates of the Alzheimer's amyloid peptide Abeta." J Mol Biol **256**(5): 870-7.

Wyttenbach, A., et al. (2002). "Heat shock protein 27 prevents cellular polyglutamine toxicity and suppresses the increase of reactive oxygen species caused by huntingtin." Hum Mol Genet **11**(9): 1137-51.

Wyttenbach, A., et al. (2001). "Polyglutamine expansions cause decreased CRE-mediated transcription and early gene expression changes prior to cell death in an inducible cell model of Huntington's disease." Hum Mol Genet **10**(17): 1829-45.

Yamamoto, A., et al. (2000). "Reversal of neuropathology and motor dysfunction in a conditional model of Huntington's disease." Cell **101**(1): 57-66.

Yang, F., et al. (2005). "Curcumin inhibits formation of amyloid beta oligomers and fibrils, binds plaques, and reduces amyloid in vivo." J Biol Chem **280**(7): 5892-901.

Yang, W., et al. (2002). "Aggregated polyglutamine peptides delivered to nuclei are toxic to mammalian cells." Hum Mol Genet **11**(23): 2905-17.

Young, A. B. (1998). Huntington's disease and other trinucleotide repeat disorders. Molecular neurology. J. B. Martin. New York, Scientific American Inc.

Zhu, C., Hickey, M.A., Gallant, K., Levine, M.S., and Chesselet, M. F. (2006). Differential effects of curcumin and coenzyme Q10 treatment on huntingtin aggregates in CAG 140 knock-in mouse model of Huntington's disease. Society for Neuroscience, Atlanta, GA.

Zuccato, C., et al. (2001). "Loss of huntingtin-mediated BDNF gene transcription in Huntington's disease." Science **293**(5529): 493-8.

VITA

Erica LeAnn Rowe was born in Knoxville, Tennessee in February 1978. She earned an Associates Degree in General Studies from Walters State Community College, Morristown, Tennessee in May 1999. In May 2001, Erica received her Bachelor of Science in Health Sciences with a Microbiology concentration from East Tennessee State University in Johnson City, Tennessee. Just after graduation, she moved to Knoxville, Tennessee and began her graduate studies in the Genome Science and Technology Program at the University of Tennessee, where she obtained a Doctorate of Philosophy Degree in Life Sciences.